AN ABSTRACT OF THE THESIS OF

James Keith Maitland for the degree of Doctor of Philosophy

in Civil Engineering presented on July 11, 1977

Title: BEHAVIOR OF CELLULAR BULKHEADS IN DEEP SANDS

Abstract approved

Dr. W. L. Schroeder

Large-scale experiments on circular model cell bulkheads were conducted to define the distribution of hoop stresses, deflections of the cells, distortion of the cell fill, ultimate overturning resistance, and the critical mode of failure. The embedment depth of the model cells was varied to investigate the effect of embedment on the behavior of circular cells. The model cells were subjected to typical service loading conditions, including backfilling and backfill surcharging and were failed by application of a large lateral load.

Hoop tension during initial cell filling was found to be the critical design consideration for sheetpiles along the back of the cell. Maximum interlock tension occurred within the lower third of the exposed height of the sheetpiles. An apparent coefficient of lateral earth pressure ranging from 1.2 to 1.6 times the active Rankine value is recommended for design of isolated cells. Maximum hoop tension and radial bulging should be assumed to occur at an elevation of one-fourth of the distance from the point of sheetpile fixity to the top of the sheetpile. The depth to fixity may be estimated

by theory of elasticity and depends on the quality of the soil in which the cells are embedded. Backfilling and surcharging increased hoop tension by about 25 and 10 percent, respectively. Crest deflections vary linearly with the magnitude of backfill surcharge.

Distortion of the model cells at failure indicates that circular cell bulkheads fail as flexible structures. The critical mode of failure for embedded cells was found to be that of tilting about a point of fixity. A plastic hinge forms in the front sheetpiles at the point of fixity. Failure of the cell fill occurs along roughly vertical planes which extend vertically only to the point of tilting.

It is shown that the method of analysis by vertical shear using the Rankine or Krynine coefficient significantly underestimates cell overturning resistance. The method of horizontal shear overestimates the overturning resistance for embedded cells by about 35 percent. An apparent coefficient of lateral earth pressure to be used with the proposed failure model is recommended. It is shown that this coefficient depends on sheetpile embedment and fill characteristics, and is significantly larger than previously suggested values.

Available field data on circular cell bulkheads, specifically hoop tension and deflection data, is presented and discussed. In general, the trends in field data compare favorably with the results from the model study.

Behavior of Cellular Bulkheads in Deep Sands

by

James Keith Maitland

A THESIS

submitted to

Oregon State University

in partial fulfillment of
the requirements for the
degree of

Doctor of Philosophy

June 1978

APPROVED

Redacted for Privacy

Professor of Civil Engineering in charge of major

Redacted for Privacy

Head of Department of Civil Engineering

Redacted for Privacy

Dean of Graduate School

Date thesis is presented July 11, 1977

Typed by Kris Thomsen for James Keith Maitland

ACKNOWLEDGEMENT

The study was made possible through the support of the Sea Grant College Program (National Oceanic and Atmospheric Administration) and Oregon State University.

I am indebted to Dr. W. L. Schroeder for his advice, assistance, and friendship over the past three years. My association with Professor Schroeder has been a distinct pleasure. The assistance of the many people who helped in all phases of the study is sincerely appreciated.

And to Debbie, who made life interesting.

TABLE OF CONTENTS

LIST FIGURES

LIST OF TABLES

BEHAVIOR OF CELLULAR BULKHEADS IN DEEP SANDS

INTRODUCTION

Cellular cofferdams are retaining structures consisting of a series of interconnected earth or rock-filled cells. These cells and the connecting arcs are constructed of interlocking steel sheetpiling arranged in a variety of geometric shapes. In this manner, two different materials, a loose shell of interlocking sheetpiles, and a soil mass, are combined to form an integrated structure capable of resisting lateral loads.

The first cellular cofferdam was built to aid with dewatering a construction site at Black Rock Harbor, New York in 1908 (Cummings, 1957). It consisted of prismatic cells with straight walls that bulged badly between the cross-walls. It was quickly realized that flat-web-bed sheetpiles required a curved surface to resist lateral pressures without large deformations. In 1910, a circular cell cofferdam was built in connection with the raising of the battleship "Maine," which had been sunk in the harbor of Havana, Cuba (Terzaghi, 1945). During the following decades, cellular cofferdams were used extensively as temporary cofferdams in connection with construction of docks, retaining walls and dams, in particular along the Mississippi River and in the Tennessee Valley.

Use of cellular bulkheads as permanent retaining structures developed directly from cofferdam construction. Cellular structures are now being commonly used as docks, retaining walls, breakwaters,

piers and drydocks, particularly in moderate to deep waters (i.e., depths greater than 45 feet).

Cellular structures have been constructed in a variety of geometric shapes. The three most common shapes, circular, diaphragm and cloverleaf, are shown in Figure 1(a), (b) and (c). Figure 1(d), (e) and (f) shows several of the many modified shapes that have been used. The geometry of the connecting arcs also has many variations. Permanent bulkhead installations have often had the configuration shown in Figure 1(e).

Circular cells have some distinct advantages over double-wall or diaphragm structures. The quantity of steel in a given length of wall constructed of circular cells is independent of cell diameter. This allows the designer to obtain additional stability without additional costs (if thicker sheetpiles are not required). For permanent structures such as docks or wharves, even the quantity of fill required is constant.

Circular cells are especially suited for construction in moderate to deep waters due to their inherent stability. Each cell is a self-contained unit and failure at one location will not lead to progressive failure of the entire structure as might be the case with an anchored bulkhead. An added important advantage is that circular cells may be filled immediately upon completion and subsequently act as working platforms for erection of successive cells. This single cell stability is particularly attractive for construction in swiftly-flowing or rough, storm-tossed waters. Cells with straight cross-walls must be filled simultaneously and do not offer this advantage.

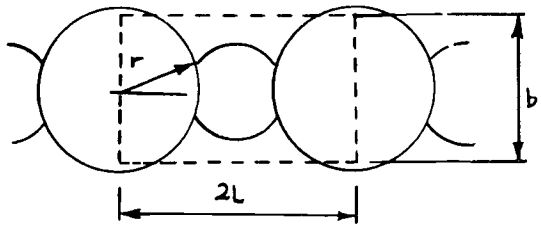

a) Circular

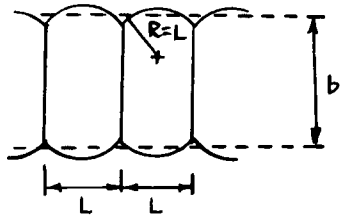

b) Diaphragm

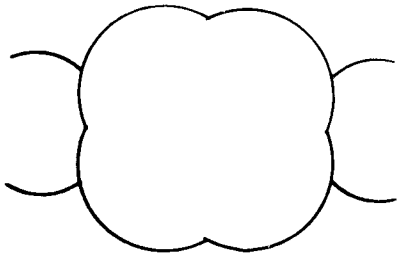

c) Cloverleaf

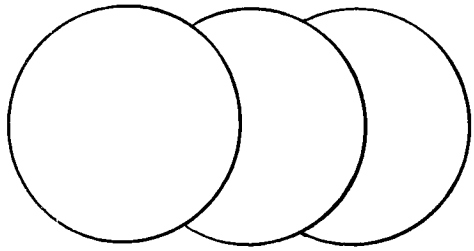

d) Modified circular

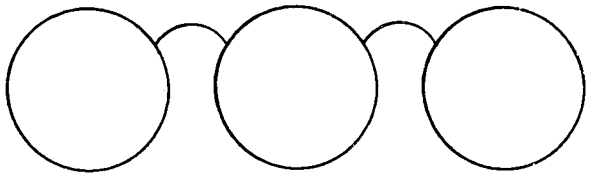

e) Circular type without back arcs

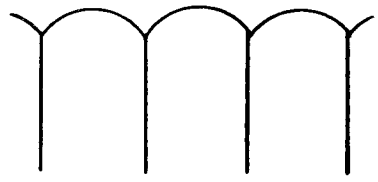

f) Modified diaphragm

Figure 1. Typical configurations of cellular structures.

Circular cell walls, therefore, are being increasingly used for a variety of special purposes. They are particularly attractive where larger dockside heights must be attained for marginal wharves.

To the casual observer cellular cofferdams and bulkheads appear to be very simple structures indeed; a thin steel cylinder filled with soil or rock and laterally loaded. However, the extreme differences in material characteristics, the complexity of the soil-sheetpile interaction, the pressure of connecting arcs and the discontinuity resulting from interlocks in the steel shell make this type of structure highly indeterminate. The ability to accurately analyze or predict cell behavior is seriously hampered by a lack of understanding of the stress distribution in the cell fill and sheetpile interlocks. Little is known about the steel/soil interaction. In addition, our ability to quantify the effects of backfill loads and surcharges on circumferential of "hoop" stresses is poor.

In spite of these deficiencies, designers must account for all possible modes of failure and design the structure to be safe under all circumstances. The secret to safe, yet economical design lies in the recognition of the critical mode of cell failure. Considerable divergence of opinion exists as to just what this critical mode is.

Practically all methods developed for cofferdam design are based, at least in part, on experiences with cellular cofferdams which have been built on rock. The analysis of cellular bulkheads in deep sands has evolved from such work with little more than simple extrapolation. To understand current design practice for bulkheads and other

permanent retaining structures, one must first look at the design considerations for construction of cofferdams on rock.

A brief description of each possible mode of failure is presented below. The applicability of current design methods to bulkhead design is discussed in detail in the DISCUSSION OF RESULTS section.

LITERATURE REVIEW AND DESIGN CONSIDERATIONS FOR CIRCULAR CELLULAR STRUCTURES

Equivalent Rectangular Dimensions

For purposes of design analysis, the cellular structure is replaced by an equivalent rectangular shape. The width, b, shown in Figure 2 is such that the assumed rectangle has either the same cross-sectional area or section modulus as the cofferdam. TVA engineers have indicated that results of analysis using either method are practically identical (TVA, 1957).

TVA engineers have suggested (TVA, 1957) that for a cell of radius r, that the equivalent width, b, be given by:

$b = 1.57\ r$ -- with 90 degree T's

$b = 1.75\ r$ -- with 60 degree T's

Terzaghi, in his 1945 paper, recommended:

$b = 1.7\ r$ for circular cells

$b = 1.8\ r$ for diaphragm cells

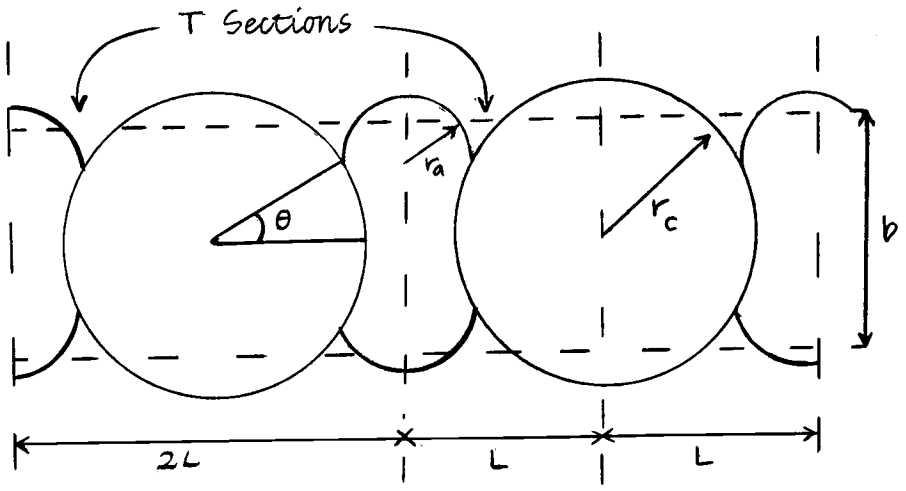

b = equivalent width

$r_{a,c}$ = arc and cell radii

2L = equivalent length

θ = angle between cell centerline and arc connection

Figure 2. Geometry of circular cell bulkhead.

Figure 2 indicates the length of the equivalent rectangular circular cofferdam. Since circular cells have two cross-walls per cell, the typical section is taken as 2L as shown. For diaphragm cells, the typical section length, L, is the distance between cross-walls.

Failure Modes

Bursting Failure

The most frequent cause of cofferdam distress has been failure of the cells near the arc connections. Experience has indicated that practically all failures by bursting of the interlocks have occurred during the cell filling stage. Terzaghi indicated that bursting

failures due to application of an overturning moment have not been recorded, unless the cofferdam was already in an advanced state of tilting (i.e. crest deflection of 20 to 25 percent of cell height) (Terzaghi, 1945).

The interlock tension is developed due to internal cell pressures acting radially outward. The calculation of this radial pressure has been a subject of considerable controversy. The interlock tension in a sheetpile may be calculated by

$$t = p \cdot r \tag{1}$$

where t = interlock tension

p = net outward horizontal pressure

r = radius of the cell or arc

The horizontal pressure, p, is equal to the combined net lateral earth and water pressure. At some depth, z, the net lateral earth pressure is the product of the effective vertical overburden pressure and the coefficient of lateral earth pressure, K.

The tension in a sheetpile due to earth pressure is

$$t = \sigma_v' Kr = z\gamma_e' Kr \tag{2}$$

where σ_v' = effective vertical stress at a depth z

γ_e' = weighted effective unit weight of cell fill

K = coefficient of lateral earth pressure.

The effect of seepage forces on hoop stress must also be considered for cellular cofferdams involved in dewatering projects. Seepage force created by large differential heads of water may significantly increase the hoop stress at the inboard sheets. Bulkhead structures, on the other hand, are seldom subjected to large differential water levels across the cell wall, except at the initial cell filling stage.

The coefficient of lateral earth pressure for cell fill has been commonly taken to be the active Rankine coefficient

$$K_A = \tan^2 (45 - \phi/2) \qquad (3)$$

where ϕ = angle of internal friction of the fill material.

Terzaghi concluded, from his analysis of the internal shearing resistance of the cell fill, that the coefficient must be larger than that obtained by the active Rankine state of stress (Terzaghi, 1945). He indicated that the value of K probably ranged from 0.4 to 0.5 and recommended an empirical value of 0.4. The value of K undoubtedly varies throughout the cell fill. It is probably higher at the middle than along peripheral areas.

Krynine recognized that the coefficient, K, was not the active Rankine coefficient but rather the ratio of horizontal to vertical stress (Krynine, 1945). The active Rankine coefficient is expressed as the ratio of the minor to major effective principal stresses (σ_3'/σ_1'). The vertical plane through the middle of a cell subjected to lateral

load is assumed to have shear stresses acting on it. It cannot be, therefore, a principal plane. Krynine suggested a modified coefficient

$$K = \frac{\cos^2 \phi}{2-\cos^2 \phi} \tag{4}$$

where ϕ = angle of internal friction of the fill. Navdock's DM-7 recommends Krynine's value of K (Navdocks, 1962).

Pennoyer stated that Terzaghi's proposed value of 0.4 for K is not in agreement with engineering practice. Cells had been built which exceeded the limits of both the height and radius set by the proposed coefficient. His experience indicated that values as low as 0.17 had been occasionally used without resulting in undue distress to the cell. He proposed that wall friction may considerably relieve the vertical stresses, that is, the weight of the cell fill may be partially relieved by "arching" effects, and carried by the sheetpile walls (Pennoyer, 1934).

The magnitude of the interlock tension may vary significantly around the perimeter of a cell. TVA suggests that the cell hoop force outside the connecting arcs and the arc hoop curve may be calculated from (TVA, 1957)

$$t = \frac{p}{12} \times r \tag{5}$$

where t = hoop force in arcs or in cell outside connecting arcs (lb/linear inch)

p = lateral unit pressure (lb/ft^2)

r = radius of arc or cell (ft)

The maximum interlock force is believed to occur in the sheet-piles directly behind the connecting arc, where the cell and arc tension are superimposed. TVA suggests that the hoop force be given by

$$t_{max} = \frac{p \times L}{12} \sec \theta \qquad (6)$$

where t_{max} = hoop force behind connecting arcs (lb/in)

L = 1/2 center-to-center distance (ft)

θ = angle between centerline of cells and point of arc connection.

Equation (6) is based on the assumption that the unit pressure, p, acting along the cell centerline also acts along a distance L at the arc connections (see Figure 3). The hoop stress behind the arc connections is then computed from static equilibrium.

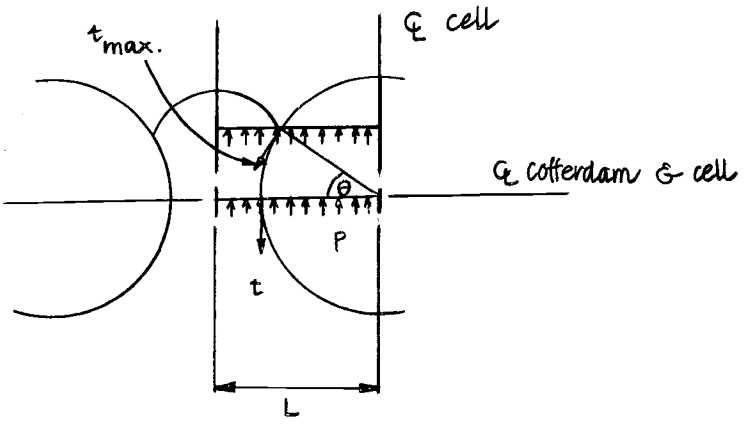

Figure 3. Interlock stress in a circular cell. (after TVA)

For single-arc cellular bulkheads the distribution of hoop forces at any level according to TVA is shown in Figure 4.

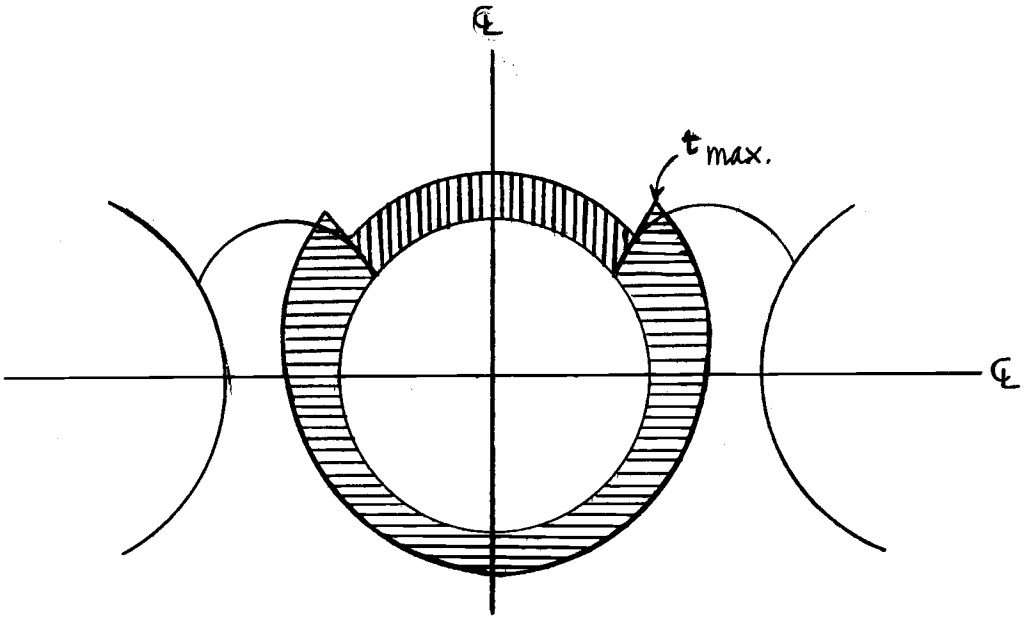

Figure 4. Distribution of hoop tension for single-arc bulkheads. (after TVA)

Field studies indicate that the increase in hoop stress due to the presence of the arcs is not as pronounced as predicted by Equation (6) (White, et. al., 1963; Khuayjarernpanishk, 1975).

Cellular cofferdams on rock or bulkheads driven into sands appear to have a point of maximum bulging at about H/4 to H/3 above the bottom of the cell and dredgeline, respectively. This is due to the radial restraint at the bottom of sheets driven into soft rock or from the sands surrounding the bulkhead at the dredgeline. TVA engineers recognized this fact and recommended the pressure distribution on the inboard sheets shown in Figure 5 (TVA, 1975).

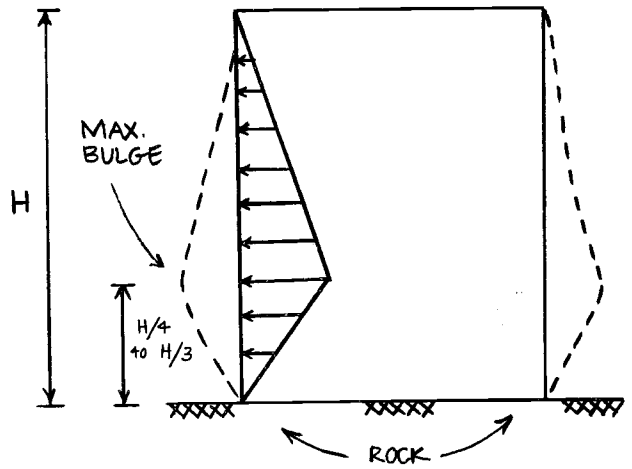

Figure 5. Assumed lateral pressure distribution.

The lateral pressure is assumed to increase linearly to a maximum value at the point of maximum bulging and then decrease to zero at the rock surface or dredgeline.

Unfortunately, interlock tension is not just a function of cell height and diameter but also depends on the soil type, water level, construction procedure and presence of backfill or cell surcharge. Tensile or compressive stresses can be introduced below the dredgeline by driving out of vertical. Pulling sheets together to ensure tight cell closure also can affect interlock forces. Many cell failures have been attributed to sheetpile damage due to overdriving out of interlock (Tschebotarioff, 1973). Sheets that have been driven out of interlock below the dredgeline may not manifest this problem in the exposed portion. Sheetpile interlocks then fail by "peeling away" during filling of the cell before developing full interlock pullout strength.

Densification of the cell fill, the sequence of stages of backfilling and the presence of surcharges can all potentially increase interlock tension.

The influence of these factors on interlock forces can be described qualitatively, or, at best, only in a rough quantitative manner. Experience and field observations must be relied upon to assess the potential contribution of each to interlock distress.

Up to 1969 most of the flat web sheetpile sections commercially available had a specified minimum pullout strength of 16,000 lb/in with a steel yield strength of 38,500 psi (Bower, 1973). A recently developed section, PSX32, has a guaranteed minimum pullout strength of 28,000 lb/in, 75% greater than the former piling (Bower, 1973). These stronger sections will probably lead to higher and larger cells.

The factor of safety against interlock pullout is defined as the ratio of the ultimate pullout strength to the sheetpile tension (i.e., F.S. = P_u/t).

A minimum factor of safety of 2.0 against interlock failure has been recommended by most manufacturers (U.S. Steel, 1975). Colburn reports that some temporary cellular cofferdams were built by TVA with a factor of safety of 1.25 without cell distress (Colburn, 1945). The only failures observed were related to driving out of interlock for sheets driven through cemented sands and gravels.

Sliding Stability

A cellular bulkhead resting on rock must resist the lateral forces imposed by the earth backfill or the water retained. The friction between the cell fill and the rock surface is equal to the effective

weight of the fill times the coefficient of friction between the fill and rock. If an earth berm is placed against the inboard side, it also provides a passive resistance to sliding. Figure 6 shows the lateral forces acting on the cell.

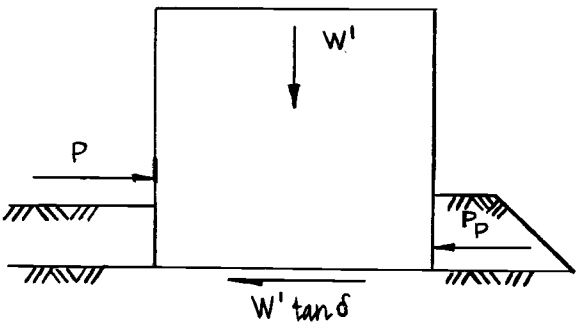

Figure 6. Sliding stability of a cell.

The factor of safety against sliding, defined as the ratio of lateral forces to potential resisting forces per unit length of wall, can be calculated from

$$F.S. = \frac{W' \tan\delta + Pp}{P} \qquad (7)$$

where W' = effective weight of cell fill

δ = coefficient of friction between fill and rock, usually taken as ϕ for rough rock surfaces.

P_p = effective passive resistance of the berm

P = total imposed lateral forces

A factor of safety of at least 1.25 (temporary structures) and 1.50 (for permanent bulkheads) is normally used (Navdocks, 1962).

Structures have been successfully built with a factor of safety against sliding of less than 1.0. Undoubtedly, the required additional horizontal shearing resistance is provided by tip penetration at the bottom of the sheetpile. The contribution to sliding stability of "toe-in" action for cells driven into soft rock can be considerable.

Failure by Overturning

Rigid Body Rotation. One of the earliest misconceptions involved in the design of cofferdams on rock has been the assumption that they can act like gravity walls subject to overturning about the toe. The cofferdam shown in Figure 7 is subjected to an overturning moment, M_o, with respect to the toe point o.

The maximum resisting moment that the weight of the cell can provide is

$$M_{max} = \frac{b^2 h \gamma_e'}{2} \tag{8}$$

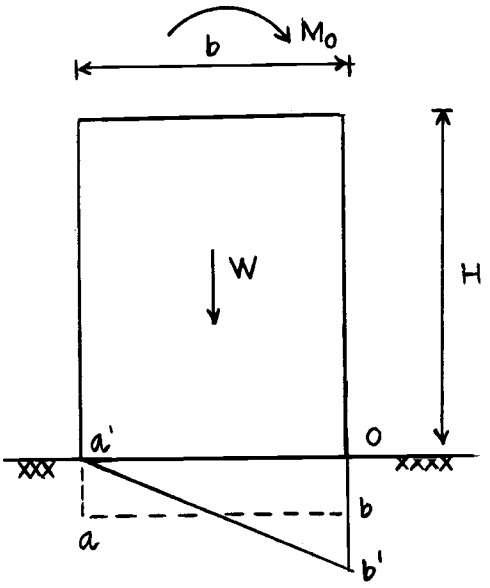

Figure 7. Cell failure by rigid body overturning.

The factor of safety against rigid body rotation is thus

$$F.\ S. = \frac{M_{max}}{M_o} \tag{9}$$

Before the application of the overturning moment, according to the usual assumptions, the pressure at the base of the cell is given by line ab in Figure 7. As the overturning moment increases the pressure distribution shifts to that of line a'b'. Ultimately, as overturning is approached, the resultant acts at the toe, which for a non-rigid cell is an impossible phenomenon. The overturning moment, M_o, required to shift the resultant of the base pressure to the inner boundary of the middle third is

$$M_o = \frac{b^2 h \gamma_e'}{6} = \frac{1}{3} M_{max} \tag{10}$$

The factor of safety against overturning for this limiting condition is

$$F.S. = \frac{M_{max}}{M_o} = 3 \tag{11}$$

Or, if a cofferdam has an equivalent width, b, of

$$b = \sqrt{\frac{6M_o}{H\gamma_e'}} \tag{12}$$

it has a factor of safety of 3.0 against overturning.

It has long been recognized that the behavior of cellular structures is not that of a rigid gravity wall. Cellular structures are flexible, i.e. they deform and distort as loads or moments are applied. The cells, therefore, can fail by excessive deformations or crest deflections before overturning occurs. Unfortunately, many designers to this day assume a factor of safety of 3.0 against overturning will actually be attained if they adhere to the "middle third" rule.

Many engineers have recognized cell behavior more realistically and have attempted to analyze the resistance of cells to overturning without the rigid-body assumptions. Several models of failure by internal shear have been proposed and are summarized below.

Failure by Vertical Shear. The concept of cofferdam failure by vertical shear was first described by Terzaghi (1945), although it had been previously incorporated into design procedure by TVA engineers (Pennoyer, 1945).

If the cofferdam shown in Figure 8 is subjected to an overturning moment, M_o, according to elementary bending theory, the foundation soil pressure response moves from that represented by line ab to a'b'. The shaded area in the figure represents the stress induced by the overturning moment. If V is the area of one of the triangles, then

$$V = \frac{3}{2} \frac{M_o}{b} \tag{13}$$

where V = total shear force acting on the neutral plane cd.

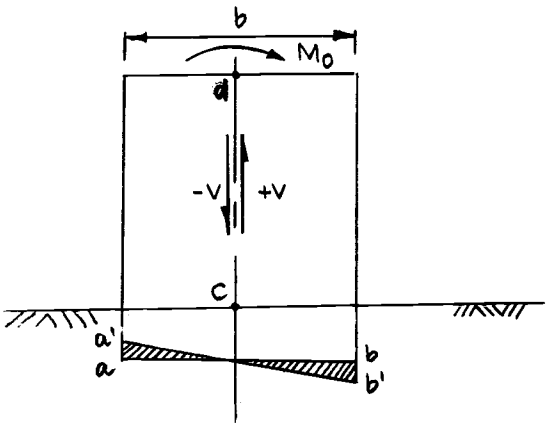

Figure 8. Vertical shear at the center of a cell.

The shearing resistance along plane cd, per linear foot of wall , is equal to the total lateral force in the vertical section times the coefficient of friction of the fill. That is

$$S' = P_c \tan\phi \tag{14a}$$

where S' = shearing resistance due to fill

P_c = effective lateral earth force on plane cd

Therefore

$$S' = \frac{1}{2}\gamma_e' H^2 K \tan\phi \tag{14b}$$

The friction between the interlocks also contributes a shearing resistance, S''. If the tension in the interlocks at a depth of z is given by

$$t = \gamma_e' z K r \tag{15a}$$

the total tension for a cell of height, H, is

$$T = \frac{1}{2}\gamma_e' H^2 K r \tag{15b}$$

Let the coefficient of friction between sheetpiles be represented by f and note that there are two such interlocks per equivalent length 2L. The total shearing resistance in the interlocks per linear foot of retaining wall is

$$S'' = \frac{2T \cdot fr}{2L} \tag{16a}$$

Substituting into Equation 16(a) the expression for T, (Equation 15(b)), then,

$$S'' = \frac{1}{2} \gamma_e' H^2 K \frac{r}{L} P \qquad (16b)$$

This shearing resistance is by no means negligible. Pennoyer (1945) reports that many cells that were only 60 percent safe by internal shear in the fill still stood without undue distress. He concluded that the remaining shearing resistance must have been provided by friction in the interlocks.

The total shearing resistance, S, along the neutral plane is equal to the sum of fill and interlock shearing resistance. Hence

$$S = S' + S''$$

$$= \frac{1}{2} \gamma_e' H^2 K \left(\tan\phi + \frac{rf}{L}\right) \qquad (17a)$$

A simplifying assumption of r approximately equal to L leads to the final expression

$$S = \frac{1}{2} \gamma_e' H^2 K \left(\tan\phi + f\right) \qquad (17b)$$

Terzaghi suggested a value of 0.3 for f (the coefficient of friction for steel on steel) while the value of K is subject to the controversy previously described.

The factor of safety against failure by internal vertical shear can be defined as the ratio of available shearing resistance to the actual shear acting on the neutral plane. Hence

$$F.S. = \frac{S}{V} = \frac{\gamma_e' H^2 bK}{3M_o} (\tan\phi + f) \qquad (18)$$

Temporary cofferdams designed by the TVA with a factor of safety of 1.25 against vertical shear performed well (TVA, 1957). Navdock's DM-7 recommends a factor of safety of 1.25 for temporary structures and 1.50 for permanent structures (Navdocks, 1962).

Krynine's ϕ-line Mechanism. In reviewing Terzaghi's classic paper (1945) on cofferdams, Krynine offered another possibility for failure by internal shear (Krynine, 1945). Figure 9 shows schematically this mode of failure.

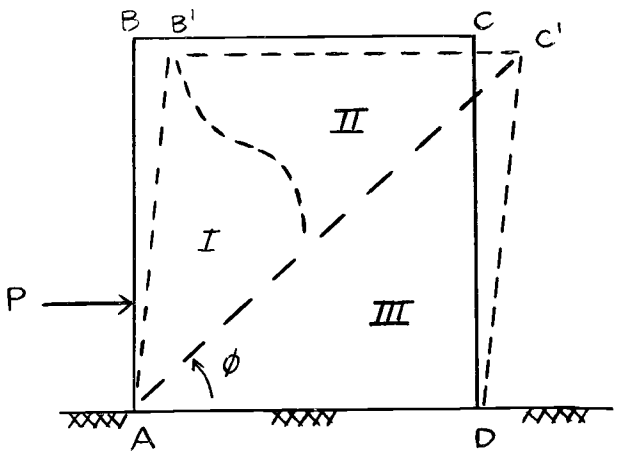

Figure 9. Failure by internal shear.

Krynine proposed that as the cofferdam tips from position ABCD to that of AB'C'D, the soil in Zone I is densified. At some critical point the soil in Zone I pushes the material in Zone II upwards. Zone III, which he termed a "quiet zone," remains stationary and presumably in an elastic state of stress. Failure, therefore, occurs by the sliding of mass ABC over the "quiet zone" along a plane making an angle of ϕ with the horizon. He theorized that the actual shape of the failure plane is curved as shown for line AC in Figure 10.

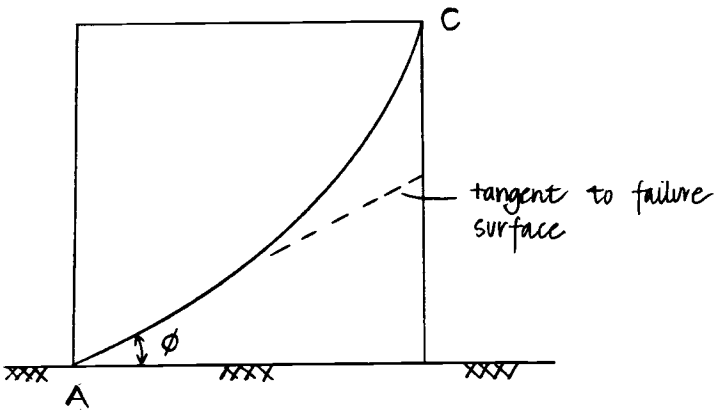

Figure 10. Internal failure surface.

Failure by Horizontal Shear. In 1957 Cummings introduced a new model for cofferdam distress, failure by tilting (Cummings, 1957). He proposed that cofferdams on rock failed primarily by internal shear of the fill along horizontal planes. Cummings' work was based on a series of small-scale model tests.

Cummings' model for cell behavior is based on the premise that the state of stress of the fill material changes upon application

of a lateral load. Before application of lateral loads, the soil above the ϕ-lines shown in Figure 11 (a) is assumed to be in the active state of stress while soil below the "ϕ-cone" is in the at-rest condition.

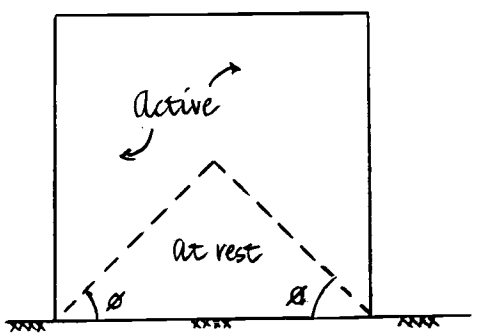

(a) Stresses in fill in an isolated cell.

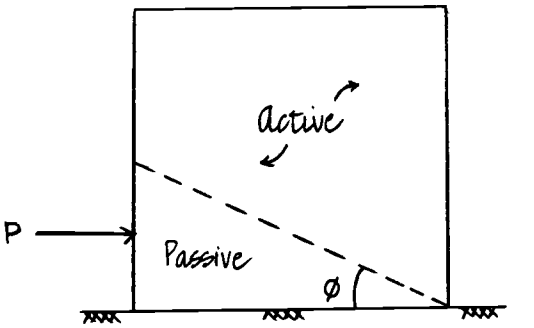

(b) Stresses in fill after application of lateral load

Figure 11. Transition of stress state. (after Cummings)

Upon application of the lateral force, P, the soil below the ϕ-line changes to the passive state while the balance of the fill remains in the active condition (see Figure 11 (b)).

As the cofferdam tilts, the angle that line ab (Figure 12) makes with the base becomes larger than ϕ, the angle of internal friction. The tendency for the fill above a'b to slide down that plane exceeds the shearing resistance to that movement.

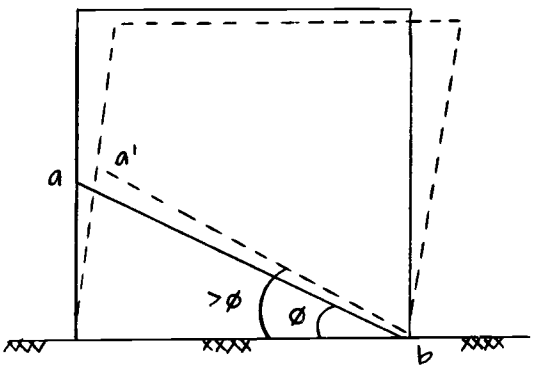

Figure 12. Cell tilting.

The soil mass then slides as the cell tilts. The soil below the ϕ-line is in the passive state of stress and is simply surcharged by the soil above. The soil mass above the ϕ-line, therefore, does not contribute to the lateral resistance (see Figure 13 (a)).

In Figure 13 (b) the ultimate lateral shearing resistance, R_y, that can be developed at any depth y below point A is equivalent to the weight, W_y, of the prism fhde times the coefficient of internal friction, $\tan\phi$. Thus

$$R_y = W_y \tan\phi \qquad (19)$$

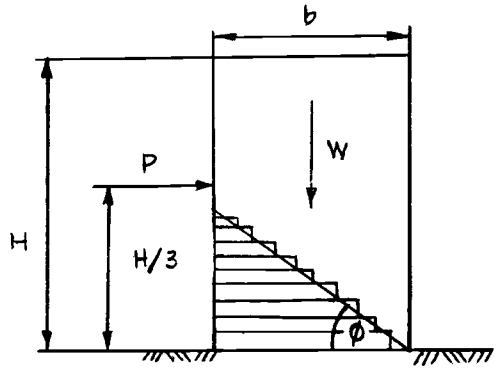

(a) Cell fill resistance to lateral force

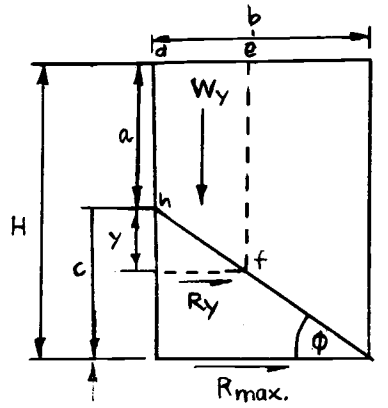

(b) Forces in tilting failure mode.

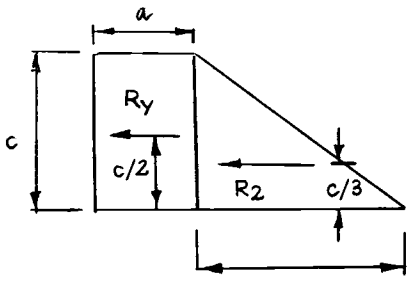

(c) Pressure diagram provided by cell fill.

Figure 13. Cummings' tilting analysis.

The weight of the arbitrary prism fhde is

$$W_y = \gamma_e'(a + y)y \cot\phi \tag{20}$$

and by substituting the expression for the weight, W_y, into Equation 19 one obtains

$$R_y = \gamma_e'(ay + y^2) \tag{21a}$$

The magnitude of the lateral resistance, R_y, is a maximum when $y = c$. R_{max} is then given by

$$R_{max} = \gamma_e'(ac + c^2) \tag{21b}$$

From the geometry of Figure 13(b) it can be noted that $c = b \tan\phi$ and $a = h - c$. Thus

$$R_{max} = \gamma_e' bh \tan\phi \tag{22}$$

that is, the maximum horizontal shearing resistance is, as anticipated, equal to the weight of the cell fill, $\gamma_e' bh$, times the coefficient of friction, $\tan\phi$.

However, this approach differs from the concept of simple sliding in that the lateral resistance, R_y, now has a moment arm and is capable of resisting an overturning moment.

Equation 21(b) may be represented graphically by Figure 13(c). The potential resisting moment due to R_y can be taken as the contribution of the components R_1 and R_2 times the respective distances to their points of application.

The potential resisting moment due to the soil, M_s, is

$$M_s = R_1 \times \frac{c}{2} + R_2 \times \frac{c}{3} \tag{23a}$$

Substituting the expressions for R_1 and R_2 obtained from Figure 13(c), into the above equation results in the equation

$$M_s = \gamma_e'\left(\frac{ac^2}{2} + \frac{c^3}{3}\right) \tag{23b}$$

If the resisting moment due to interlock friction is considered, then, using the same assumptions described by Terzaghi (1945) and TVA (1957), the expression for the total resisting moment, M_r, is given by

$$M_r = \gamma_e'\left(\frac{ac^2}{2} + \frac{c^3}{3}\right) + Pfb \tag{24}$$

Rotational Failure. Brinch Hansen introduced in 1953 a different method of cellular bulkhead analysis (Hansen, 1953), based on rigid body rotation. The method, known as the equilibrium method, assumes a single rupture line near the base of the cell consisting of a circular slip-line.

For cells driven to shallow depths, the rupture line is a single convex upward arc (Rupture X) and the entire structure is assumed to rotate about a point below the bottom of the sheets (see Figure 14(a)). The earth below the circle remains in the at rest condition. Exterior earth pressures are independent of the location of the rotation center.

If the cell is driven to greater depths, the center of rotation moves up into the cell. The rupture line is then the concave upward arc

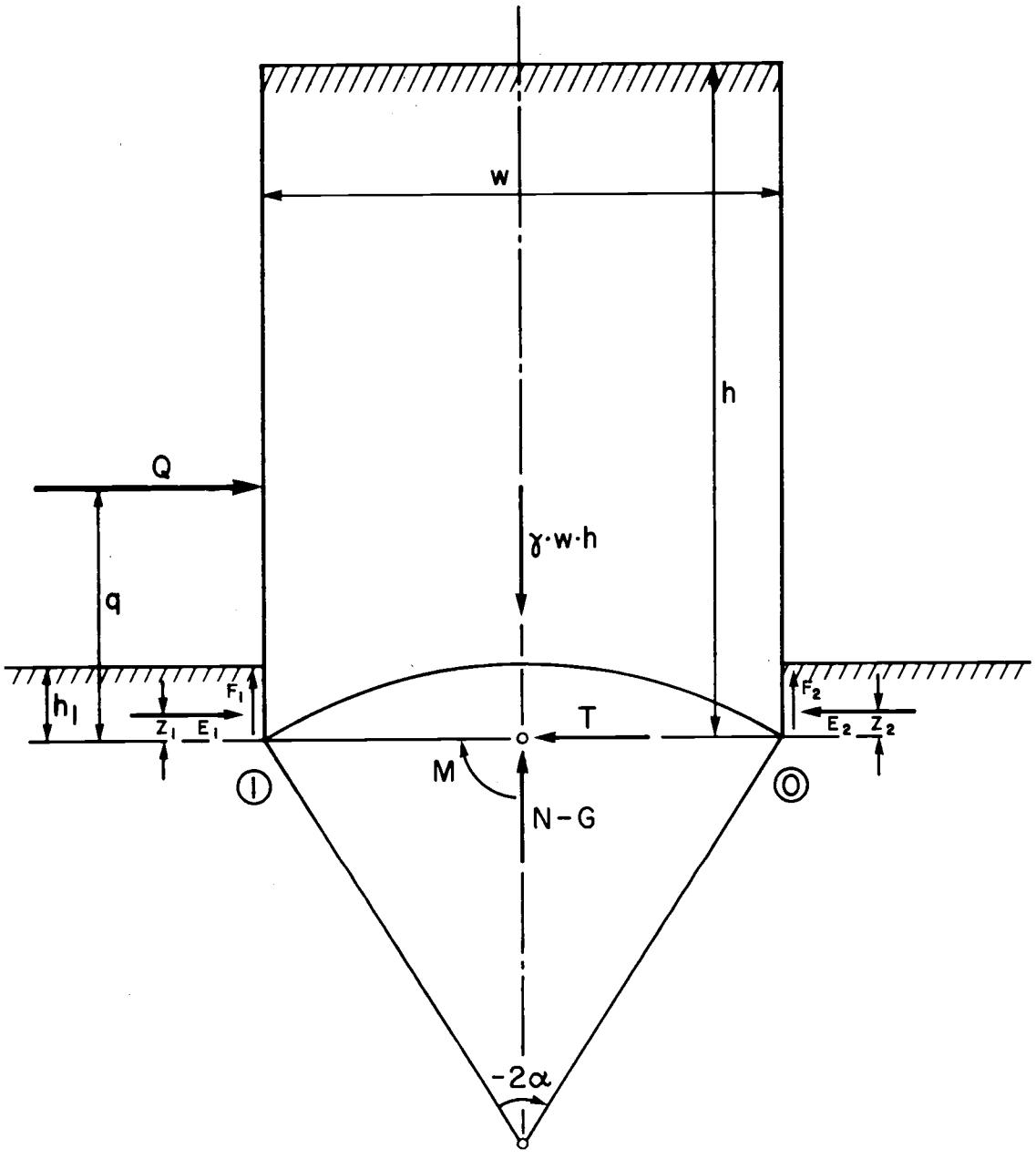

(a) X failure mode

Figure 14. Rotational failure of a cell (after Ovesen).

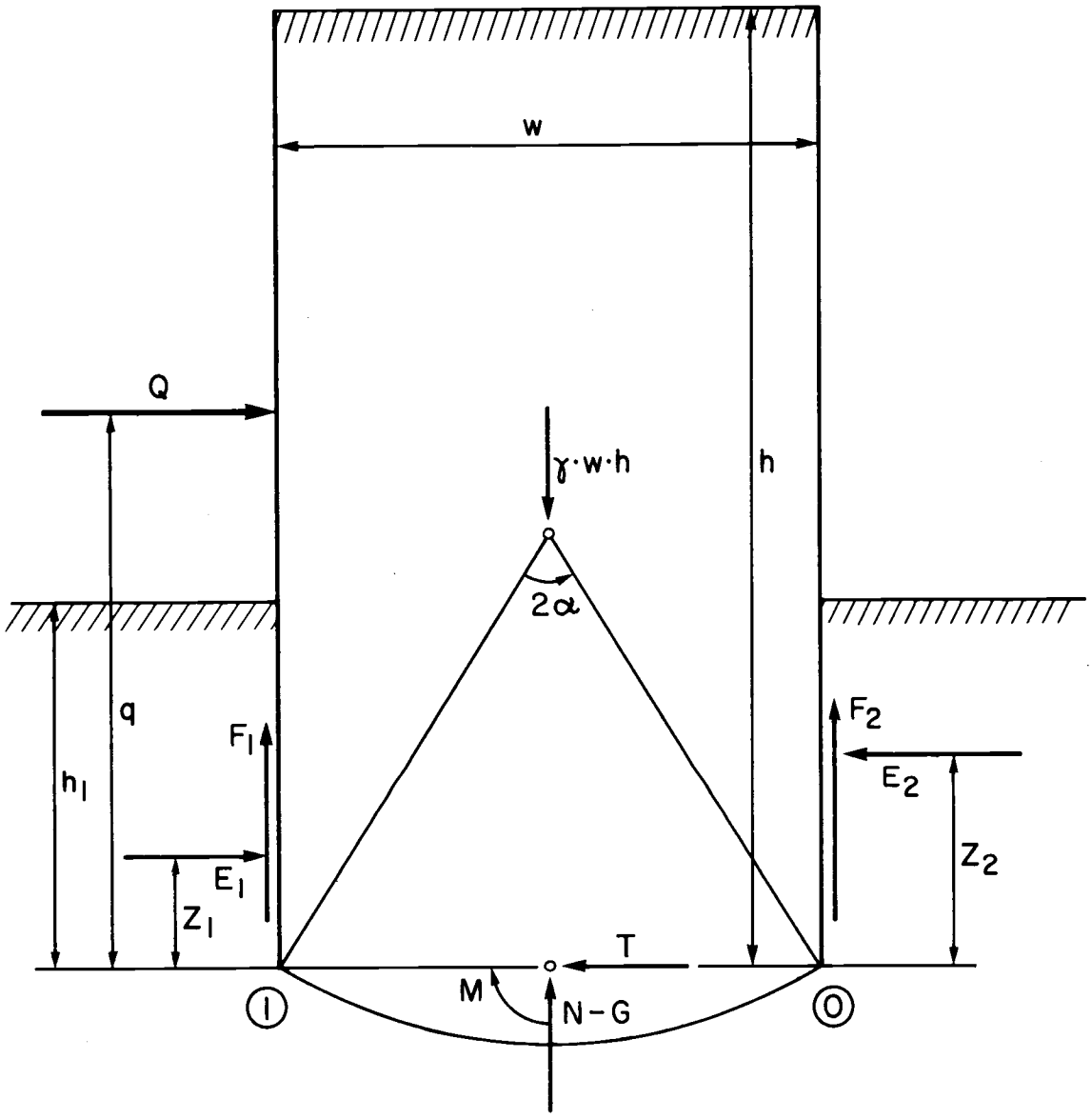

(b) A failure mode

Figure 14. continued

(Rupture A) shown in Figure 14(b). The exterior earth pressures now depend on the location of the center of rotation.

Referring to Figure 14(a) and (b) and summing forces in the horizontal and vertical directions and summing moments about the center of the chord one obtains

$$Q = T - E_1 + E_2 \tag{25a}$$

$$\gamma wh = G - N - F_1 - F_2 = 0 \tag{25b}$$

$$M + \frac{1}{2} w(F_1 - F_2) + E_1 Z_1 - E_2 Z_2 = 0 \tag{25c}$$

All the terms used in the method of equilibrium are defined in Table 1.

The above three equations are solved by the following trial and error procedure: trial values of α (the half central angle of the rupture circle) are used in Equation 25(b) to obtain trial values of t° (the stress at one end of the rupture circle). Using the trial value of t°, Q is computed from Equations 25(a) and 25(c). The correct value of α has been chosen when the value obtained from Equations 25(a) and 25(c) converge.

T, N and M (see Table 1) are functions of α, ϕ and t°. Their relationships have been developed (Hansen, 1957) using Koetter's equation for the variation of stress along the rupture circle

$$\frac{\partial t}{\partial v} + 2t \tan\phi + \gamma r \sin (v + \phi) = 0 \tag{26}$$

Bent Hansen indicated formulas that can be used to calculate the values of T, N and M (Hansen, 1958). The necessary calculations are fairly involved and time consuming.

Table 1.

Definition of Terms for Hansen's Analysis

Term	Definition of Term
$E_{1,2}$	Normal components of total earth pressure on wall
F	Tangential component of total earth pressure on wall
G	Total weight of earth mass
M	Moment of internal forces about point of rotation
N	Component (normal to the chord) of internal forces
Q	External forces on cellular cofferdam
T	Component (parallel to the chord) of internal forces
w	Equivalent cell width
$Z_{1,2}$	Distance from cell base to normal earth pressure components

A simpler method of analysis, known as the extreme method, was also employed by Brinch Hansen (Hansen, 1953). It is based on the same principles as those used in the equilibrium method, but assumes that the circular slip surface may be approximated by a logarithmic spiral. The spiral is assumed to pass through the tip of the cell walls and is defined by the polar equation

$$r = r_o e^{\theta \tan\phi}$$

The moments of the external and gravity forces about the pole of the spiral are computed and the ratio

$$f = \frac{M_{stabilizing}}{M_{driving}}$$

is computed. The position of the spiral is then changed and the ratio of stability, f, is recomputed. The critical spiral is the one for which the ratio is a minimum. If f is equal to one, the correct failure surface has been assumed.

Slipping Stability

One mode of failure frequently considered is that of slippage between the sheetpiles and the cell fill. As an overturning moment is applied to the cofferdam, there is a tendency for the steel shell to rotate about the toe. As the shell rotates, slippage occurs between the outboard sheets and the cell fill while the cell fill runs out the heel. The resisting moment with respect to the inboard toe is due to the frictional forces acting on the inboard face. The magnitude of this frictional force is assumed to be equal to the applied lateral load, P, times the coefficient of friction between the cell fill and the sheetpiles (see Figure 15).

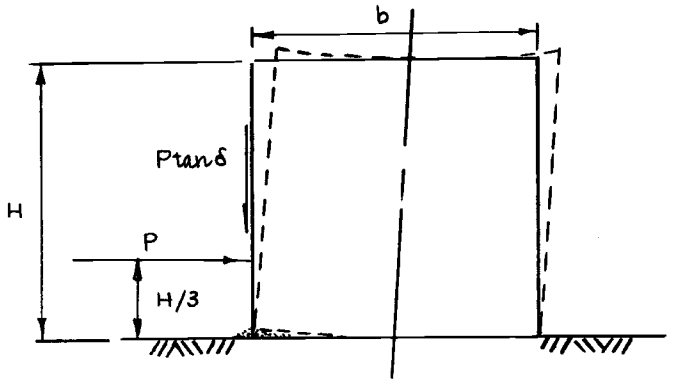

Figure 15. Slipping stability of a cell.

The factor of safety against slippage can be taken as

$$F.S. = \frac{(P\tan\delta)b}{P \cdot H/3} \tag{27}$$

where δ = friction angle between the fill and the sheetpiles.

Since slippage occurs between the cell fill and sheetpiles, the fill weight does not contribute to the resisting moment. A factor of safety against slippage of at least 1.25 has been recommended.

If the sheetpiles are driven into sand, a resisting moment can be developed with respect to rotation about the toe, due to the friction along the sheets at the heel. The pullout of sheetpiles at the heel is sometimes considered as a separate mode of failure.

Problems Associated with Presence of Water

No element in nature is more insidious than water. Its presence can probably be associated with most failures or distress of foundations

and earth retaining structures. Cellular cofferdams are no exception. Cofferdams are used primarily in the dewatering of construction sites and must sometimes withstand tremendous differential heads of water. Terzaghi has described comprehensively the problems associated with underseepage in cofferdams (Terzaghi, 1945).

Figure 16 shows a partial flow net for underseepage for a cell driven in sand. Potential problems that are usually considered are listed below:

1. The exit gradient at point "a" must not exceed the critical gradient, which can lead to formation of a pipe, boils or heave of the soil mass in front of the toe.

2. Upward seepage forces at the toe must not excessively reduce the passive resistance of the soil.

3. Seepage forces acting on the soil at the inboard face must not increase the hoop stresses in the sheetpiling excessively.

Terzaghi concluded that potential failures due to excessive underseepage were so critical that he recommended that the sheetpiles be extended to a depth of (2/3)H below the dredgeline to extend the flow lines and thereby reduce gradients at critical locations (Terzaghi, 1945).

Permanent bulkhead structures, however, are generally not exposed to large differences in water levels across the sheetpiles. Therefore, many, if not most, comments concerning underseepage directed at the design of cofferdams are not relevant to permanent waterfront retaining structures.

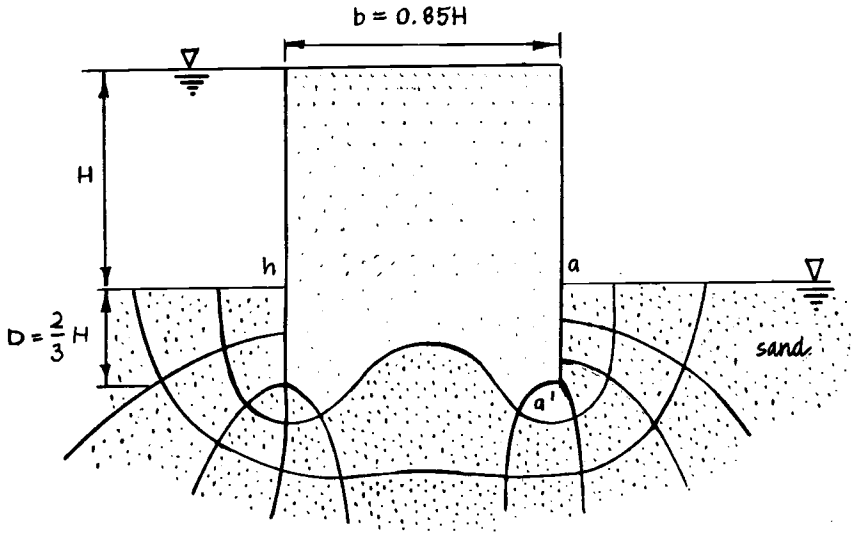

Figure 16. Seepage beneath a cell on sand.

TVA has suggested two simplified phreatic lines within cofferdam cells for free draining and non-free draining soils (TVA, 1957). Figure 17 (a) and (b) indicate both cases.

Tidal fluctuations in permanent waterfront bulkheads are generally small enough that seepage-associated problems may be generally neglected. Probably the most important affect of tidal fluctuation is due to a lag in the cell's phreatic surface with respect to the level of the river or ocean. The effect of a drop or rise in the phreatic surface on the interlock hoop stresses has been described in the literature (Schroeder, et al., 1977).

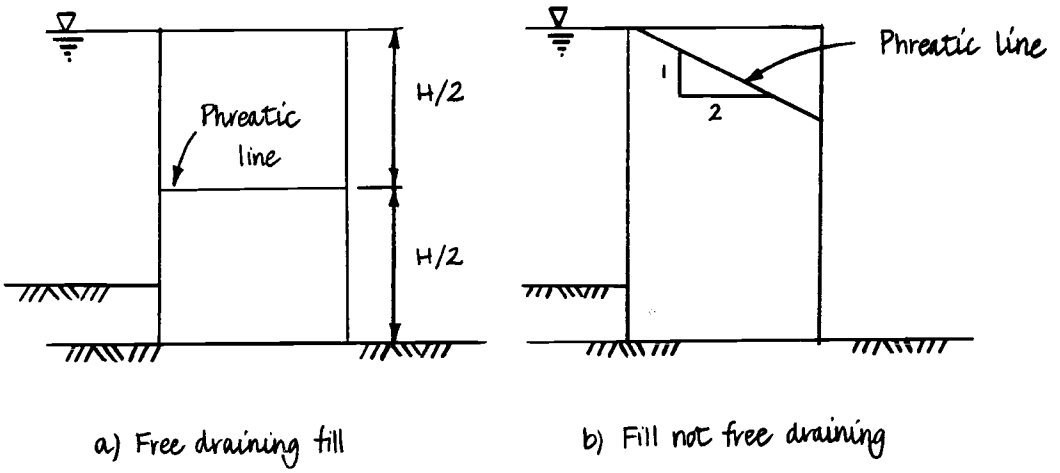

Figure 17. Location of phreatic line for cofferdam design.

Foundation Failures

The methods of analysis described previously deal with the stability of the cofferdam or bulkhead structure. The designer, however, must not lose perspective of the overall stability of the system comprised of the cellular structure and the soil surrounding it. Failure to examine the adequacy of the foundation or limited subsurface investigations can lead to serious cell distress.

In general, problems related to inadequate foundations result from the presence of a soft, weak or highly compressible soil layer at or near the base of the cell (Swatek, 1967).

Figure 18 indicates a possible bulkhead failure due to the presence of a weak soil beneath the cell. A bearing capacity failure of the entire structure or a partial foundation failure at the toe can occur, causing the cell to sink or rotate excessively.

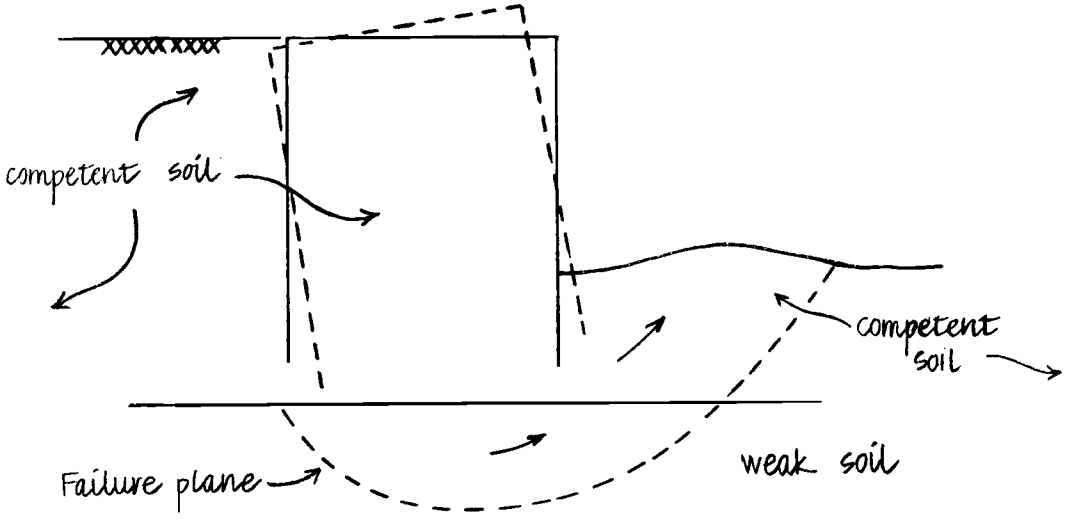

Figure 18. Bearing capacity failure.

Shear failure in a relatively thin, weak zone can occur in a different manner. As the cell is filled, the soft material is squeezed out laterally in a mud "wave". Large settlements in the middle of the cell may result.

The cell shown in Figure 19 might have adequate resistance against sliding along the base of the cell through the sand, but could fail if a soft, thin soil layer or a stratum with high excess pore pressures acted as a zone of weakness.

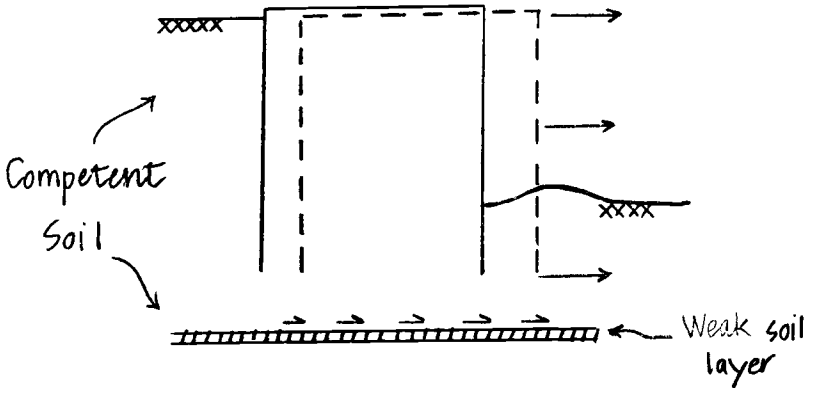

Figure 19. Sliding due to zone of weakness.

A highly compressible layer, such as a soft clay or organic silt, could also result in distress to the cellular structure. Compression of this layer can cause large settlements of the cell, leading to distress of the surface topping a bulkhead. If the compressible material occurs in pockets beneath the cell, differential settlements may cause excessive tilting.

Experience with recent bulkhead construction (Schroeder et al., 1977) indicates that settlements in excess of nine inches can occur even where foundation conditions are good. Although such settlement may be uniform and occur mostly during construction, it can cause problems of alignment with appurtenant attached structures such as fender pile systems.

The State-of-the-Art

A number of methods for analysis of cellular cofferdam and bulkhead behavior have been proposed, as may be surmized from the preceeding discussion. The possible modes of failure that are investigated are numerous. Many aspects of the analysis and design of cellular structures are subject to considerable controversy or uncertainty.

Some of the particular areas of concern are summarized below:

1. Hoop stress distribution. Designers are still not able to accurately predict the location and magnitude of maximum interlock tension. The influence of backfilling, surcharging and compacting on the magnitude of interlock forces is still relatively unknown. Methods of estimating the coefficient of lateral

earth pressure, K, vary within the literature. The influence of connecting arcs and lateral forces from backfills or water loads are additional complicating factors.

2. Critical mode of shear failure. Many theories have been advanced as to the mechanism by which cofferdams or bulkheads fail when subjected to ultimate lateral load. Neither the state of stress in the cell fill nor the mechanics of failure within the cell are really understood.

3. Deflections. Detailed profiles of sheetpile deflection during construction have been compiled in only a few instances (White, et al., 1963, and Khuayjarernpanishk, 1975). Field observations (White, et al., 1963, and Khuayjarernpanishk, 1975) have indicated that crest deflections are sometimes highly erratic and very sensitive to the sequence of construction events.

4. Effects of embedment. It has long been known that restraint of the bottom of the cell, due to "toe-in" of the sheetpiles, affects the magnitude and location of sheetpile bulging and maximum hoop stress. The maximum bulging, and consequently hoop stress, is assumed (TVA, 1957) to occur at H/4 to H/3 above the rock surface. The effect of embedment on hoop stresses and radial deflections is even more significant for bulkheads driven into sand (Khuayjarernpanishk, 1975). To date, no one has attempted to quantify the affect of embedment on these two parameters or the manner in which it might affect cell stability.

Progress toward resolution of the problems with understanding cofferdam and bulkhead behavior has been made by work on three fronts; field studies, analytical methods, and model studies. A summary of such work follows.

Field Studies

Data describing full-scale structures have been obtained primarily from two field studies (White, et al., 1963, and Khuayjarernpanishk, 1975). They provide a direct opportunity to observe and compare field data with predicted, design, or assumed values.

In 1963 A. White, J. Cheney and C. Duke published the results of a comprehensive field investigation of a 33-circular cell bulkhead, at Pier E in Long Beach, California. Tests were conducted on a pilot cell and then on a fully instrumented (62 ft. diameter) cell and adjacent arc (see Figure 20). Sheetpiles were instrumented to measure strains in the steel (to obtain hoop stress). Piezometers and settlement plates were used to observe the pore pressure and settlements in the cell fill. Sheetpile deflections were measured and cell and arc crest deflections were surveyed. The free water level in the cell and tidal fluctuations were also monitored.

Thanasarn Khuayjarernpanishk conducted a similar investigation of the 12-cell wharf at Terminal No. 4, along the Willamette River, in Portland, Oregon, (Khuayjarernpanishk, 1975). The 65.8 ft. diameter cells were unique in that a stepped sheetpile configuration was used to save steel along the backfilled side. In addition, thinner sheetpiles were used along the back portion of the cells. Vibrating wire strain gages were used to monitor strains at four elevations on eight

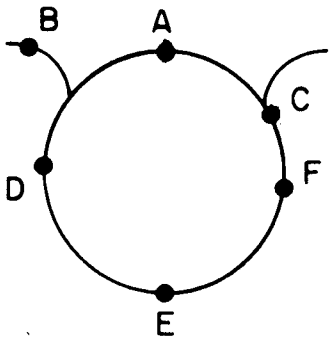

(a) Location of instrumented sheetpiles

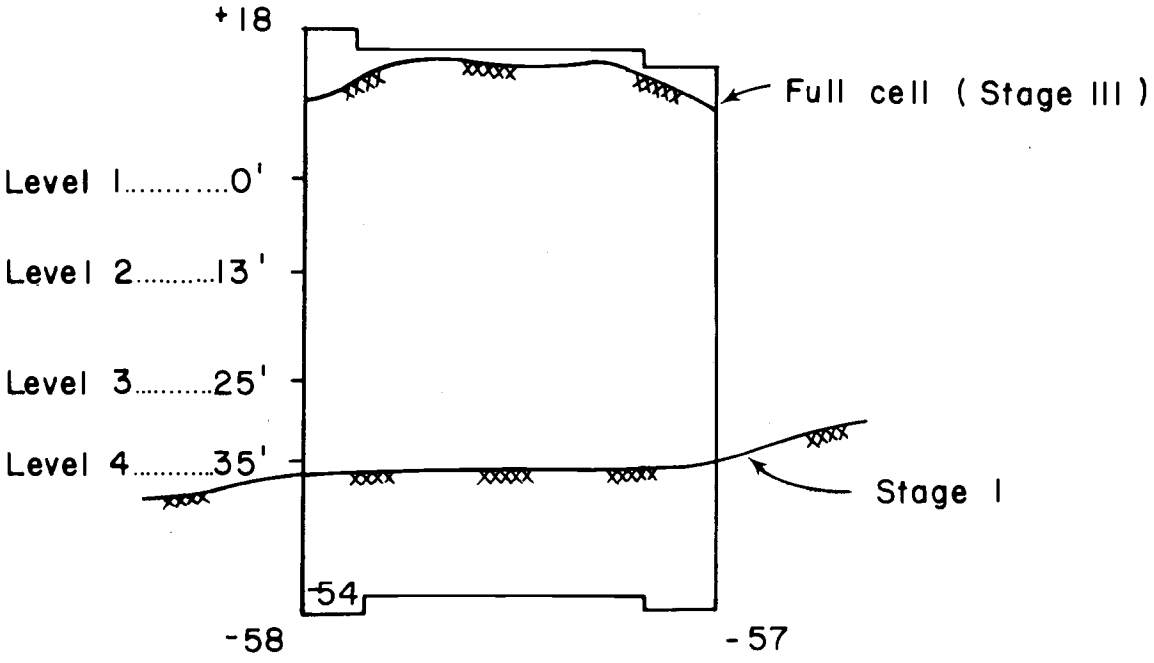

(b) Cell profile

Figure 20. Long Beach cell (after White)

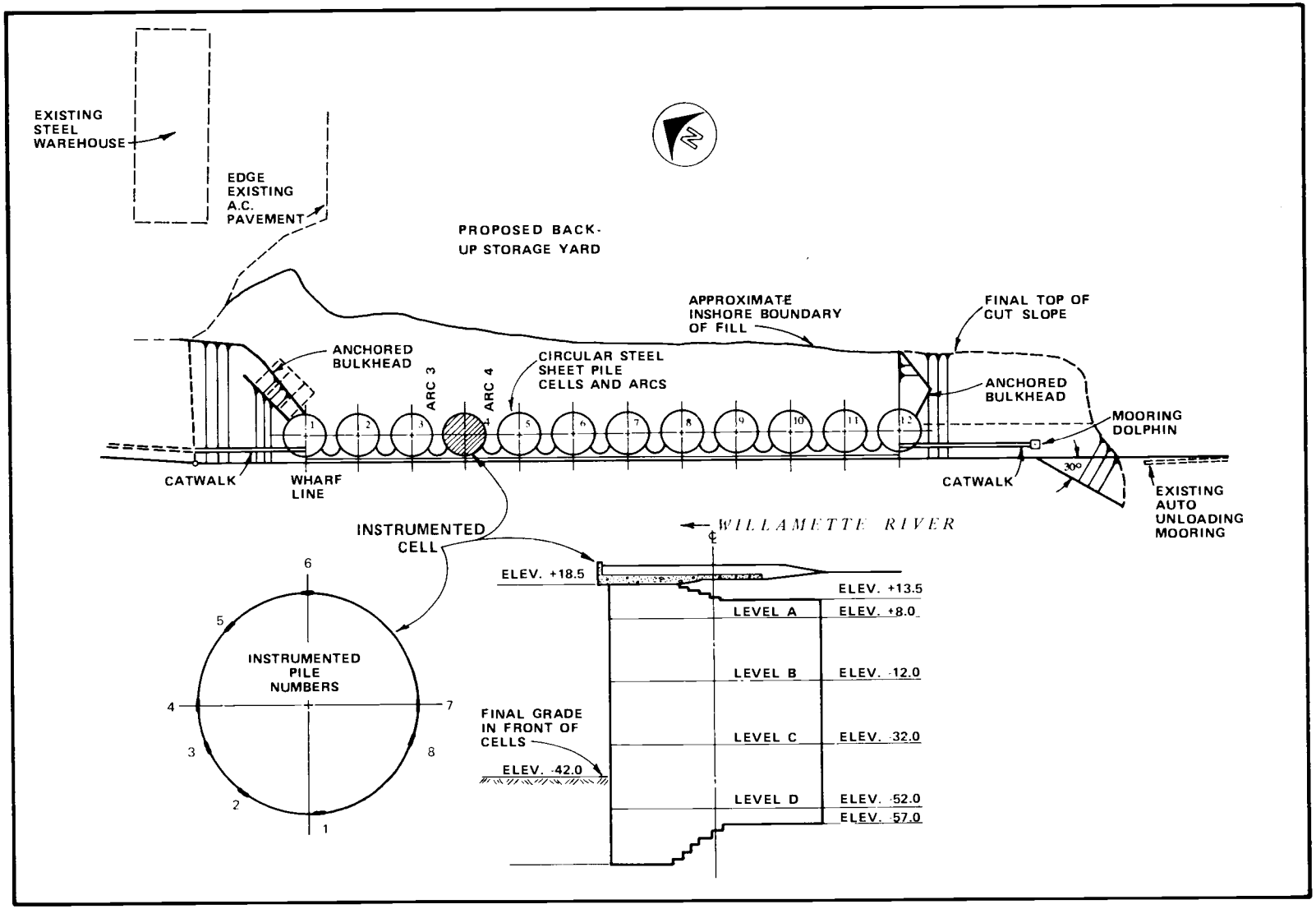

Figure 21. Terminal 4 cell. (after Khuayjarernpanishk)

different sheetpiles. Figure 21 shows a typical cell cross-section along with the location the instrumented sheetpiles.

In addition slope-meter tubes were used to monitor radial deflections, while land-based surveys measured cell crest movements and sheetpile settlements during construction. The free-water level in the cell was also monitored and compared with the adjacent river level.

A summary of important data for both field studies are provided in the DISCUSSION OF RESULTS section of this thesis.

Analytical Techniques

Closed Form Solution. Philip Brown proposed, in his discussion of the field study by White, et al., 1963, an analytical approach to the problem of predicting bulkhead deformations (Brown, et al., 1963).

Referring to Figure 22, he proposed that the expression for the curvature of a beam (based on elastic theory)

$$\frac{d^2y}{dh^2} = -\frac{M}{EI} - \frac{K}{AG}\frac{dQ}{dh} \qquad (28)$$

where M = moment
A = cross-sectional area
E = modulus of elasticity
K = shape factor (1.5 for rectangle)
I = moment of inertia
G = shear modulus
Q = shear force
h = elevation

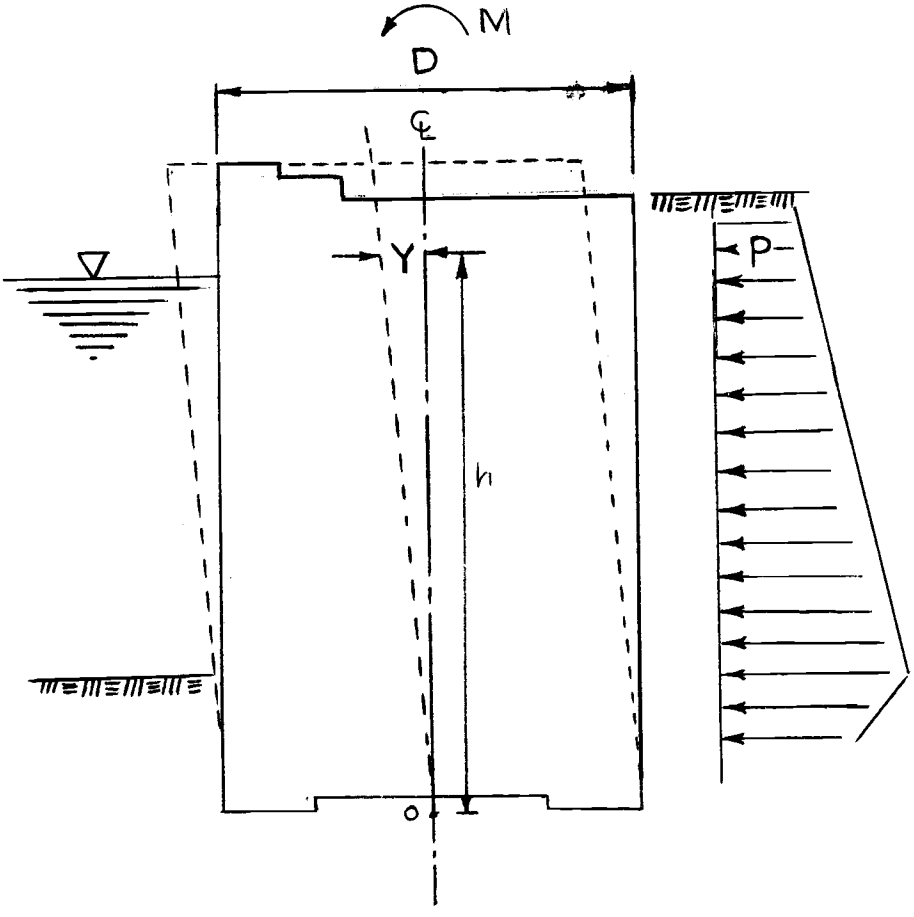

Figure 22. Cell deflection. (after Brown)

could be written in an alternate form, using $G = \frac{E}{2(1-u)}$ and pressure $p = \frac{dQ}{dh}$, as

$$\frac{d^2y}{dh^2} = - \frac{1}{EI} \left[M + \frac{K(1 + \mu)D^2}{6} P\right] \tag{29}$$

where D = the cell width.

A curvature diagram may then be plotted from Equation 29. The slope at the base of the cell is determined from the horizontal shear (Q_B) along the base and the tilting of the base foundation plane respectively, by

$$\frac{dy}{dh} = \frac{K}{AG} Q_B \tag{30a}$$

and

$$T = \frac{(1 - a^2)}{E} \Delta pm \tag{30b}$$

where: T = tilting angle (in radians)

m = dimensionless parameter determined by the shape of the loaded area.

Δp = difference in base pressure at heel and toe

The curvature diagram is integrated graphically to obtain the slope diagram. To this curve, is added the base tilting determined from Equations 30a and 30b.

A deflection curve can then be obtained from the graphical integration of the slope diagram. This integration is performed incrementally from bottom to top, allowing variable values of the modulus of elasticity of the soil, E, to be introduced. The influence of the steel sheetpiles on the elastic curve is neglected throughout the analysis.

Finite Element Analysis. A computer program was developed at Oregon State University by L. Kittisatra to analyze cellular bulkheads by the finite element technique (Kittisatra, 1976).

The program uses two basic finite elements: the quadrilateral axisymmetric ring elements for the soil and cylindrical shell-of-resolution elements to represent the steel sheetpiles. The sheetpiles were assumed to form a thin, continuous steel cylinder and no slippage between sheetpiles was allowed. Figure 23 shows the typical finite element mesh used in the study.

The program permits a three-dimensional analysis to be performed under typical bulkhead loading conditions. Case 1 analysis is that of an isolated cell loaded axisymmetrically due to the weight of cell fill. Case 2 permits analysis of a cell subjected to asymmetric loading resulting from backfill and arc tension. The distribution of loads from the backfill and the two adjacent arcs is approximated by Fourier series.

Stresses within the steel shell within the soil mass and nodal displacements are computed at various sheetpile locations. Up to seven arbitrary locations may be requested.

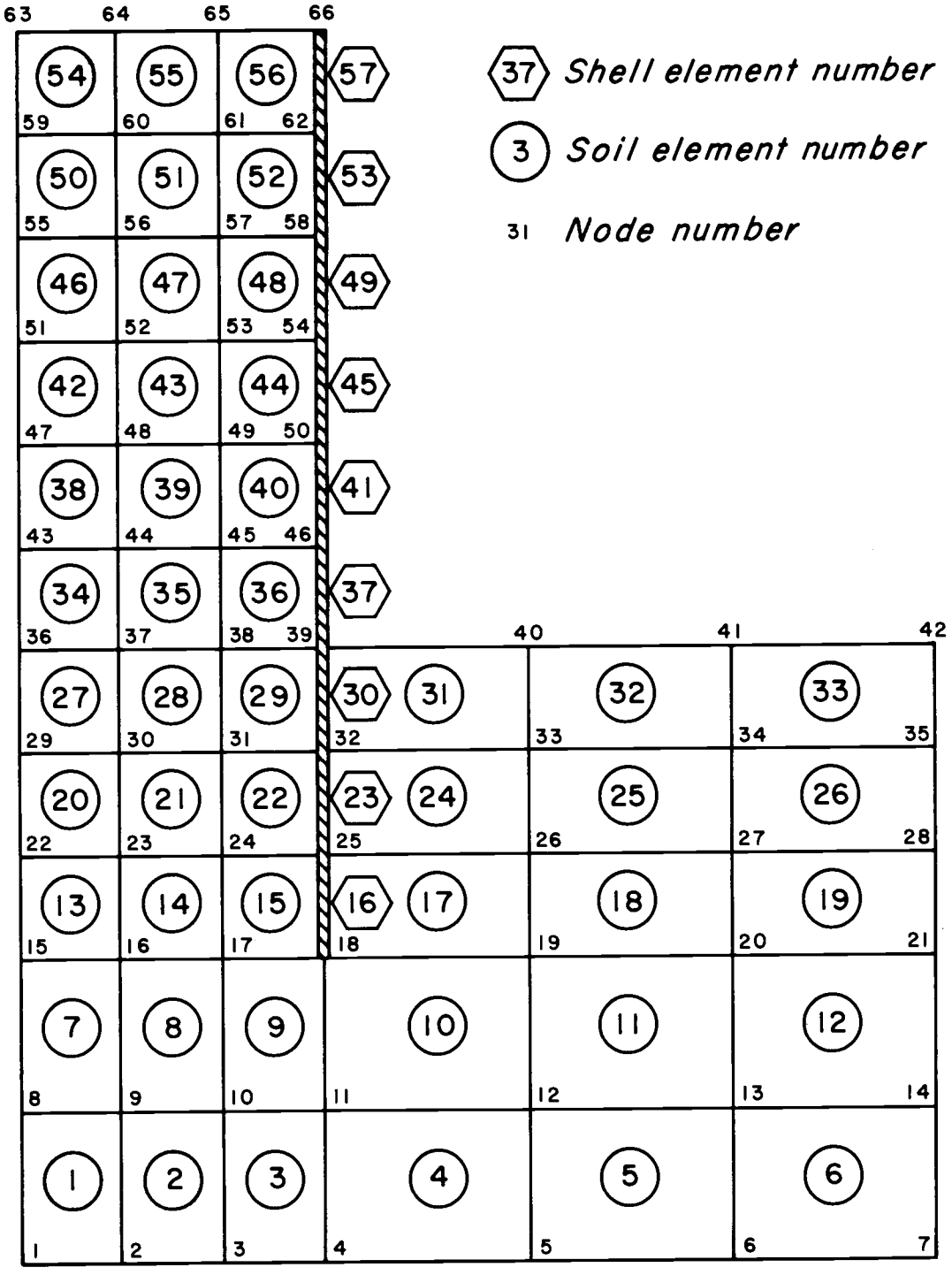

Figure 23. Finite element modeling a circular cell.
(after Kittisatra)

Previous Model Studies

A popular approach to investigating the behavior of cellular structures has been through model studies. In general, these studies have consisted of relatively small scale models loaded to failure. Cell stability, i.e. determination of the force (or moment) required for failure, has been of primary concern.

In 1957, E. M. Cummings published results of his model studies of cofferdams on rock (Cummings, 1957). It is probably the best known model study and forms the basis for his theory of internal cell failure by horizontal shear. Cummings' model consisted of 24.5 inch diameter, 24 inch high circular cells and rectangular cells with the equivalent 19.5 by 24.5 inch dimensions.

Wood staves, 5/16 by 1 1/2 inch, were used as model sheetpiles. These staves were held together by a thin wire threaded through screw-eyes located at the top, middle and bottom of the sheetpiles. The cell was threaded together loosely, with no contact between the wood staves, so that very little friction could be developed between model sheetpiles. All the cells rested on a rough concrete base one inch thick. The fill consisted of 1/2 inch minus, graded crushed rock which would not run through the interlock as sand might. Lateral loads were applied by a wire loop, 1/3 H from the base. Cable loads were measured with proving rings.

Cummings was also concerned with the change in the state of stress in the fill resulting from lateral loads. Pullout tests of wood slats buried in the cell fill were conducted before and after application of the lateral load to provide data for calculation of these stresses.

N. K. Ovesen conducted a series of model tests at the Danish Geotechnical Institute (Ovesen, 1962). The model set up consisted of four interconnected cells (20 cm in diameter), each consisting of 20 interlocking sheetpiles. The typical cross-section of his model sheetpile is shown in Figure 24.

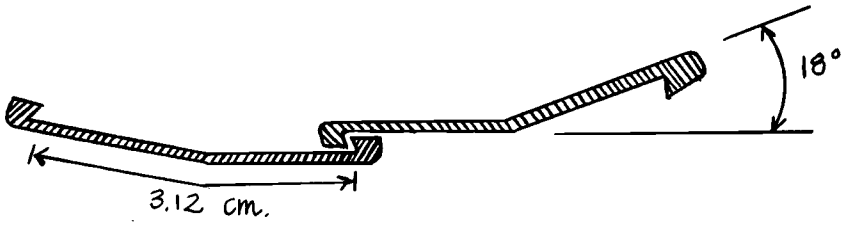

Figure 24. Model sheetpile. (after Ovesen)

Loads were applied incrementally by a system of nylon wires, pulleys and beams. Both loads and cell deformations were monitored for each load increment. A well-rounded, uniform beach sand was used during the study. Density measurements were made before and after cell failure.

Results from this model study along with the work of B. Hansen form the basis for the method of rigid body rotation for analysis of cofferdam stability (Hansen, 1953).

J. J. Polivka conducted a series of tests on a 5 cell model cofferdam during the course of his preliminary investigation on cellular cofferdams in the Kaiser shipyards at Richmond, Calfiornia (Polivka, 1945). The testing set up consisted of five circular cells,

3 to 7 inches in diameter, 6 inches high and arranged in an arc-shaped wall. The cell walls consisted of a continuous cylinder, made from 0.004 inch thick sheet metal. In his discussion, Polivka attempted to correlate the model test results with field data and with Terzaghi's theory of vertical shear.

Although cofferdam and bulkhead behavior is explicitly a three-dimensional action, some valuable information may be obtained from two-dimensional studies.

G. Schneebeli and R. Cavaillé-Coll conducted a series of model tests to investigate the resistance to overturning of double-walled cofferdams on rock (with straight walls). Cell widths of 15 and 30 cm were used. The side walls were only 4 cm apart to ensure two-dimensional action (Schneebeli and Cavaillé-Coll, 1957). The walls were tied together at the top to simulate tie-rods. Glass walls permitted visual examination of the sand movement. They also performed several tests on circular cells and on equivalent rectangular cells, with a set up similar to that of Cummings. Canvas, reinforced by wood staves, served as the retaining cylinder.

They proposed the equation

$$M_r = \frac{0.03}{6} \gamma_e' h^3 \nu\phi \qquad (31)$$

where ν = width-height ratio

h = cell height

ϕ = angle of friction (in degrees)

for the maximum overturning moment, M_r, per linear foot of wall that a straight double-walled cofferdam can sustain. Equation 31 is based on the slip-line theory (Koetter's equations); (Schneebeli and Cavaillé-Coll, 1957). They proposed circular slip lines that intersected the sheetpiles for the failure planes within the cell fill. Equation 31 yields values that are closer to the "middle-third" formula for rigid body overturning and considerably higher than Terzaghi's vertical shear theory.

B. K. Mazurkiewicz also conducted an investigation into the two-dimensional behavior of double-walled cofferdams (Mazurkiewicz, 1976). He used photographic techniques to monitor the movement of sand grains during model failure. He concluded that the mechanism of behavior of straight-walled cofferdams could be explained by consideration of closely spaced circular failure planes as proposed by B. Hansen (Hansen, 1953). His model tests indicated a combination of eight straight (Rankine-type) and circular slip lines.

PROJECT DESCRIPTION

Design of cellular bulkheads and cofferdams is based on highly simplified, semi-empirical analyses. Usual procedures are based on several relatively simplistic theories, some small-scale model studies, and field observations. Performance observations on cells in the field are relatively rare. This is due partly to expense and partly to the reluctance of contractors to become involved in an instrumentation and observation program that might hinder or interfere with their construction schedule. Field data is at best scarce and the experiences of contractors are rarely documented. Consequently, designers rely heavily on their own experience and the observations of local contractors. Both may be severely limited. Several good summaries of design methods for cellular structures can be found in the literature (Belz, 1970; Lacroix, 1970; Swatek, 1967.)

A substantial gap exists in the state-of-the-art between analysis and design of cellular bulkheads and cofferdams. The present study was conducted to partially bridge this gap.

A study was needed to observe the behavior of cellular bulkheads subjected to a wide range of loading conditions. The model study described herein provided the opportunity to make such an investigation under controlled laboratory conditions. A model study can, of course, only partially fill the existing gap in information. Field instrumentation programs are needed to observe directly the behavior of these structures.

Holding Basin

The large size of the cell model needed imposed certain conditions on the design of the holding basin. The structure had to: a) accommodate a four foot diameter cell plus two adjacent arcs; b) hold approximately 25 to 30 cubic yards of sand; c) sustain the lateral soil pressure without significant deflections and d) allow easy transfer of sand and construction materials. In particular, it was important to minimize any edge effects, i.e., the influence of the walls and floor on the sand fill.

The final design consisted of a 16 x 11 x 8 foot steel tank, constructed of 10 gage corrugated steel plates bolted together along vertical seams. Rolled sections were used as corner plates. The interior of the tank allowed a minimum wall or floor clearance of 1 radius (two feet) of the test cell. A 4 x 4 foot opening provided easy access to the inside.

The steel tank was reinforced by a framework of heavy steel angles bolted along all edges and plate seams. This resulted in a very stiff structure. Wall deflections due to the sand backfill and surcharge loads were negligible. Limiting these deflections was essential to prevent mobilization strength in the sand along the walls laterally and thereby adversely affect the lateral forces on the cell due to the backfill.

Two heavy aluminum beams formed an overhead coordinate system and provided support for the dial gage installation. Walkways and scaffolding provided access to the cell without disturbance of the sand bed. A one-half ton overhead electric hoist aided in the

construction, testing and removal of the model. Figure 25 provides a plan view of the facility.

Cellular Bulkhead Model

Figure 26 shows a typical plan view of the model bulkhead sections tested. Each section consisted of one cell plus two adjacent arcs. Since embedment depth was considered to be the primary variable, all cells had the same cross-sectional dimensions and approximately the same exposed height (H).

All the cells were circular, with a diameter of 4.08 feet and consisted of 58 interlocking sheets. Total sheetpile lengths ranged between four and six feet.

Single, semi-circular arc sections, 1.78 feet in diameter and consisting of 12 similar sheetpiles were connected to the cell on adjacent sides. The arc sections at the backfill side were absent, as is typical of bulkhead wharf installations.

Table 2 summarizes the pertinent cell dimensions for the four main series. Note that Series III represented a "stepped" cell, i.e., the length of the sheetpile varied. Figure 27 shows the cell profiles.

Table 2.

Dimensions of cells for Main Test Series (feet).

Series No.	Total Length (L)	Exposed Height (H)	Embedment Depth (D)
I	6.0	4.17	1.83
II	5.0	4.17	1.83
III	6.0 (front)	4.0	2.0 (front)
	4.83 (back)		1.67 (back)
IV	4.0	4.0	0

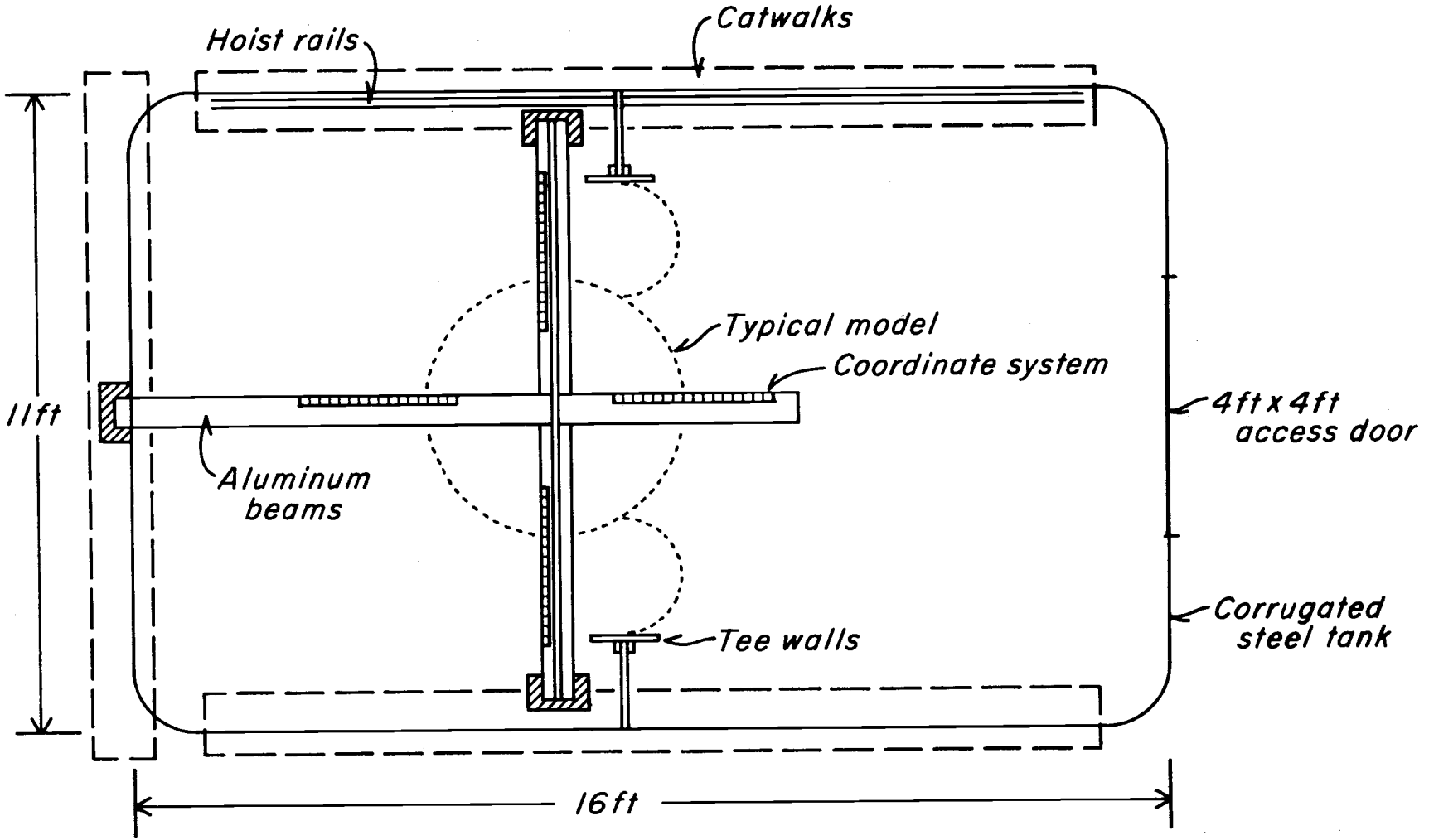

Figure 25. Plan view of testing basin.

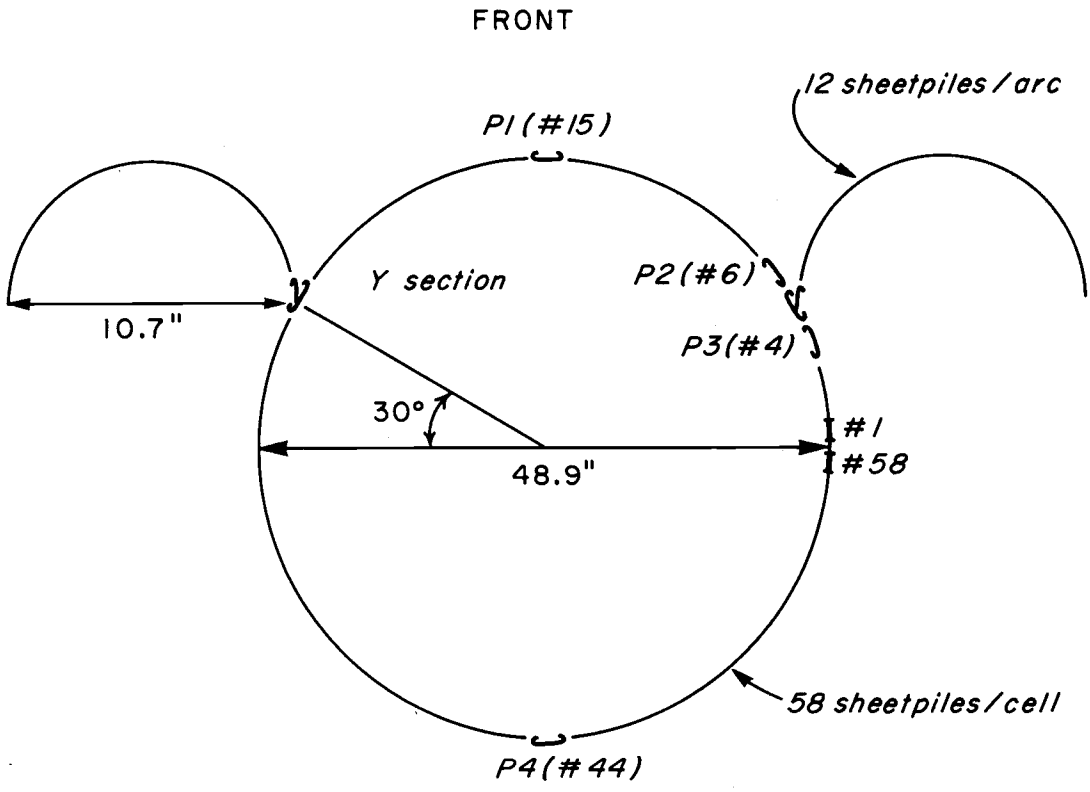

Figure 26. Location of instrumented sheetpiles.

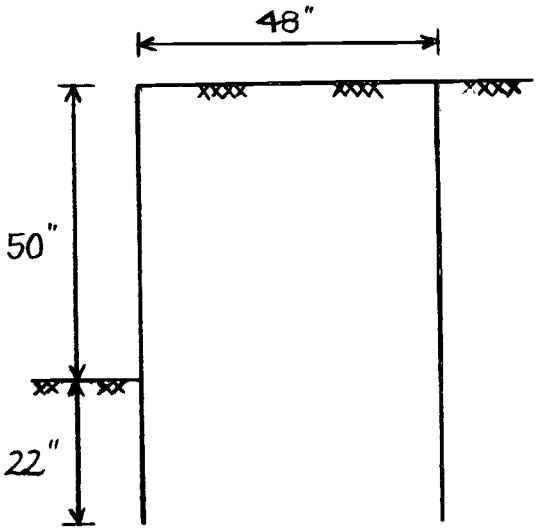

(a) Series I

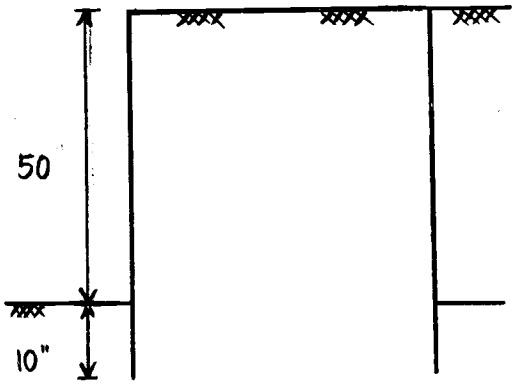

(b) Series II

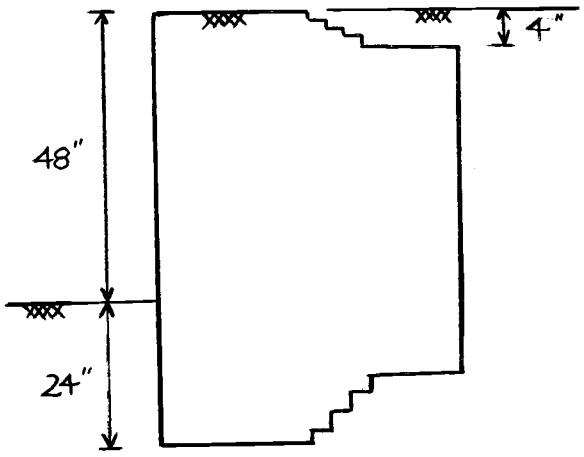

(c) Series III

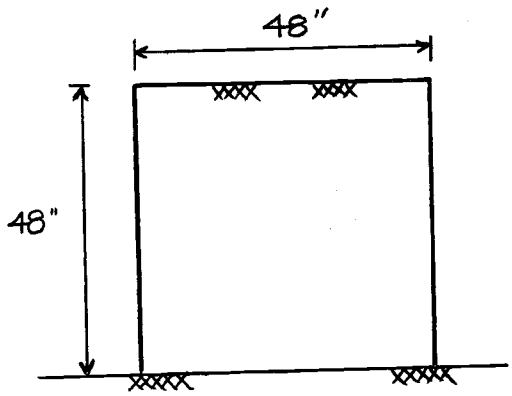

(d) Series IV

Figure 27. Profile of model cells.

Typical Model Installation

As in the field, templates were required as working platforms for threading the model cells and to maintain their shape during driving. The cell templates consisted of two one-half inch plywood rings spaced apart by six threaded rods. The support spacing could be changed to accommodate variable sheetpile lengths. The arc section templates consisted of two 1.6 foot diameter, semi-circular plywood rings, with the same rod spacing as the cell template. All the templates had a three inch foam lining along the entire ring perimeter to provide interlock tension without damage to the interlocks or the strain gages.

The cell template was set on a four foot thick sand bed, aligned and weighted down with steel bricks. The cell was then threaded by hand (see Figure 28). Arc templates were then set in place and the arcs threaded, beginning at the Y-sections. A rigid T-wall provided the support for the far ends of the arc sections.

Typically, the cell and arcs were out of vertical and twisted after threading. Good alignment was attained by applying pressure to the template and to the top of the sheets. The cell and arcs were then driven into place. Driving was done by hand using a heavy hammer. Sheets were driven in pairs, one-quarter inch at a time to prevent interlock splitting. Small wood blocks served as pile cushions and minimized web damage. Driving to a depth of 1.5 feet was relatively fast and easy. However, the final six inches of driving was difficult and required Plexiglas sheet cushions. Throughout the driving operation, cell and arc alignment was checked by plumb bob and hand level.

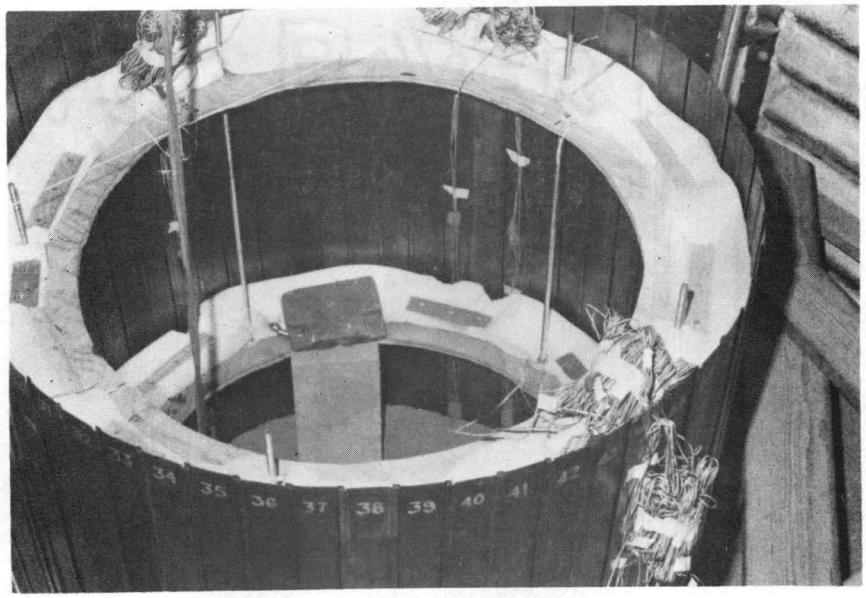

(a) Construction of a typical cell.

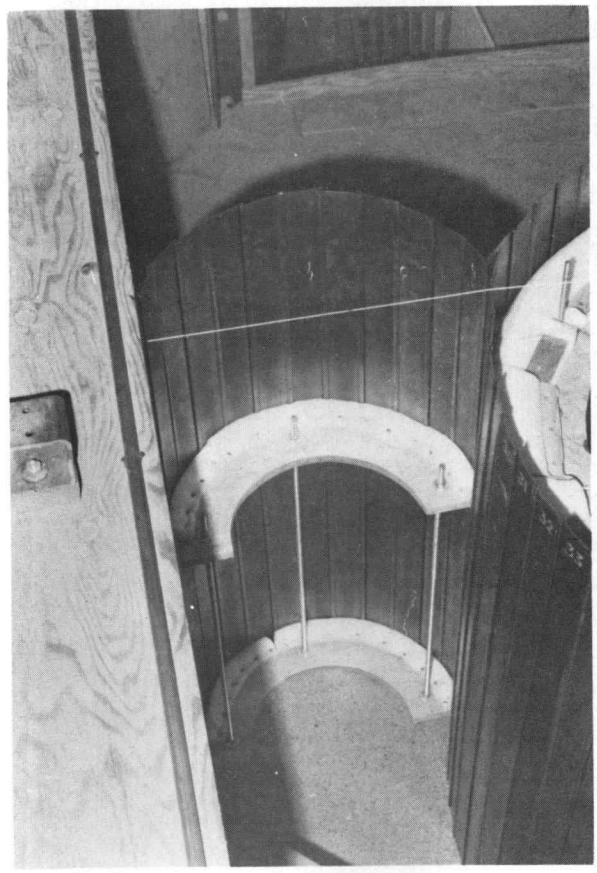

(b) Typical arc installation with template in place.

Figure 28. Construction of a model bulkhead.

Even with the above precautions, problems with sheetpile alignment arose. Cell No. 1 had, at the end of driving, a slight twist (of about 5°). This was due to an uneven sheetpile driving pattern. The driving technique was modified to that of driving diametrically opposite pairs of sheets, thereby eliminating any uneven pull on the cell. Subsequent cell alignments using this method were excellent (see Figure 29).

Only two out of 328 sheetpiles installed were driven out of interlock. Both times problems were overcome by drilling small holes through the interlocks, drawing them together and bolting them along the split portion. These bolted sheets were far removed from any instrumented sheets and thus had little influence on the stress distribution pattern.

The cell template was removed with care to minimize disturbance of the sheets. The arc templates remained in place until after cell filling was complete. Removal of the cell template prior to filling did have a significant effect on the magnitude of hoop stresses (see the DISCUSSION OF RESULTS).

Model Sheetpiles

The basic requirements for a model sheetpile are much the same as those for the prototype: a) the model sheetpile must be inexpensive and easy to fabricate; b) the sheetpiles must allow easy assembly of the cell and arc sections; c) the interlock must show a consistent pull-out strength and d) the interlock must be capable of developing the full web yield strength.

The last requirement is by far the hardest to satisfy. A sheetpile would have to be essentially a miniature or "scale" model of the

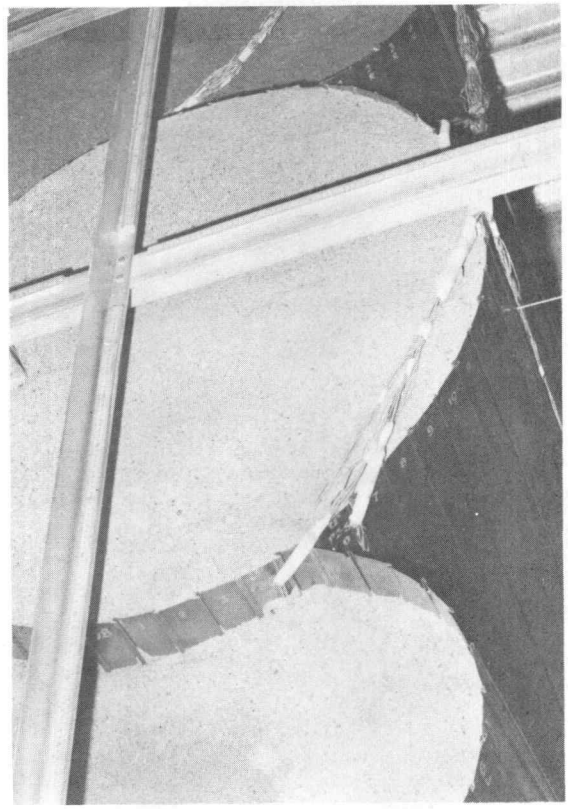

(a) Completed and backfilled bulkhead model.

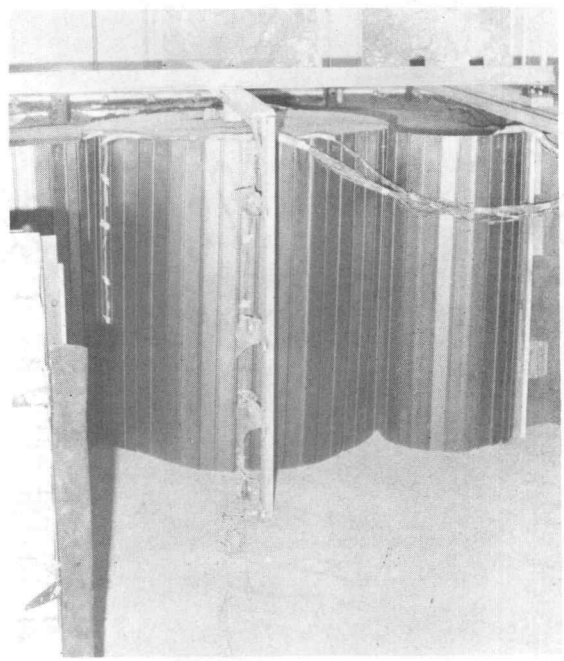

(b) Complete bulkhead model.

Figure 29. Completed model installation.

prototype. Such a model sheetpile would be extremely difficult and expensive to fabricate.

The feasibility of using a commercially produced sheetmetal edge crimp as an interlock was examined. Pull-out tests were conducted on sheetmetal strips of various gages and crimp configurations.

The final design consisted of a three inch wide, double crimped sheetpile model, made from 22 gage cold-rolled steel. This edge crimp is commonly used in heating and ventilating work and could be easily and inexpensively fabricated by local sheetmetal shops. Figure 30(a) shows a typical model sheetpile. Several types of model Y-connections were fabricated and tested.

The 30° Y-section shown in Figure 30(b) was finally selected as the most convenient for cell construction. It is built from a standard sheetpile, together with a 30° bent section tack welded every five inches on center. Tests conducted on sheetpile specimens indicated a consistent pull-out strength of 87 lbs/in.

Cold rolled steels sometimes show fairly erratic values of Poisson's ratio due to residual stresses from the fabricated process. Testing of sheetmetal used in the model indicated an average value of 0.32, slightly higher than the value of 0.285 normally assumed. The measured value was used throughout the analysis and reduction of strain gage data.

Any bent or crimp-type interlock will fail due to local bending stresses long before developing the full web strength. Interlock pull out capacity, therefore, dictated sheet thickness rather than web strength. In addition, the sheets had to be capable of being driven in

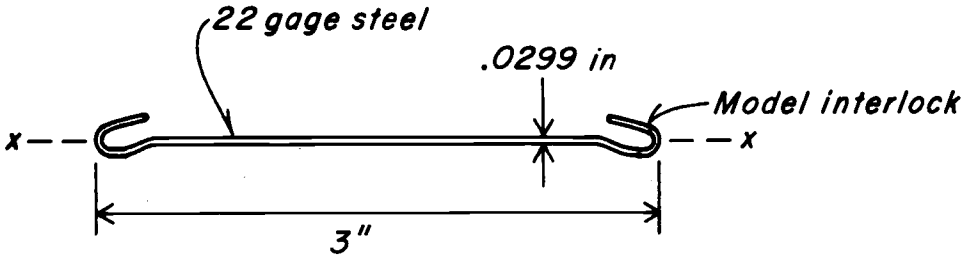

(a) Typical model sheetpile

$E_m = 30 \times 10^6$ psi

$\mu = 0.32$

$I_x = 4.6 \times 10^{-4}$ in^4

$P_{ult} = 87$ lb/in

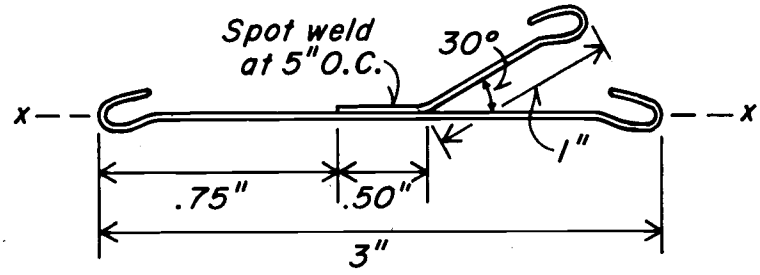

(b) Typical Y-connection

Figure 30. Model sheetpile details.

the sand without buckling or sustaining significant web damage. The 22 gage sheetpiles satisfied all these criteria.

Testing Program

Model Testing. Four complete models were assembled and tested in the main test series. Each phase of testing simulated, as best possible, the different stages of field construction. In addition, cell and backfill surcharges were imposed that were out of the normal range of bulkhead service loads. The sequence of cell testing events is described below.

The cell and arc sections, after being threaded, were driven to their final elevations. This stage was taken as the reference point for all deflection and strain measurements. The cells were then filled using the "raining" technique (see Density Control). During the cell filling stage, pressure cells and wax markers were buried at several levels of fill. A four foot sand backfill was placed using uniform lifts to avoid non-symmetrical loadings. A surcharge was applied to the backfill area using layers of iron bricks (see Figure 31). The surcharge was gradually increased by addition of more brick layers. The number of layers of iron bricks varied from one to eight. Table 3 summarizes the surcharges applied to the backfill area.

Figure 31. Backfill and surcharge.

Table 3.

Surcharges for Testing.

No. of Brick Layers	Equivalent Backfill Surcharges (psf)
1	65
2	129
3	193
4	258
8	437

A cyclic cell surcharge was also applied during Series III and IV. Both the surcharge and the backfill was then removed and measurements of cell rebound were made.

During Series I (and only then) the sand in front of the cell was excavated down to the bottom of the sheets prior to removal of the surcharge and backfill. This sand was subsequently replaced before failure levels were applied.

Strain gages and dial gage readings were recorded at the end of every testing stage.

Tables 4, 5, 6, 7 summarize the sequence of events during testing.

Table 4.

Sequence of Testing Event (Series I)

Stage No.	Construction Event
1	Driven Cell (empty, 22.2" embedment, template in place)
2	Cell filled 13.5" (≃ 27% full)
3	Cell filled 24.9" (50% full, w/o template)
4	Full cell
5	Backfilled 25.5" (52.2% backfill)
6	Backfilled 45.6" (91.5% backfill)
7	1 layer of surcharge (65 psf)
8	2 layers of surcharge (129 psf)
9	3 layers of surcharge (193 psf)
10	4 layers of surcharge (258 psf)
11	8 layers of surcharge (437 psf) reduced
12	8 layers of surcharge + 5.0" of excavation at front
13	8 layers of surcharge + 16.6" of excavation at front
14	8 layers of surcharge + 21.2" of excavation at front

Table 5.

Sequence of Testing Event (Series II)

Stage No.	Construction Event
1	Driven cell (empty) no template
2	Cell filled 13.78" (≃ 28% full)
3	Cell filled 20.94" (≃ 42% full)
4	Full cell
5	Backfilled 21.71" (44% backfill)
6	Backfilled 31.89" (64% backfill)
7	Full backfill = 48.0"
8	1 layer surcharge (65 psf)
9	2 layers surcharge (129 psf)
10	4 layers surcharge (258 psf)
11	Surcharge removed

Table 6.

Sequence of Testing Event (Series III)

Stage No.	Construction Event
1	Driven cell (empty)
2	Cell filled 13.7" (28.4% full)
3	Cell filled 23.5" (48.5% full)
4	Full cell (level with back sheets)
5	Backfilled 23.1" (47.7% backfill)
6	Full backfill (level with front sheets (≃ 92% backfill)
7	2 layers surcharge (129 psf)
8	4 layers surcharge (258 psf)
9	4 layers backfill surcharge and cell surcharge (65 psf)
10	All surcharge removed

Table 7.

Sequence of Testing Events (Series IV)

Stage No.	Construction Event
1	Driven cell (empty)
2	Cell filled 10.8" (22.5% full)
3	Cell filled 23.5" (48.9% full)
4	Cell filled 36.1" (75.2% full)
5	Full cell
6	Backfilled 23.8" (50% backfill)
7	Backfilled 34.5" (71.9% backfill)
8	Full backfill: 2.4" below top (95% backfill)
9	2 layers of surcharge (129 psf)
10	4 layers of surcharge (258 psf)
11	4 layers + cell surcharge (65 psf)
12	4 layers - cell surcharge removed
13	4 layers + cell surcharge reloaded
14	All surcharges removed

Cell Tests to Failure. As a final phase of testing, the behavior of the model under failure conditions was observed. Loads well beyond service load range were applied laterally to the isolated cells.

Figure 32 shows the loading system used to fail the cells. The load was applied to the cell by a steel cable loop, using a two-ton winch, braced against a steel I-beam. Nine 4 x 6 x 2 inch wood blocks distributed the cable force to the sheets to minimize stress concentrations. A 4 x 8 inch timber was used as a loading yoke, ensuring that the cable load was applied evenly and without interfering with the dial gages. A strain gage load element permitted direct measurement of the applied loads. Loads were applied incrementally and continued until large cell deflections had occurred.

Deflections of the front sheets, sheetpile strains, and cable force were monitored throughout cell failure. At the end of testing, measurements were made of cell fill displacement, interlock shear, and passive failure zones at the dredge lines. The cell was then carefully disassembled and samples of bent sheets from the front, sides and back were preserved.

Thin wax markers had been buried at several levels in the cell fill. The rupture points along these markers gave some indication of the cell fill deformation.

Small Cell Series. A series of small-scale models was built to further investigate the pattern of internal failure planes. The cells were two feet in diameter (i.e., one half of the previous model scale) with embedment depths varying in the same proportion as the original cells (see Figure 33).

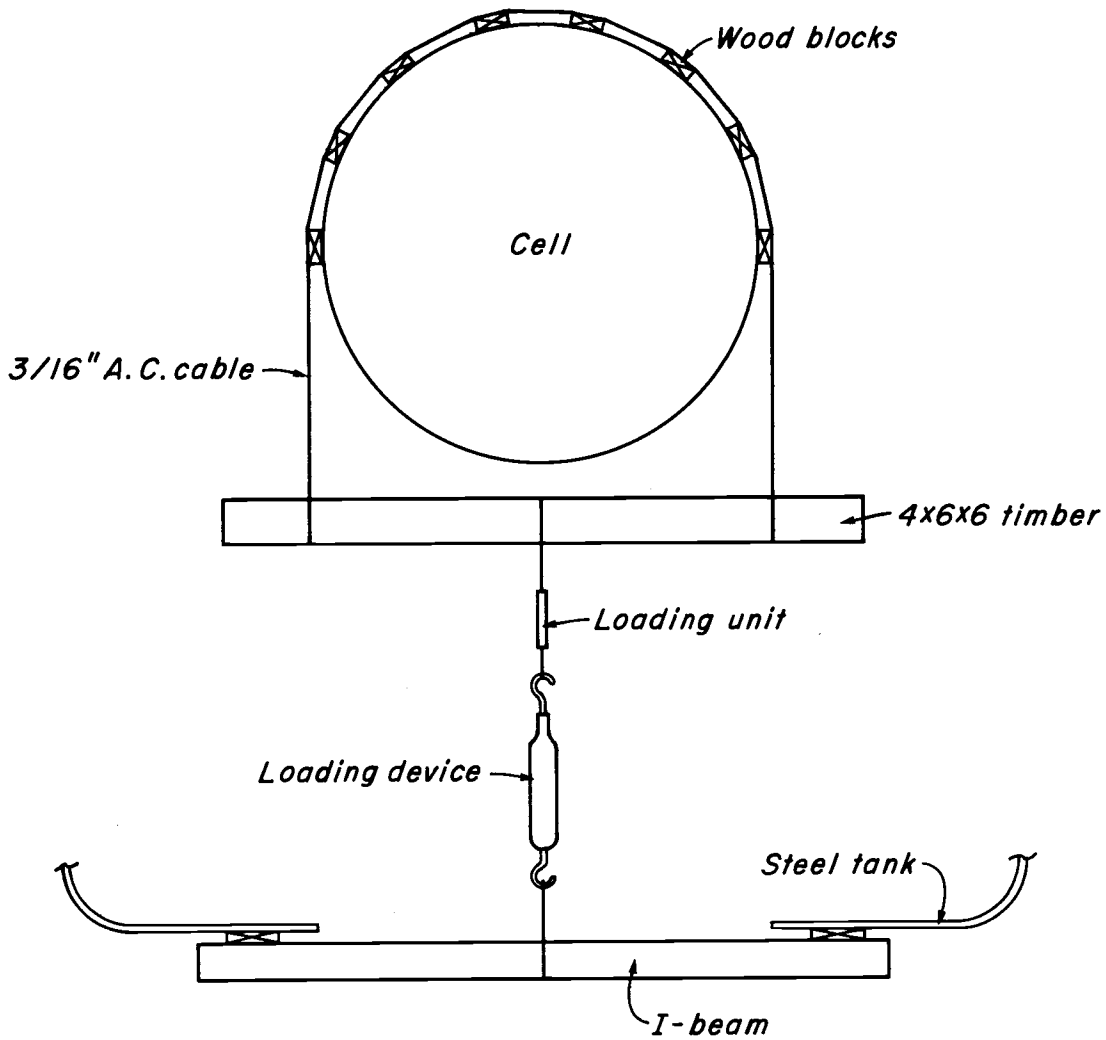

Figure 32. Set-up for failing model cells.

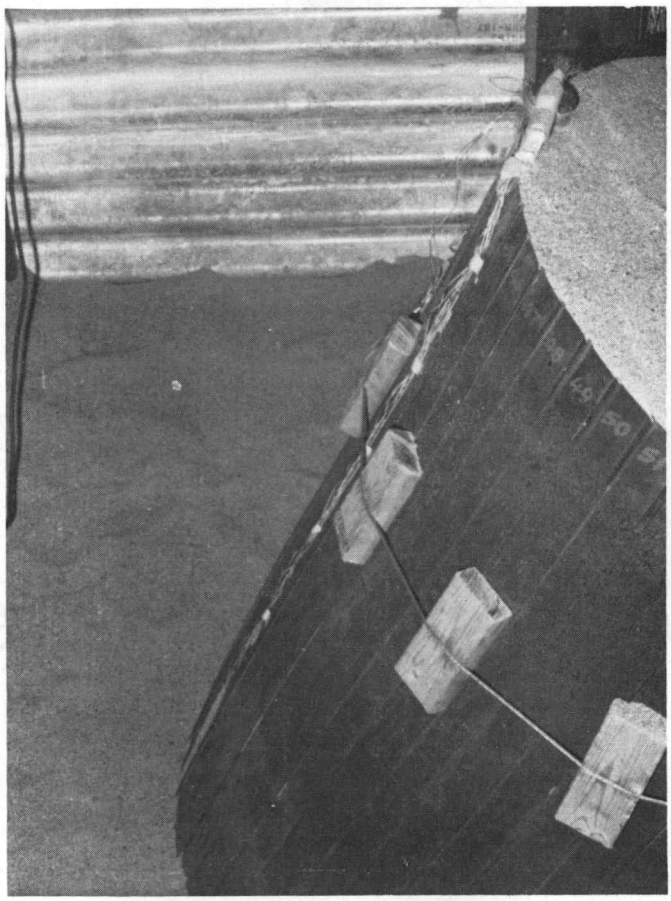

(b) Application of lateral loads.

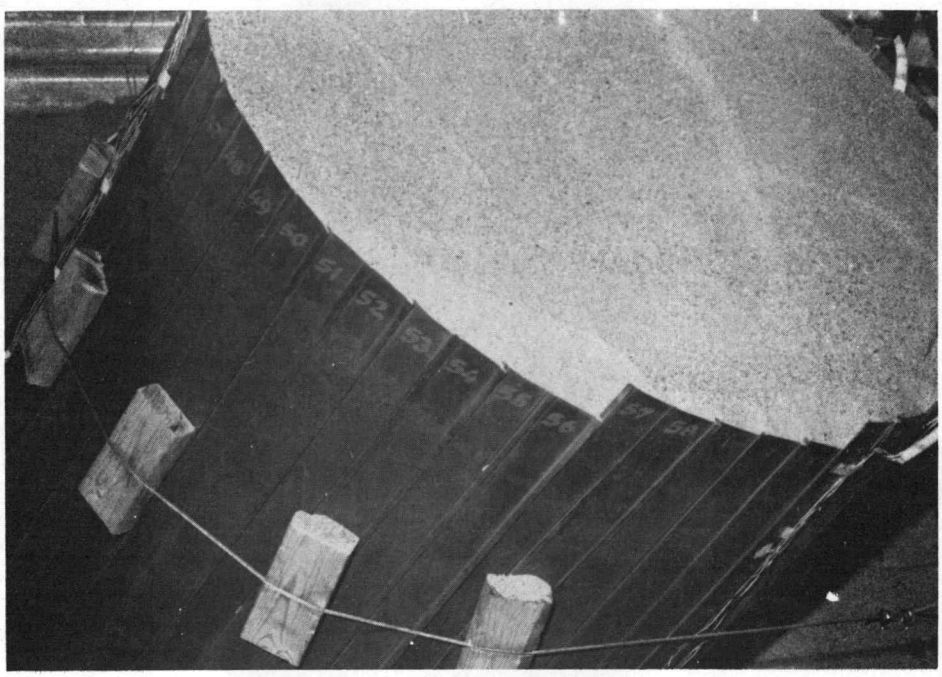

(c) Interlock slippage at failure.

Figure 32. continued

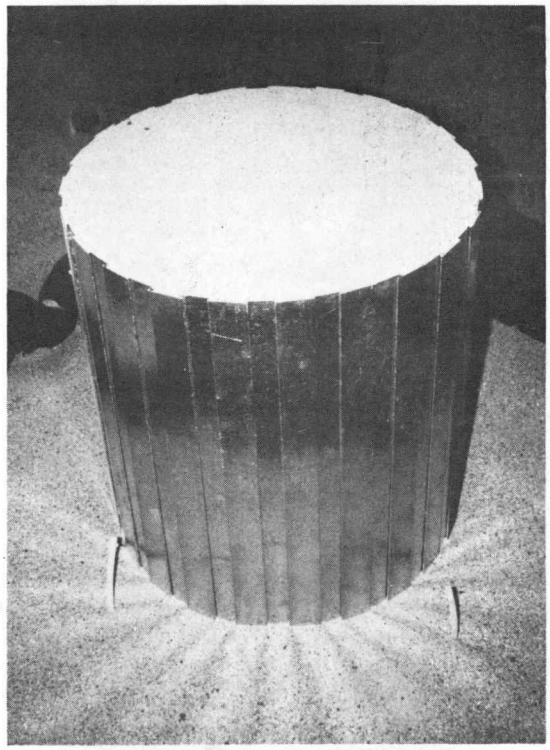

(a) Typical small cell.

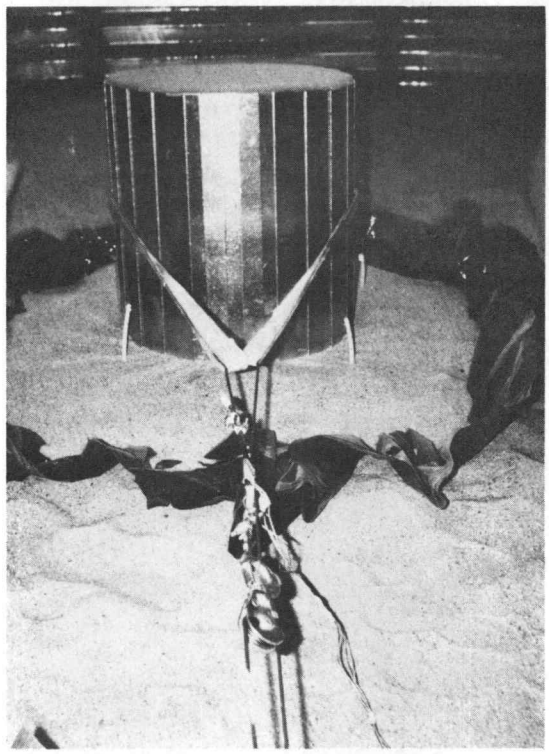

(b) Failure of small cells.

Figure 33. Small model cells.

The sheetpiles were two inches wide and made from 28 gage sheet-metal. They were threaded around a small plywood template and driven into place. Thin (1/16 inch) beds of dyed sands were placed at several levels within the fill. A vertical marker bed was also formed during the filling of Cell No. 3 (see Figure 34). Each cell was loaded to failure. The cell fill and surrounding sand was then saturated with a solution of AM-9 (a two-component grout)[1] to preserve interior deformation patterns. A thin plastic membrane placed at the bottom contained the seepage of the grout solution. Upon hardening of the grout, some of the sheets were removed and a portion of the cell fill excavated. In this manner, entire cross-sections of the cell fill and base bed were exposed, revealing patterns of shear displacements. Even minute offsets of the marker beds could be traced through several levels. Typical cell cross-sectional views are shown in the PRESENTATION OF RESULTS section.

Instrumentation

Strain Gages. Foil mounted, resistance-type strain gages are, by far, the most popular type of strain gage presently used in experimental stress analysis. They afford an easy, economical and flexible method of measuring strains in a variety of materials and under a wide range of environmental conditions. Their reliability and accuracy along with ease of installation made them practical for the model study.

---

[1] American Cyanide Company, Wayne, New Jersey.

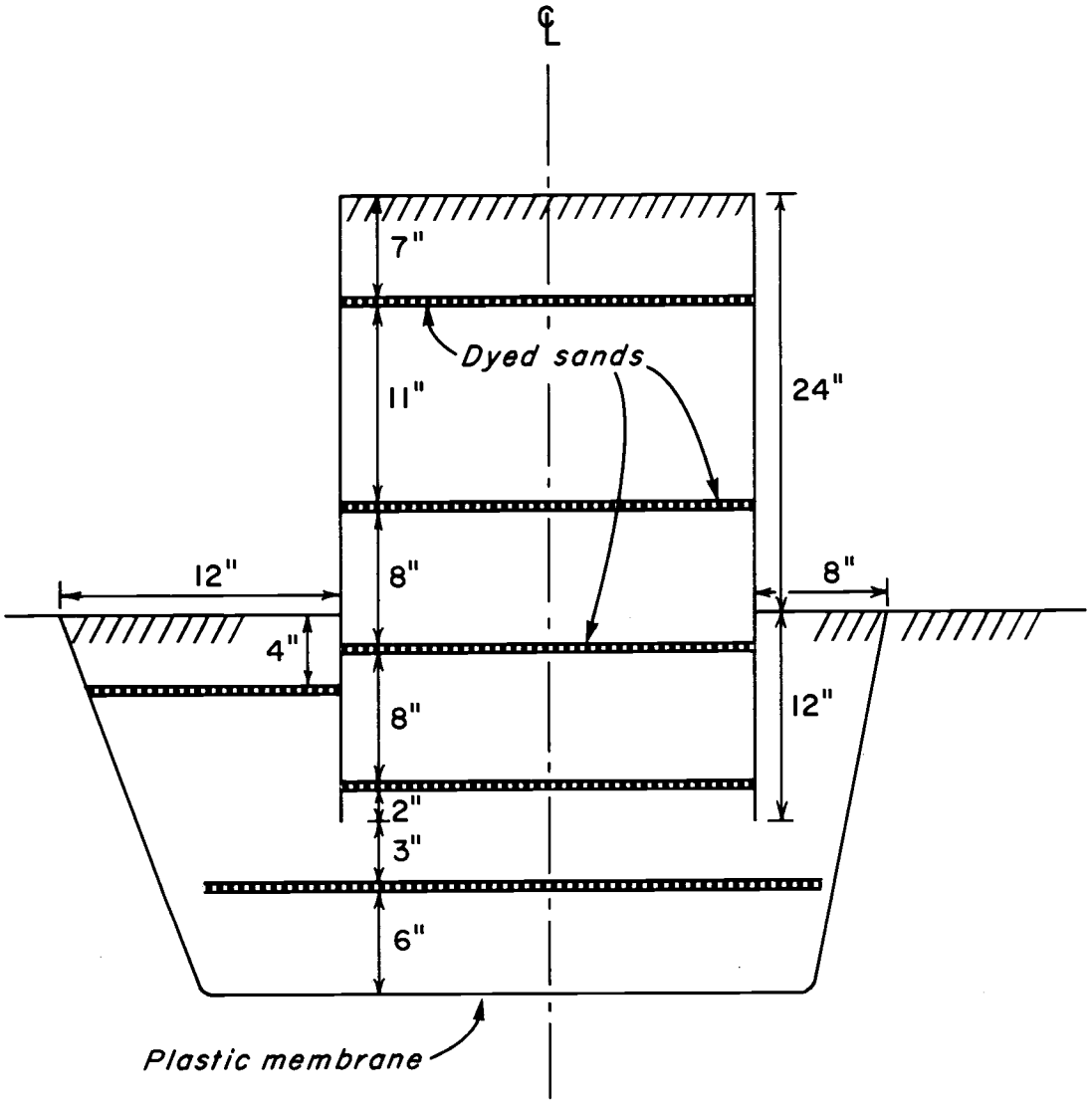

Figure 34. Typical profile of small cells.

Two types of strain gages were used in the stress analysis program: the CEA-06-187UW single gage and the CEA-06-125WT 90° stacked rosette gages, both manufactured by Micro-Measurements[2]. Characteristics of both these gages are summarized in Table 8.

Table 8.

Summary of Strain Gage Characteristics

	Single Gage	90° Stacked Rosette Gage
Resistance (ohms)	20.0 ± 0.3%	120.0 ± 0.5% (top) 120.0 ± 0.5% (bottom)
Gage Factor	2.10 ± 0.5%	2.14 ± 1.0% (top) 2.14 ± 1.0% (bottom)
Transverse Sensitivity (K_t) (percent)	+ 0.8	+ 1.4% (top) + 1.4% (bottom)

Strain Gage Installation. The strain gages were mounted on opposite sides of the sheetpiles along the centerline of the web. Gages were mounted on the prepared steel surface using M-Bond 200 adhesive[3] (a quick drying epoxy-type adhesive). Previously etched orientation lines helped in providing good gage alignment. Twenty-five foot, 24 gage, three strand leads were soldered directly to the gage contact pads. Strain relief loops were not used since reuse of the sheets was not anticipated. A small dot of epoxy adhesive fixed the leads to the web two inches above the gage to prevent pullout during cell

---

[2] Micromeasurements, Romulus, Michigan.

[3] Ibid.

construction. A flexible, moisture-resistant coating (M Coat-G) provided added gage protection during sheet driving. All leads were brought up vertically along the sheet interlock and bundled at the top. Wires from all instrumented sheets were then wrapped in one bundle, leading to the instrumentation cabinet.

The lead wires were connected to three, 10-channel Vishay SB-1 switch and balance units[4]. These units were wired in parallel to a Vishay P-350A digital strain indicator (Null meter type)[5]. A quarter bridge, Wheatstone bridge circuit was used throughout the entire project to allow measurements of both axial and bending strain components.

Strain Gage Corrections. Both types of strain gages used show a relatively flat temperature-apparent strain curve at 75°F (24°C) and approximately zero apparent thermal strain at that temperature. Although temperature variation in the testing room was less than $\pm$ 10°F a three-lead wire was used. This provided a temperature compensation loop within the bridge circuit and eliminated practically all apparent strain due to thermal changes.

Strain gages are essentially very accurate resistors. Long lead wires can substantially alter the resistance of the gage within the bridge circuit (a phenomenon called lead wire desensitization). To compensate for the 25 foot lead wires, the nominal gage factors were corrected by calibrating the gage plus leads installation against an

---

[4] Vishay Instruments, Malvern, Pennsylvania

[5] Ibid.

internally shunted resistor of known characteristics. This corrected gage factor was used in strain gage data reduction (see Appendix B).

Initial readings were taken before and after driving to investigate possible web overstrains. The readings taken after driving were considered as initial values. Subsequently, readings were taken at the end of each filling or surcharging phase.

A total of 150 gages were used. Of this total, only two gages failed. No problems were evident in gages driven into the sand.

Strain Gage Location. Figure 35 shows the typical locations of the strain gage instrumentation for positions P1 (front) and P4 (back). Instrumentation at position P2 was eliminated after Series I. Each sheet was instrumented with four to six levels of strain gages. Generally, the instrumentation of sheet P3 (behind the Y-connection) was the same as position P1 (front).

Dial Gages. Dial gages were used to monitor deflections of the front sheet throughout the entire testing procedure. In addition, deflections along the back sheetpile was monitored for the cell-filling phase.

Four 0.001-inch dial gages with a five inch throw were used at the front of the cell. They were mounted on adjustable aluminum bars that were attached to a vertical aluminum bar (see Figure 36). Spacings of the dial gage bars were variable and were normally set to provide concentrated measurements near the point of maximum bulging. A similar set-up was used along the back sheet, although the dial gages used had only a one inch range. The shorter range of these gages made frequent resettings necessary.

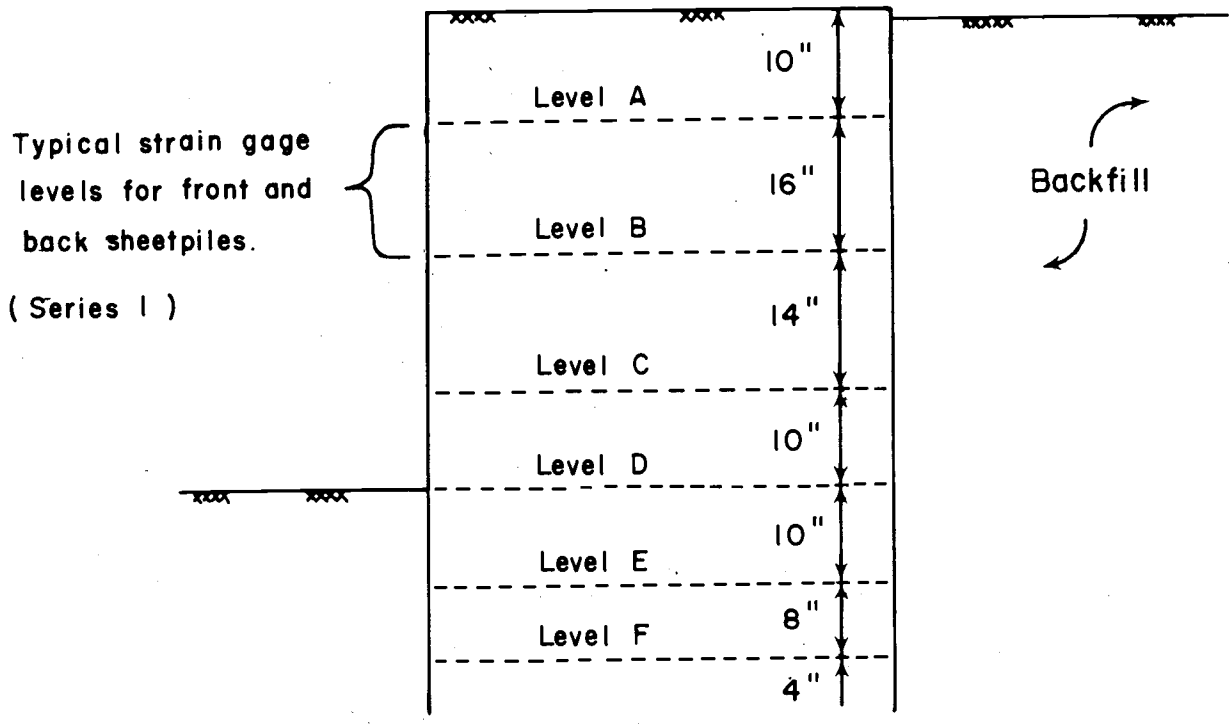

Figure 35. Typical location of strain gages.

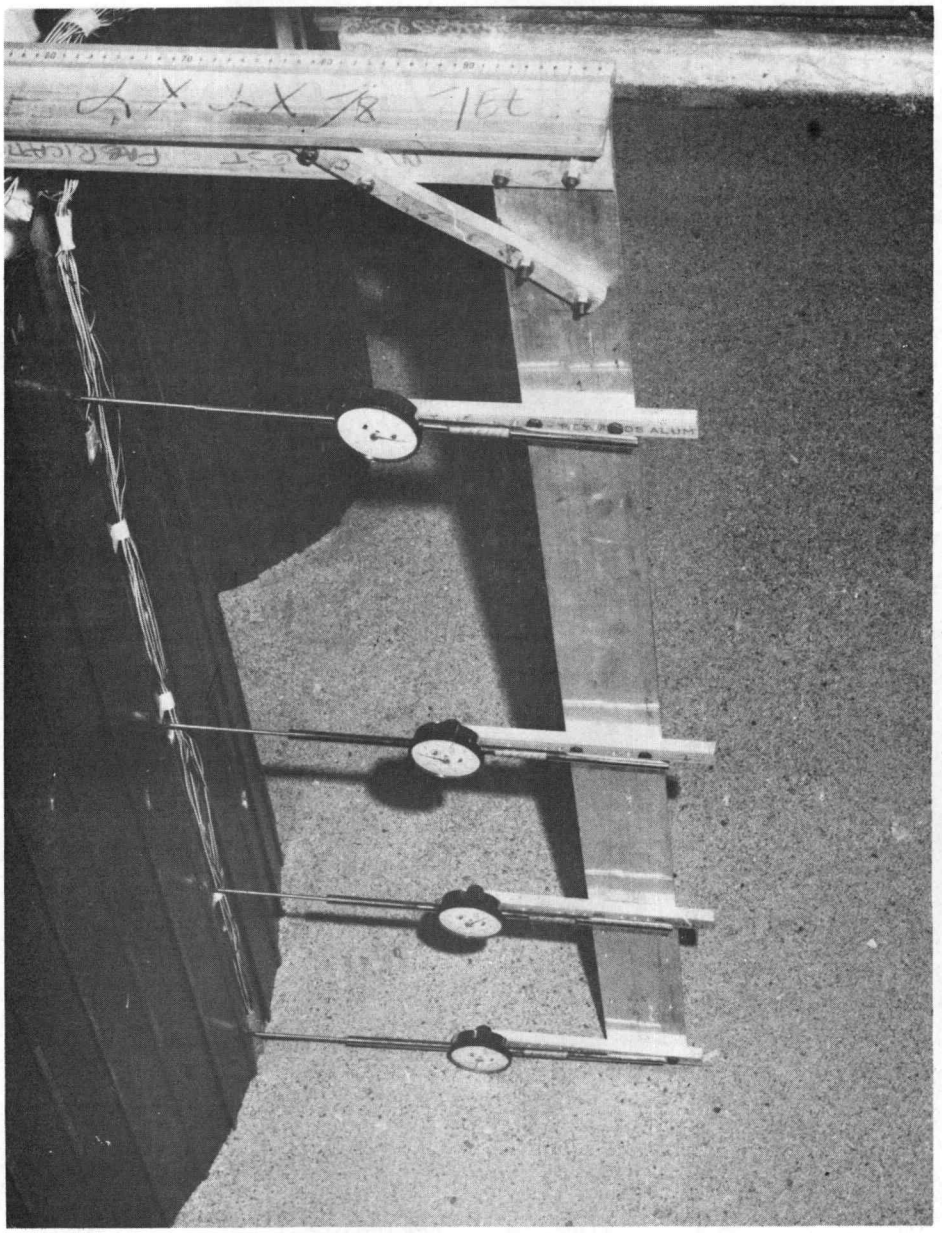

Figure 36. Dial gage installation.

Pressure Cells. An attempt was made to monitor the changes in soil pressures in the cell fill during backfilling and surcharging stages. Commercially available total pressure gages are expensive (in the range of $200 to $350) and require a special readout unit.

Several total-pressure diaphragm-type cells were built in the laboratory to measure soil pressures more economically and using the available strain indicator. These cells consisted of a 2.5 inch diameter rings, 0.25 inch thick and two thin steel diaphragms sealing the ring. A single strain gage was mounted on the under surface of the top diaphragm.

The cells were calibrated hydrostatically in a specially built pressure vessel. The curve of total pressure versus strain obtained for each cell showed good repeatability with little hysterisis.

A number of these cells were placed at various levels of cell fill. Unfortunately, the level of stress at the base of cell was low and the response of the pressure cell was within too small a range of the calibration curve to provide meaningful results. Increase in vertical pressure could be observed in the front portion of the fill but only in a qualitative manner. Pressure cells in the back half of the cell did not show the anticipated drop in vertical pressure. The use of pressure cells was discontinued after Series II.

Fill Density Control

Many techniques are available in the field to densify sands. In the laboratory, however, the additional problem of density constancy and control exists. This control is necessary if density,

shear strength, angle of internal friction, etc. are to be eliminated as variables in the study.

Several methods of sand placement and densification were tested. A uniform, medium dense sand fill was desired without grain size segregation. Tamping of thin layers proved ineffective in achieving the desired density. Dropping heavy weights provided good densification but with damaging effects on the cell fill and instrumentation. Concrete vibrators lowered through the sand provided very high densities but with an unacceptable densification gradient in the sand mass.

The "raining" technique has been used successfully in providing uniformly dense sand beds for model studies (Kelly, 1969). Basically, the technique involves raining sand through a series of sieves with a constant height of drop and raining intensity (i.e. the volume or weight of sand raining per unit area per unit time). Surprisingly high densities can be attained using this method.

Sample sand beds were built using this technique under a wide range of sieve sizes, heights of drop and intensities. It was felt, upon evaluation of these variables, that the raining technique could be used to provide a uniform, medium dense sand fill with good density control and little disturbance to the cell.

A large (8 x 3 foot) sieve box was constructed for placement of the 4 foot base bed and cell backfill. The sieve box consisted of slotted plywood sheet underlain by two layers of expanded metal mesh separated by one inch wood spacers (see Figure 37). The slotted plywood top distributed the sand over the entire sieve box while the mesh split the sand into a fine rain. The sieve box was supported

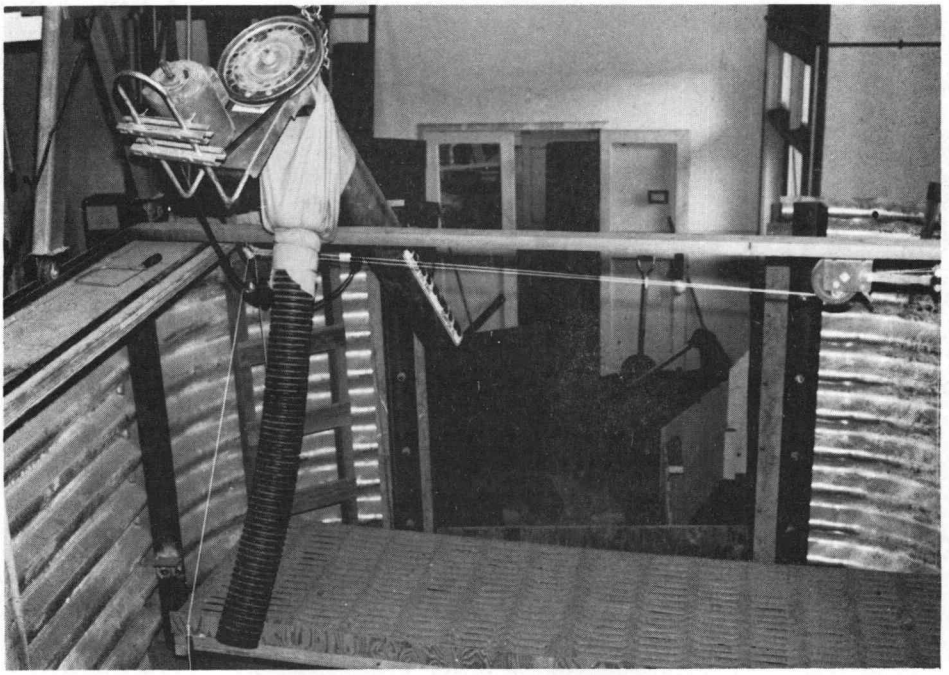

(a) Auger and sieve box set-up.

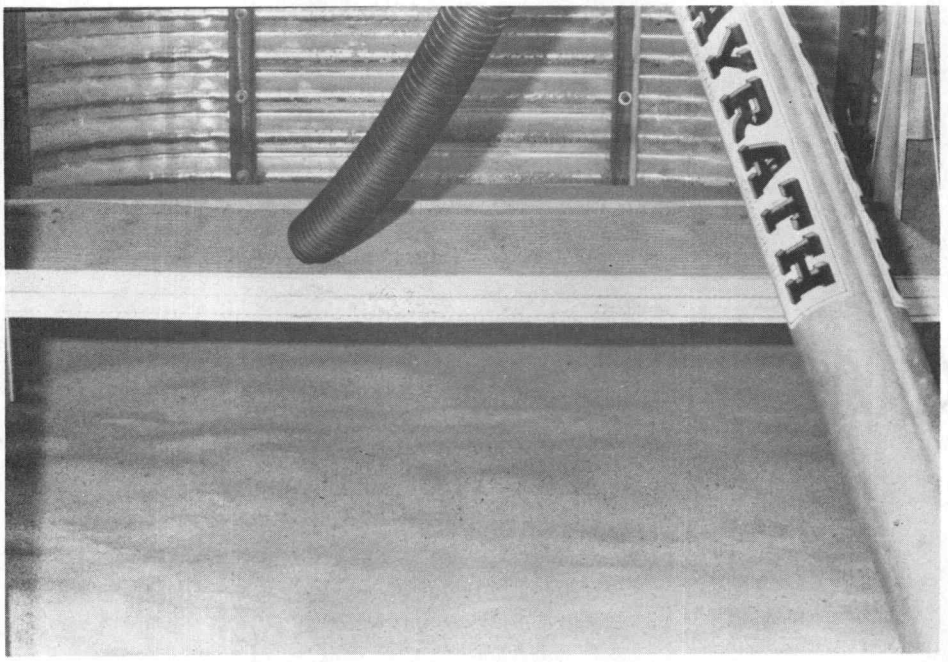

(b) Typical sand bed.

Figure 37. Raining technique for sand placement.

by a winch and pulley system that permitted adjustment in the height of drop. A smaller (3 x 3 foot) sieve box of similar construction was used to place the sand in the cell and behind the arc sections. The sand was transported by two six inch grain augers and supplied to the sieve box by a four inch flexible plastic hose.

The sieve box was periodically moved to avoid excessive build up of sand in one location. This prevented the formation of slopes along the perimeter of the sieve box, a possible zone of loose sand.

The density of the sand fill was periodically checked. Density control tests were conducted using 0.10 ft^3 molds placed in the sand and filled during the sieving operation.

Sand layers whose densities fell out of the control limits were removed and replaced. At the end of each series of experiments, the sand was removed and the operation repeated. A total of about 200 tons of sand was placed using the above technique during the course of testing.

Laboratory Testing

The sand used in the model study was tested in the laboratory to evaluate its strength, density, grain size, distribution and frictional characteristics.

Grain size distribution was determined by two separate sieve analyses (ASTM D422). The upper and lower limit of relative density were obtained from the ASTM D2049 relative density tests.

A series of standard direct shear tests and triaxial tests was conducted for several sand densities. The direct shear tests were run on dry sand. The triaxial specimens were formed under water with

previously boiled sand to ensure full saturation. The sand was densified in the mold with a shaking table and a vibrating wire probe. Sample volume changes were monitored throughout the tests to evaluate the frictional component of the shear strength.

Results from these tests were plotted as a function of confining stress and are summarized in Appendix A. Comparison of these results are found in the discussion section.

The microscopic characteristics of the sand grains, such as angularity and sphericity, were studied using a binocular microscope under low to medium power (see Appendix A).

PRESENTATION OF RESULTS

Characteristics of the Sand Fill

The sand used during the model testing was a uniformly graded dune sand from Monterey, California. Curves from sieve analysis indicated average values for the coefficients of uniformity (C_u) and curvature (C_c) of 3.8 and 1.2, respectively. Values of 4 and 6 are commonly taken as the lower limit for the coefficient of uniformity for well-graded sands. The sand was very clean, with less than 0.3 percent finer than the No. 200 sieve. It was air dried for use in the project. Microscopic examination of the sand showed the grains to be generally blocky, subangular and consisting of mostly quartz with some feldspars. Relative density tests (ASTM D2049) indicated a minimum dry density of 103.6 pcf and a maximum dry density of 120.3 pcf.

The sand fill was placed in the holding basin and model cell by the raining technique described in the PROJECT DESCRIPTION section. The in-situ dry density of the sand was monitored throughout the project. Table 9 shows the results from density measurements. The in-place fill had an average density of 115.2 pcf with a standard deviation of 1.34 and an average relative density of 72.6 percent.

Direct shear and triaxial tests were conducted to determine the strength characteristics of the sand. Results from the two tests indicated an average angle of internal friction, ϕ, of 50°. This relatively high value results, in part, from the low confining stresses in the test models.

Table 9.

Density Test Results for Models in Main Test Series

Test Number	Test Location (Series No.)	Dry Density (pcf)	D_r(%)
1	Sand Bed (S-I)	114.1	66.1
2	Sand Bed (S-I)	115.5	74.1
3	Sand Bed (S-I)	115.8	75.7
4	Sand Bed (S-I)	115.3	73.0
5	Sand Bed (S-I)	116.5	79.8
6	Sand Bed (S-I)	116.7	80.9
7	Sand Bed (S-I)	117.0	82.5
8	Sand Bed (S-I)	115.8	75.9
9	Cell Fill (S-I)	115.9	76.4
10	Cell Fill (S-I)	116.9	82.0
11	Cell Fill (S-II)	115.6	74.8
12	Back Fill (S-II)	109.4	38.2*
13	Sand Bed (S-III)	115.4	73.7
14	Cell Fill (S-III)	113.4	62.2
15	Cell Fill (S-III)	114.2	66.9
16	Cell Fill (S-IV)	115.1	72.0
17	Cell Fill (S-IV)	113.2	61.1
18	Back Fill (S-IV)	112.4	56.4

* Sand Fill Replaced

Table 10 summarizes the results of the tests conducted on the sand. A more detailed description of the sand is found in Appendix A, along with a summary of data from the tests conducted.

Table 10.

Summary of Test Results on Monterey Sand

Test	Parameter	Value
Sieve Analysis	C_u	3.8
	C_c	1.2
Relative Density	$\gamma_{d(min)}$	103.6 pcf
	$\gamma_{d(max)}$	120.3 pcf
Sand Placement	$\gamma_{d(avg)}$	115.2 pcf
(raining technique)	$D_{r(avg)}$	72.6%
Triaxial	ϕ	50°

Data Reduction for Stresses in the Sheetpiles

Figure 38 shows one face of a typical instrumented model sheetpile. The strain gages consisted of 90° stacked rosettes oriented along the axes shown.

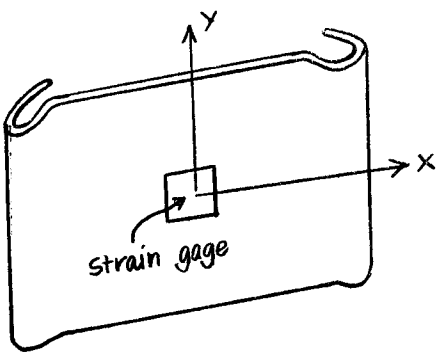

Figure 38. Orientation of strain gages.

Strains along the x-axis (hoop or circumferential axis) as well as the y-axis (vertical axis) were measured. A similar strain gage installation was placed on the opposite face of the web.

The problem of data reduction consisted, therefore, of utilizing the set of four strains measured at one level to determine the components of vertical and hoop stress along with the corresponding bending stresses.

Figure 39 shows the typical strains in one face of the steel web.

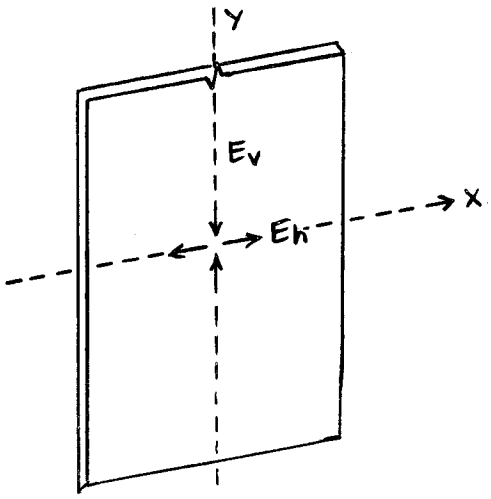

Figure 39. Typical strains on sheetpile web.

Assume, for the moment, that the horizontal and vertical strains shown in the figure are principal strains, (ε_1 and ε_2, respectively), and that Hooke's law applies.

For a biaxial stress field, Hooke's law gives

$$\sigma_2 = \frac{E}{1-\mu^2} (\varepsilon_1 + \mu \varepsilon_2) \qquad (32a)$$

$$\sigma_2 = \frac{E}{1-\mu^2} (\varepsilon_2 + \mu\varepsilon_1) \qquad (32b)$$

where σ_1, σ_2 = principal stresses

ε_1, ε_2 = principal strain

μ = Poisson's ratio

E = modulus of elasticity

and with the assumption that positive strains produce elongation.

For the present case Equations 32a and 32b become

$$\sigma_h = \frac{E}{1-\mu^2} (\varepsilon_h + \mu\ \varepsilon_v) \qquad (32c)$$

$$\sigma_v = \frac{E}{1-\mu^2} (\varepsilon_v + \mu\ \varepsilon_h) \qquad (32d)$$

where σ_h = horizontal stress at the surface

σ_v = vertical stress at the surface.

The stresses on each face can now be calculated from measured strains. Completion of the analysis for stresses requires determining axial and bending components.

Consider first the horizontal stresses. A typical section about the vertical axis (for a unit length of sheetpile) is shown in Figure 40(a).

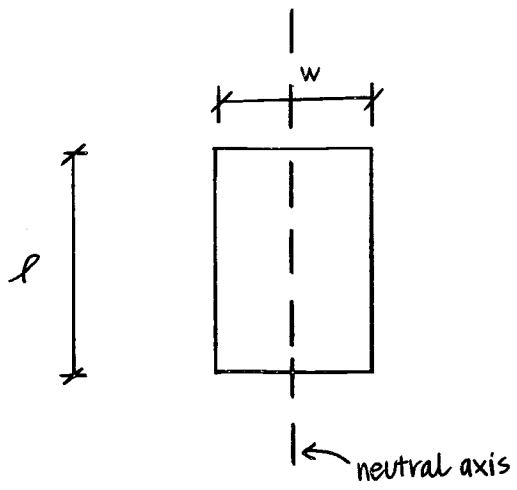

(a) Vertical section

Figure 40. Vertical section for stress analysis.

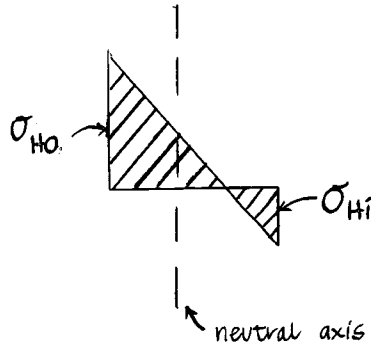

(b) Horizontal stress distribution

In Figure 40 w is the web thickness and 1 is the length (unit) of the section. Subscripts o, i refer to outside and inside face of the web, respectively.

The hoop stress will be the axial stress at the vertical axis, or

$$\sigma_{AH} = \frac{\sigma_{Ho} + \sigma_{Hi}}{2} \tag{33}$$

The bending stress component in the horizontal direction at one face will be

$$\sigma_{BH} = |\sigma_{Ho} - \sigma_{A}| = |\sigma_{Hi} - \sigma_{A}| \tag{34}$$

where the sign associated with the bending stress, σ_{BH}, depends on the web face considered.

The interlock force, t, may be calculated by

$$t = \sigma_{AH} \cdot w \cdot \ell \tag{35}$$

If we are considering the typical sheetpile section about the horizontal axis shown in Figure 41(a), the distribution of vertical stresses is now that shown in Figure 41(b). The stress distribution is now asymetrical because of the offset in the neutral axis due to the presence of the interlock.

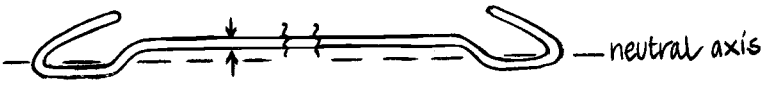

(b) Vertical cross-section

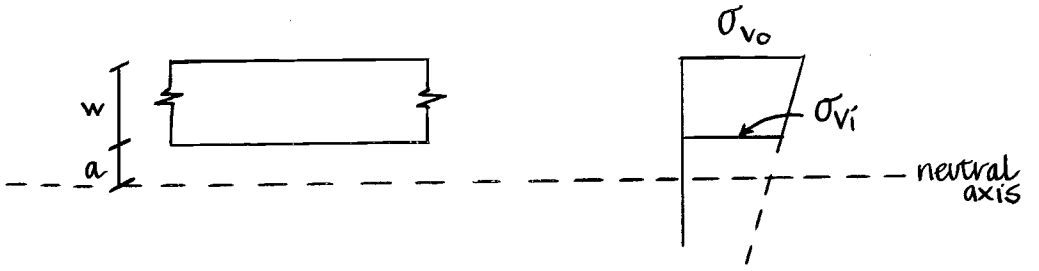

(b) Distribution of vertical stresses

Figure 41. Typical vertical section.

The axial vertical stress is now

$$\sigma_{AV} = \sigma_{Vo} - (\sigma_{Vo} - \sigma_{Vi})(\frac{w+a}{w}) \tag{36}$$

and the bending stress component in the vertical direction is given by

$$\sigma_{BV} = |\sigma_{Vo} - \sigma_{AV}| \tag{37}$$

Application of Hooke's law (Equations 32(c) and 32(d)) to the experimentally determined strains on each web face revealed three facts:

1. A large horizontal bending stress was present.
2. The horizontal axial (hoop) stresses were relatively small.
3. Both the axial and bending stresses in the vertical direction were relatively small and usually erratic.

The large horizontal bending stress is due partly to the eccentricity of the interlock connection. As the hoop force is applied the crimp tends to open, thereby transmitting a moment through the web.

Hoop stresses in excess of 1300 psi had been anticipated based on calculations with K assumed as 0.5. However, the maximum hoop stresses measured were in the range of 400 to 450 psi. The bending stress component was, therefore, much greater than the axial or hoop stress component, and tended to mask it.

The magnitudes of vertical strains were usually only a small fraction of the horizontal strains. The magnitude of these strains many times fell, therefore, within the range of the accuracy of the readout unit ($\pm$ 0.1% of the reading or $\pm$ 5×10^{-6} in/in, whichever is greater). The direct use of Equation 32(c) to calculate hoop stresses therefore resulted in highly erratic values. Compressive hoop stresses, for instance, were calculated along an entire sheetpile when other physical evidence definitely indicated tension. The sheetpile interlocks in these cases were incapable of transmitting compressive hoop forces of any substantial magnitude without separating, and no such separations were observed.

A possible explanation for this behavior appears to lie in the relative magnitudes of the axial and bending stresses. Use of Equation

33 to calculate axial and hoop stresses involves the addition of two large stresses of opposite signs to obtain a relatively small hoop stress. The relative error for such an operation (considering the $\pm$ 5$\mu\varepsilon$ readout accuracy) is extremely high. Direct application of Equation 33 to obtain hoop stresses was therefore unsatisfactory.

An alternate approach was needed to obtain the hoop stresses. If we note that the bending strains were considerably larger than axial strains we could reason that the relative error associated with their use in Equation 34 would be significantly smaller. It was felt that a correlation between bending stresses caused by interlock eccentricity and hoop stresses could be obtained. The device shown in Figure 42 was used to perform a series of tests on the model sheetpile section to do this. It allowed a variable axial force (hoop force) to be applied uniformly along the interlock of a six inch test specimen. The sheetpile interlock could also be subjected simultaneously to a shearing force.

A six inch sheet was instrumented with three pairs of strain gages to investigate the strains developed in the web as a function of hoop forces. Bending stresses computed from these strains were then plotted versus hoop force (in lb/inch). The resulting curve (see Figure 43) showed good repeatability in readings up to hoop forces of 16.0 lb/inch. It is interesting to note that the axial (hoop) forces computed directly by Equation 33 from measured strains showed poor correlation with the applied load, in particular for

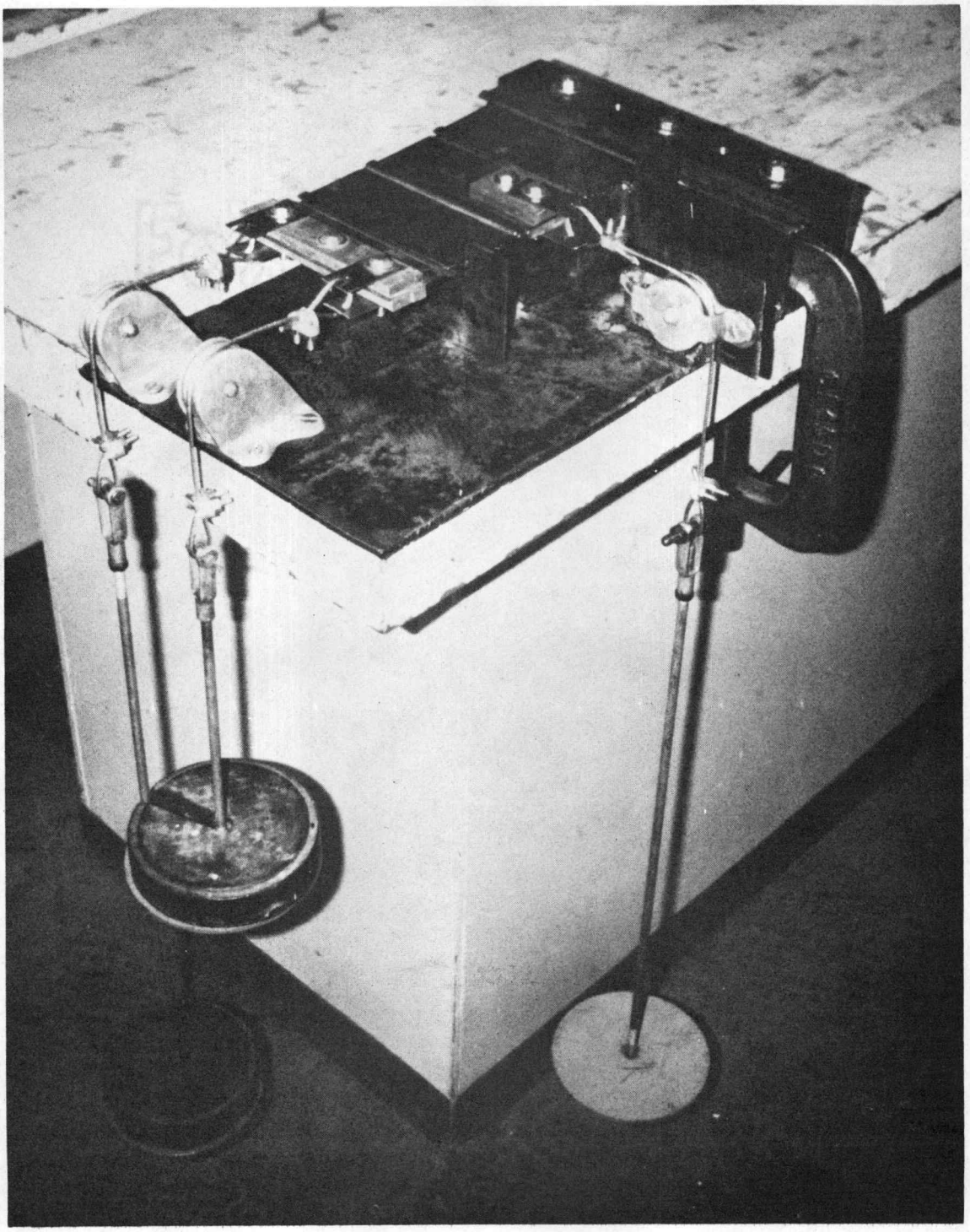

Figure 42. Sheetpile testing apparatus.

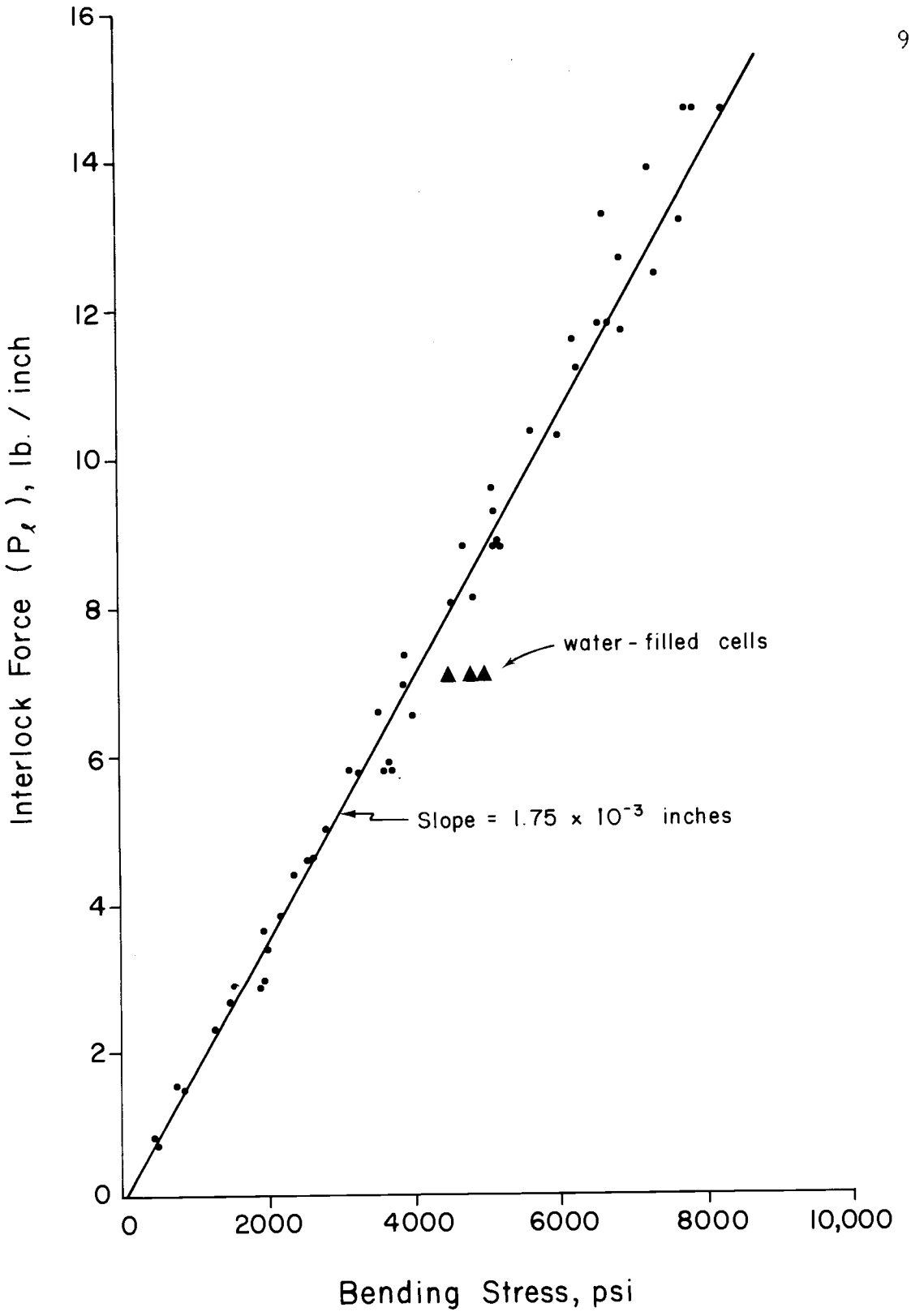

Figure 43. Correlation curve for interlock tension.

small hoop forces. This reaffirmed the belief that the bending strains were masking the axial strain component in the cell tests and preventing accurate calculation of hoop stress by Equation 33.

The correlation curve discussed above was obtained from tests run on a six inch long specimen and conceivably could be different from the response of full-length sheetpiles. It was necessary, therefore, to investigate the validity of the bending stress-hoop force relationship for full sheet lengths and within the actual cell set-up.

Two four-foot diameter, four-foot high cells with three instrumented sheets were built on a concrete slab. The interior of the cells was lined with a thin, loose plastic membrane and filled with water. The sheets rested on a thin bed of sand to minimize radial restraint along the bottom. Strains in the sheet were recorded as a function of water height. Values of hoop force obtained from the correlation were compared to those derived theoretically by the relationship

$$P_{hoop} = \gamma_w \cdot z \cdot r \tag{38}$$

where P_{hoop} = hoop force in lb/in.

γ_w = unit weight of water (lb/in^3)

z = depth from the surface (in)

r = radius of cell (in)

In general the hoop forces obtained from the water filled cells were significantly higher than those measured from the Series IV

sandfilled cell (i.e., no embedment case). Since the unit weight of water and sand and the anticipated coefficients of lateral pressure (K_w = 1.0 and K_{sand} = 0.5) differ by offsetting factors of about 2, the magnitudes of hoop forces for both cases were anticipated to be about the same. The difference in measured values indicated that the radial pressures due to the sand fill were significantly below the anticipated values. This matter will be discussed in the DISCUSSION OF RESULTS section.

Only the lowermost values of hoop forces measured in the water-filled cells were within the range of the correlation curve shown in Figure 43. These points, however, indicated that the presumed hoop force-bending stress relationship was valid for long sheets as well as for the test specimen.

The correlation curve shown in Figure 43 presumes that the hoop forces are applied along a horizontal axis. In fact, a typical sheetpile as shown in Figure 44, is subjected to both a radial pressure and a hoop force making an angle θ with the axis of the web. The angle θ is due to the fact that the sheetpile actually

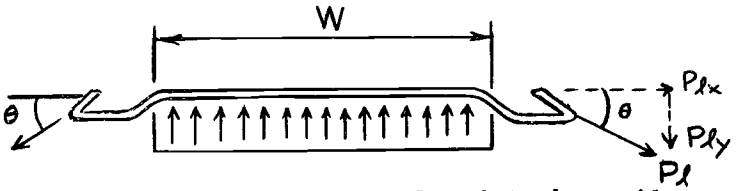

Figure 44. Free body of model sheetpile.

where P_ℓ = hoop tension per unit length

w = lateral pressure per unit length

W = width of sheetpile.

forms a small chord rather than an arc section with respect to the center of the cell. The average value of θ for the cells in the present study was 6°.

Summing forces per unit length in the y direction shown in Figure 44 gives

$$w = \frac{2(\sin\theta)P_{\ell}}{W} \tag{39}$$

The pressure, w, on the inner web face is, therefore offset by the y-component of the hoop force, P_{ℓ}. It also creates a bending stress at the center of the web.

The bending stress due to the interlock eccentricity, however, depends on the orientation of the interlocks. For position P1 (front) the open face of the interlock opened outward and the bending stresses are additive with the web bending stresses. The sheets in positions P2, P3 and P4 were oriented in the opposite sense and the end moment due to interlock eccentricity had an effect opposing that of web flexure due to lateral pressures.

Figure 45(a) and 45(b) summarizes the two cases.

(a) End moments (front sheetpile)

Figure 45. Combined bending effects of lateral pressure and interlock eccentricity for model sheetpiles.

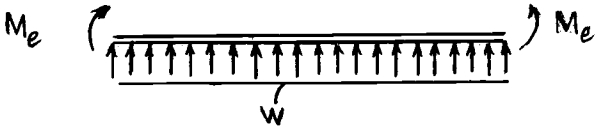

(b) End moments at side and back sheetpiles

If M_w is defined as the moment at the center of the web caused by the lateral earth pressures then the total moment, M, can be defined as

$$M = -(M_e + M_w) \text{ (for P1)} \tag{40}$$

and $$M = -(M_w - M_e) \text{ (for P2, P3, P4)}$$

Since the correlation between hoop force and bending stress involves only the component due to interlock moments, it was necessary to remove the effect of the bending moment due to lateral pressure, M_w. This last correction was made in a relatively simple manner.

The hoop forces at cell sheets at a given level are expected to, and should, be about the same, for the isolated cell case. The hoop stresses were decreased at the front sheetpiles and increased at other locations by about 13.5 percent.

For instrumentation levels where only a single horizontal strain gage was used (at some side sheets), the vertical strains were extrapolated from other sheets or adjacent gages and used in step 1 of the data reduction procedure.

Summary of Hoop Stress Data

Figures 46 through 49 summarize the hoop stresses measured in all tests. The level of the dredgeline is indicated on every figure along with the top of the cell fill.

Vertical Stresses

The magnitude of vertical stress was consistently low and usually within the range of accuracy of the readout unit. No attempt was made, therefore, to analyze the vertical stress. In general, however, the vertical stresses were maximum near the point of maximum bulging and then reduced to very small values below the dredge line.

Movement of the Cell

Deflection Data

The deflection of the model bulkhead and sheetpile deformations were monitored principally by means of large-throw dial gages attached to a vertical bar at the front of the cell (see Figure 36). A more detailed description of the dial gage set up is found in the PROJECT DESCRIPTION section. The deflections of the cell for all phases of testing except the pullover tests were so small that radial displacements of the top of the cell along the perimeter could not be measured by the overhead coordinate system with any degree of reliability.

Figures 50 through 53 show the radial deflections of the front sheet as a function of construction events for all four test series.

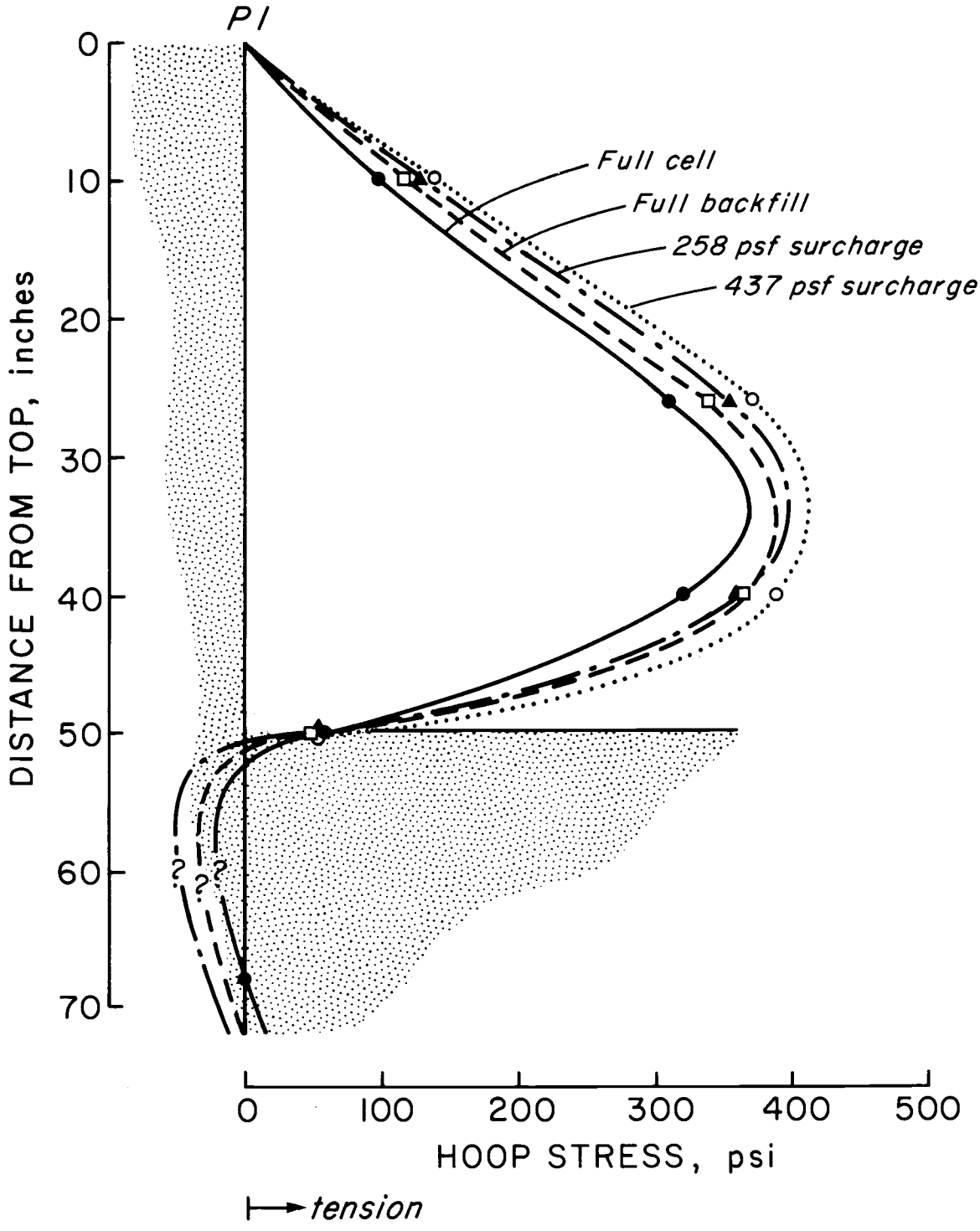

(a) Hoop stress distribution at front sheetpile (P1)

Figure 46. Hoop stress distribution for Series I.

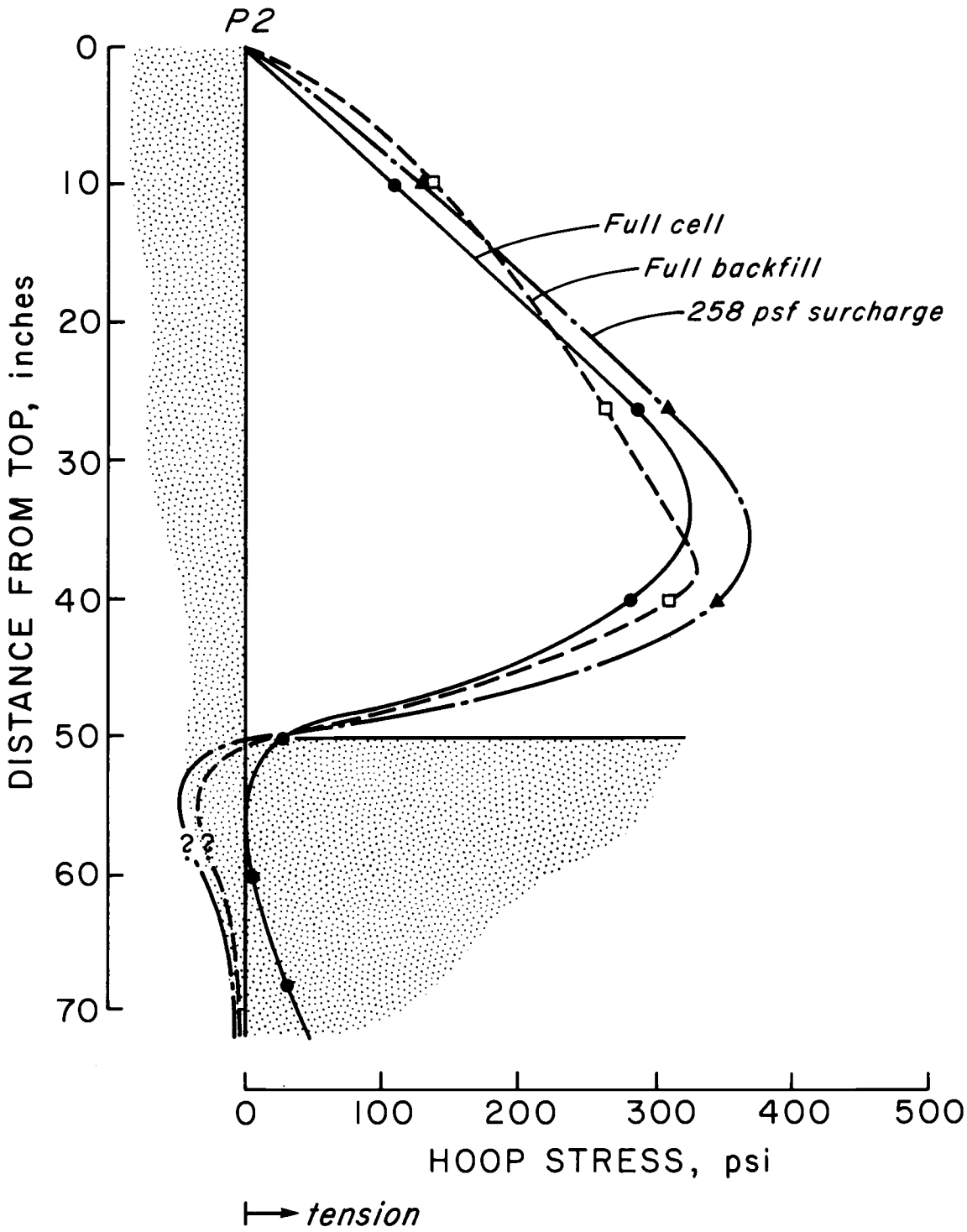

(b) Hoop stress distribution at side sheetpile (P2)

Figure 46. continued

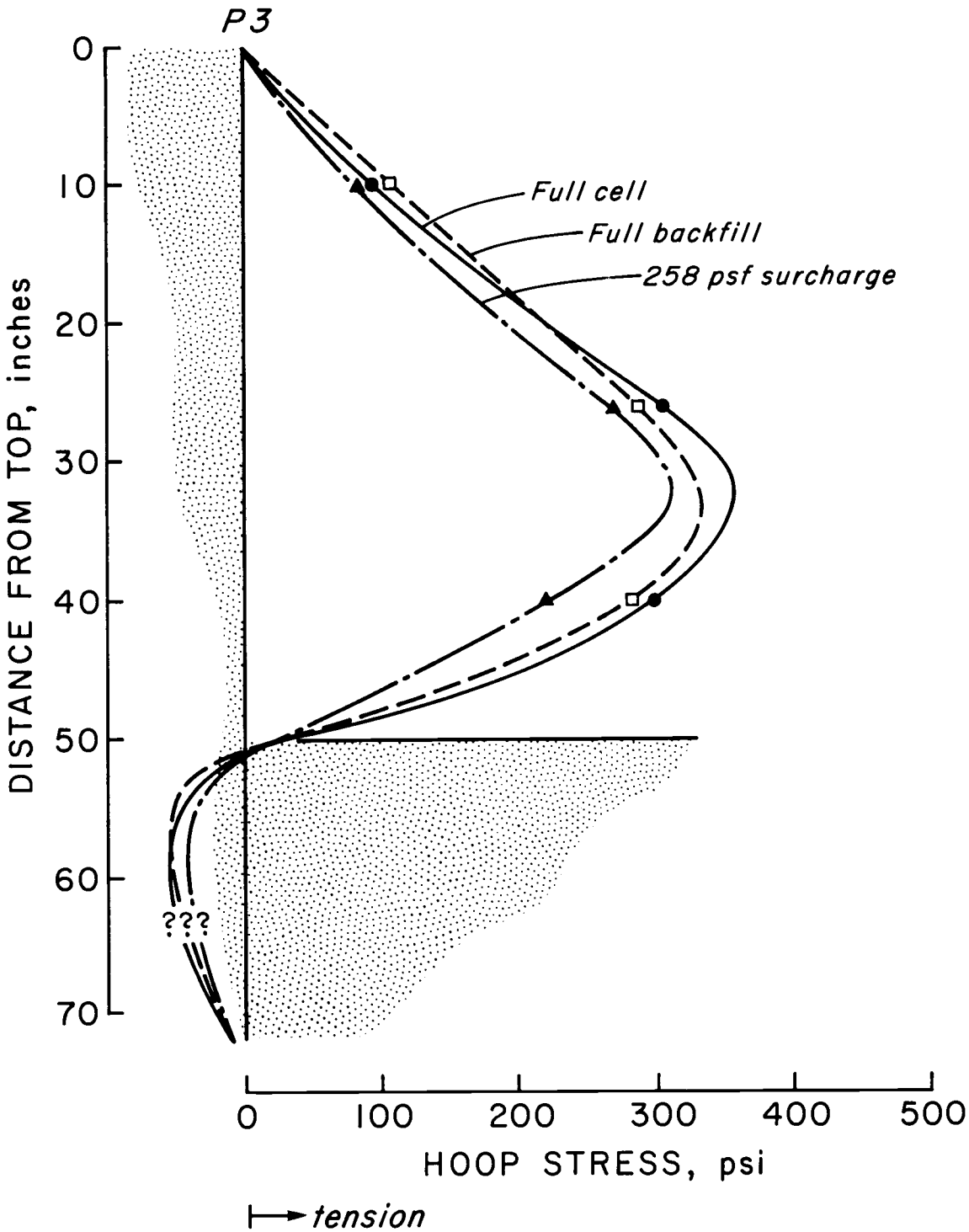

(c) Hoop stress distribution for side sheetpile (P3)

Figure 46. continued

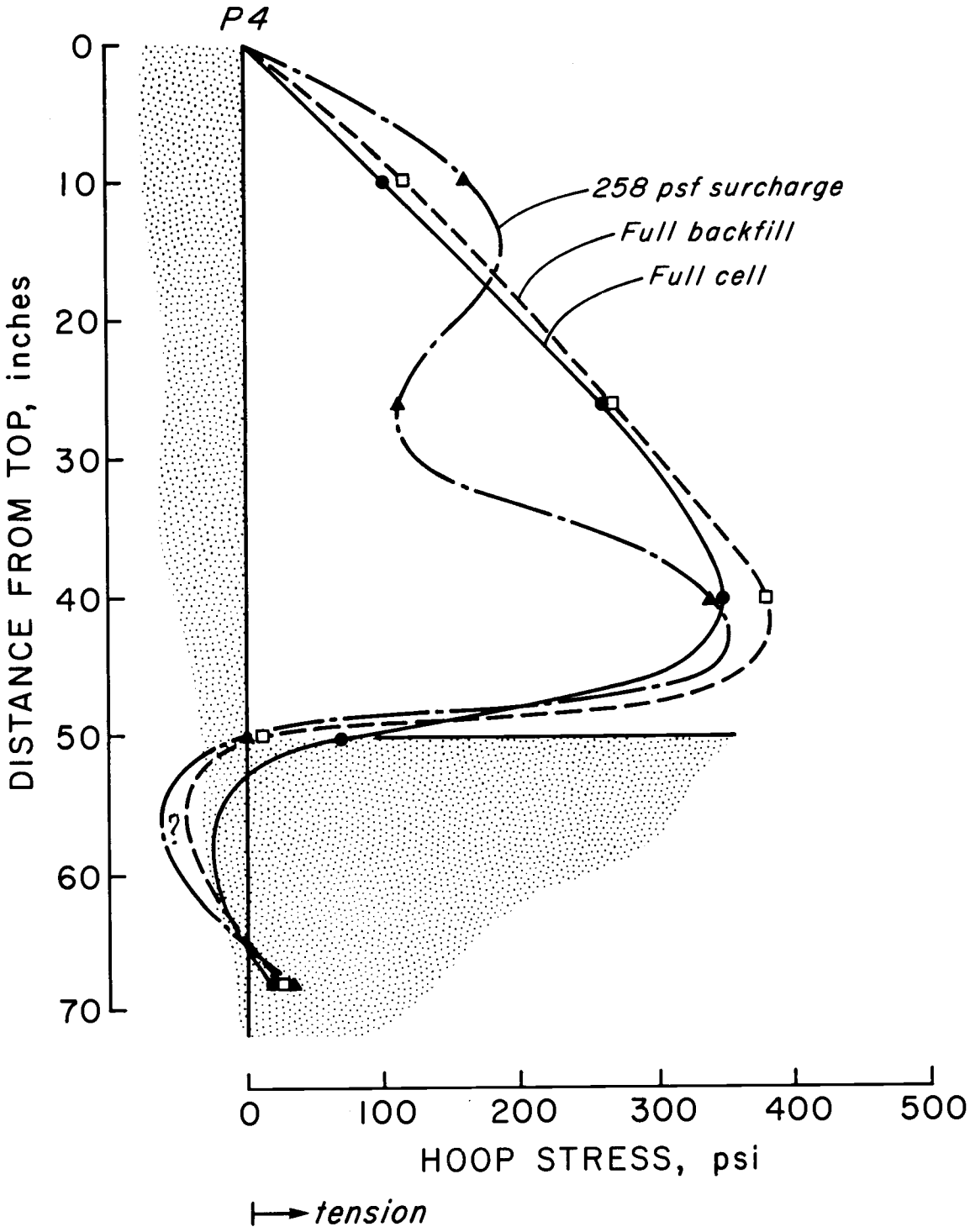

(d) Hoop stress distribution for backsheetpile (P4)

Figure 46. continued

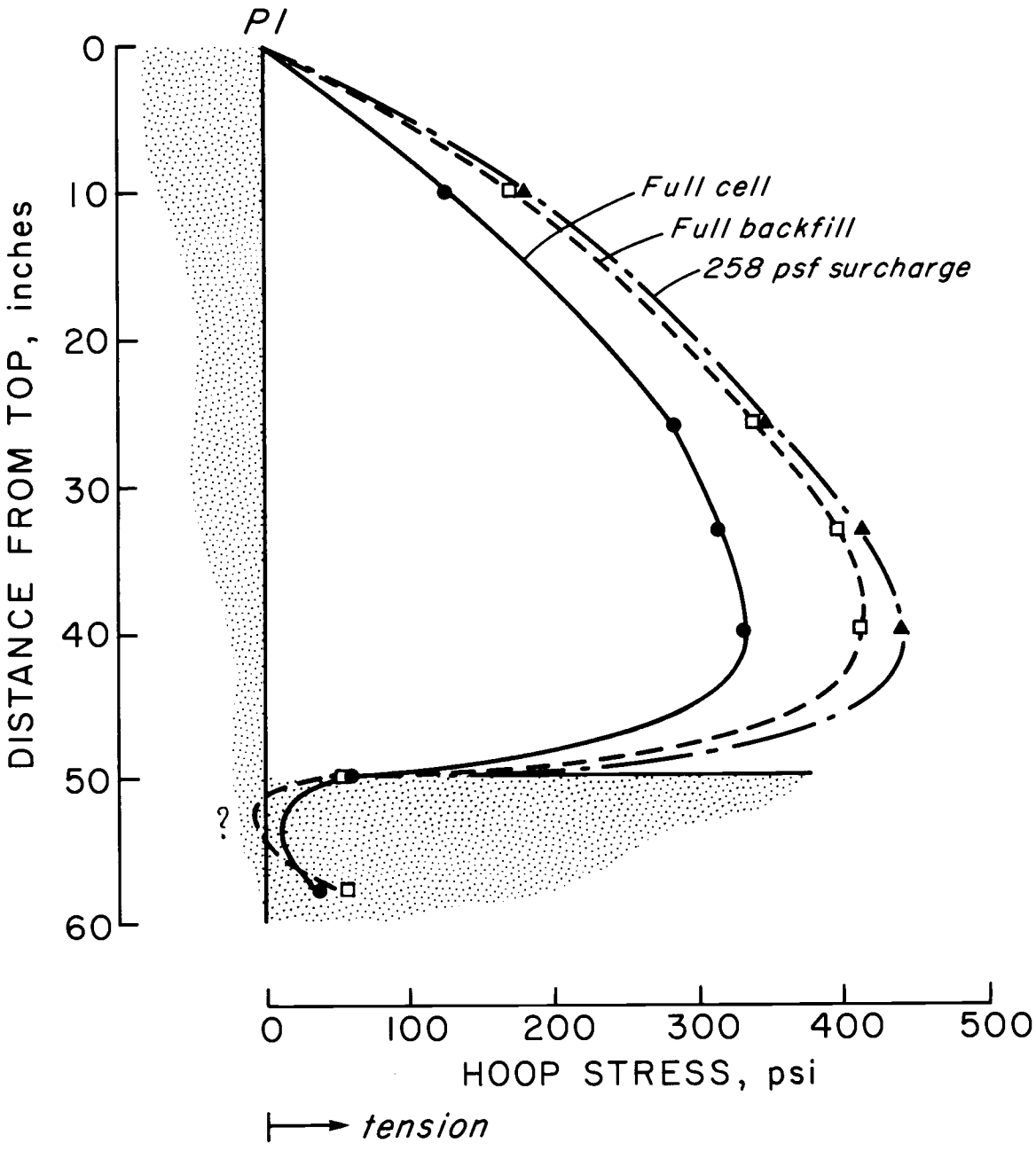

(a) Hoop stress distribution at front sheetpile (P1)

Figure 47. Hoop stress distribution for Series II.

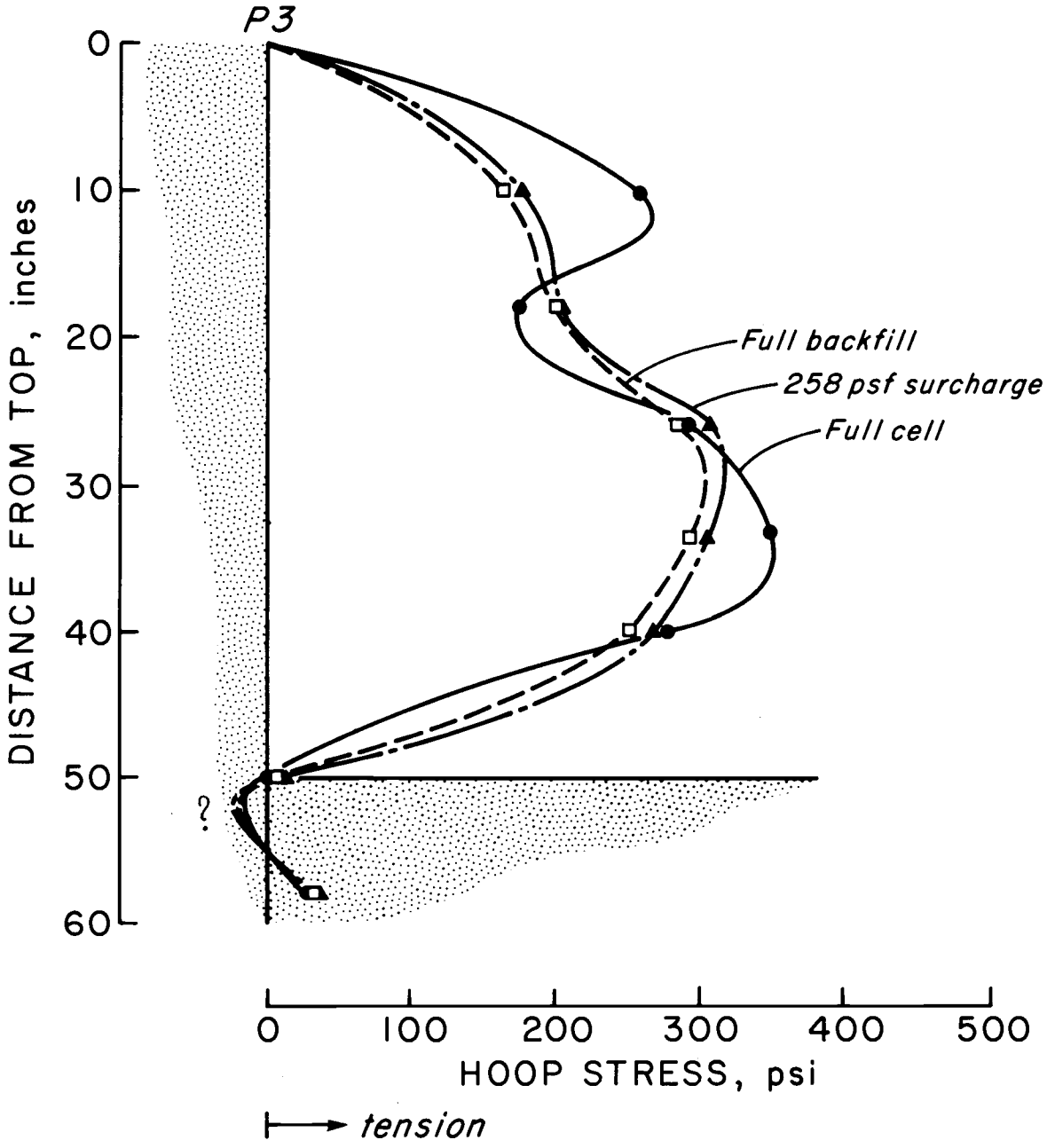

(b) Hoop stress distribution at side sheetpile (P3)

Figure 47. continued

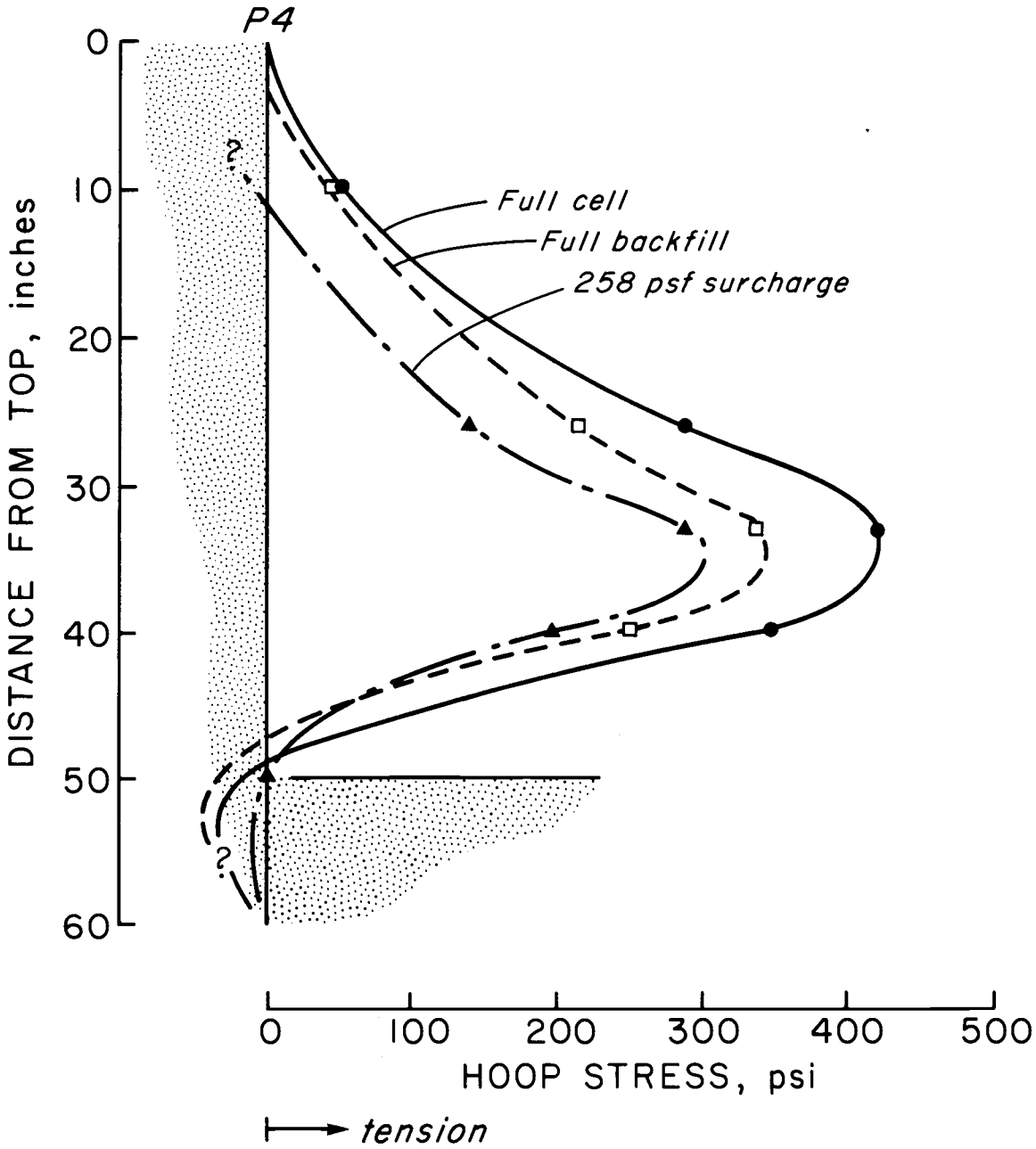

(c) Hoop stress distribution at back sheetpile (P4)

Figure 47. continued

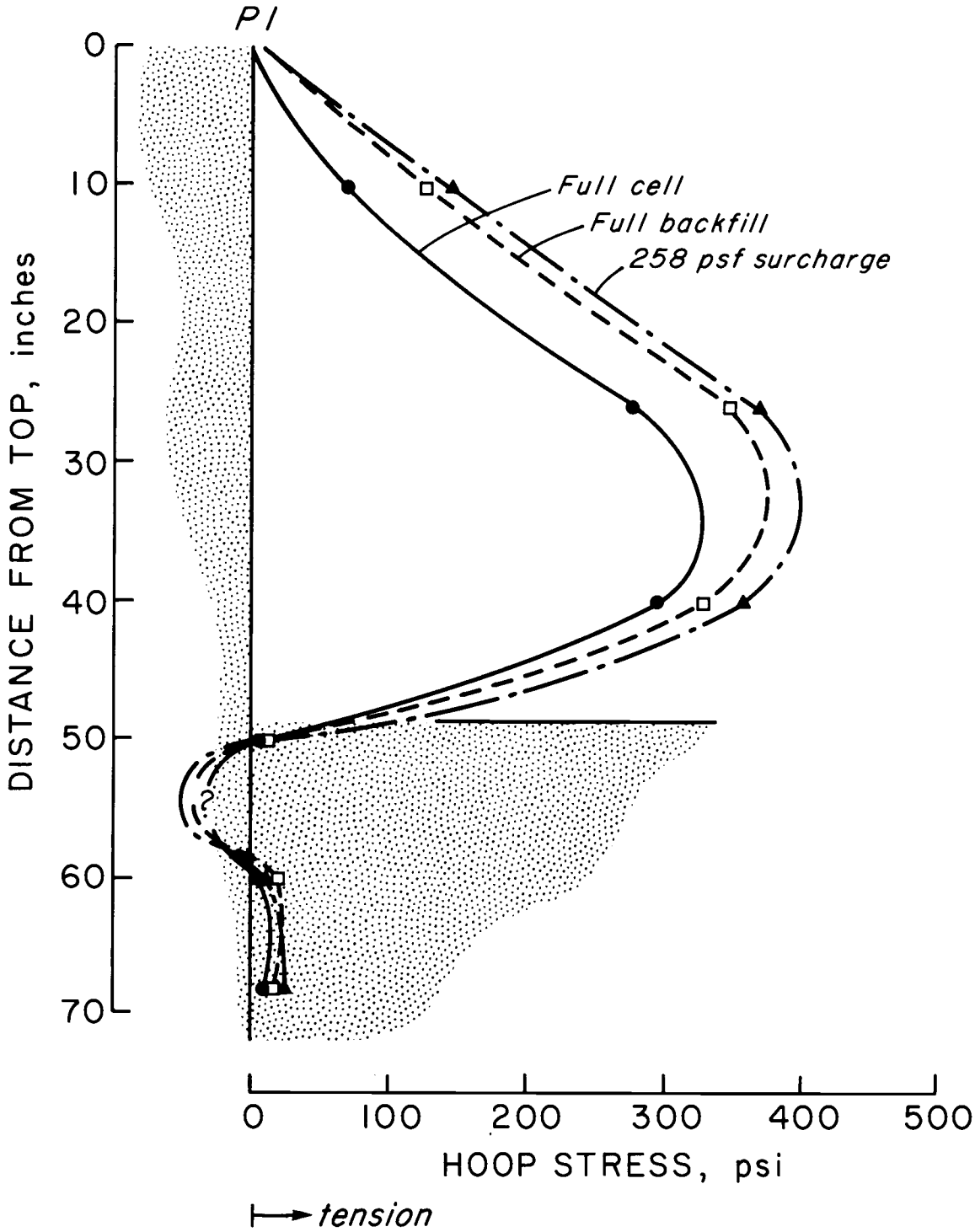

(a) Hoop stress distribution at front sheetpile (P1)

Figure 48. Hoop stress distribution for Series III.

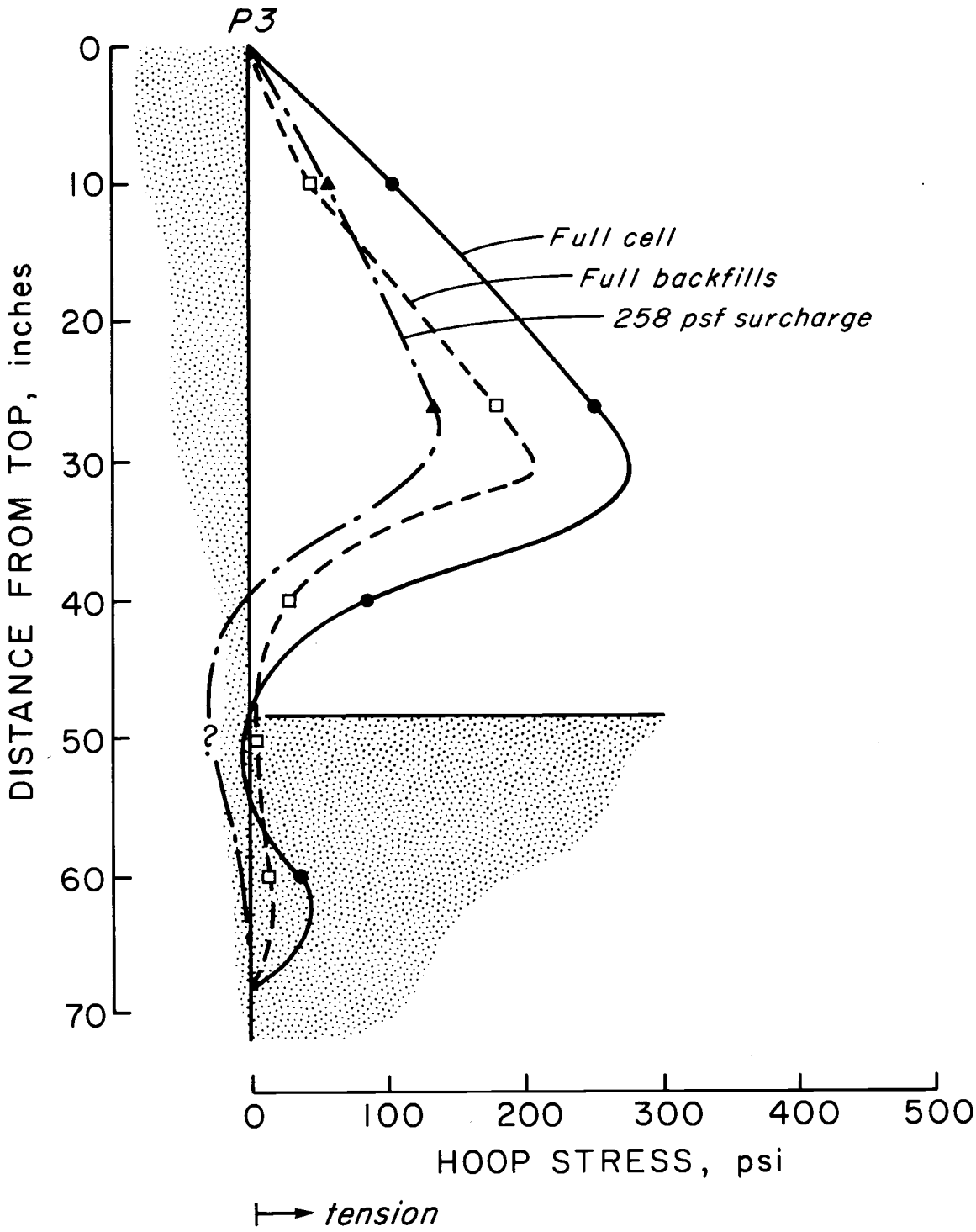

(b) Hoop stress distribution at side sheetpile (P3)

Figure 48. continued

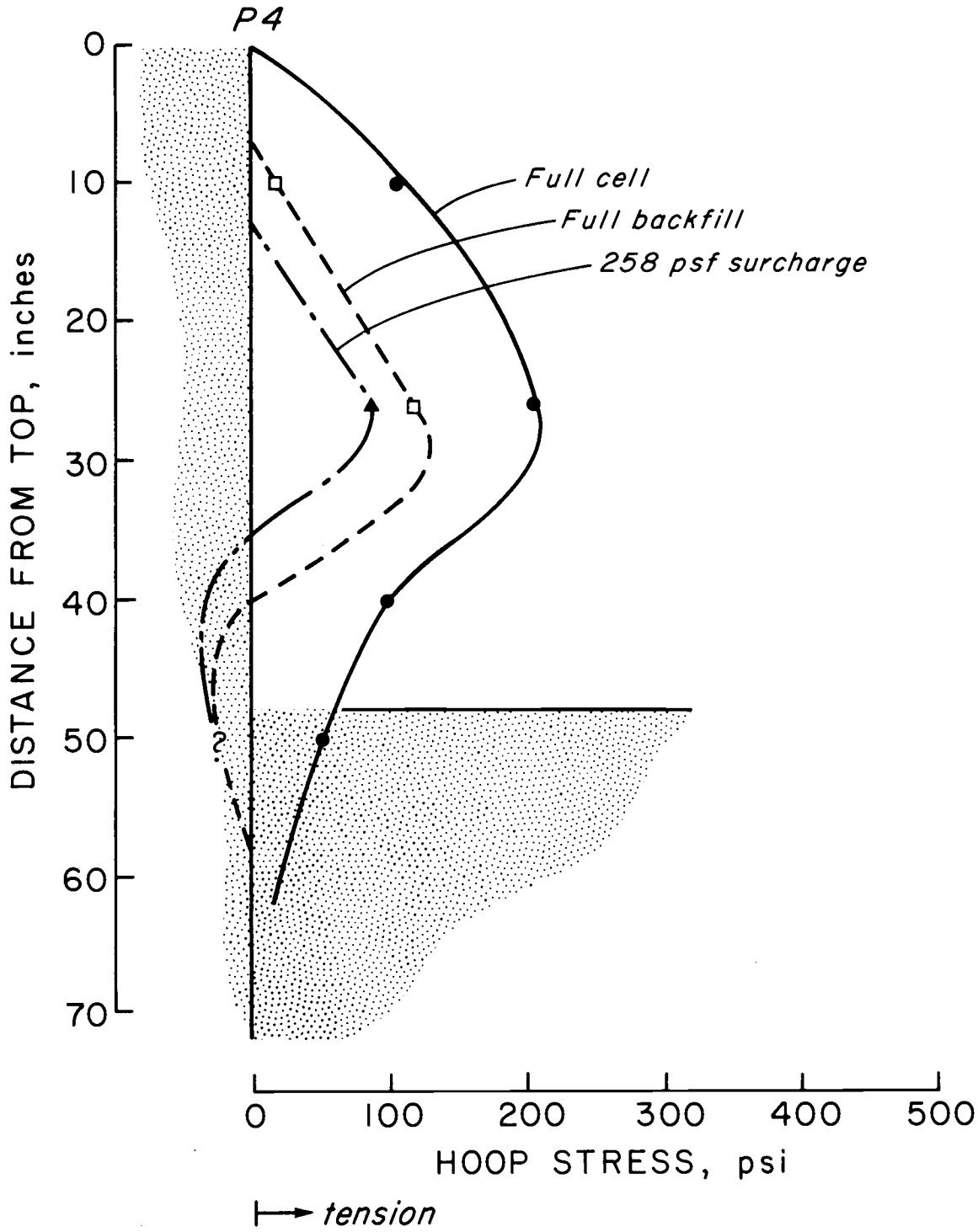

(c) Hoop stress distribution at back sheetpile (P4)

Figure 48. continued

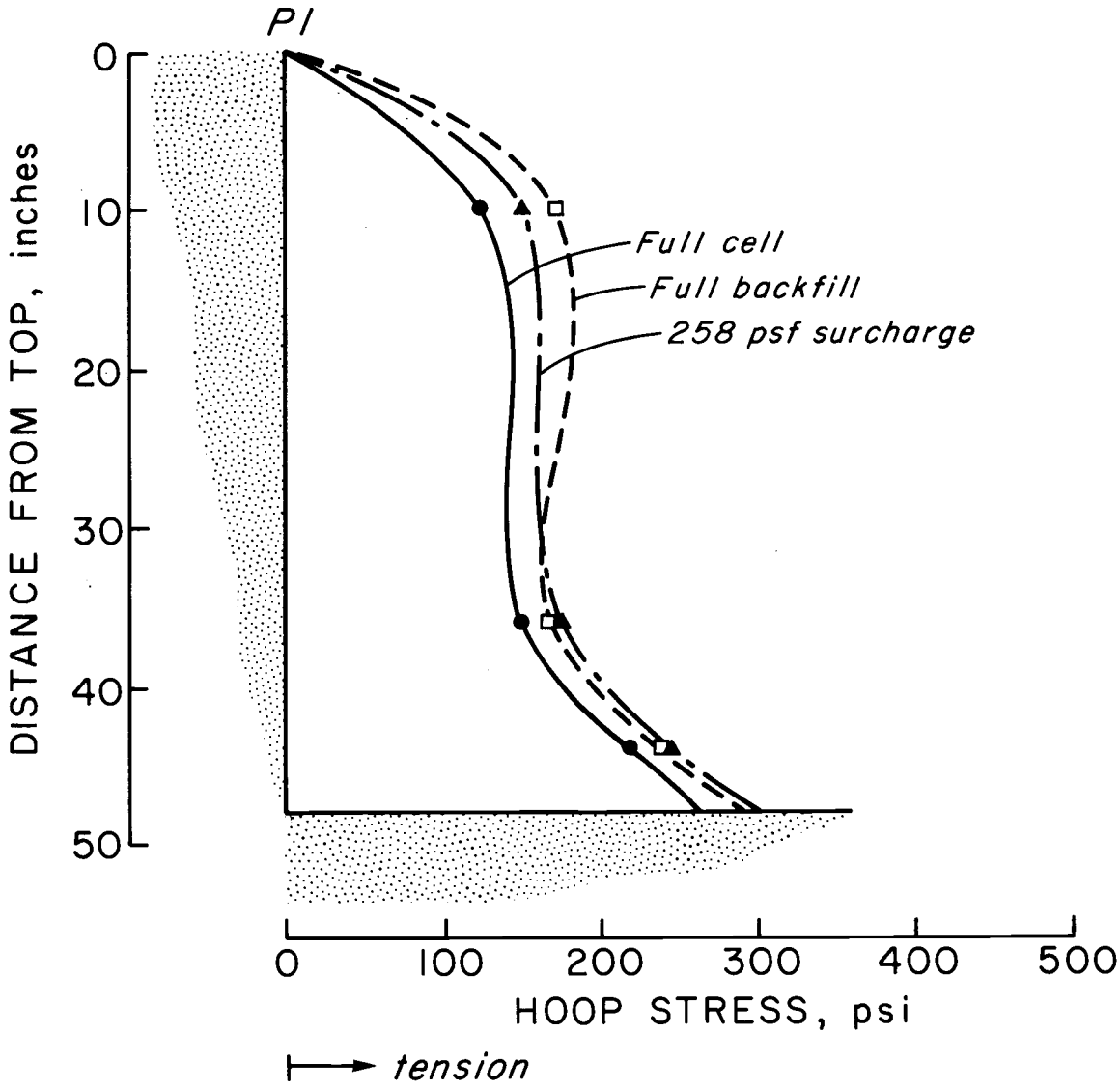

(a) Hoop stress distribution at front sheetpile (P1)

Figure 49. Hoop stress distribution for Series IV.

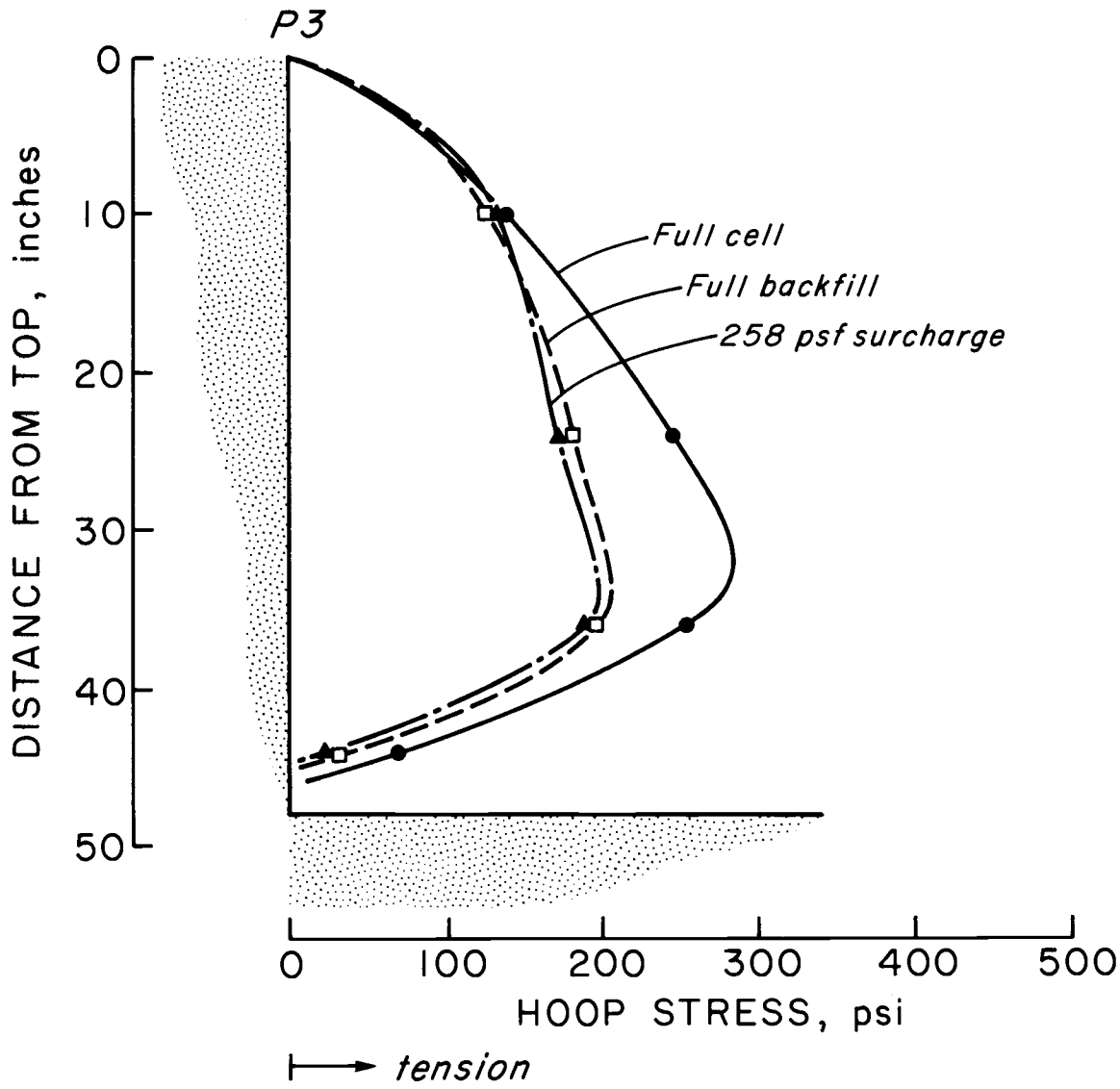

(b) Hoop stress distribution at side sheetpile (P3)

Figure 49. continued

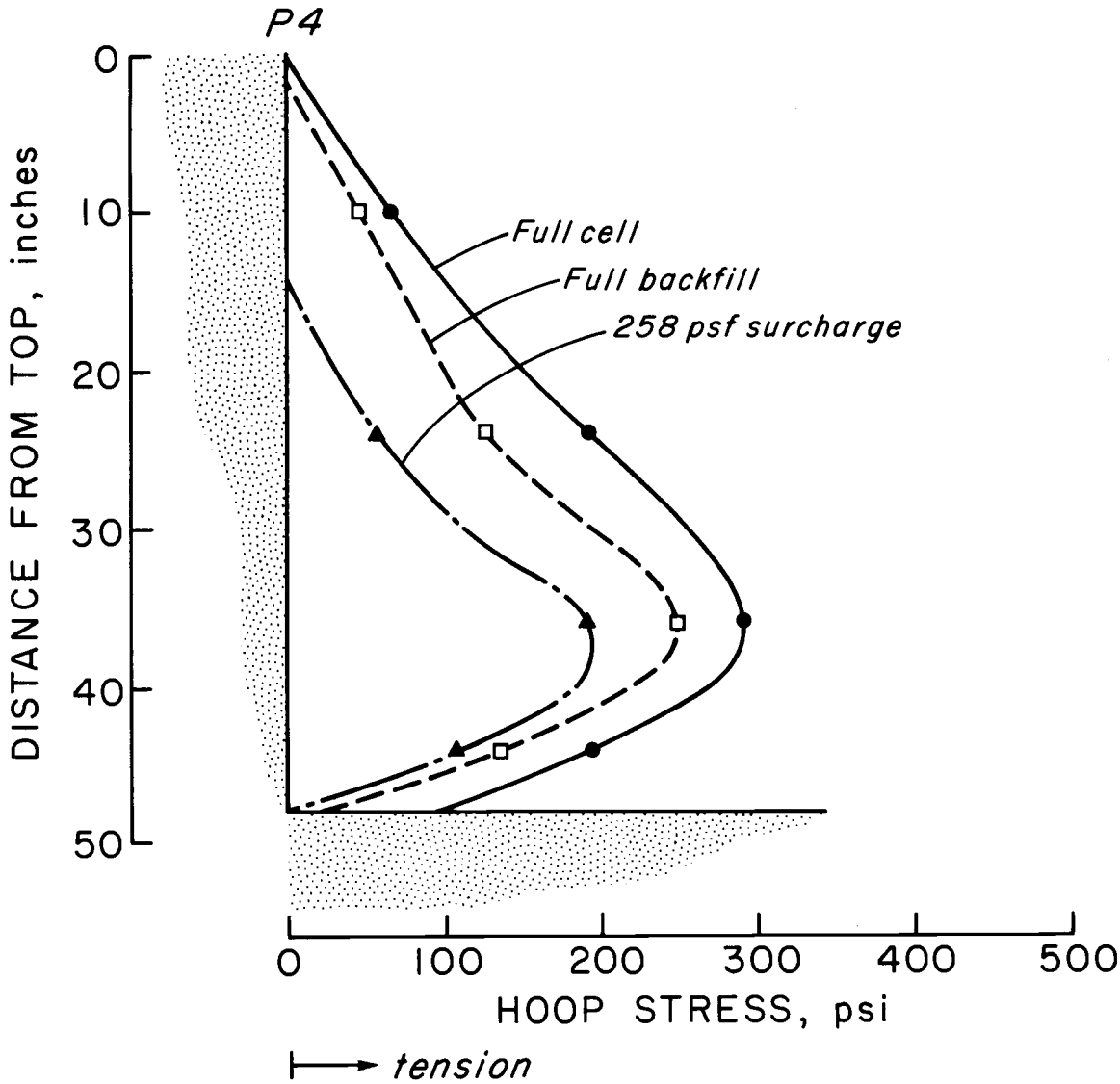

(c) Hoop stress distribution at back sheetpile (P4)

Figure 49. continued

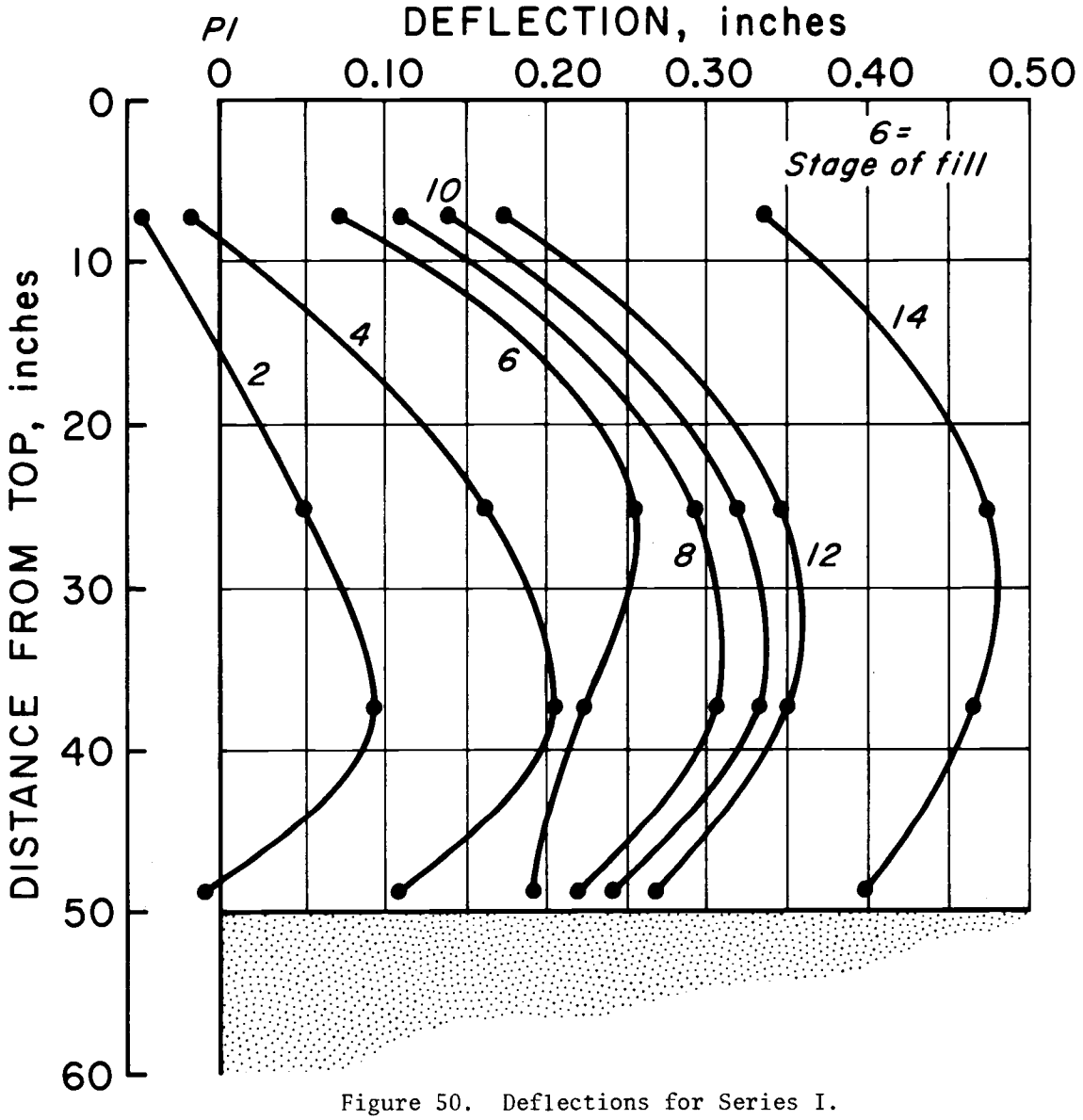

Figure 50. Deflections for Series I.

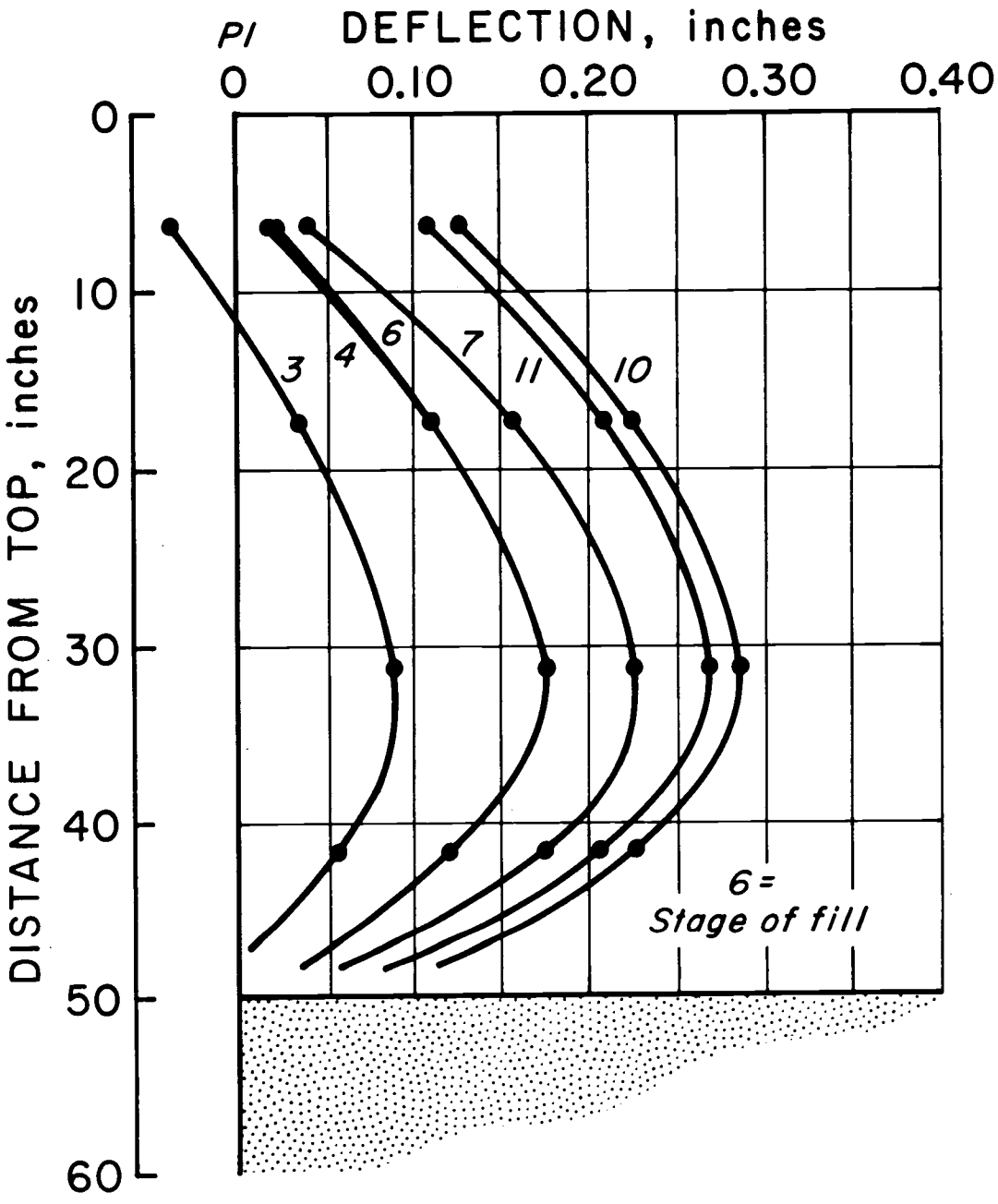

Figure 51. Deflections for Series II.

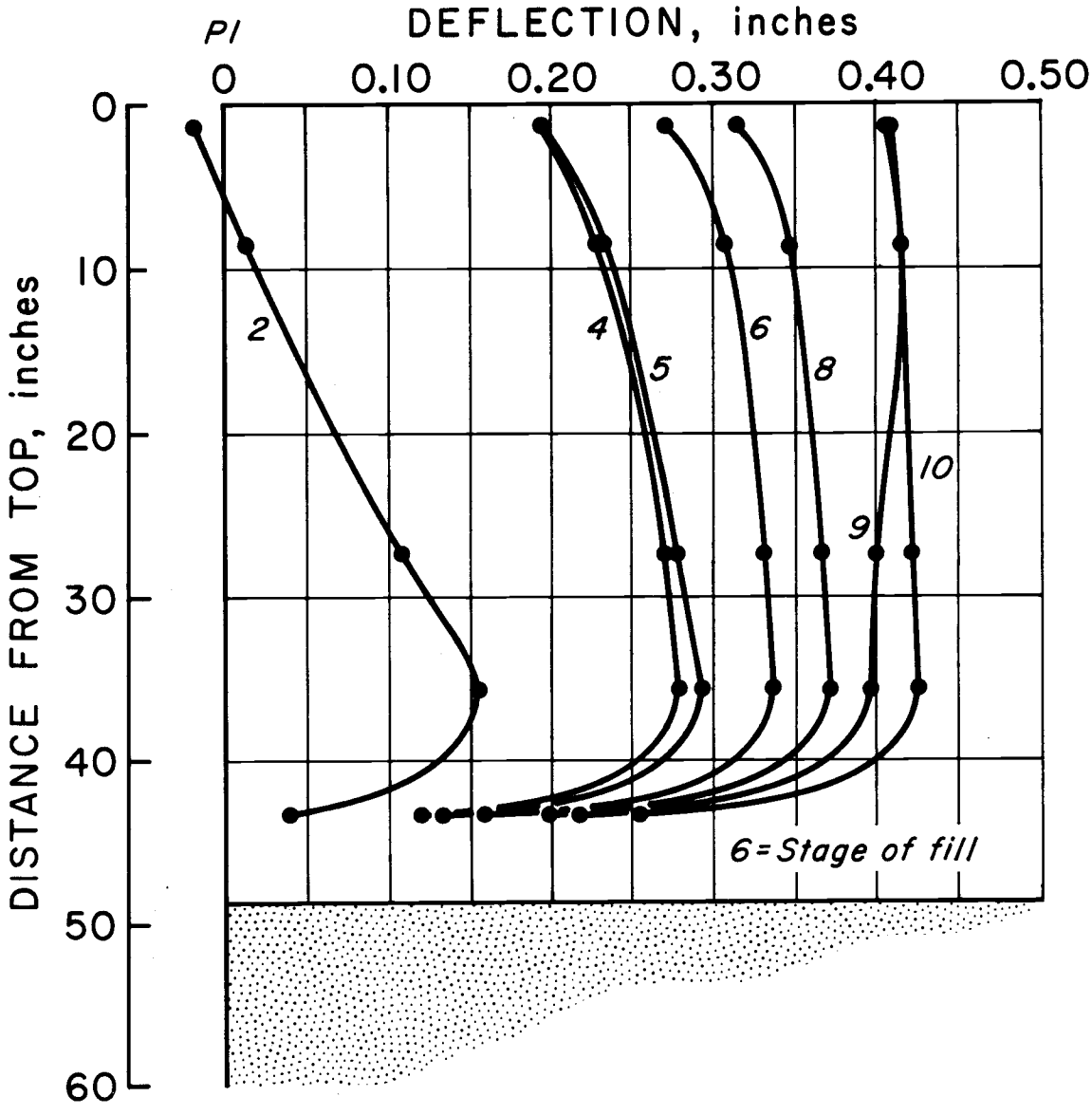

Figure 52. Deflections for Series III

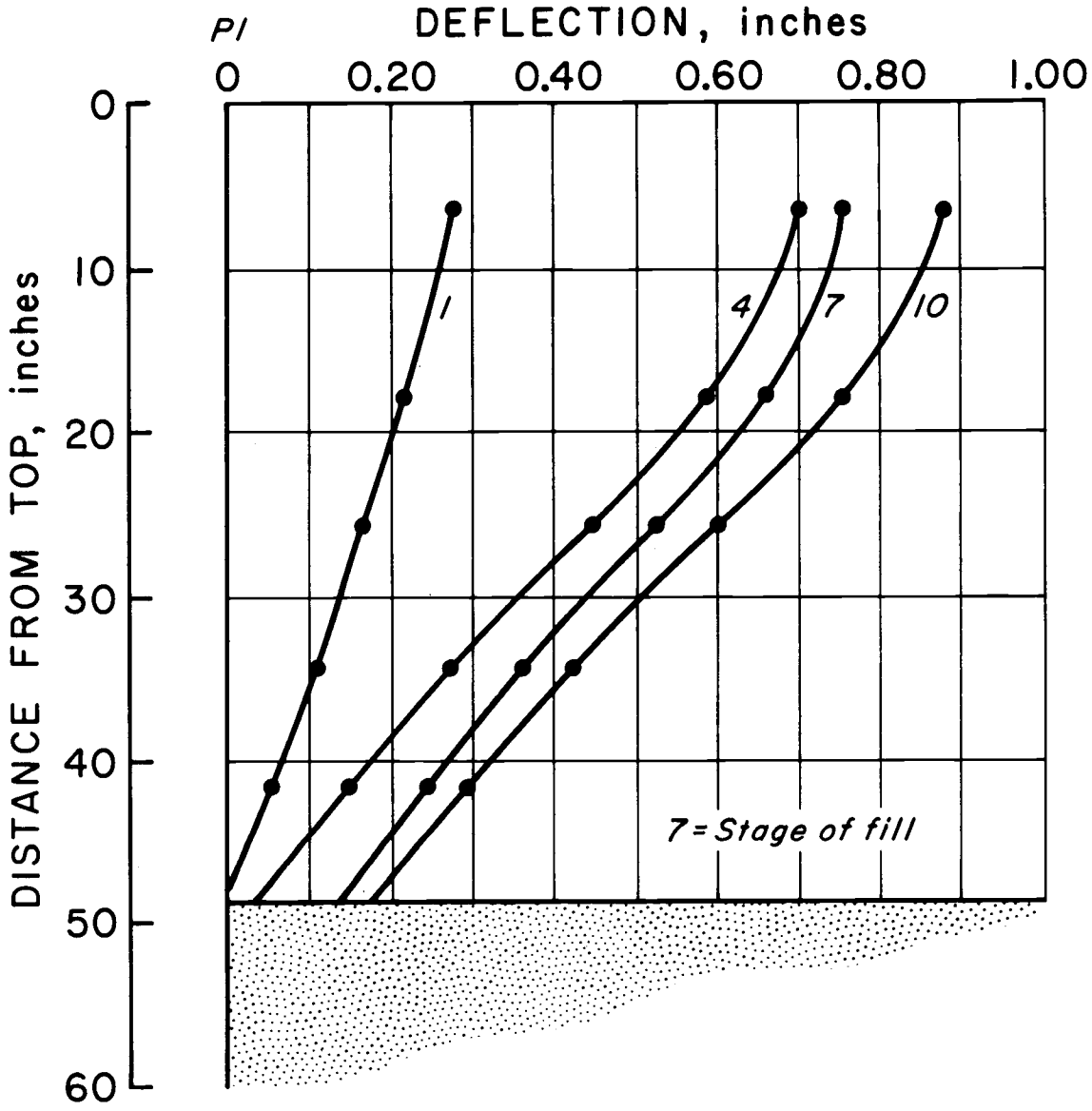

Figure 53. Deflections for Series IV.

It should be noted that the levels of dial gage readings varied with the test series since they were placed at the locations where they would best define anticipated deformation. Additional dial gages were placed at some intermediate levels to better define the deflection curves.

Measurement of deformations of the back sheetpile (P44) were also monitored for the full cell stage during Series III and IV.

A comparison of front sheetpile deformations for all cells at the full cell stage is shown in Figure 54. The circled numbers represent the stage of construction and are summarized in Tables 4, 5, 6 and 7.

To investigate the deflections of the cell due to backfilling and surcharging operations, the radial displacement due to initial cell filling was subtracted from subsequent readings when the cell were subjected to lateral load. This also removed deflections due to initial interlock slack.

The incremental deflections (beyond the full cell stage) of the front sheetpile are summarized in Figures 55 through 58. Deflections at dial gage No. 3 for Cell No. 1 appear to be inconsistent with observations of physical behavior. The dashed line indicates the assumed curve between Gages No. 2 and 4.

As a final phase of testing each model was loaded to failure. Very large deflections were measured during the overturning of the cells. Figures 59 through 66 show the profile of the front sheet at various stages of overturning.

The location of the dredgeline is indicated on all figures.

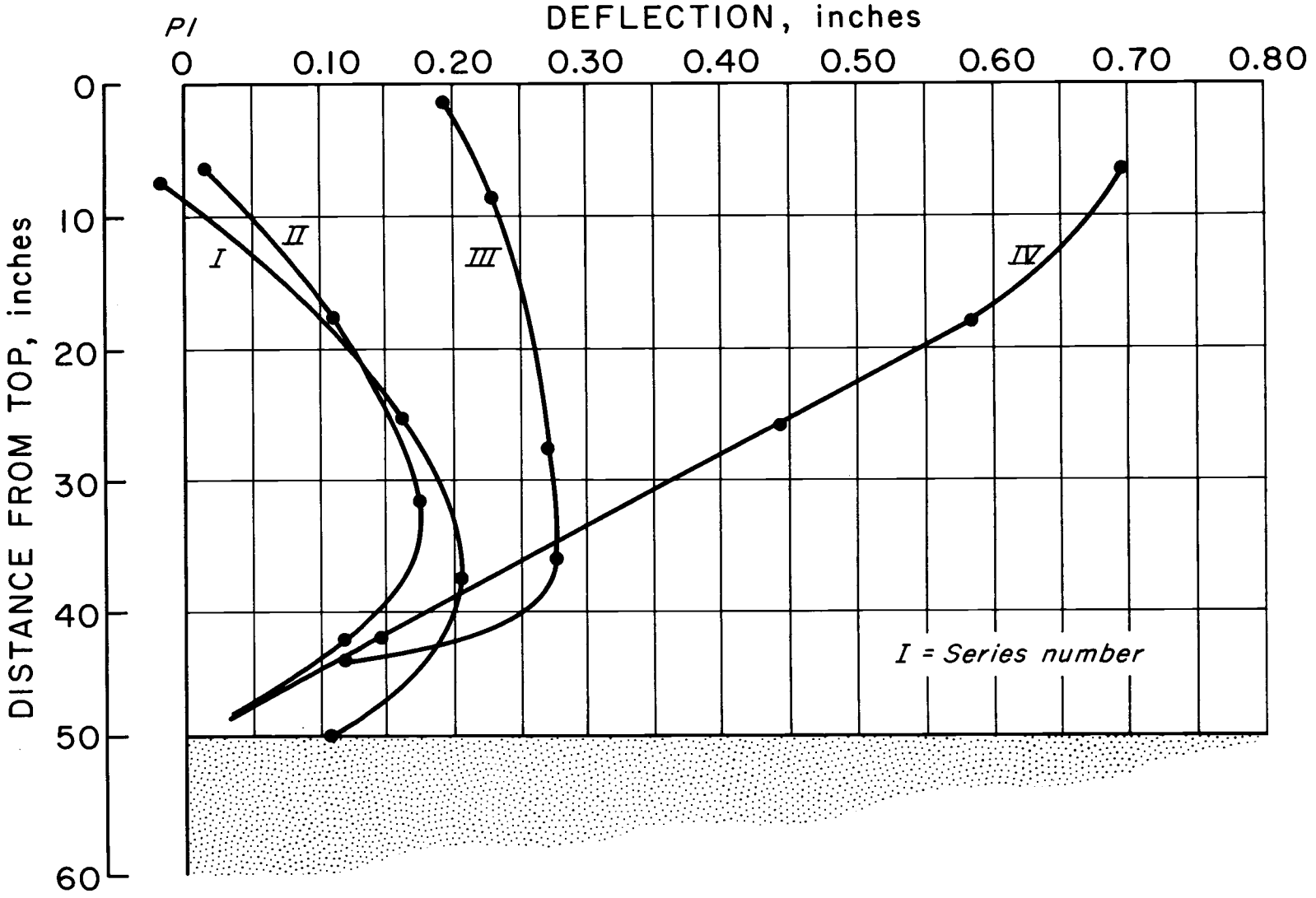

Figure 54. Comparison of deflections of full cells.

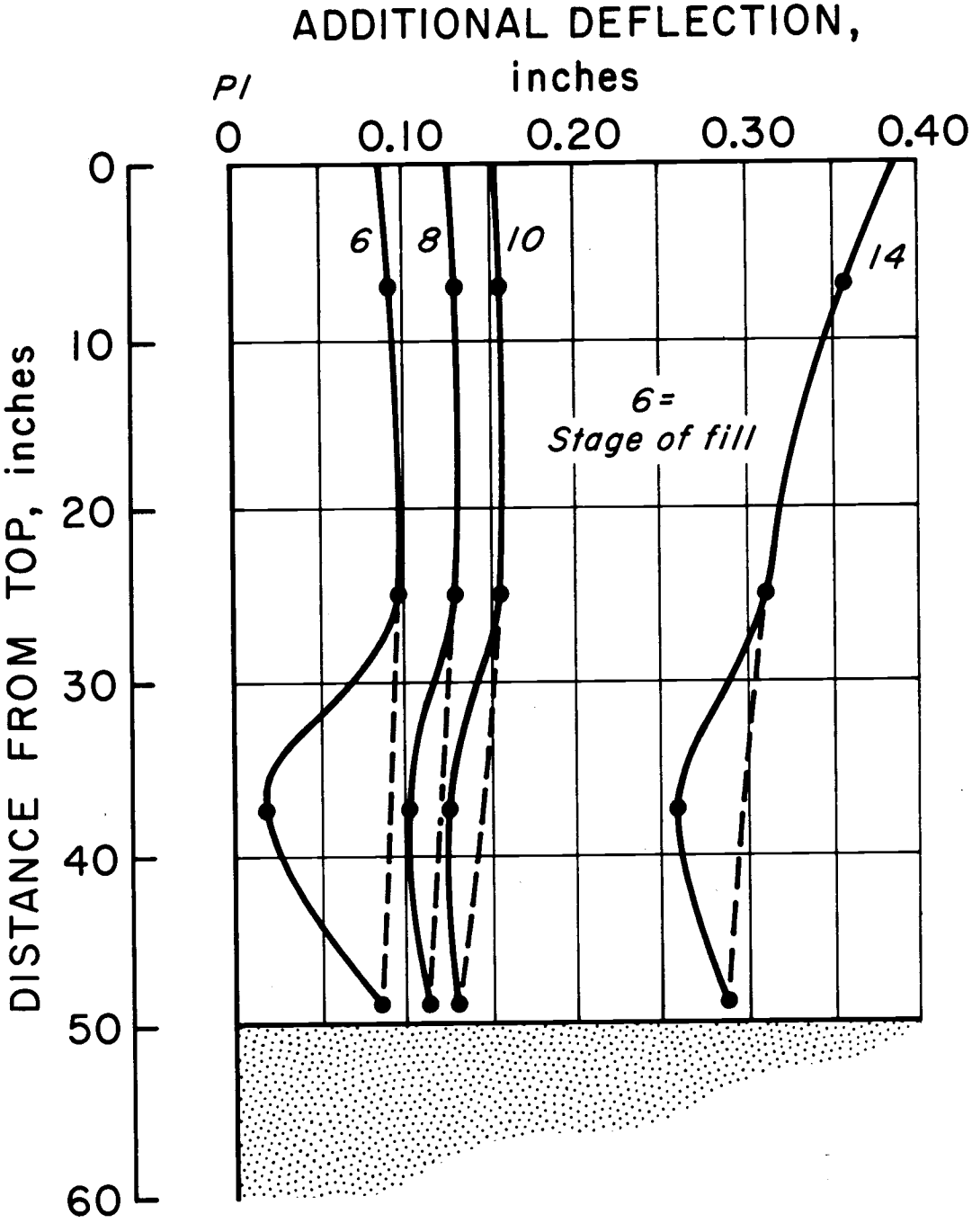

Figure 55. Additional deflections beyond full cell stage (Series I).

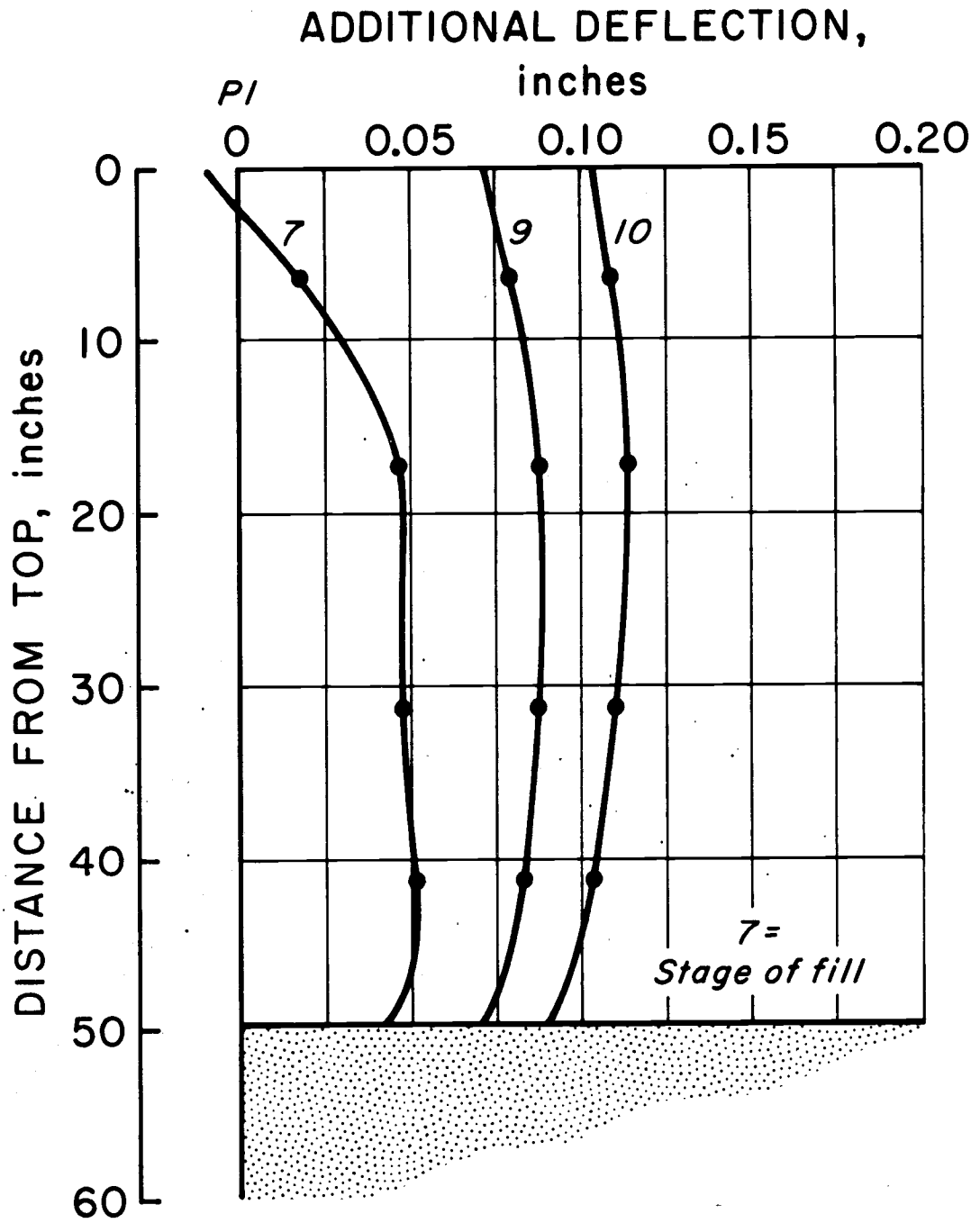

Figure 56. Additional deflections beyond full cell stage (Series II).

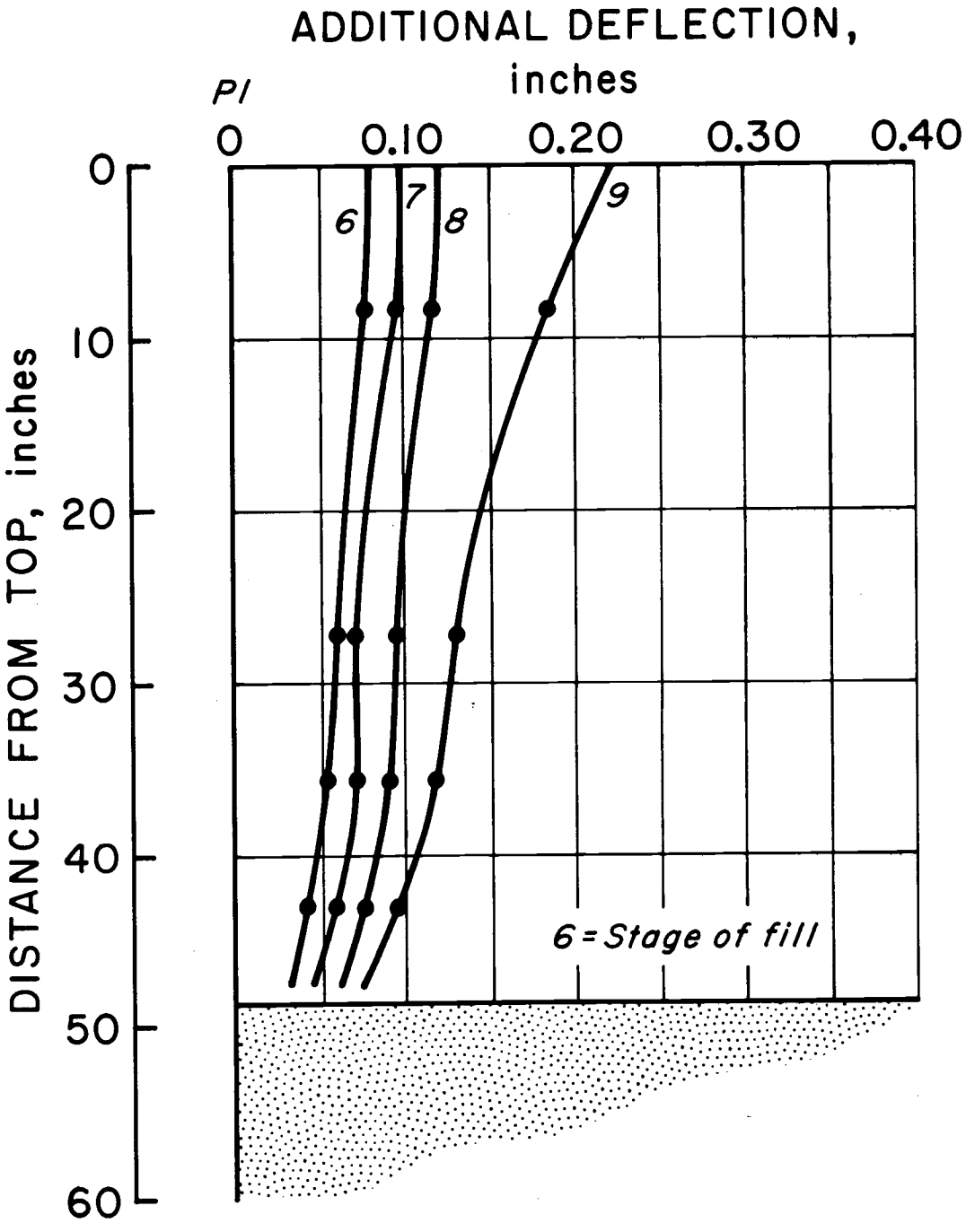

Figure 57. Additional deflections beyond full cell stage (Series III).

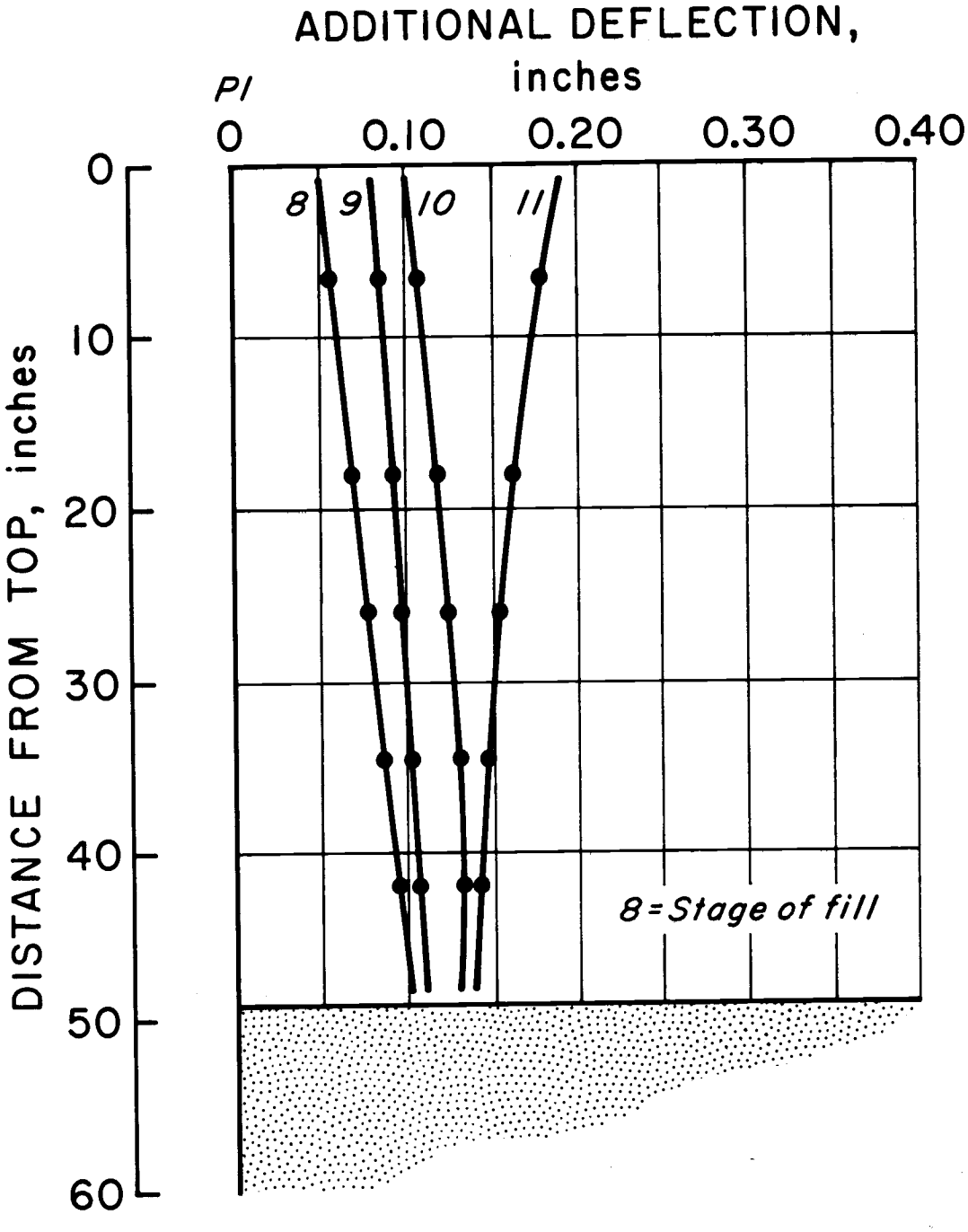

Figure 58. Additional deflections beyond full cell stage (Series IV).

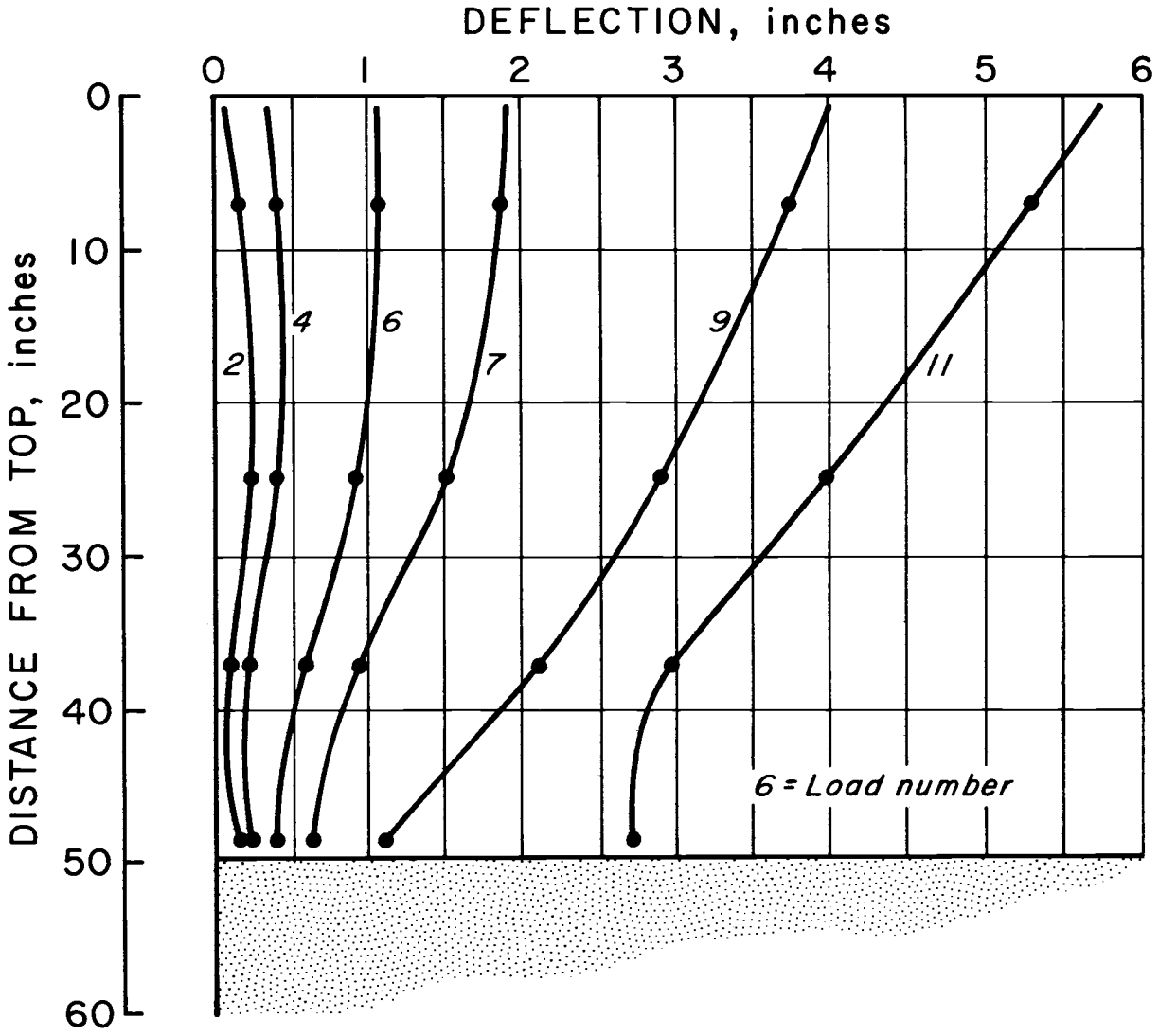

Figure 59. Deflections during failure (Series I).

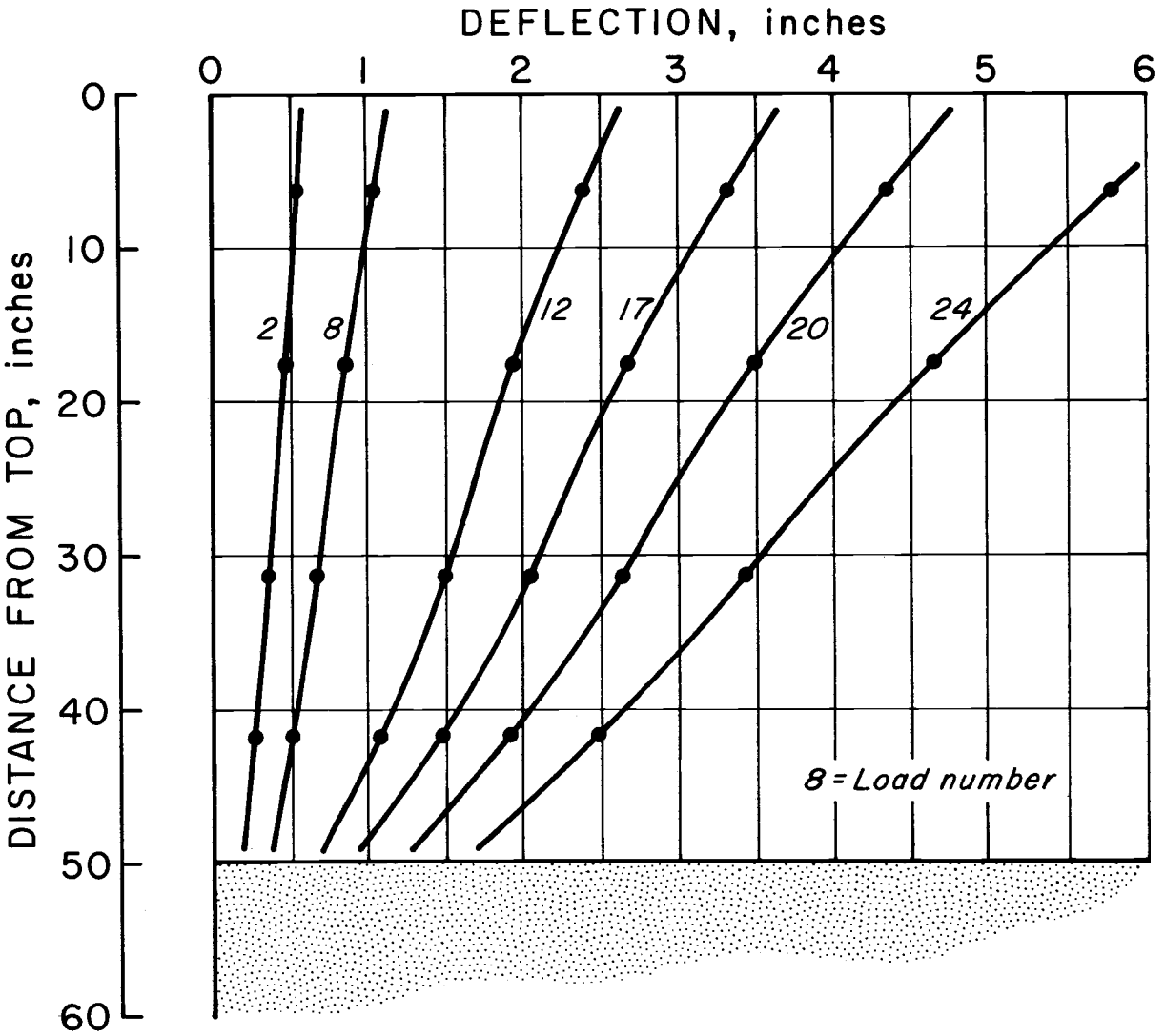

Figure 60. Deflections during failure (Series II).

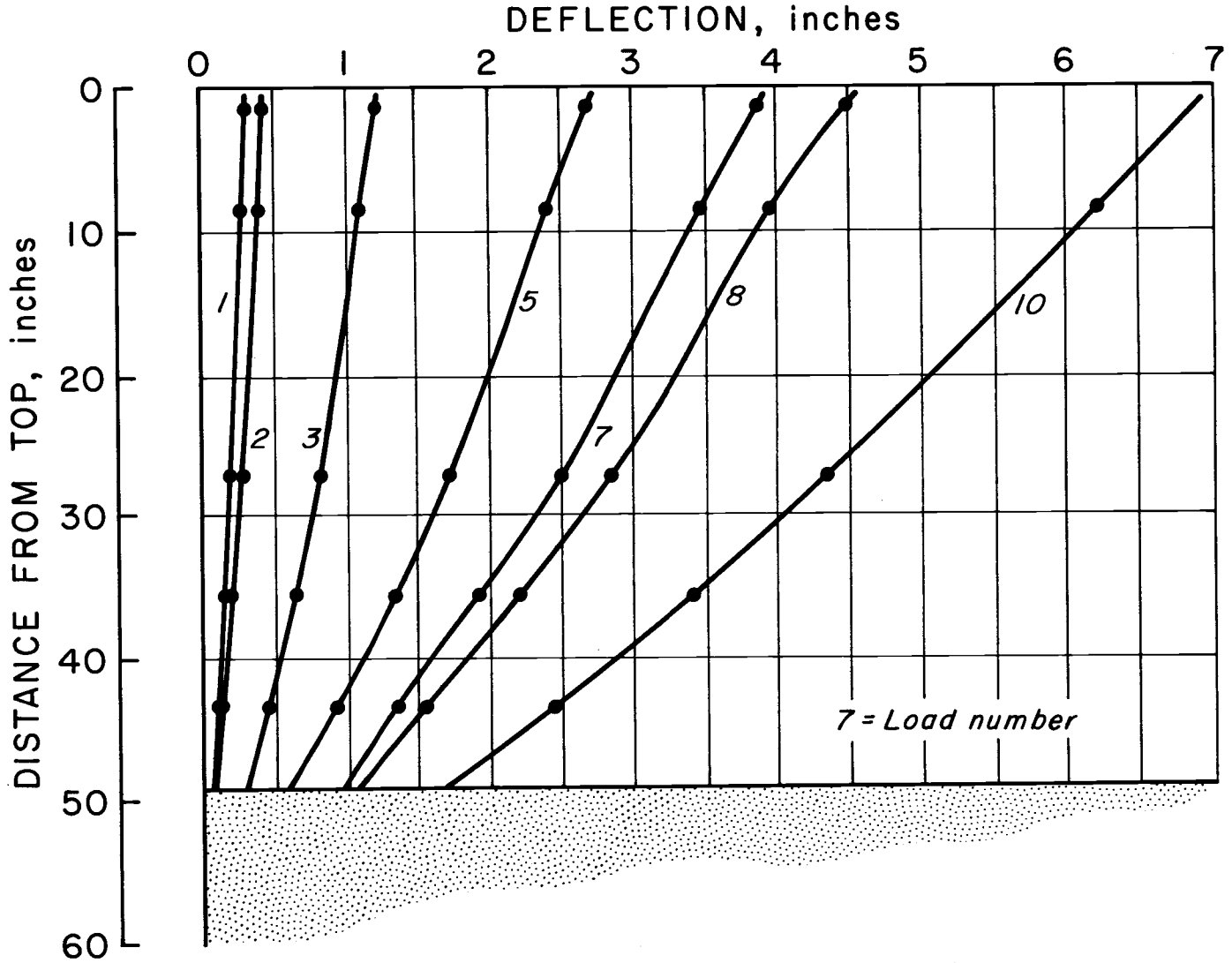

Figure 61. Deflections during failure (Series III).

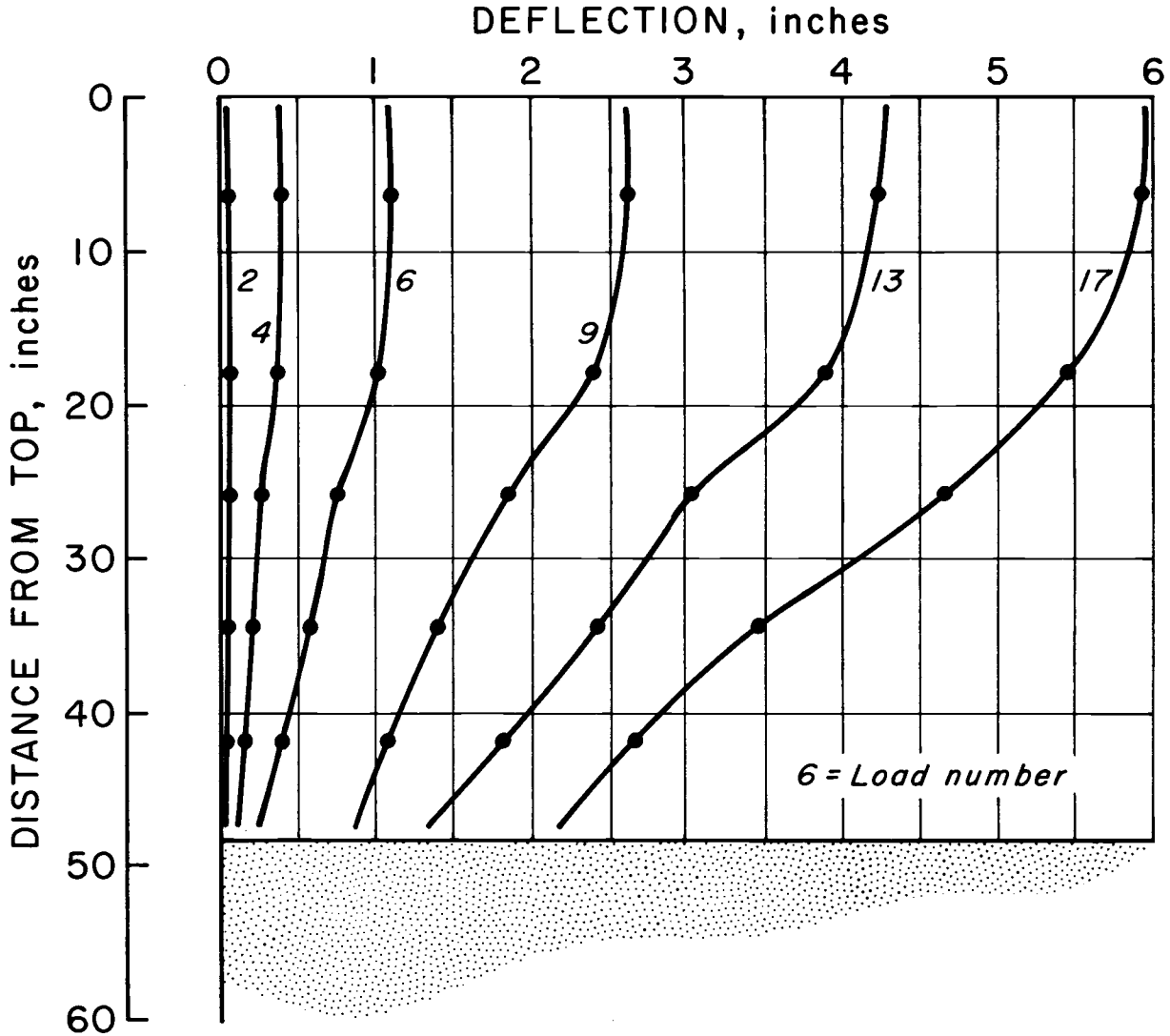

Figure 62. Deflections during failure (Series IV).

Sheetpile Deformations

After cells had been loaded to failure, the sheetpiles were carefully removed for examination. The sheetpiles at the front, side and back portion of each cell showed distinct differences in deformed shapes.

Figure 63 shows the typical shape of the front sheets from Series I, II and III. The sheetpiles from Series IV (zero embedment case) exhibited little permanent deformation. The level of the dredgeline relative to the sheets is indicated in the photos by a dark line.

Figure 64 shows a comparison of the deformed shapes of the front sheetpiles.

An outline of the sheetpiles was traced on paper to study the geometry of the deformations. Figures 65 through 68 show a sketch of the deformed shape for each sheetpile of the final stages of testing.

The front sheetpiles for Series I and III (two feet of embedment) had almost identical deformed shapes (see Figures 65 and 67). The sheetpile embedment was sufficient to essentially "fix" the sheets, even during large overturning rotations. A plastic hinge formed in the steel at a depth of 6.3 inches (0.26D) and 5.0 inches (.21 D) below the dredgeline for Series I and III, respectively. The front sheetpile for Series II (12 inches of embedment) showed the incipient formation of a hinge at a depth of 6.1 inches (0.51 D) below the dredgeline. The sheetpiles for Series IV (no embedment) were essentially straight, even during severe cell rotation. In all cases the angle the front sheetpiles made with the vertical was measured. It was then possible, from the geometry of the deformed sheet, to define at the end of testing, the shape of the sheets below the dredgeline.

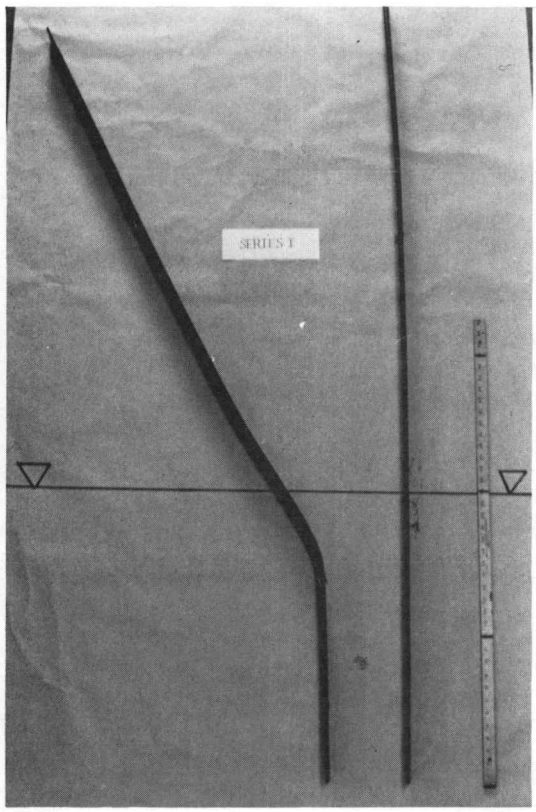

(a) Series I.

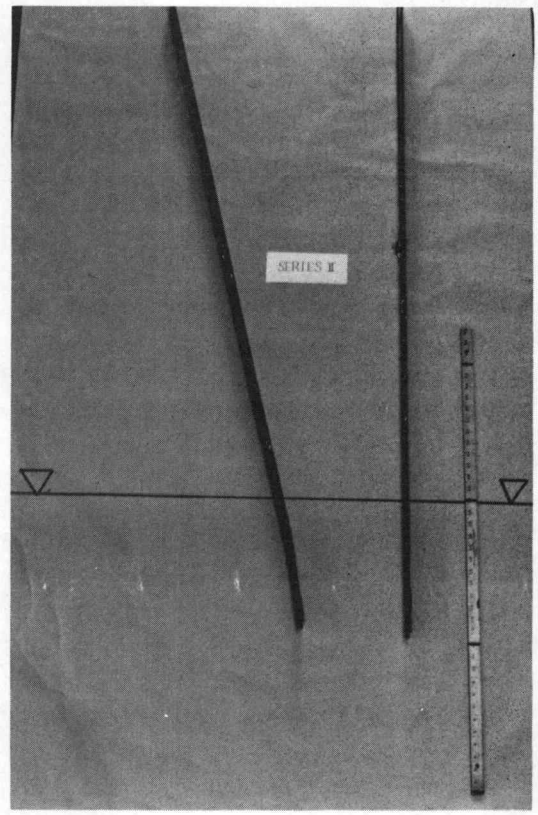

(b) Series II.

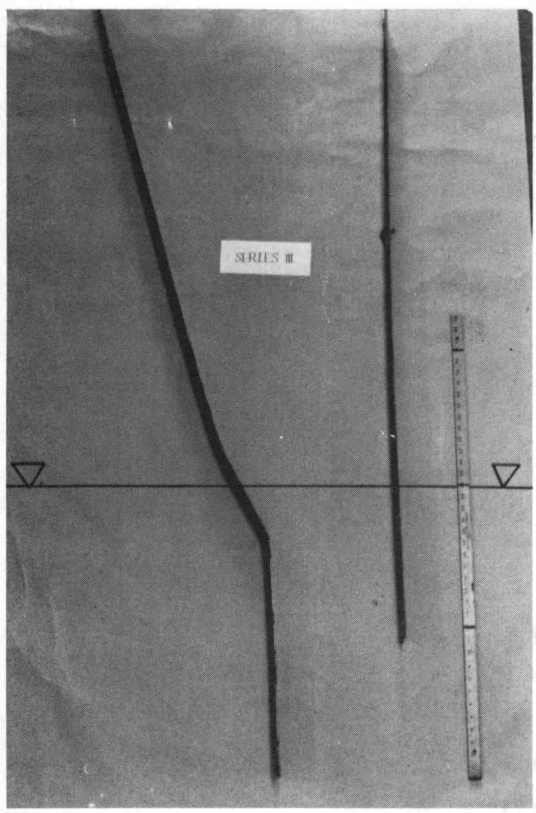

(c) Series III.

Figure 63. Typical deformation front sheetpiles.

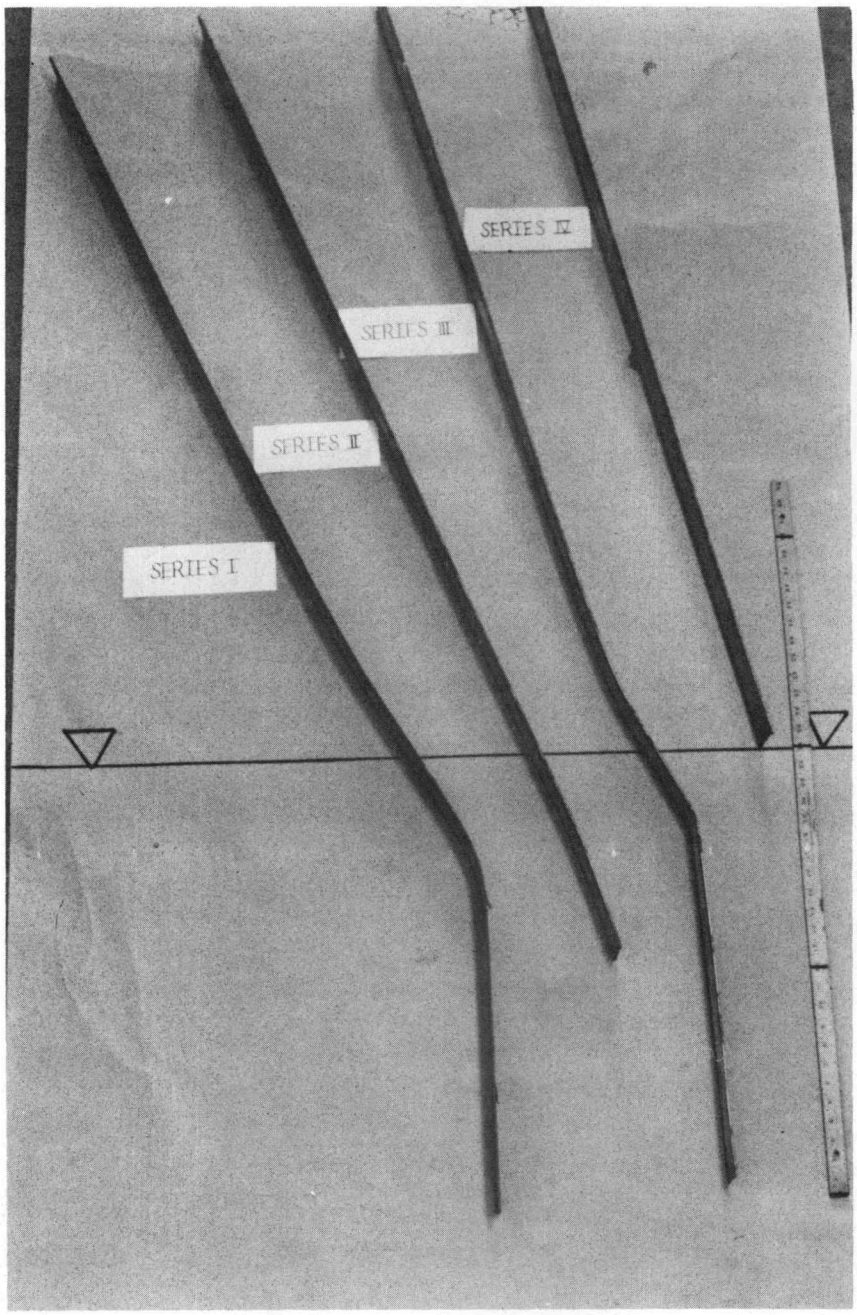

Figure 64. Summary of deformation of front sheetpile.

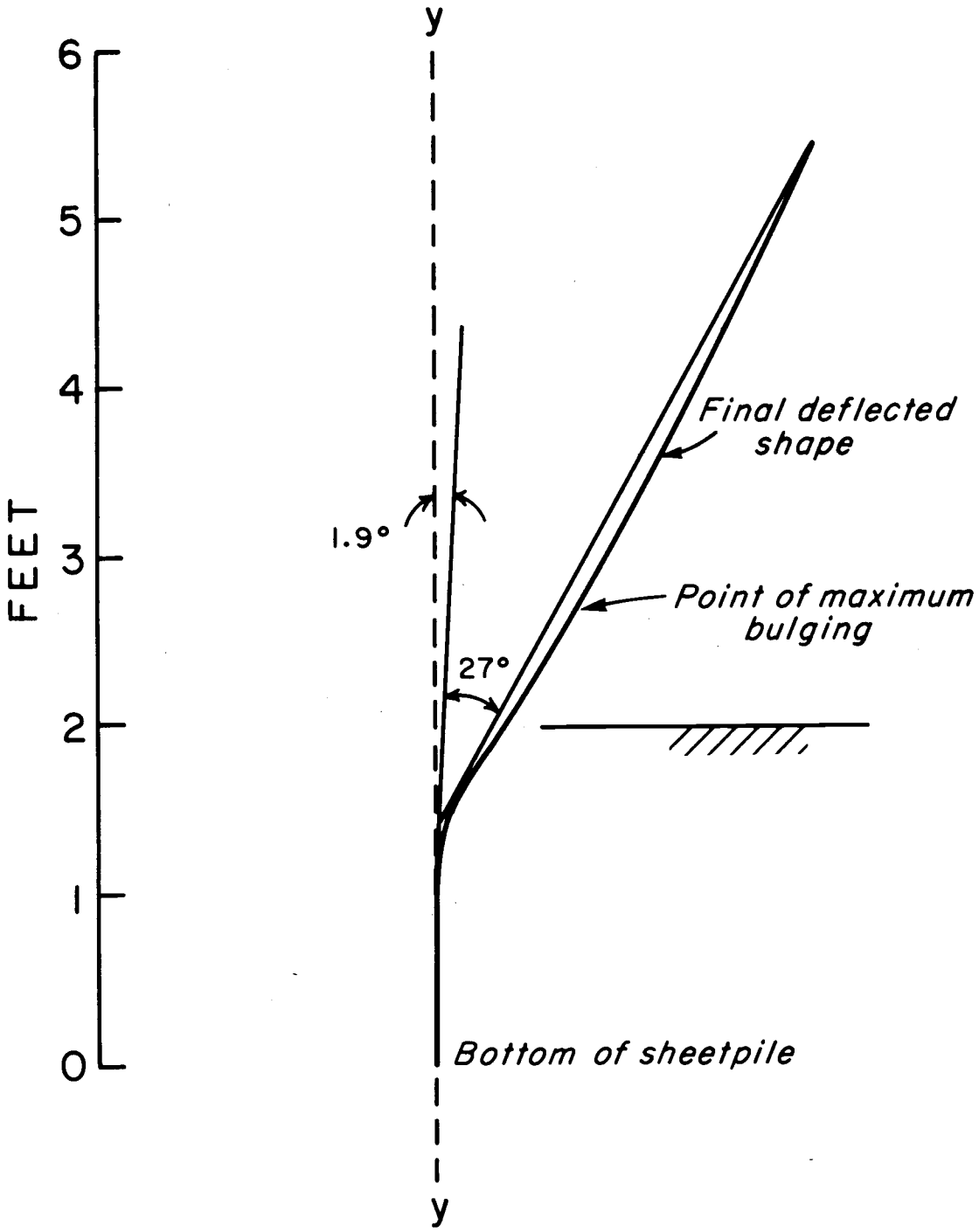

Figure 65. Deflected shape of front sheetpile (Series I).

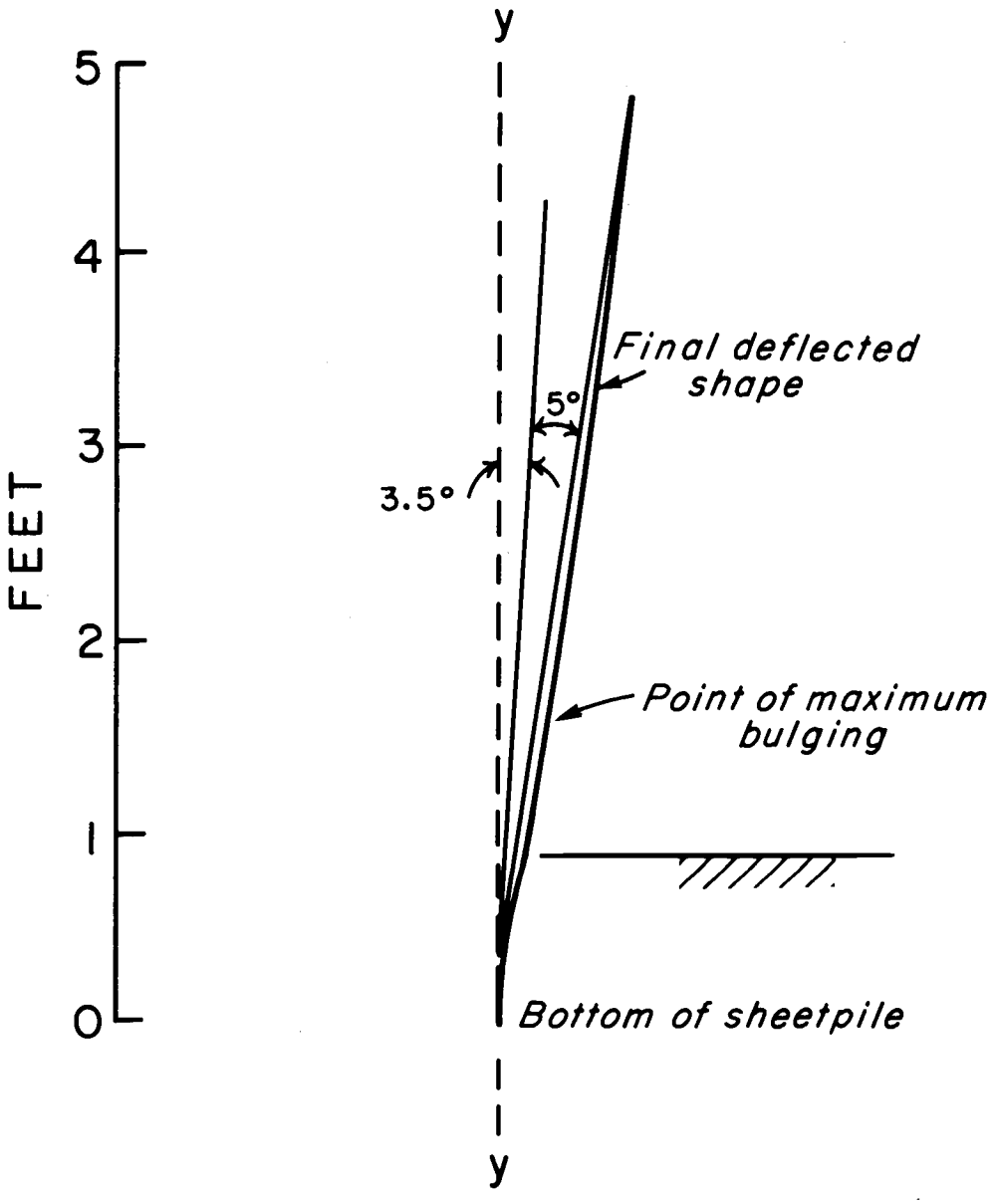

Figure 66. Deflected shape of front sheetpile (Series II).

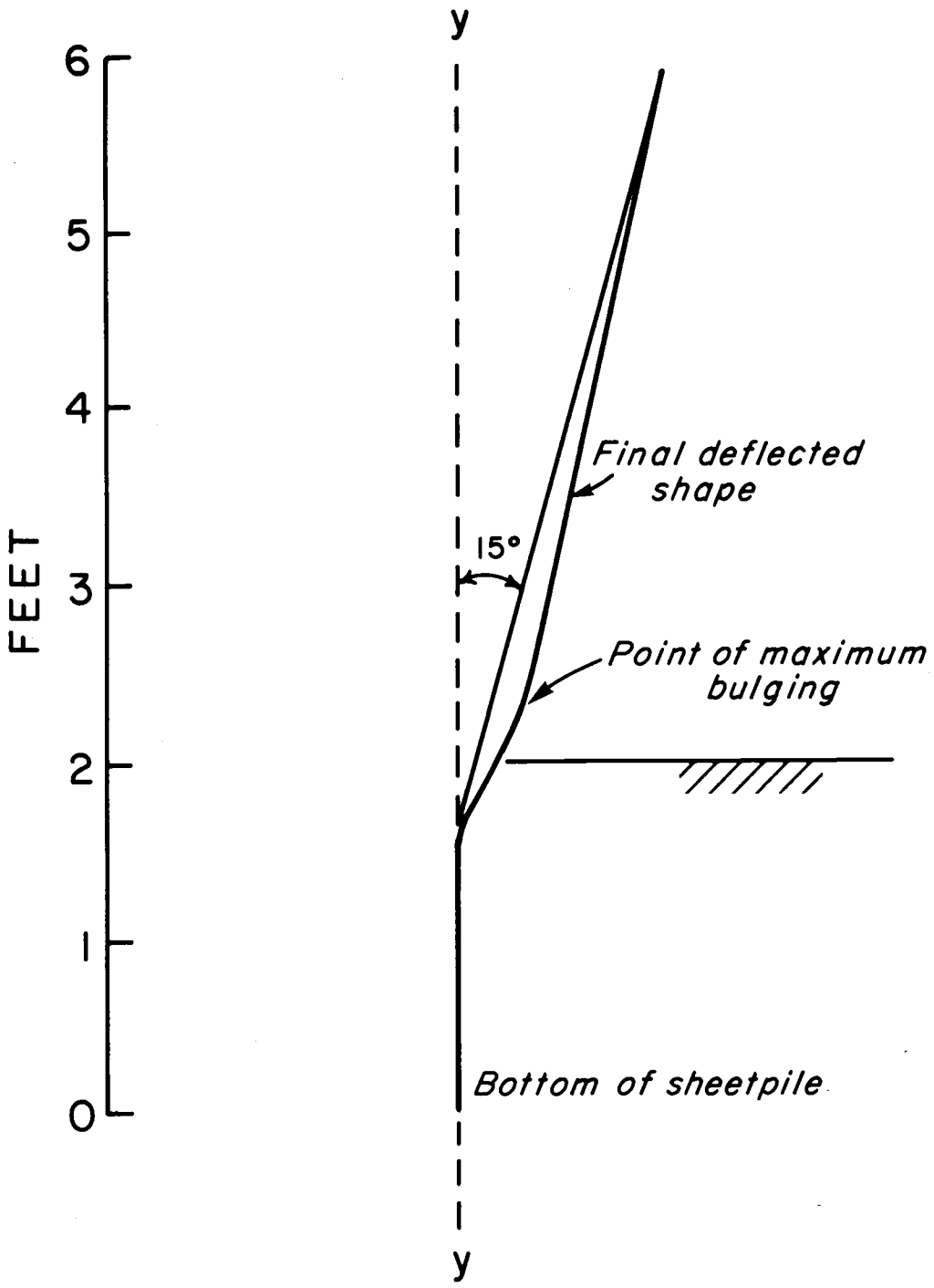

Figure 67. Deflected shape of front sheetpile (Series III).

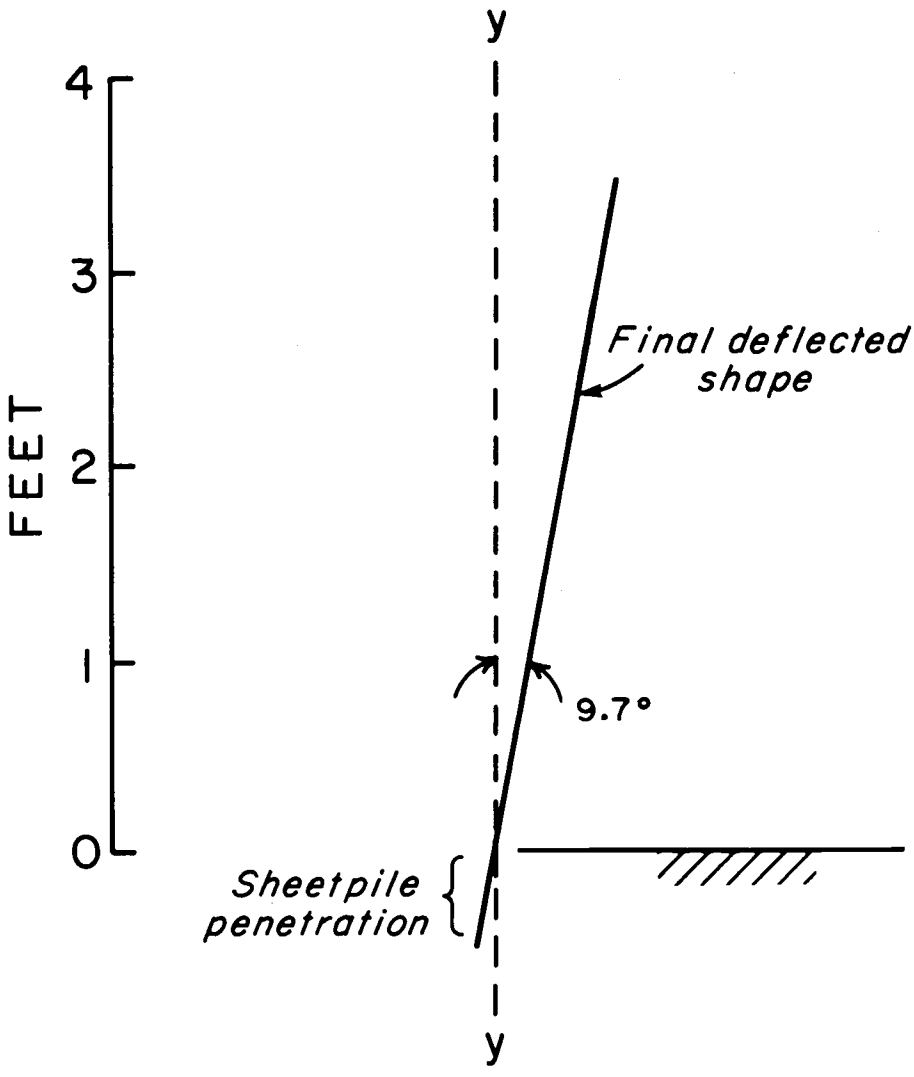

Figure 68. Deflected shape of front sheetpile (Series IV).

stresses for the uncorrected bending stress were plotted for all the sheets at the full cell stage. The values of hoop stress at the front sheet (P1) were consistently higher than the other sheets. The true hoop forces were calculated as the average between the value at P1 and the average values of P2, P3, and P4. The average differences between the two values and the true hoop stress calculated for all sheets at all levels was $\pm$ 13.2 percent. The hoop stresses at position P1 for all levels were, therefore, reduced by 13.2 while hoop stresses at positions P2, P3 and P4 were increased by 13.2 percent. The contribution to the total bending stress in the web due to lateral soil pressure is, therefore, relatively small. Consequently, this same correction was applied to subsequent stages of testing (such as backfill), even though the lateral pressures may vary from front to back.

In summary, the hoop stresses were calculated from measured strains through four steps: 1) apply Hooke's Law for a biaxial stress field to obtain stresses at each face of the web, 2) calculate, from the combined stresses acting on a face, the component of horizontal bending stress, 3) determine the hoop force (or stress) using Figure 43, 4) correct for orientation of sheetpile's interlock.

Calculations, based on the measured coefficient of interlock friction, indicate that, even at failure during overturning, the major principal stress in the sheetpile webs, σ_1, is rotated only about 13° from the horizontal axis. Since backfilling and surcharging did not cause any observable interlock displacement, the vertical shear stresses in the webs present during these loading stages must have been fairly small. The assumption that the hoop stress represents a principal

stress is, therefore, reasonable, even at side sheetpiles (P2 and P3), and even during overturning.

The sheets along the back side of the cell remained essentially straight for all cells. During severe tilting or rotation of the cell, the sheetpiles along the back side tended to lift out of the sand. Consequently, no plastic hinge formed. A slight inward bulge was observed during cell failure due to the cable loads. These deflections, however, were small, due to the distribution of the cable force by the wood blocks.

The amount of sheet deformation near the dredge line decreased from the front of the cell towards the arc sections. At failure, the sheetpiles at the sides of the cell (i.e. along the centerline-to-centerline axis) showed varying degrees of web buckling near the dredge-line. Deformation of sheetpiles adjacent to the Y-connector were significantly reduced by the added stiffness of the Y-section.

Cell Distortion

Figures 69 through 72 show a cross-sectional view of each cell at the end of testing. Distortion of the cell was continued well past the "point of failure" (i.e. the maximum applied lateral load). Overturning of the cells was halted at arbitrarily selected stages. The shapes of the cell, therefore, are not directly comparable from one test to another.

Note that the sheets at the front of the cell are almost parallel to those at the back side. The angle that the sheetpiles forms with the vertical was measured for Series I, III and IV. The angle of deflection for Series II was calculated from dial gage data. In all cases the difference in deflection angles was less than two degrees.

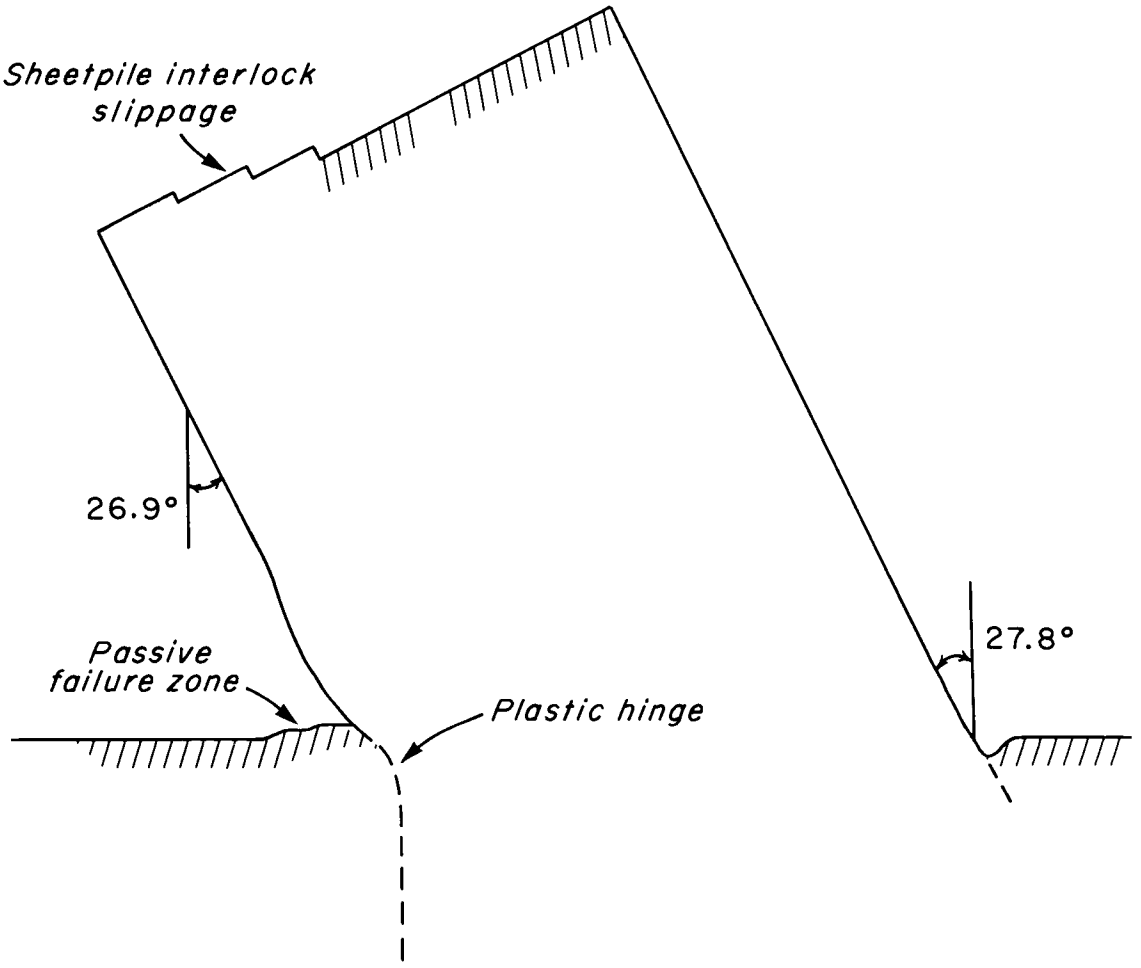

Figure 69. Cell distortion (Series I).

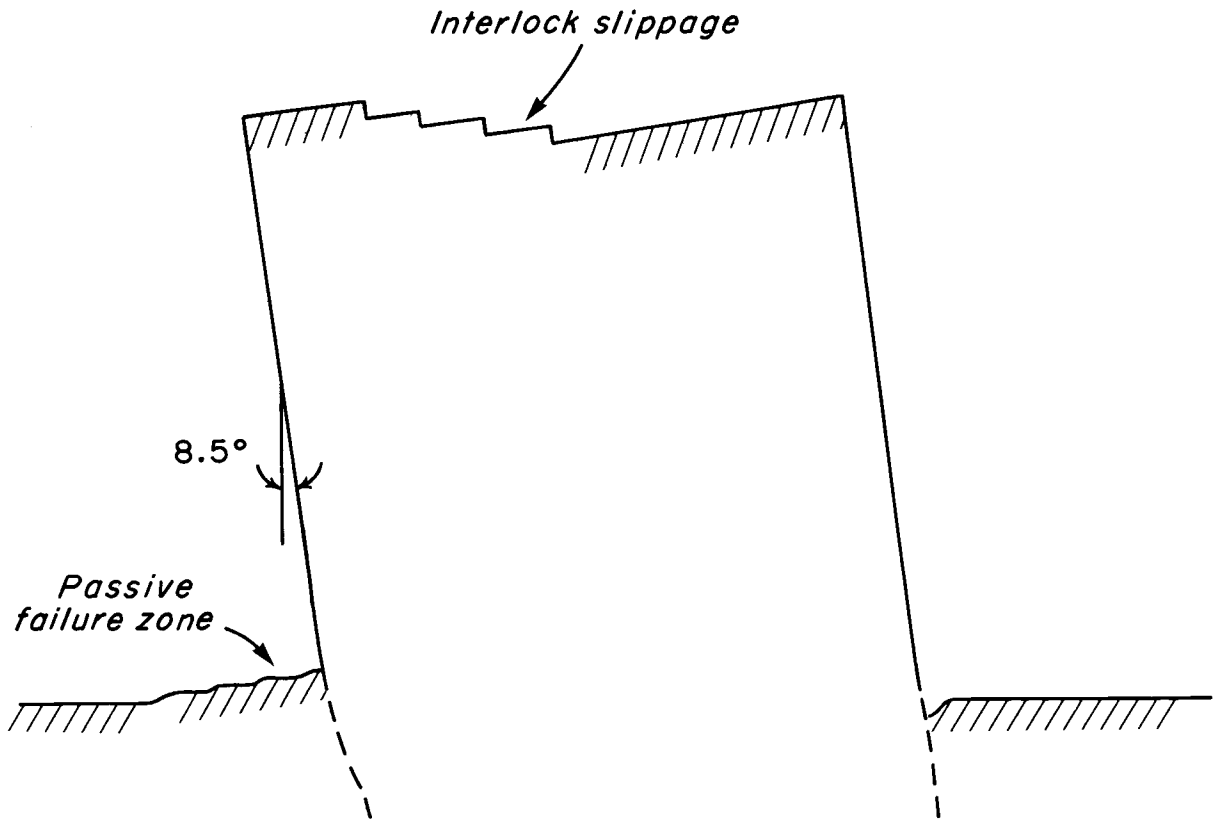

Figure 70. Cell distortion (Series II).

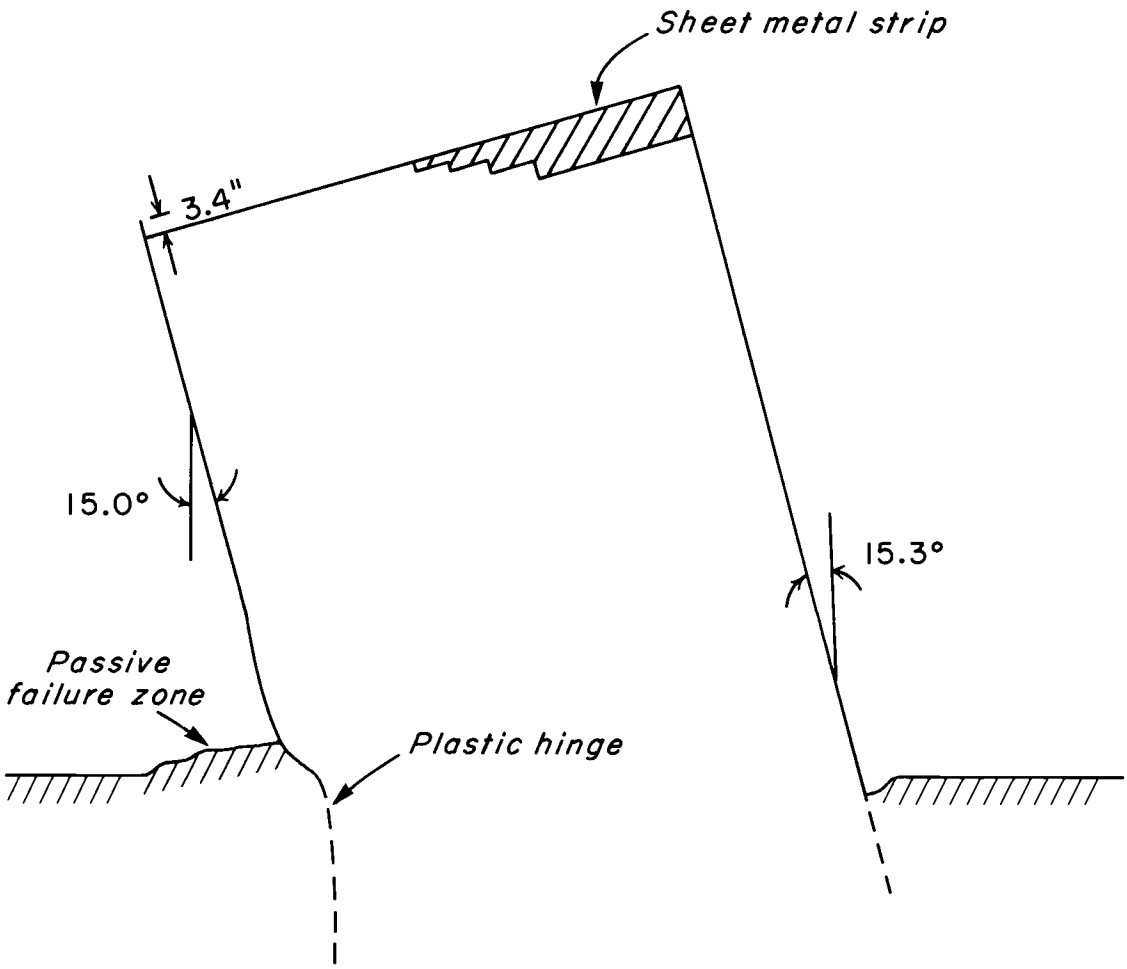

Figure 71. Cell distortion (Series III).

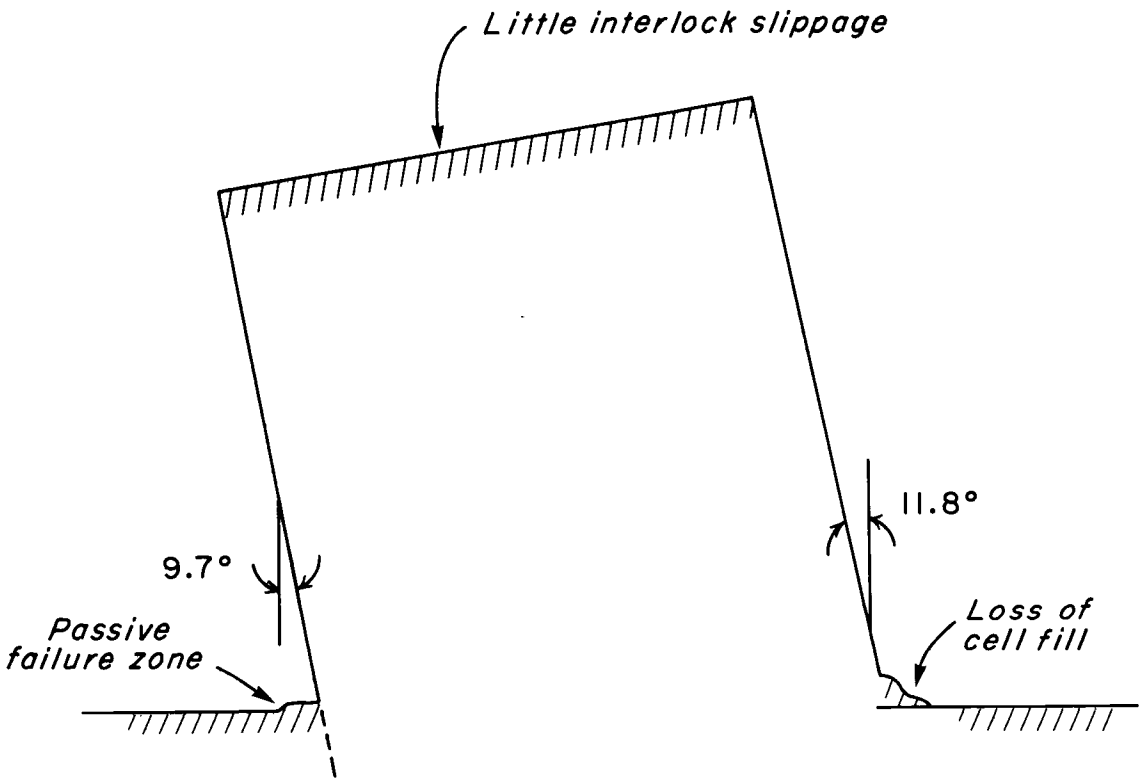

Figure 72. Cell distortion (Series IV).

The sheetpiles at the front and back, therefore, are parallel during cell failure.

Interlock Displacement

The deflections of the sheetpiles and the cell during testing stages (comparable to service loads) were very small. Interlock displacement during these stages was negligible. However, significant interlock slippage did occur during cell failure tests.

The pattern of interlock slippage varied from cell to cell, although, typically, the maximum slippage occurred near the bulkhead axis (cell centerline axis) and became smaller towards the front. There was no slippage of consequence behind the bulkhead axis. Interlock slippage did not occur beyond sheet number 54 (i.e., behind the back third of the cell). In all cases, the slippage pattern was symmetrical, i.e. equal interlock displacements occurred at the right and left hand sides of the cell (refer to Figure 26 for sheetpile location).

In Series I a maximum slippage displacement of about one inch occurred between sheetpiles No. 29 and 30 (and symmetrically at No. 58 and 1) and decreased to about half that amount at the front. Typically, the locations of interlock slippage were separated by several sheets which showed little or no slippage. No slippage of the interlock occurred behind sheetpile No. 30 (i.e., in the back half of the cell).

In Series II the maximum slippage (about 1/2 inch) occurred between sheetpiles No. 2 and 3 (and on the opposite side, between sheetpiles No. 26 and 27). Slightly less slippage occurred between sheetpiles No. 56 and 57, No. 5 and 6, and No. 8 and 9. No slippage was observed behind sheetpile No. 56 (approximately the bulkhead centerline).

The maximum interlock slippage (0.75 inches) in Series III occurred between sheetpiles No. 9 and 10 (and symmetrical, between sheetpiles No. 20 and 21). Sheetpile interlocks between the Y-connectors and the point of maximum slippage, displaced approximately one half inch. Smaller displacements (between 1/4 and 1/2 inch) were observed between the "stepped" sheetpiles although measurements were hindered by the presence of a four inch wide strip of sheet metal used to contain the cell fill above the "stepped" sheets. Approximately 0.75 inches of slippage was again observed between sheetpiles No. 54 and 55, although the displacement at the symmetrical location (sheetpiles No. 35 and 36) was only 0.25 inches.

Interlock slippage in Series IV was significantly lower. Displacement of 0.25 inches were observed between sheetpiles No. 57 and 58 and No. 27 and 28. All other interlocks showed very slight or no movement at all.

Movement of the Sand

To accurately analyze cellular bulkhead behavior under lateral load (especially at or near failure), one must be able to define the state of stress and movements of the soil below the dredgeline, in the backfill and within the cellular structure. It was felt that considerable insight into the contribution of the cell fill to bulkhead behavior could be gained by monitoring the deformation of the sand surface in the cell, the movement of sand at the dredgeline in front of the cell and the movement of the sand mass within the cell.

Surface Deformations of the Cell Fill

Deformations of the sand surface at the top of the cells were noted in two of the four models tested, Series I and II. Figure 73(a) shows a plan view of the cell No. 1 indicating the pattern of the terraces developed at the sand surface during pullover tests. A typical cross-section of one such sand terrace is shown in the inset. The vertical offset at the center of the cell (section A-A) was approximately one inch. The vertical offset decreased to about one half inch on other terraces towards the back of the cell. Note that the surface pattern of the individual terraces are wavy.

Figure 73(b) shows the two distinct terraces found at the surface of the cell for Series II. The terrace near the front of the cell had a vertical offset of about 0.8 inches while the one towards the back portion had an offset of about 0.4 inches.

The cell in Series III did not show any distortion of the sand surface. Possibly, the sand above the "stepped" sheets (which was restrained by a strip of sheetmetal around the back perimeter of the cell) was insufficiently restrained and essentially masked the displacements occurring in the cell fill below.

The surface of the cell in Series IV also did not indicate any offset terraces, but rather, rotated continuously with the cell as a smooth plane of sand.

It is interesting to note that as the cell rotated, approaching failure, the sand surface at the back of the cell rose with the sheetpiles while it subsided at the front of the cell. The slippage between the sand and the sheetpile of the front of Cell No. 2 for example, amounted to 2.68 inches. The phenomenon of sand rising at the back and

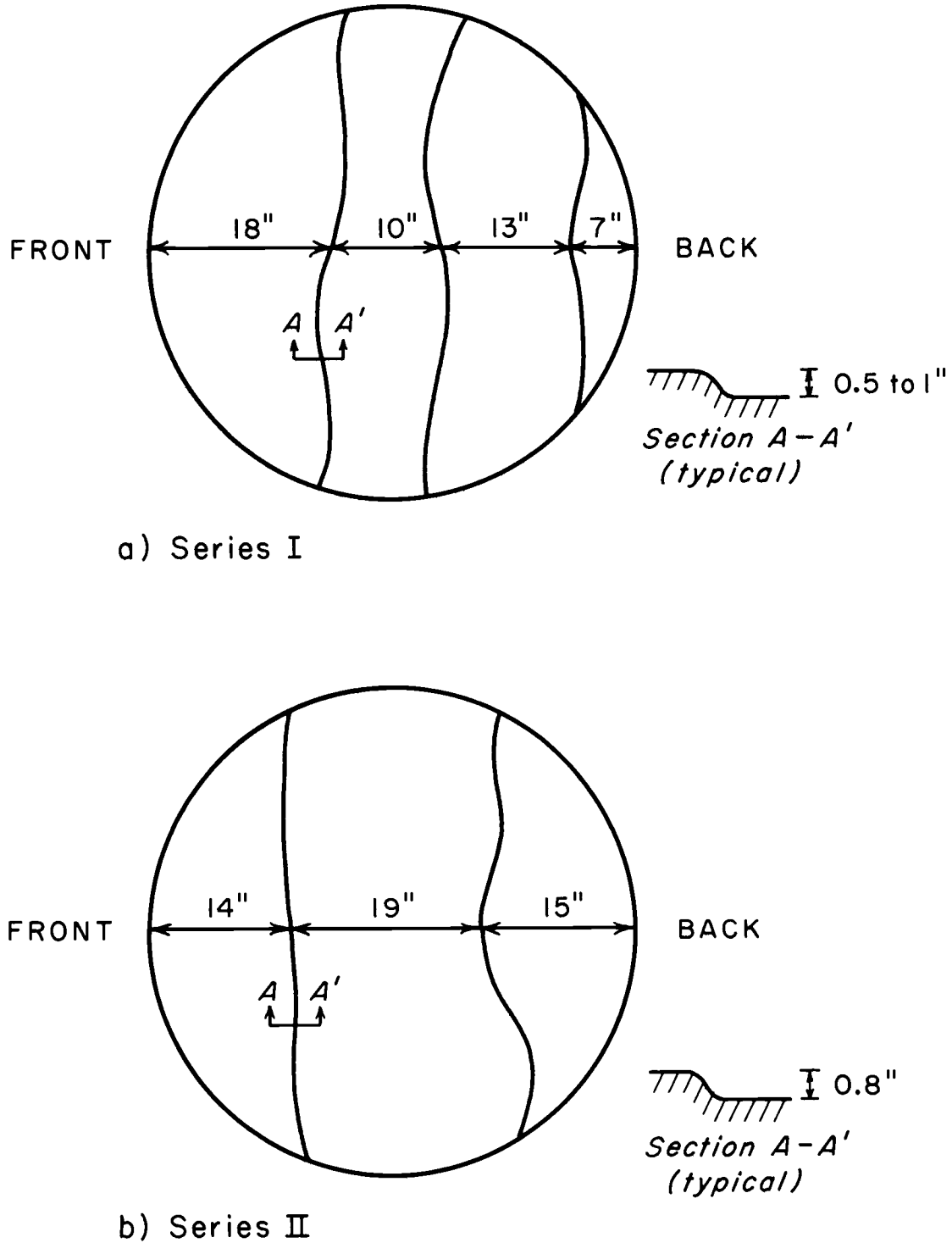

Figure 73. Surface deformation of cell fill.

subsiding in the front of the cell was also observed in previous model studies (Cummings, 1957).

Sand Movement at the Dredgeline

During cell failure, the sheetpiles at the toe tended to rotate into the sand at the dredgeline. A zone of passive failure was then formed along the front portion of the cell.

The plan view of the failure zones for the four cells are shown in Figure 74. Typically these failure zones consisted of a semi-circular or quasi-rectangular area of disturbed soil with a width (measured radially) of approximately 12 to 16 inches at the front of the cell. A typical cross-section of the failure zone (see Section A-A, Figure 74(a)) showed the disturbed zone to consist of a series of stepped terraces. As the sheetpiles continued to rotate into the sand, successively higher terraces were formed.

Note that the shape of the failure zone for Series I and III (both with about two feet of embedment) were almost identical. Although the Series II cell had no initial embedment, the front sheetpiles penetrated the sand at the toe during cell overturning and subsequently rotated into the sand. The resulting disturbed zone showed a more pronounced width at the front (sheetpile No. 15) than near the arc section.

The disturbed zones shown along the back of the cells were the result of cell rotation. As the cells rotated, the sheetpiles at the heel moved away from sand at the dredgeline, leaving a small depression approximately five inches wide. If there had been backfill behind the cells during failure, the effect of rotation would have been evidenced by a very distinct active zone behind the cell.

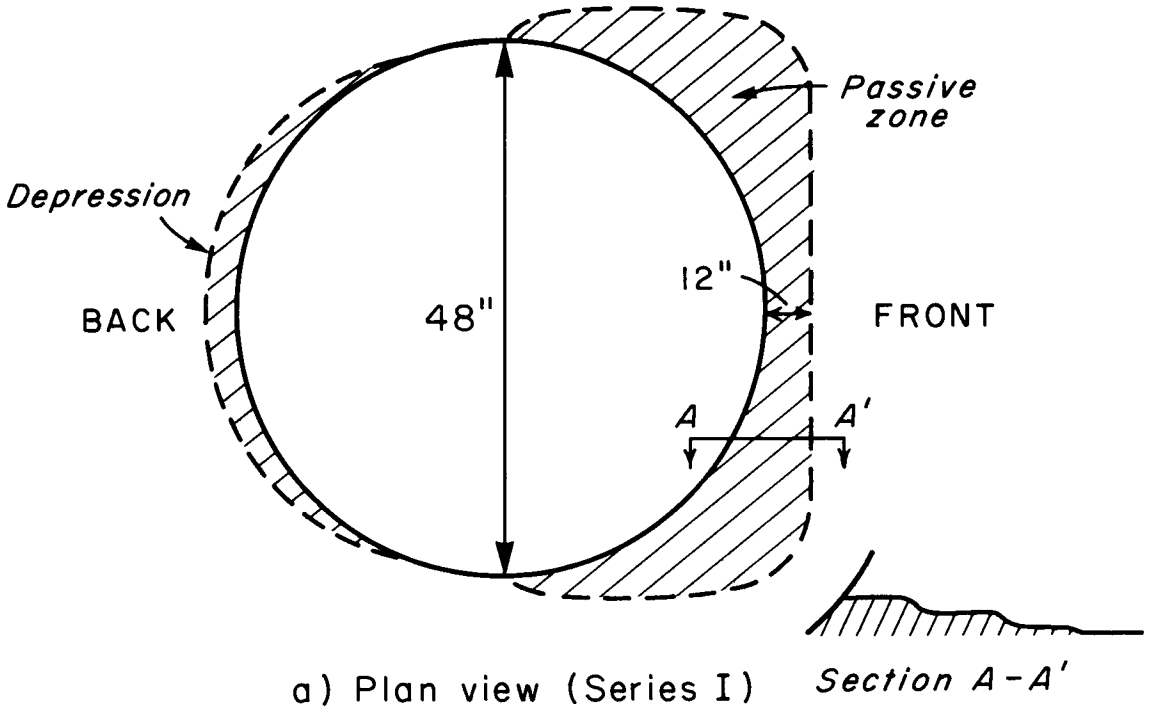

a) Plan view (Series I)

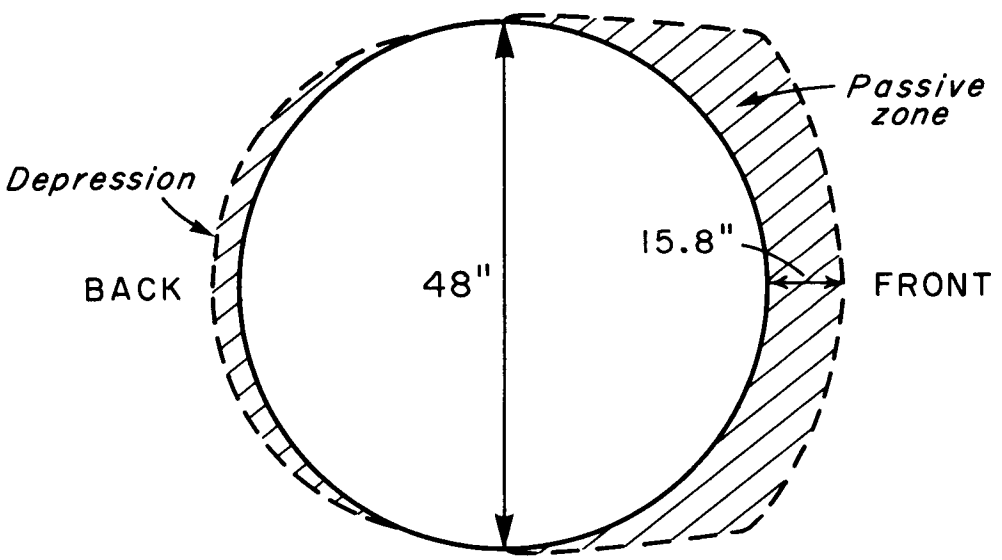

b) Plan view (Series II)

Figure 74. Disturbance of sand at the dredgeline.

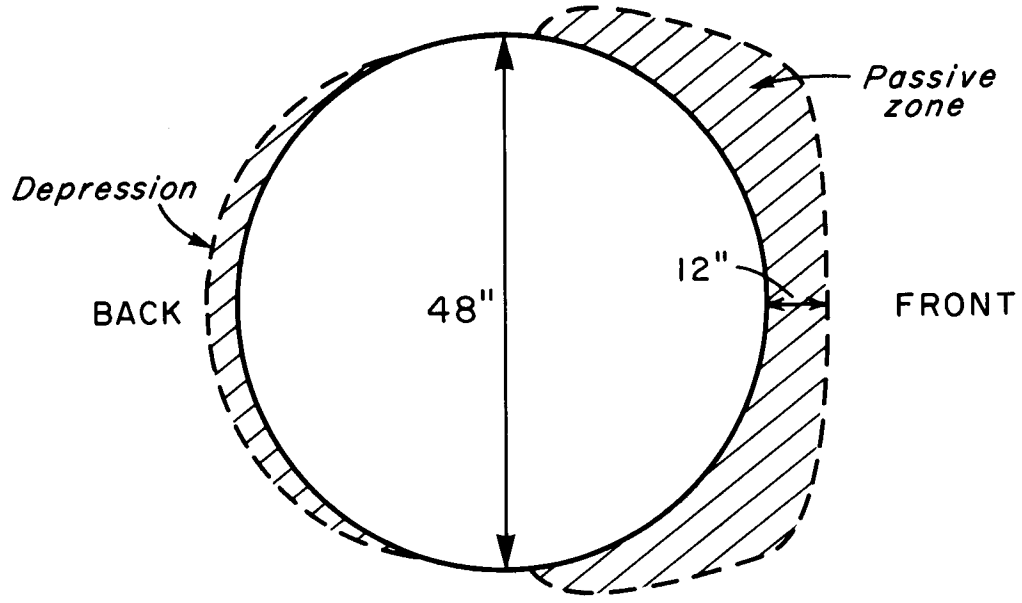

c) Plan view (Series III)

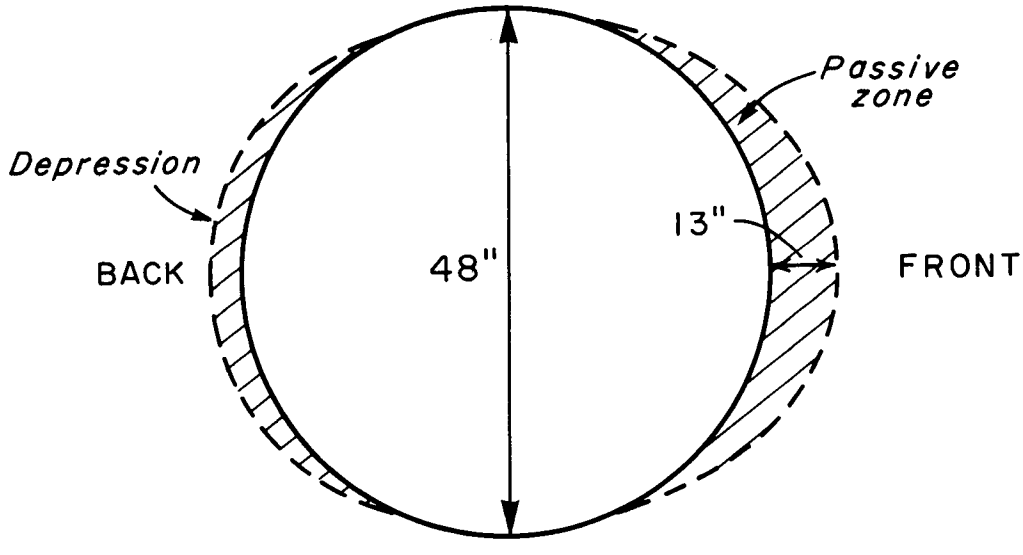

d) Plan view (Series IV)

Figure 74. continued

In the final stages of overturning of Cell No. 4, the sheetpiles at the heel lifted above the depression and cell fill ran out the back until the opening was covered.

Distortion of the Cell Fill

Formulation of a model for cellular bulkhead behavior must include a model for the distortion and the state-of-stress of the cell fill. It was felt that insight into the behavior of the cell fill could be gained, if one could define the pattern of failure planes within the cell fill. These planes were defined in the large cells by the method described below.

Thin colored wax strips (1/2 inch wide by 1/8 inch thick) were buried in the cell fill at various levels prior to testing. Wax strips (48 inches long) were placed at the center of the cell along the toe-heel diameter while shorter strips (24 and 36 inches) were placed at points near to the sides and parallel to the central wax marker. It was assumed that the wax strips did not affect the behavior of the fill. Wax strips were not placed in Cell No. 1 due to the presence of the pressure cells. At the end of testing (i.e. cell failure) the cell fill was slowly removed and the wax markers carefully exposed to minimize disturbance. Cracks, bends or displacement of the wax strips were recorded.

Figure 75(a) shows the cross-sectional view of Cell No. 2 at failure. Figure 75(b) shows a plan view of the cell indicating the typical location of the wax strips.

Figures 76 and 77 show sketches of the cross-section for cells No. 3 and 4, respectively.

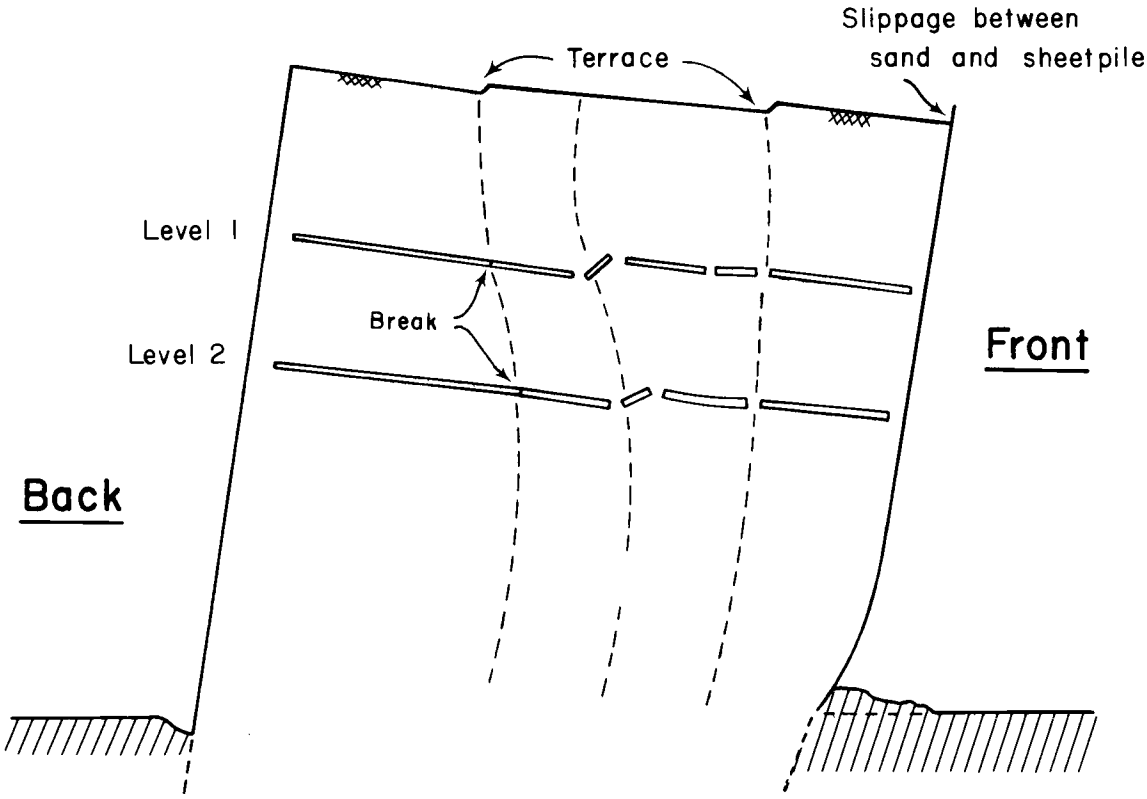

(a) Profile of cell fill

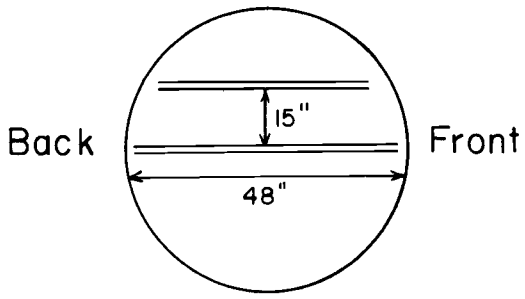

(b) Plan view of Level 2 (typical)

Figure 75. Distortion of cell fill (Series II).

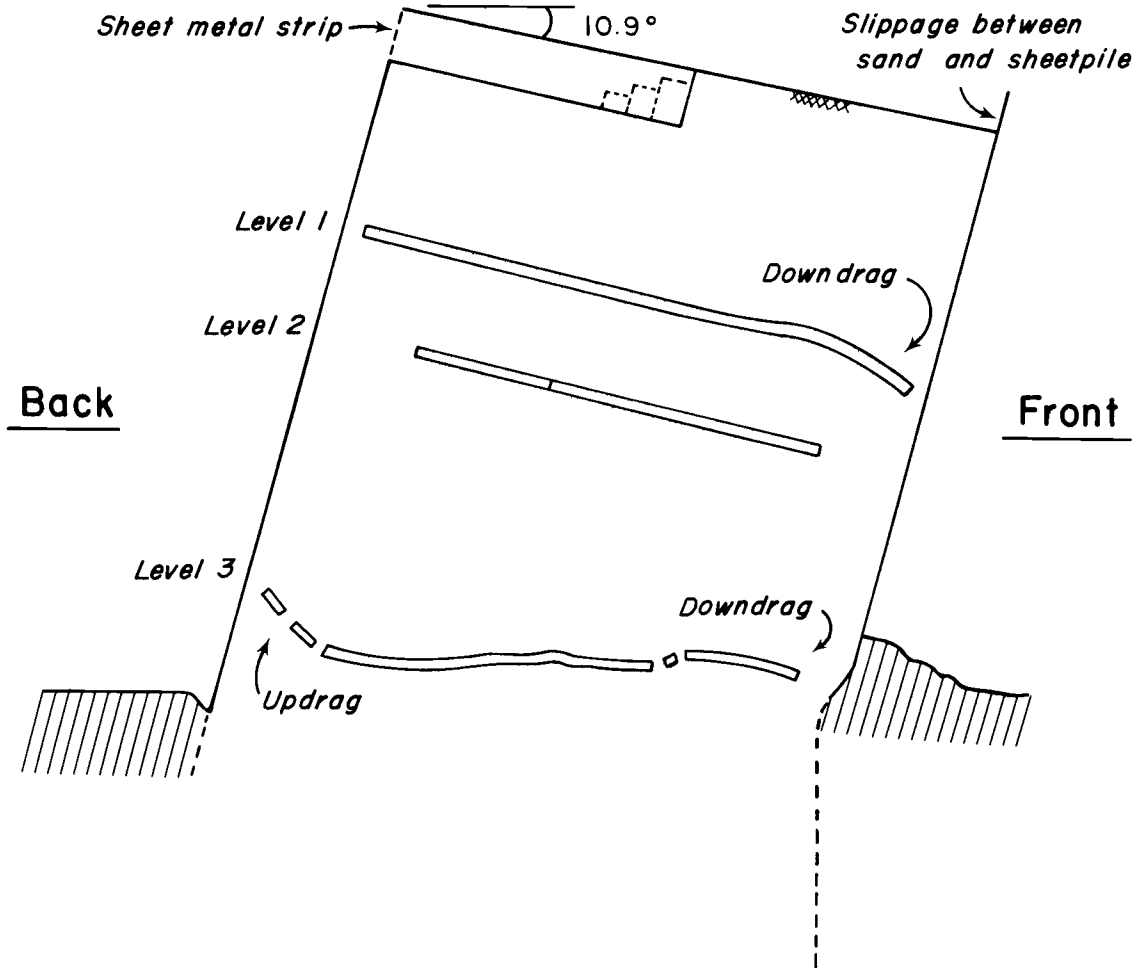

Figure 76. Distortion of cell fill (Series III).

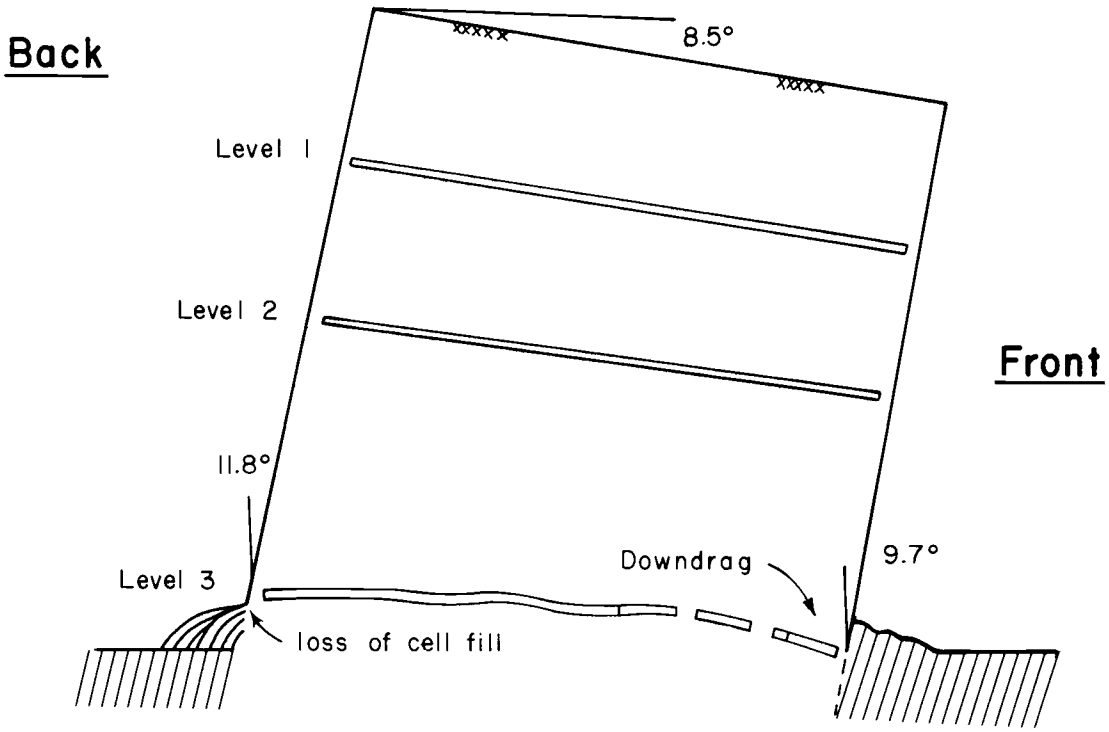

Figure 77. Distortion of cell fill (Series IV).

Small-Scale Model Study

The distortion of the wax markers provided significant information about the displacement of the cell fill under failure loads. The wax strips, however, were located at only three levels within the cell fill and the definition of zone of relative displacement would involve extrapolation between these levels.

A series of smaller-scale models was constructed to investigate the displacement of the cell fill throughout the entire cross-section. Thin beds of dyed sand were placed at several levels (see Figure 34) in the cell fill and in the surrounding sand mass. After failure, the cell fill and surrounding sand was grouted and the cells cut open (see the PROJECT DESCRIPTION section for a more complete account). Displacements of sand across the marker beds were reflected by distinct offsets in the dyed sands.

Figure 78 shows the typical geometry of small cell No. 1 at failure along with the plan view of the model.

Figures 79 and 80 show cross-sectional views of the cell fill for small cells No. 1 and 2 at various cuts. The location of the cuts given at the top of the figures refers to the distance of the cut from the unopened side of the cell (the cut at 12 inches is at the center of the cell). Note that the sand fill at the back of cell No. 1 was not saturated by the grout and subsequently fell out during the opening of the cell.

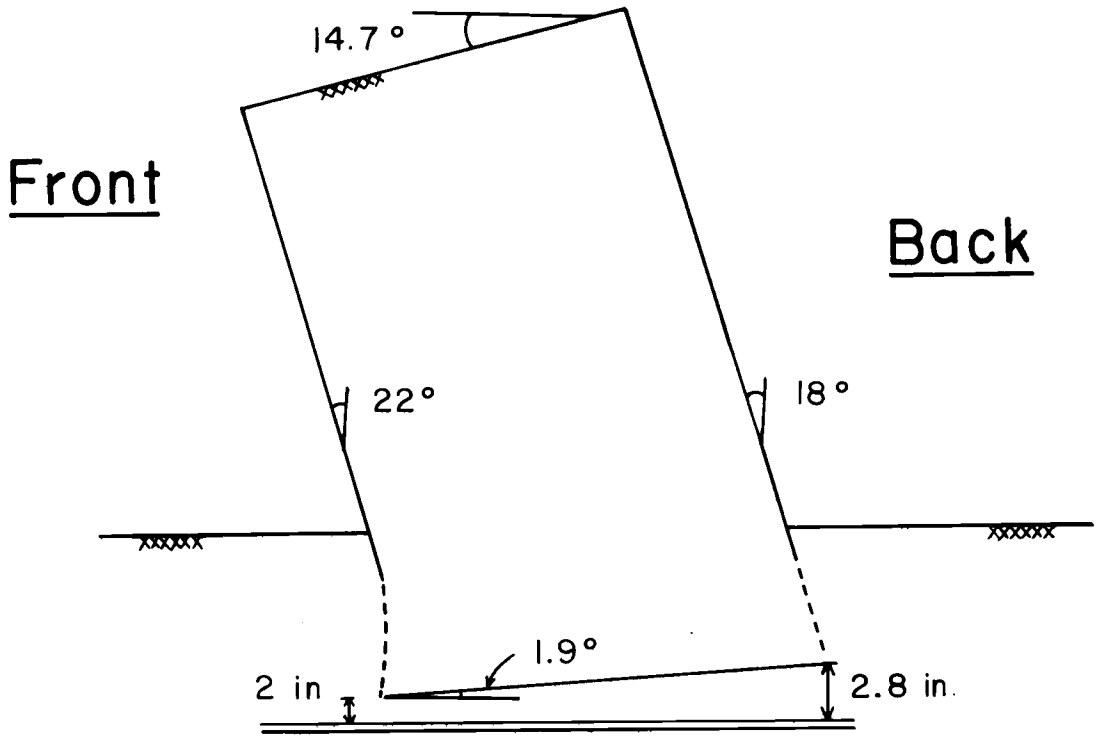

(a) Cell profile.

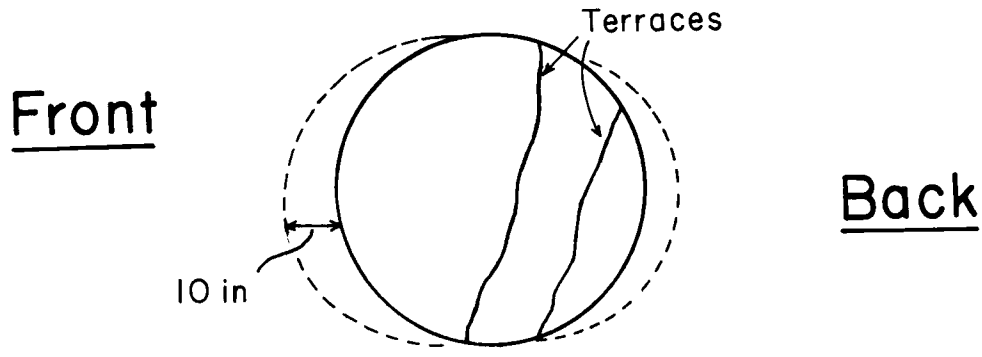

(b) Plan view.

Figure 78. Small Cell No. 1 at failure.

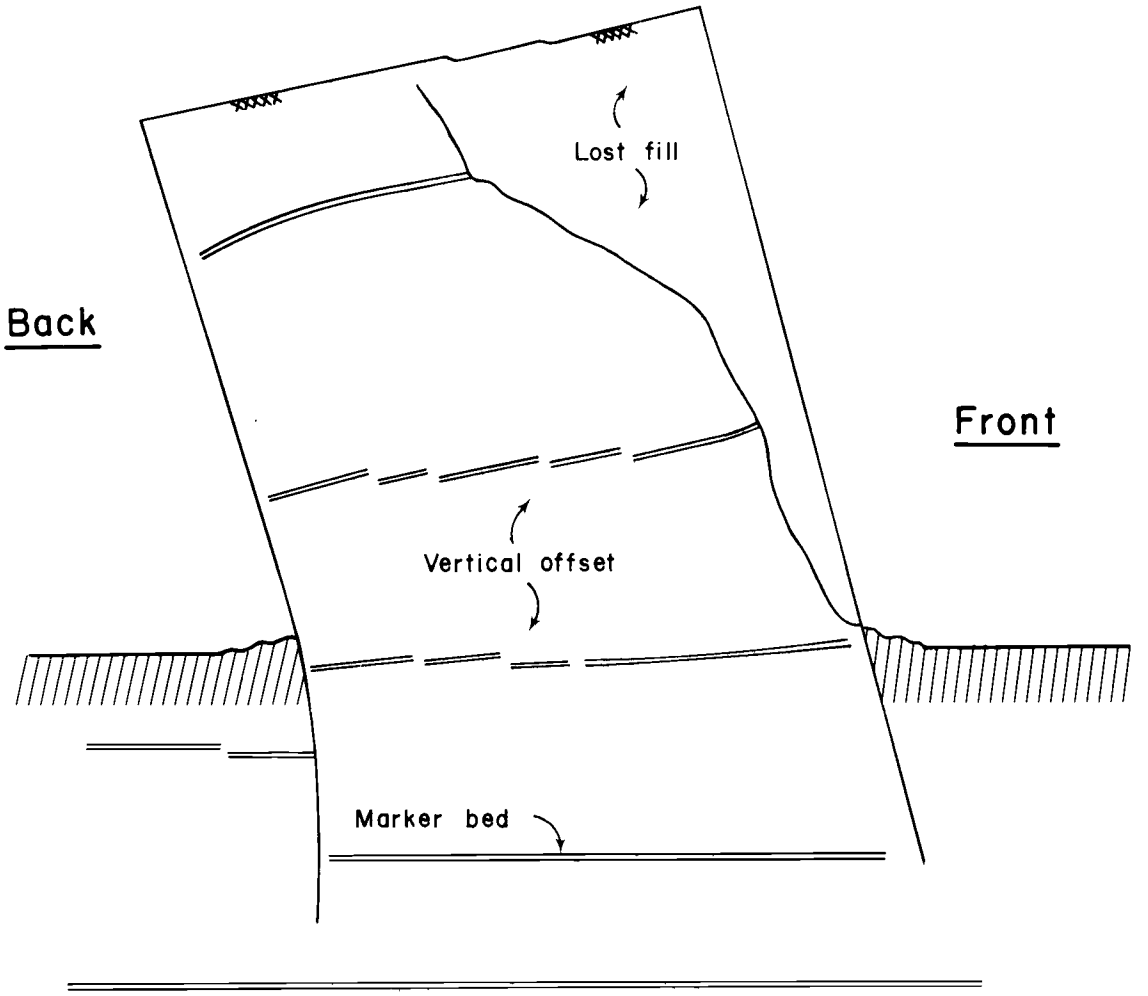

(a) Cut at 17-in. from undisturbed side

Figure 79. Distortion of cell fill (small Cell No. 1).

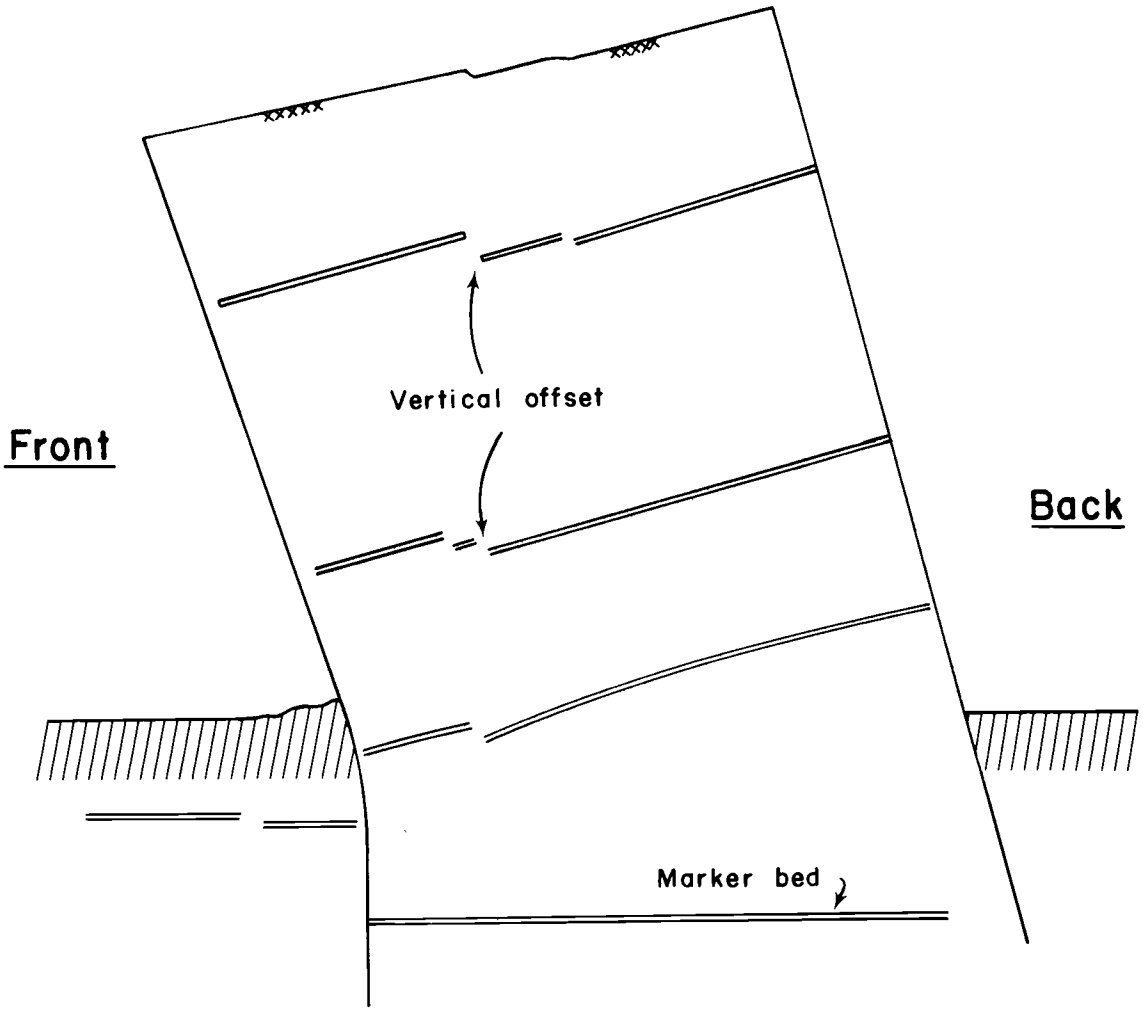

(b) Cut at center of cell

Figure 79. continued

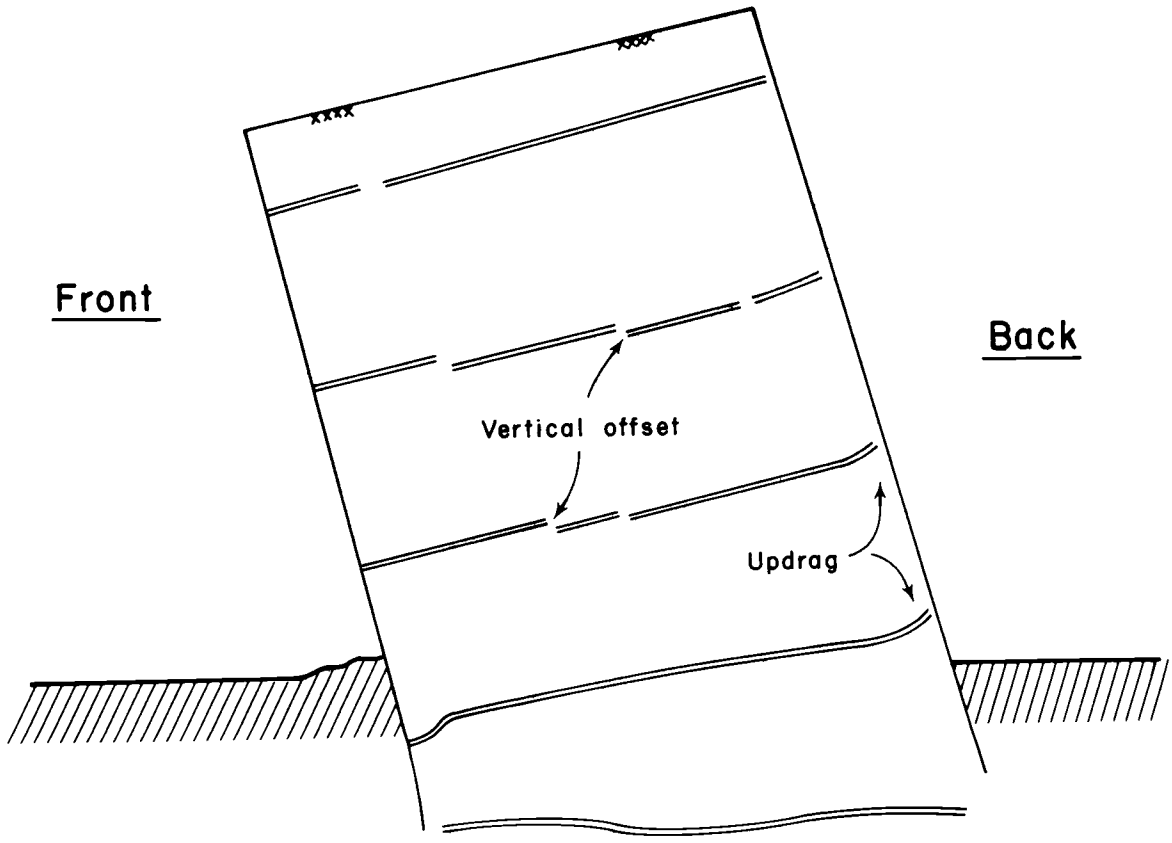

Figure 80. Distortion of cell fill (small Cell No. 2).

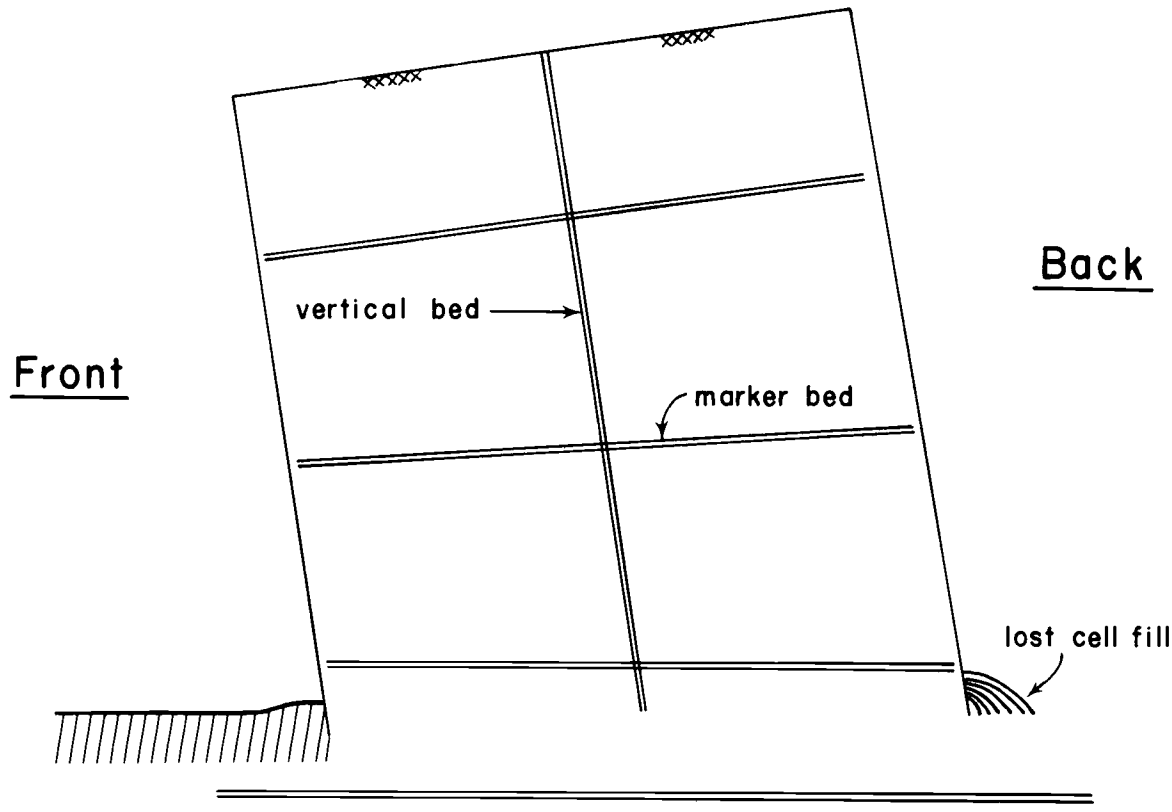

Figure 81. Distortion of cell fill (small Cell No. 3).

Figure 81 is the presumed shape of the cell cross-section of cell No. 3 (no embedment ease). In this case the grout did not harden sufficiently to support the open cells. The shapes of the marker beds were observed but the cell fill collapsed before measurements could be made.

Overturning Tests

Each of the large cells was failed by a cable-applied lateral load (see the PROJECT DESCRIPTION section). The load was applied 18.5 inches from the top of the cell for Series I, III and IV, and 21.2 inches from the top in Series II. The magnitude of the load was measured by a load element consisting of a 1/4 x 1" bar instrumented with 4 strain gages. Deflections of the front sheetpiles were measured during cell failure.

A plot of lateral force versus sheetpile deflection (at dial gage No. 1) is shown in Figure 82 for Cell No. 1. Typically, the load initially increased almost linearly with cell deflection, then reached a maximum and either leveled off or dropped slightly with increasing deflection. The load in the cable dropped off very quickly with cell movement. Points lying below the curve usually are indicative of late readings of the load element strains.

Figure 83 shows a comparison of the lateral load versus crest deflection curves for all four cells.

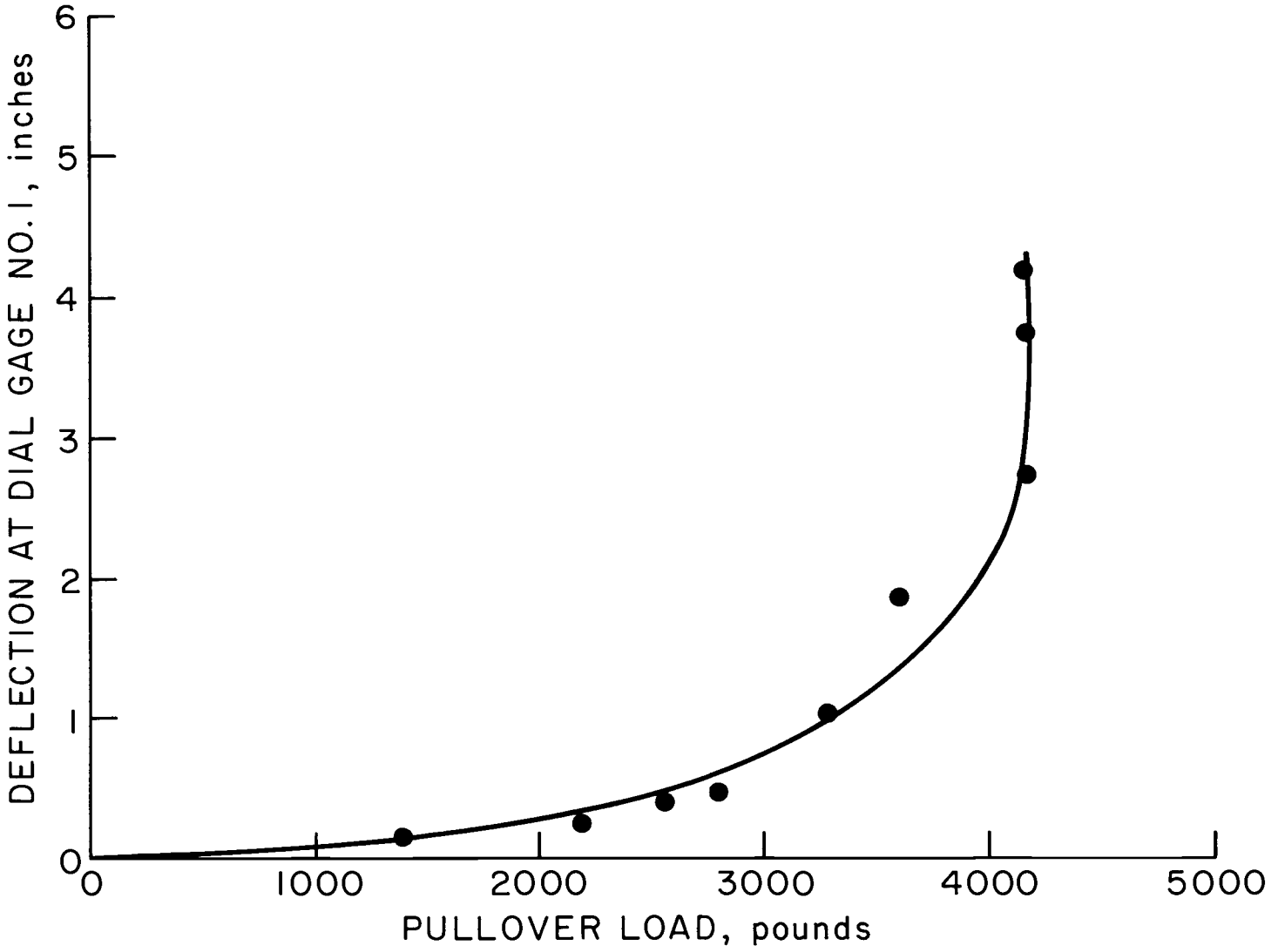

Figure 82. Deflection versus lateral load (Series I).

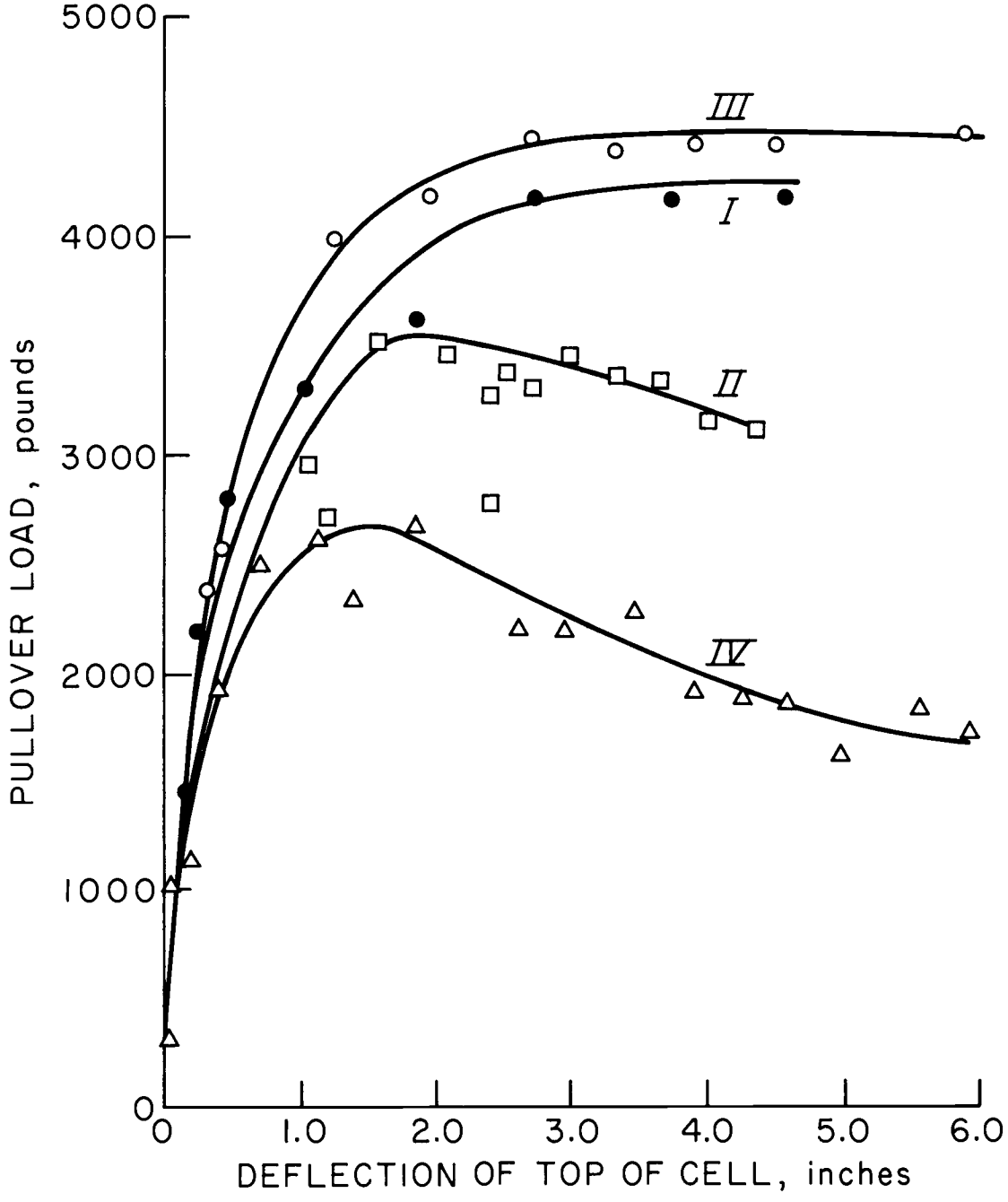

Figure 83. Crest deflection versus lateral loads.

Miscellaneous Tests

During the course of the main project several smaller investigations were conducted to resolve questions incidental to the main effort. To investigate the pullout strength of the model sheetpile interlocks, a series of tests were conducted on one inch wide test specimens (Pietrak, 1974). Test samples of various gage metals were tested on an Instrom Tension testing machine. Test results are summarized in Table 11.

Table 11.

Tests for Interlock Strength

Test No.	Strain Rate (in/min)	Sheet Metal Gage	Max. Load (lbs.)
1	0.20	24	55
2	0.20	24	59
3	0.50	24	60
4	0.10	24	55
5	.05	24	56
6	.20	26	36
7	0.50	26	41
8	0.10	26	41
9	0.20	22	87
10	0.10	22	86
11	0.10	24	58

One inch test specimens were also instrumented with four SR-4 type strain gages and tested in tension to investigate the magnitude of stress concentrations due to the crimped interlock. Stress-strain

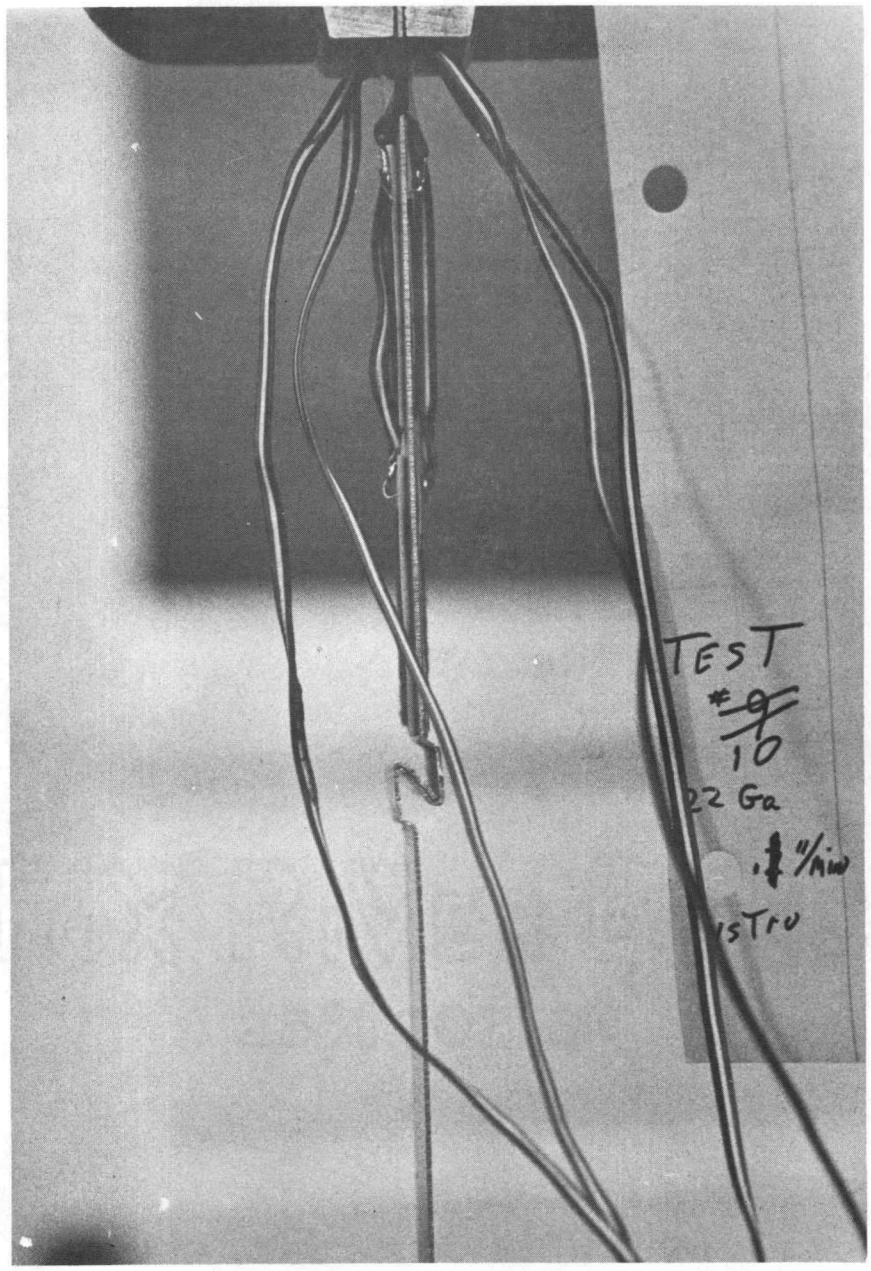

Figure 84. Typical sheetpile testing.

curves were developed for each gage location. It was found that, typically, the stresses due to interlock bending three inches away from the tip of the sheetpile were very low even while the metal near the crimp was yielding.

Figure 84 indicates the typical testing set-up.

Interlock Friction Tests

Since interlock friction plays an important role in the overall stability of the cell, it is important to evaluate the coefficient of friction for the steel interlocks.

A six inch specimen was tested in the device shown in Figure 42 for this purpose. An axial (or hoop force) was applied evenly over the six inch interlock. A shearing force, V, was then applied incrementally until slippage occurred.

At the moment of slippage, the forces acting on the test specimen are those shown in Figure 85.

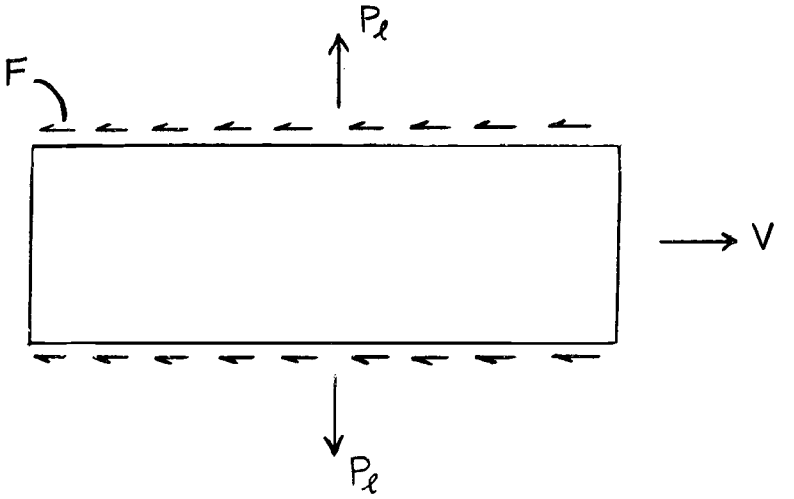

Figure 85. Forces acting on test specimen.

where V = shearing force

P_ℓ = total lateral force on interlock

F = total interlock friction force

For equilibrium, the resisting frictional forces, F, must be equal to the shearing force V. The total frictional force, F, acting along both interlocks is given by

$$F = 2 \cdot \mu_s \cdot P_\ell = V \tag{41a}$$

where μ_s = static coefficient of friction.

Therefore, the coefficient of friction, μ_s, can be calculated by

$$\mu_s = \frac{V}{2P_\ell} \tag{41b}$$

Sixteen shear tests were run using a large range of lateral force, P_ℓ. The average value computed for the static coefficient of friction, μ_s was 0.24 with a standard deviation of 0.037. A value of 0.30 is often used as the coefficient of friction for steel on steel. A thin, residue of carbon and oil on the sheetmetal surface may account for the slightly lower value observed in these tests.

DISCUSSION OF RESULTS

Shear Strength of Monterey Sand

The Monterey Sand used in the project was very clean (< 0.3 % passing the No. 200 U. S. Standard Sieve). All the sand was air dried so that the effect of apparent cohesion due to moisture could be disregarded. The shear strength of the sand can, therefore, be defined as

$$\tau = \sigma' \tan \phi' \tag{42}$$

where τ = shear strength

σ' = effective normal stress

ϕ' = apparent angle of internal friction.

Cohesionless soils derive their shear strength from a combination of interparticular friction and grain interlocking. Interlocking contributes a significant portion of the shear strength in dense sands. This contribution to shear strength decreases with decreasing relative density. The apparent angle of friction (ϕ'), therefore, does not depend solely on internal friction, since a portion of the shearing stress is used in overcoming interlocking.

Taylor has shown that the friction angle of sands depends on relative density, confining stress, particle angularity, grain size distribution, and to some extent, on the mineralogical content of the grains (Taylor, 1948). Confining stress influences the magnitude of

the friction angle because of the energy involved in overcoming interlocking. At low confining stresses, the sands dilate and work is performed by the confining stress which is proportional to the amount of volume change. At high confining stresses the particles are prevented from riding over each other and the shear strength becomes more purely frictional in character, since little work is performed in overcoming interlocking. Consequently, the apparent friction angle is higher at low confining stress.

Figure 86 represents a summary of shear strength tests on the sand used in the study (both triaxial and direct shear). Taylor has indicated similar trends (Taylor, 1948). The sand in the cell and backfill were subjected to average vertical overburden depths of 2 to 3 feet of sand (1.60 and 2.40 psi, respectively). A value of 50° was picked as the average angle of friction (ϕ') for the range of confining stress encountered in the project and was used in all calculations.

Discussion of Isolated Cells

Cell Deflections

Figure 54 shows the deflections of the front sheetpile for the isolated cells superimposed. Sheetpiles P1 for Cells No. 1, 2 and 3 have approximately the same relative magnitude of deflections while Cell No. 4 shows roughly 3-fold greater displacements. The difference in these magnitudes is due to lack of sheetpile embedment. The sheetpiles in Cell No. 4 had no embedment while Cells No. 1, 2 and 3 had embedments ranging from 10 to 24 inches. Since the empty,

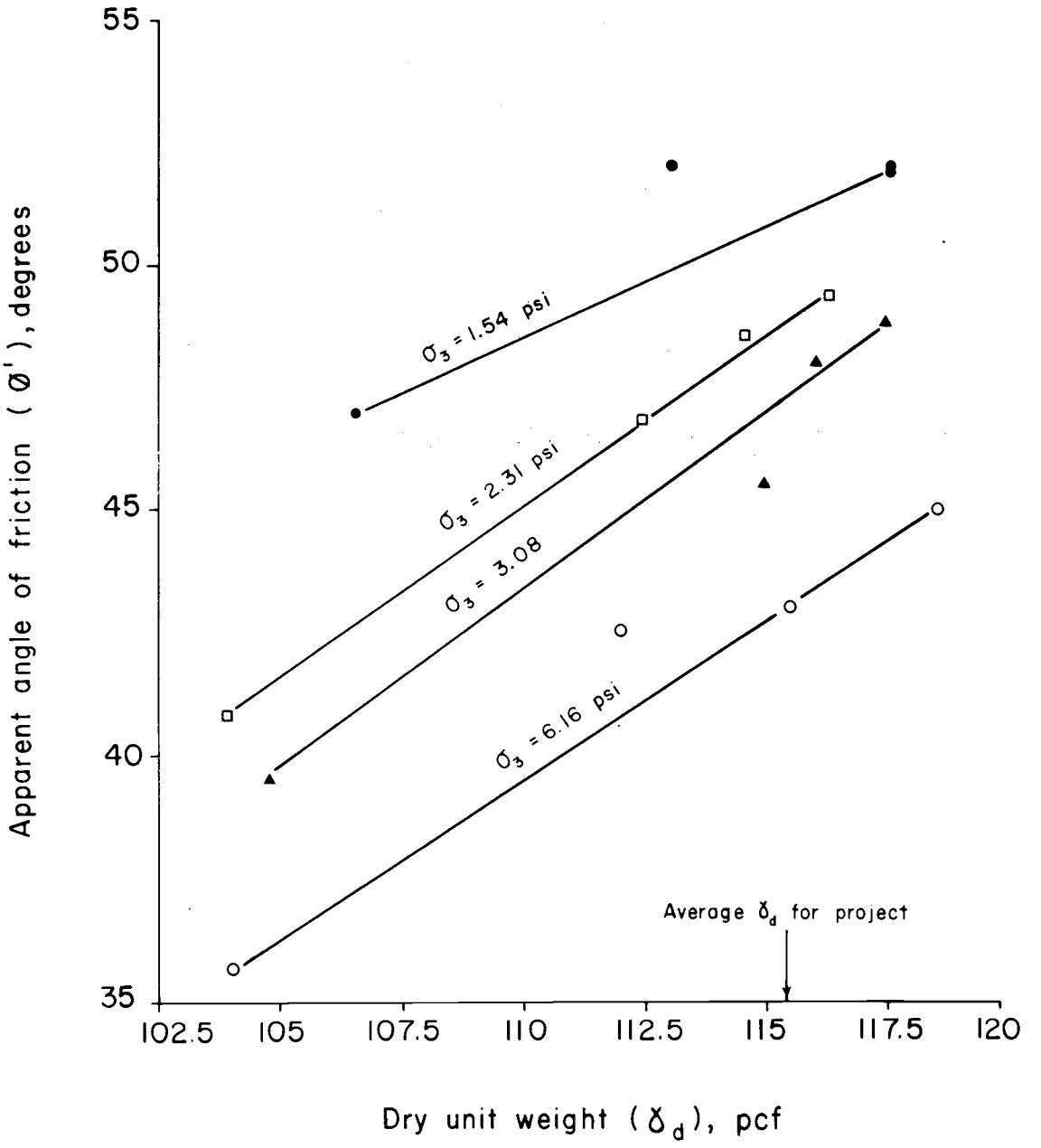

Figure 86. Shear strength of Monterey sand.

free-standing cells were taken as the point of initial displacements, the sheetpiles of Cell No. 4 (which has considerable interlock slack) indicated much larger radial displacements due to cell filling.

Table 12 summarizes the magnitude and location of the maximum radial displacements (bulging).

Table 12.

Radial Displacements of Front Sheetpile (P1)

Series No.	Max. ΔR (in.)	Y (in. from D.L.)	$\bar{y} = y/H$
I	0.20	13.0	0.26
II	0.17	16.9	0.34
III	0.28	13.1	0.27
IV	0.69	top	-

The deflection of the front sheetpile in Cell No. 4 is maximum at the top (due to interlock slack). The point of maximum bulging is, therefore, virtually masked by initial non-elastic radial displacements. In subsequent testing stages, the radial displacements due to the isolated cell were subtracted to account for the effect of initial interlock slack.

Hoop Stress

Series I. Cell No. 1 consisted of a four foot diameter cell, formed with sheetpiles six feet long with 22 inches of embedment. This distribution of hoop stress for the isolated cell is shown in Figures 46(a) through 46(d). The shape of all curves are remarkably

similar. Maximum hoop stresses occurred within the lower third of the sheetpile. Table 13 summarizes the maximum hoop stress, $\sigma_H(max)$, the distance from the dredgeline to the point of maximum hoop stress, y, the exposed height, H, and the ratio of y to H, $\bar{h}$. The ratio of embedment to exposed cell height (d/H) was 0.44.

Table 13.

Maximum Hoop Stresses (Series I)

	$\sigma_H(max)$ (psi)	y(in)	H(in)	$\bar{h} = y/H$
P1	370	15	50	0.30
P2	315	17	50	0.34
P3	355	17	50	0.34
P4	350	10	10	0.20

The maximum hoop stresses experienced by all four instrumented sheetpiles are nearly equal. The average maximum hoop stress for the cell was 346 psi. The average point of maximum hoop stress was 14.8 inches above the dredgeline, that is, an average value of $\bar{h}$ of 0.30. The point of maximum hoop stress for the sheetpiles adjacent to the Y-section was slightly higher. This upward shift may have been caused by the added stiffness of the Y-sections.

Series II. Cell No. 2 consisted of a cell similar to Cell No. 1 with a total length of five feet (60 inches) and an embedment depth, d, of ten inches. Figures 47(a) through 47(c) show the hoop stress curves for Series II. The hoop stress distribution of the front sheetpile

was similar to that of Cell No. 1, but differs somewhat from the side sheetpile (P3) and the back sheetpile (P4). Sheetpile P3 shows an inward dip in its hoop stress curve near the middle of the exposed height. Most probably the stiffness of the Y-section was again affecting the behavior of adjacent sheets. Table 14 summarizes the results of tests for Cell No. 2. The cell represents a ratio of embedment to exposed height (d/H) of 0.20.

Table 14.

Maximum Hoop Stresses (Series II)

	σ_{Ho}(max)(psi)	y(in)	H(in)	$\bar{h}$ = y/H
P1	331	10	50	0.20
P3	350	14	50	0.28
P4	423	17	50	0.34

The average maximum hoop stress for Cell No. 2 was 368 psi. Sheetpile P4 (back) had a maximum hoop stress that was about 15% above the average value. The point of maximum hoop stress occurred, on the average, at 13.7 inches above the dredgeline (i.e. $\bar{h}$ = 0.27).

Series III. Cell No. 3 models a "stepped" cell; one with the sheetpiles having larger embedment at the front than at the back. The lengths of the sheetpiles are reduced towards the back in a stepped fashion. The embedment at the front and side sheetpiles was 23.6 inches and reduced to 13.6 inches along the back portion of the cell. In addition the sheetpiles along the back were four inches shorter at

the top of the cell. The full isolated cell stage represents cell fill level with the back sheetpiles (i.e. four inches less fill than in other cells).

The hoop stress curve for sheetpile P1 was very similar to the curves for the front of Cells No. 1 and 2. The maximum hoop stress (330 psi) was about 8 to 10% below the averages of Cells No. 1 and 2. This was due to smaller lateral pressures, since there was less cell fill (four inches) at the full cell stage. The maximum hoop stress decreased towards the back portion of the cell. The elevation of the point of maximum hoop stress also increased significantly from the front to the back of the cell.

Table 15 summarizes the hoop stress data for Cell No. 3. Hoop stress curves are shown in Figures 48(a) through 48(b).

Table 15.

Maximum Hoop Stresses (Series III)

	σ_H(max)(psi)	y(in)	H(in)	$\bar{h}$ = y/H
P1	330	14	48.4	0.29
P3	278	18	48.4	0.37
P4	205	20	48.3*/44.4	0.41

*to top of cell

The average maximum hoop stress was 271 psi and the average distance from the dredgeline to the point of maximum hoop stress was 17.3 inches (or $\bar{h}$ = 0.36).

Series IV. Cell No. 4 represented the zero embedment case. Hoop stress curves for Series IV are shown in Figures 49(a) through 49(b). Hoop stress in sheetpile P1 was seen to increase with depth in a quasi-hydrostatic fashion. Strain gage readings from level B of this sheetpile were considered to be spurious because they were unstable. Sheets P3 and P4 had hoop stress curves that were similar. Note that the hoop stresses at the lower most level (D) were much lower than those at level C.

Table 16.

Maximum Hoop Stresses (Series IV)

	σ_H(max)(psi)	y(in)	h(in)	$\bar{h} = y/H$
P1	260	0	48	0
P3	288	16	48	0.33
P4	290	12	48	0.25

The average maximum hoop stress was 279 psi and occurred at an average of nine inches above the dredgeline or an average value of 0.19 for $\bar{h}$.

The behavior of sheetpile P1 was consistant with the zero embedment conditions. Sheetpiles P3 and P4, however, showed trends similar to those seen in previous cells. Apparently there was either a slight embedment of these sheetpiles or the friction at the base of these sheetpiles was sufficient to partially restrain them.

Hoop Stress Envelopes. The hoop stress curves for each series have been superimposed and are shown in Figures 87 through 91. The

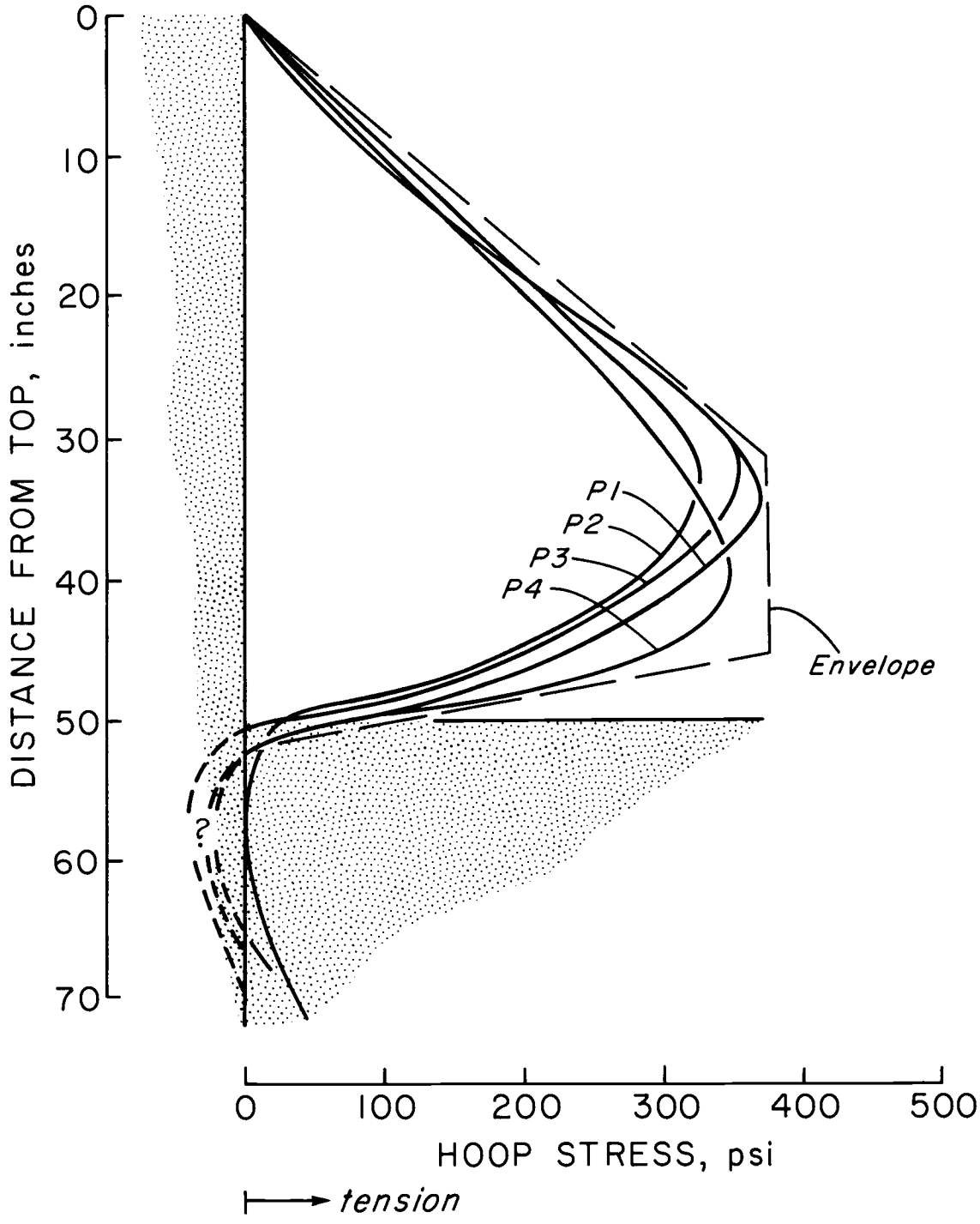

Figure 87. Superposition of hoop stresses (Series I).

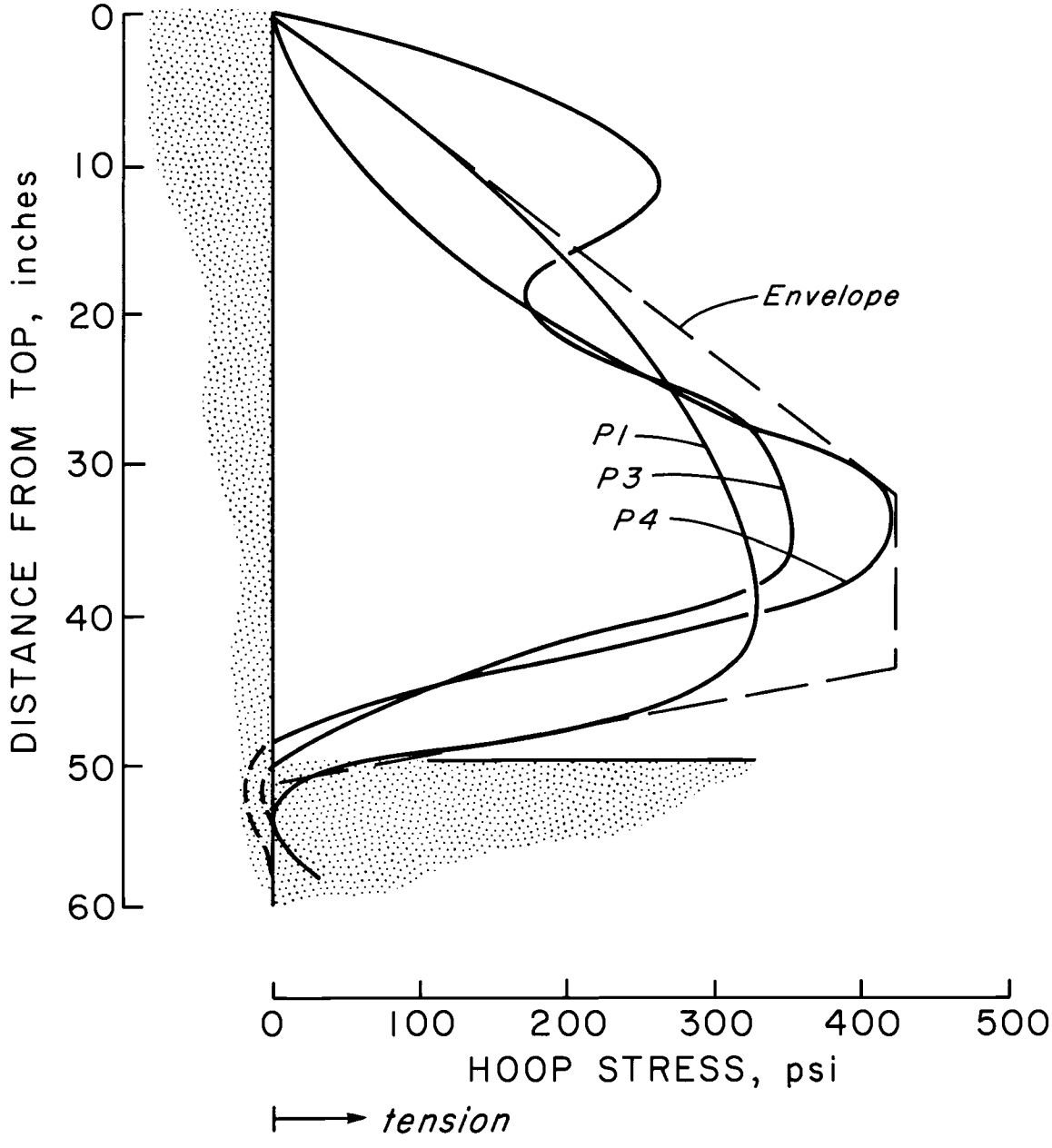

Figure 88. Superposition of hoop stresses (Series II).

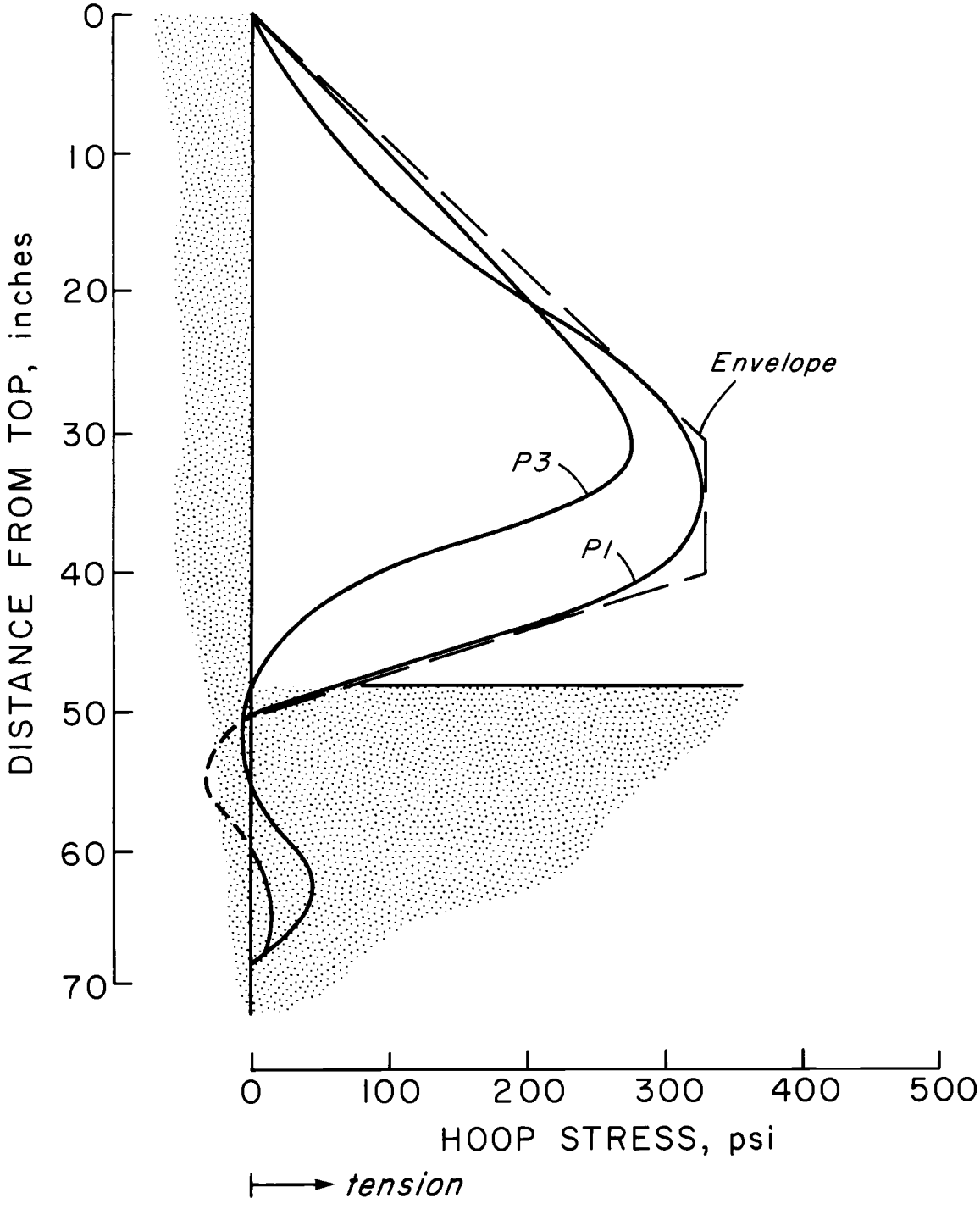

Figure 89. Superposition of hoop stresses (seres III).

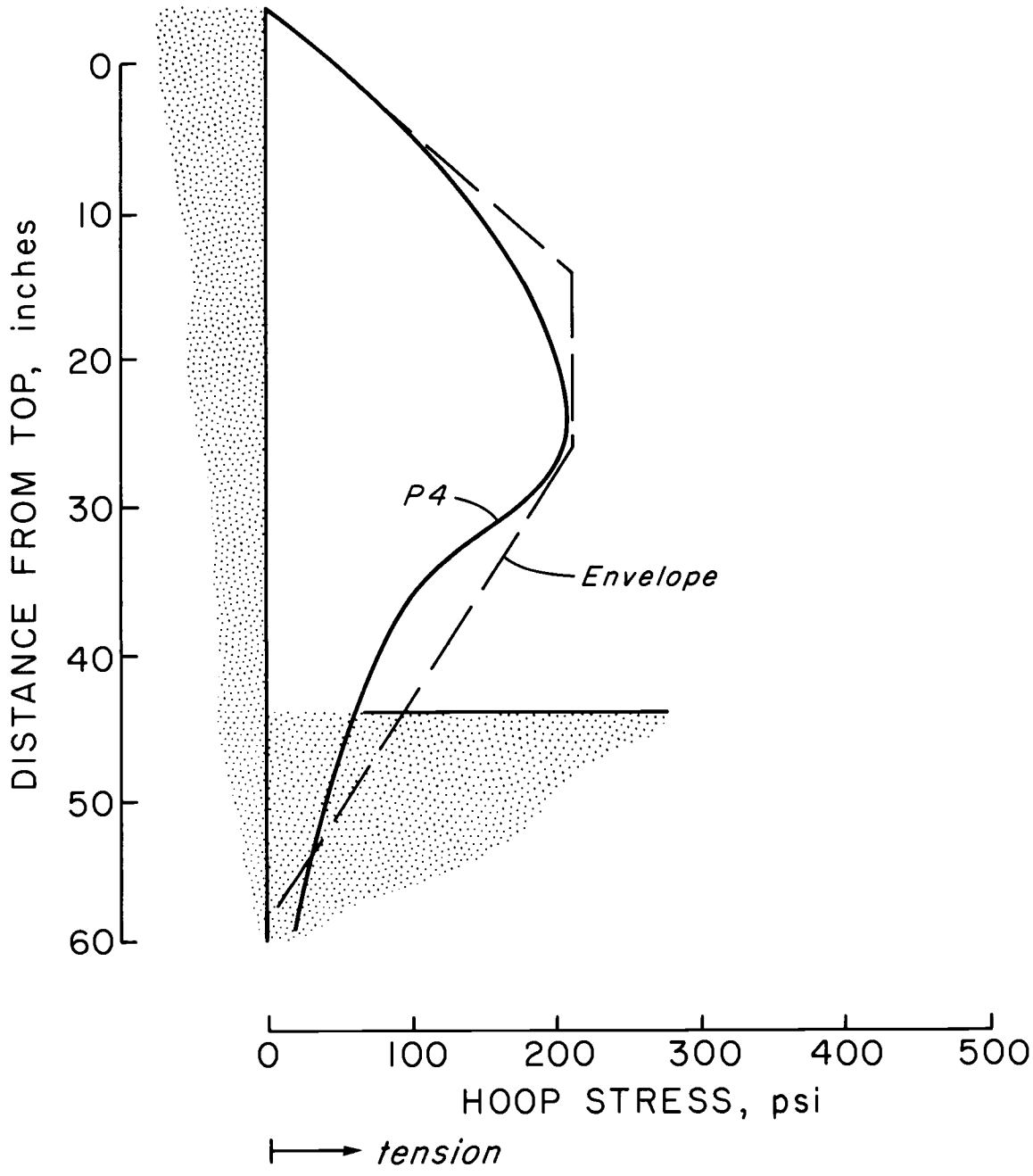

Figure 90. Hoop stress at P4 (Series III).

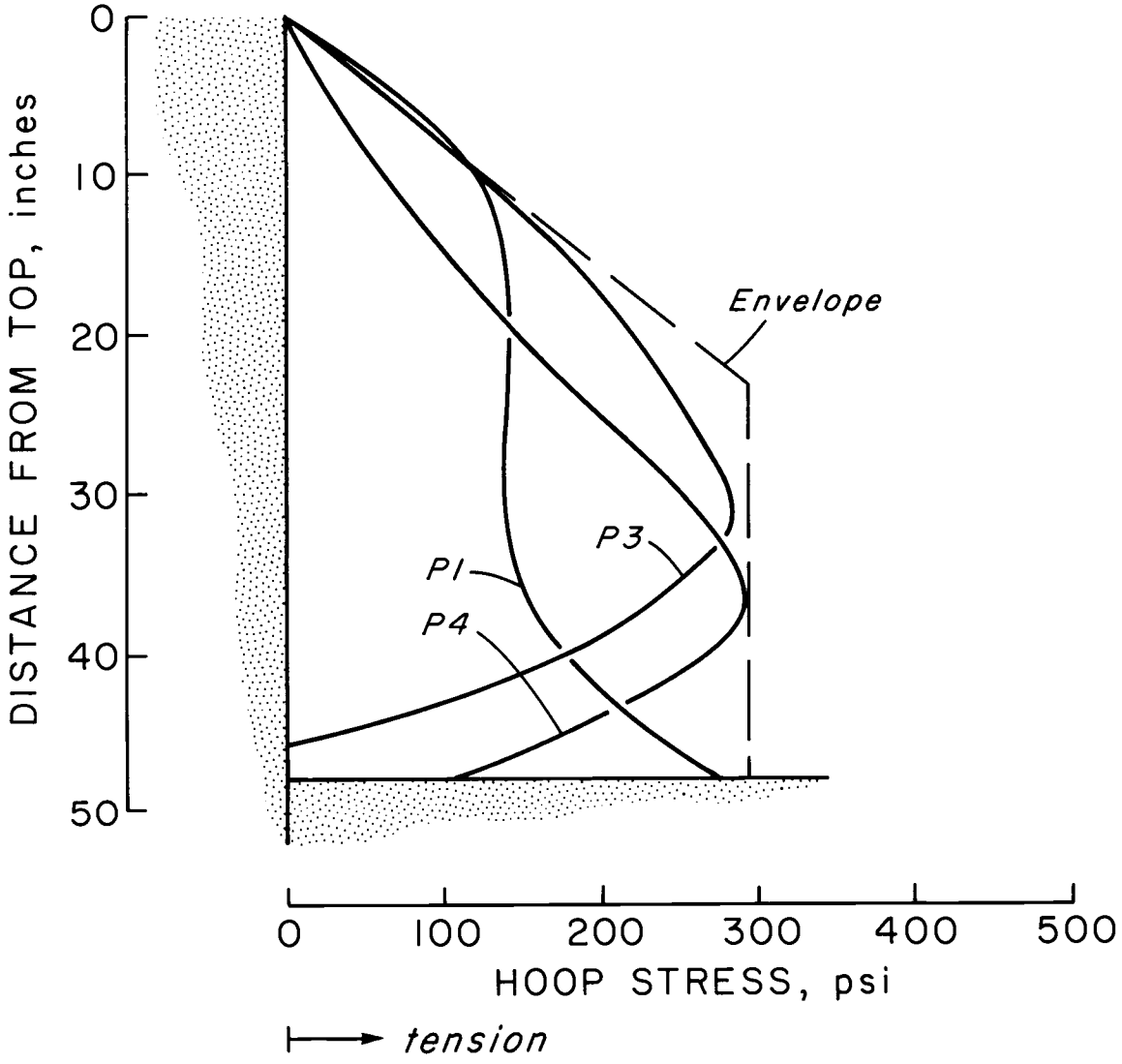

Figure 91. Superposition of hoop stresses (Series IV).

hoop stress distribution for the isolated cell can be characterized by an approximate stress envelope, roughly trapezoidal in shape. In almost all cases, the hoop stress increased linearly to some maximum level, $\sigma_H(max)$. This region of maximum hoop stress was within a height of about H/5 to H/2 from the dredgeline, depending on the embedment conditions. The hoop stress then dropped dramatically due to sheetpile embedment. In most cases the hoop stress appeared to reduce to zero within 5 to 30% of the exposed height, H, below the dredgeline. For the shorter, (i.e. stiffer) sheetpile at the back of Cell No. 3 the hoop stress was not reduced as quickly by the sheetpile embedment.

Below the point of zero hoop stress, most sheetpiles indicated a variation between a slight compressive stress and a small tensile stress near the base. The sheetpiles in the study were not capable of sustaining any significant compressive hoop stresses due to the type of model interlock. The regions of compression shown in the curves are therefore extrapolated from adjacent data points and made necessarily small.

The hoop stress envelope for the back sheetpiles of Cell No. 3 did not show as dramatic a reduction in stress near the dredgeline. This was due to shorter and, therefore, stiffer sheetpiles at the back. The region of maximum hoop stress also appears to shift upwards. Although there is a small residual hoop stress at the bottom of the sheetpiles, the hoop stress at the dredgeline was still reduced from the maximum value by about 71%.

The hoop stress envelope for Cell No. 4 indicates a maximum hoop stress (at approximately H/2) which extends to the base.

Lateral Earth Pressure

Hoop stresses develop in the sheetpiles during cell filling due to soil pressures. The behavior is similar to that of a thin-walled cylinder subjected to a radial pressure. The hoop stress, σ_H, can be expressed as:

$$\sigma_H = \frac{p \cdot r}{t} \tag{43}$$

where σ_H = hoop stress in web (psi)

p = radial soil pressure (psi)

r = radius of cell (inches)

t = thickness of sheetpile web (inches)

or, in terms of tension per unit length, P_ℓ, of sheetpile as

$$P_\ell = p \cdot r \tag{44a}$$

The lateral soil pressure, p, at some depth is equal to the effective vertical overburden pressure times the coefficient of lateral earth pressure, K. That is,

$$p = \sigma_v' \cdot K = \gamma_e' Z \cdot K \tag{44b}$$

where γ_e' = unit weight of soil

z = depth from the top of cell.

In our study $\gamma_e' = \gamma_d = \gamma$, and the less cumbersome, γ, will be used in subsequent discussion.

The hoop stress can then be expressed as a function of unit weight, γ, and the depth from the cell surface, z, by

$$\sigma_H = \frac{\gamma z K \cdot r}{t} \tag{45a}$$

with the average unit weight of the sand equal to 115.2 pcf, the radius of the cell, 24.48 inches, and the thickness of the web, 0.0299 inches in Equation 45(b), one obtains

$$K = \frac{\sigma_H}{54.58 \cdot z} \tag{45b}$$

Values for the apparent coefficient of lateral earth pressure, K, were calculated for the point of maximum hoop stress. Results are summarized in Table 17.

Table 17.

Apparent Coefficients of Lateral Earth Pressure
Computed from Measured Hoop Stresses

Sheetpile No. (Series)	σ_H(max)	z(in.)	K
P1 (SI)	370	35	0.194
P2 (SI)	315	33	0.175
P3 (SI)	355	33	0.197
P4 (SI)	350	40	0.100
			K_{avg}=0.182(SI)
P1 (SII)	331	40	0.152
P3 (SII)	350	36	0.178
P4 (SII)	423	33	0.235
			K_{avg}=0.188(SII)
P1 (SIII)	330	30.8	0.196
P3 (SIII)	278	26.8	0.190
P4 (SIII)	205	24.8	0.151
			K_{avg}=0.179(SIII)
P1 (SIV)	260	48	0.099
P3 (SIV)	288	32	0.165
P4 (SIV)	290	36	0.148
			K_{avg}=0.137(SIV)

The average values of K are relatively close for the first three cells but significantly lower (about 25%) for the fourth cell. In all cases, the values are smaller than those typically associated with cellular structures.

For a given angle of friction, ϕ, the coefficient of active earth pressure can be computed by the Rankine equation

$$K_A = \tan^2(45 - \frac{\phi}{2}) = \frac{1 - \sin\phi'}{1 + \sin\phi'} \tag{46}$$

A friction angle of 50° results in a value of 0.132 for K_A. The coefficient of active earth pressure for conditions that include wall friction can be obtained from the Coulomb equation

$$K_A = \frac{\sin^2(\alpha + \phi')}{\sin^2\alpha \sin(\alpha-\delta)\left[1+\sqrt{\frac{\sin(\phi+\delta)\sin(\phi-\beta)}{\sin(\alpha-\delta)\sin(\alpha+\beta)}}\right]^2} \tag{46a}$$

where α = angle the wall makes with the horizontal

β = angle of included backfill

δ = wall friction angle

With a vertical wall ($\alpha = 90°$) and a horizontal cell fill surface ($\beta = 0$), the expression becomes

$$K_A = \frac{\sin^2(90 + \phi')}{\sin(90-\delta)\left[1+\sqrt{\frac{\sin(\phi+\delta)\sin(\phi)}{\sin(90-\delta)}}\right]^2} \tag{46b}$$

A value 17° ($\phi/3$) for the wall friction angle appears reasonable and agrees with the value proposed by Bowles for steel sheetpiles backfilled with clean sands (Bowles, 1977). Values of 50° and 17° for ϕ and δ, respectively, result in an active (Coulomb) coefficient of 0.125.

The coefficient of at-rest pressure, K_o, is usually estimated from the expression

$$K_o = 0.9(1 - \sin\phi) \tag{47}$$

A value of 0.211 is obtained for K_o for a sand with a friction angle of 50°.

The average between the at-rest coefficient, K_o, and the active Coulomb coefficient, K_A, is 0.168. The average measured value of the coefficient of earth pressure in the first three series was .183. The state of stress of the cell fill in Cells No. 1, 2 and 3 therefore lies between the at-rest and the active case. Cell No. 4, however, has a measured coefficient very close to the active coefficient. The cell fill in Cell No. 4 was presumably, therefore, very nearly in the active state of stress.

An explanation for the apparent discrepancy in values of earth pressure coefficient can be found in the construction procedure. Cells No. 1, 2, and 3 all represent cells which were driven into the sand. The template was then removed and the cell filled. Cell No. 4 was built around the template, without driving. The template was removed and the cell filled. The cell was essentially free standing

during the filling operations. Small strips of tape kept the sheets from collapsing inward at the top. Consequently, in the first three cells, the outward radial expansion of the cell was partially restrained by the sheetpile embedment. As the cell was filled, the radial movements were probably sufficient to partially mobilize the shear strength of the fill but not enough to create an active condition. The slack in the sheetpile interlocks of Cell No. 4 was substantially larger. There was also little or no restraint along the bottom of the sheetpiles. The radial displacements were, therefore, apparently sufficient to fully mobilize internal shear resistance. The cell fill could be considered to have been in the active state of stress (see Figure 54 for a comparison of radial displacements).

Comparison with Field Data

A considerable amount of information has been obtained concerning the behavior of circular bulkheads from two comprehensive field studies. The field studies conducted by White, et. al. (White, et. al., 1963) and T. Khuayjarernpanishk (Khuayjarernpanishk, 1975) have been described in the LITERATURE REVIEW AND DESIGN CONSIDERATION section. Typical cross-sections of the cells studied are shown in Figure 20 and 21.

Field Data (White, et. al.)

Table 18 summarizes the average hoop stress for the full cell (Stage III) of the Long Beach bulkhead, built in 1952-53. The front sheetpile had an embedment-height ratio (d/H) of about 0.28. The hoop tensions (in kips/in) are tabulated as a function of strain gage level (see Figure 20 for locations of these levels).

Table 18.

Average Hoop Tensions for Full Cell (kips/in) (after White)

Pile	Level 1	Level 2	Level 3	Level 4
A	2.7	2.7	3.8	5.6
C	3.0	1.7	3.7	4.2
D	2.2	3.1	2.9	5.9
E	1.7	2.3	-	3.2
Avg	2.4	2.3	3.5	4.7

Figure 92 shows a plot of the average hoop tension as a function of depth. The range of values at each level is also indicated. The higher values of hoop stress occur at Pile A (front) while the lower values occur at Pile E (back). The authors indicated that the difference may have been due to the higher elevation of the natural ground surface at the back of the cell. The back sheets were also embedded almost entirely in a fine to medium sand while the front piles are associated with embedment in silts and clays.

The average radial displacements for the cell are summarized in Figure 93. The authors proposed that the large initial radial displacements at the bottom of the cell were due to either injury to the interlock or lack of definition of the curve at that depth (White, et. al., 1963).

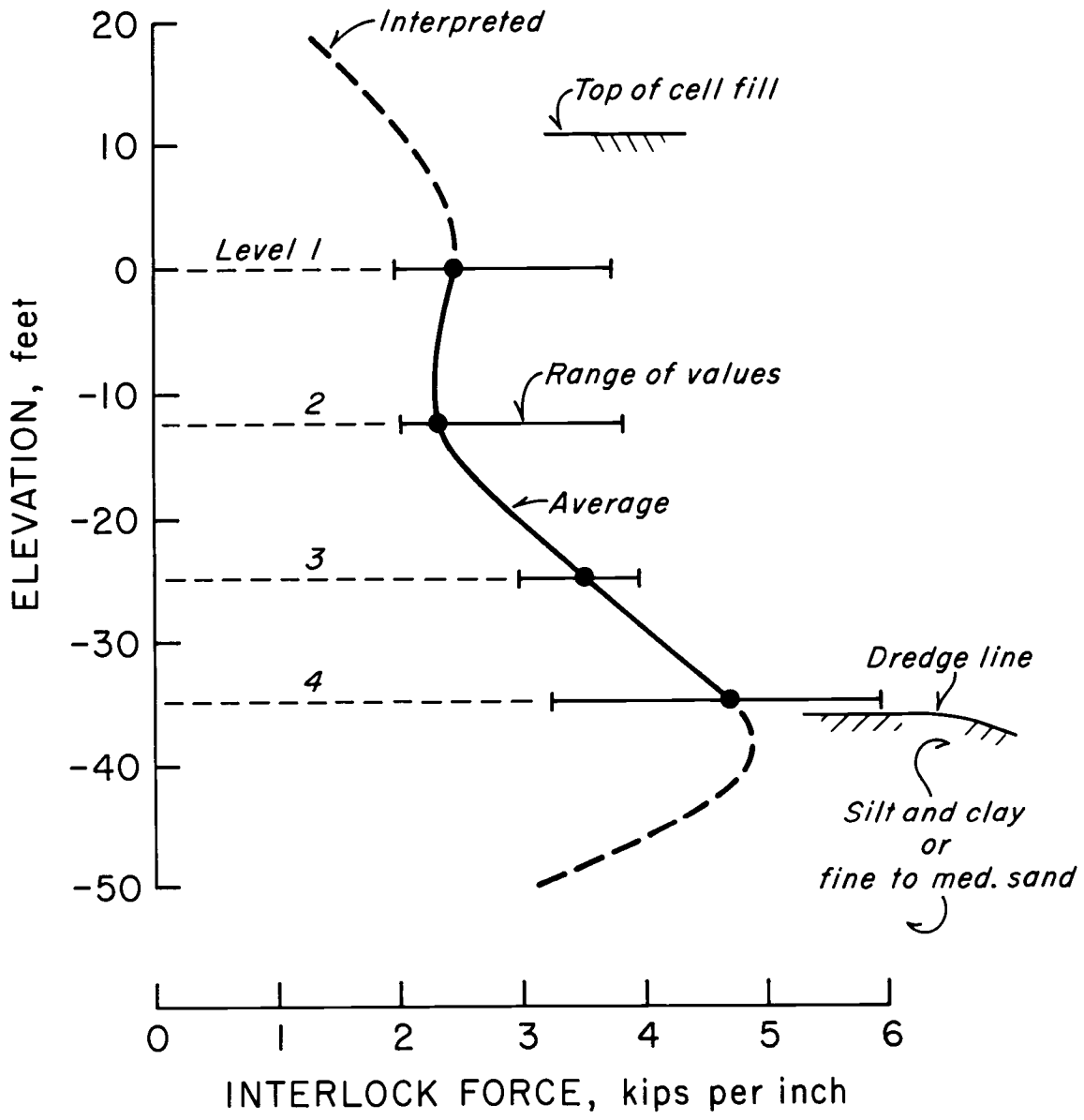

Figure 92. Average hoop tension at full cell.

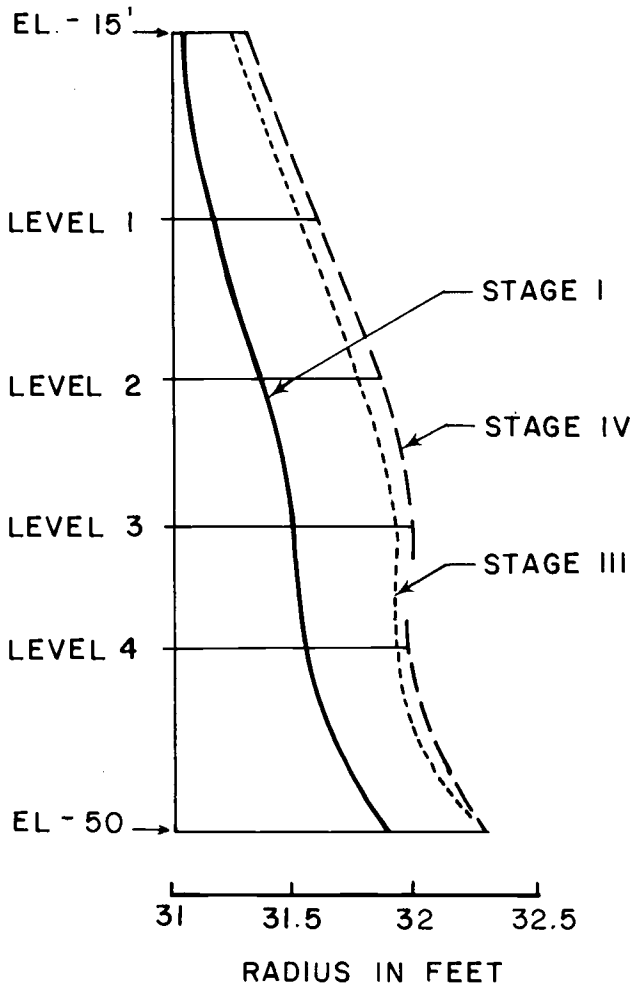

Figure 93. Average radii of Long Beach cell (after White).

Field Data (Khuayjarernpanishk)

Figure 94(a) through 94(h) summarizes the hoop stress data obtained during construction of the cellular bulkhead at Terminal 4, in the Port of Portland (Khuayjarernpanishk, 1975). Event No. 3 represents the full cell stage. Because the cells were "stepped", the full cell stage represents cell fill that is level with the top of the back sheetpiles. The front sheetpile has an embedment-height ratio (d/H) of 0.32.

Figure 95 indicates the average interlock tension, in kips per inch, along with the range of values at each level (see Table 19). All but two sheetpiles (at positions 4 and 5) showed a linearly increasing interlock force to an elevation of -32 feet (i.e. 10 feet above the dredgeline). The sheetpiles at positions 4 and 5 showed a decrease in interlock tension at level C.

Figures 96(a) through 96(f) show the radial deflections due to the cell filling operation ($R_o - R_2$). Figure 97 summarizes the location of the maximum bulge point as a function of sheetpile position. The point of maximum bulging at the side and back of the cell (positions 4, 5 and 7) occurs at a higher elevation than at the front of the cell.

Table 19.

Average Interlock Force (kips/in) (after Khuayjarernpanishk)

	t_{low}	t_{high}	$t_{average}$
Level A	- .55	1.13	0.62
Level B	1.10	2.50	1.85
Level C	0.84	3.84	2.69

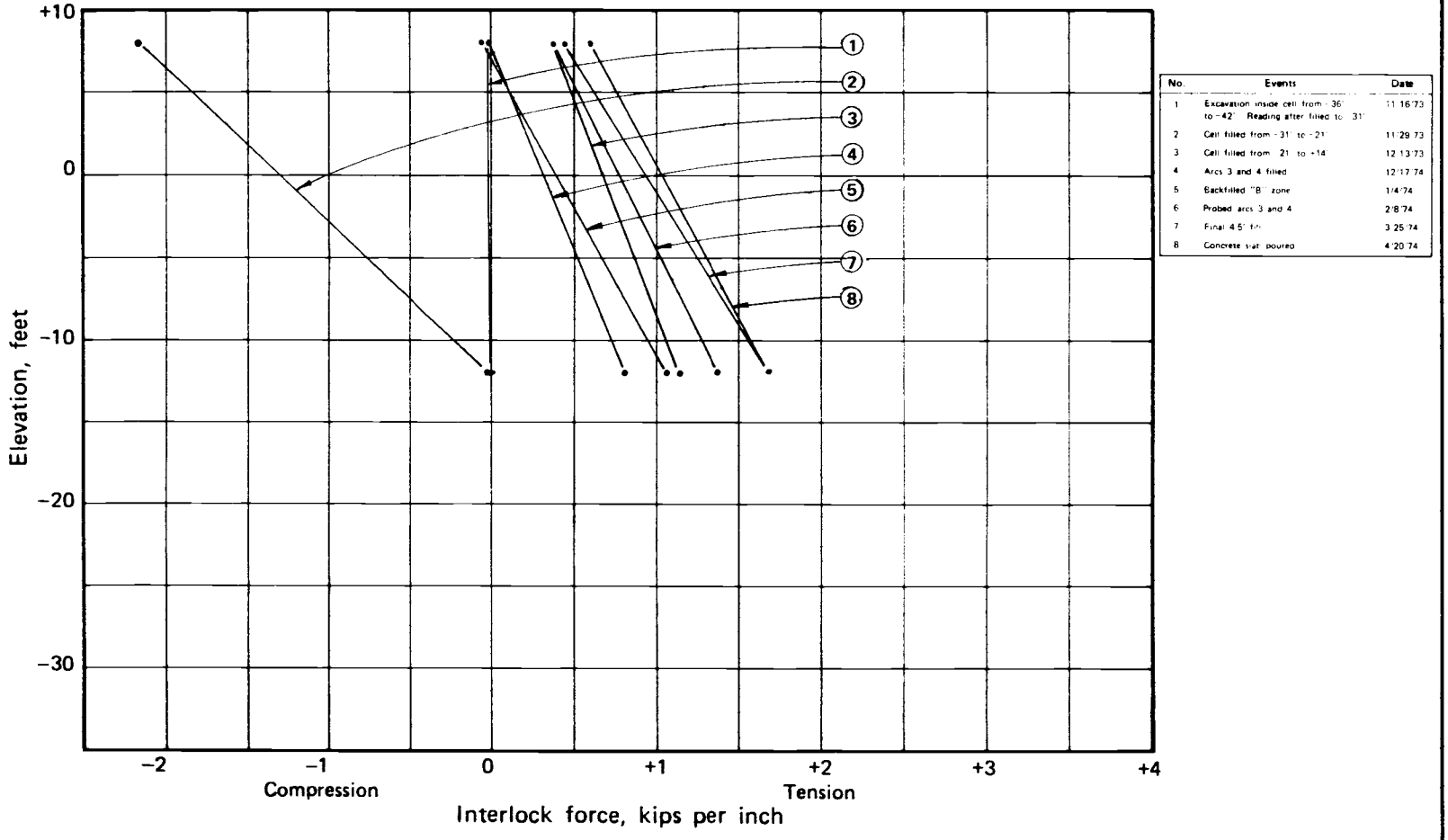

(a) Interlock force at position 1.

Figure 94. Interlock forces of Terminal 4 cell (after Khuayjarernpanishk).

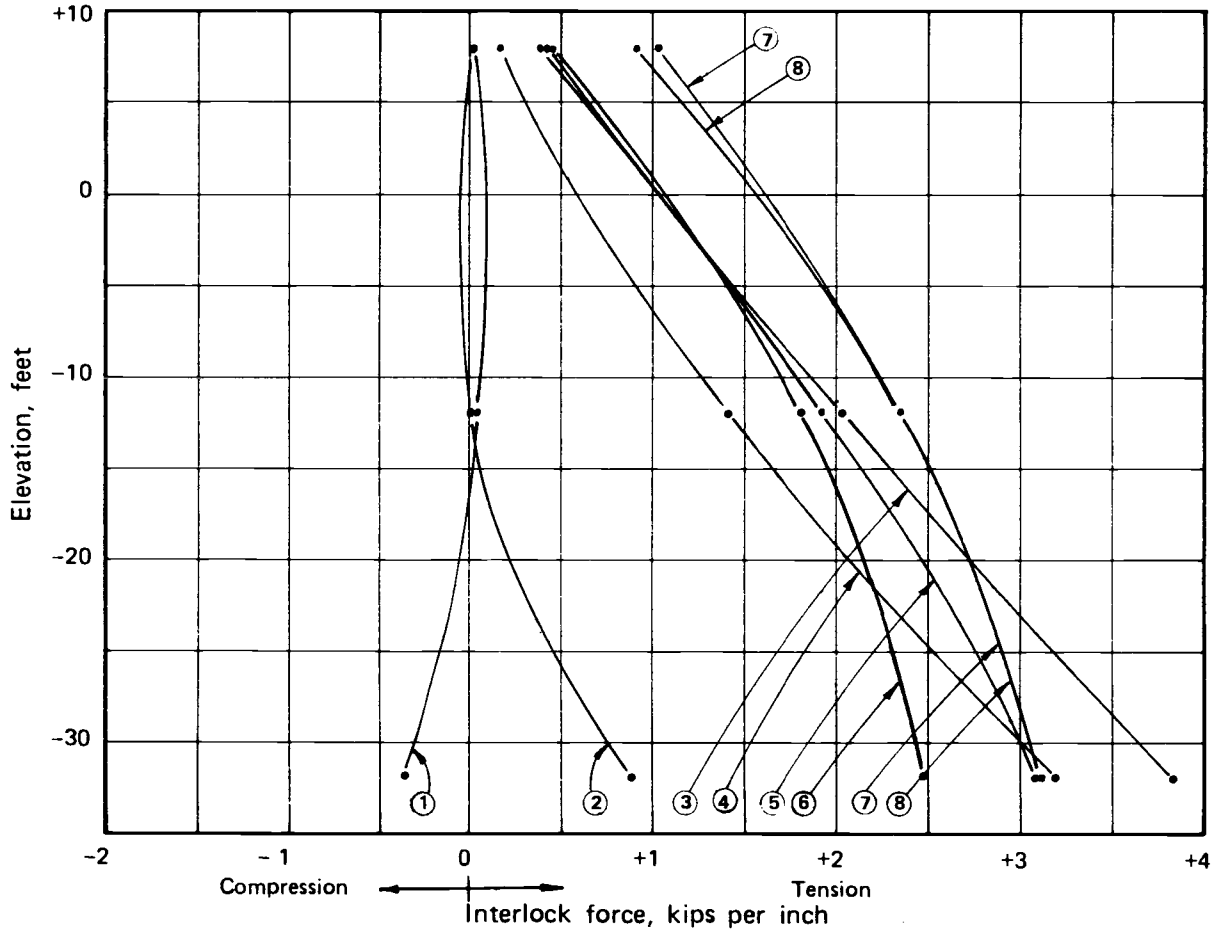

No.	Events	Date
1	Excavation inside cell from -36' to -42'. Reading after filled to -31'	11 16 73
2	Cell filled from -31' to -21'	11 29 73
3	Cell filled from -21' to +14'	12 13 73
4	Arcs 3 and 4 filled	12 17 74
5	Backfilled "B" zone	1 4 74
6	Probed arcs 3 and 4	2 8 74
7	Final 4.5' fill	3 25 74
8	Concrete slab poured	4 20 74

(b) Interlock forces at position 2.

Figure 94. continued

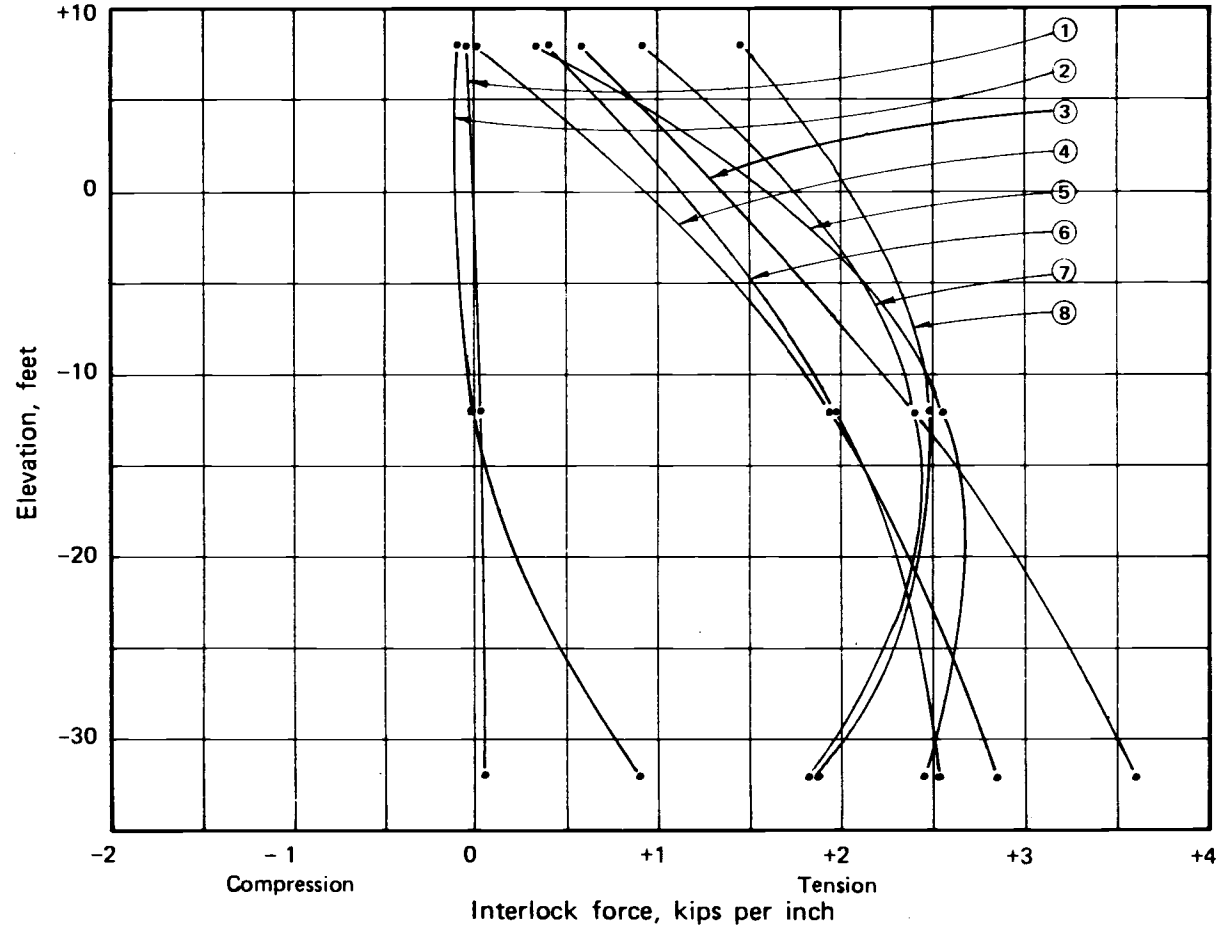

No.	Events	Date
1	Excavation inside cell from -36' to -42'. Reading after filled to -31'	11 16 73
2	Cell filled from -31' to -21'	11 29 73
3	Cell filled from -21' to +14'	12 13 73
4	Arcs 3 and 4 filled	12 17 74
5	Backfilled "B" zone	1 4 74
6	Probed arcs 3 and 4	2 8 74
7	Final 4.5' fill	3 25 74
8	Concrete slab poured	4 20 74

(c) Interlock forces at position 3.

Figure 94. continued

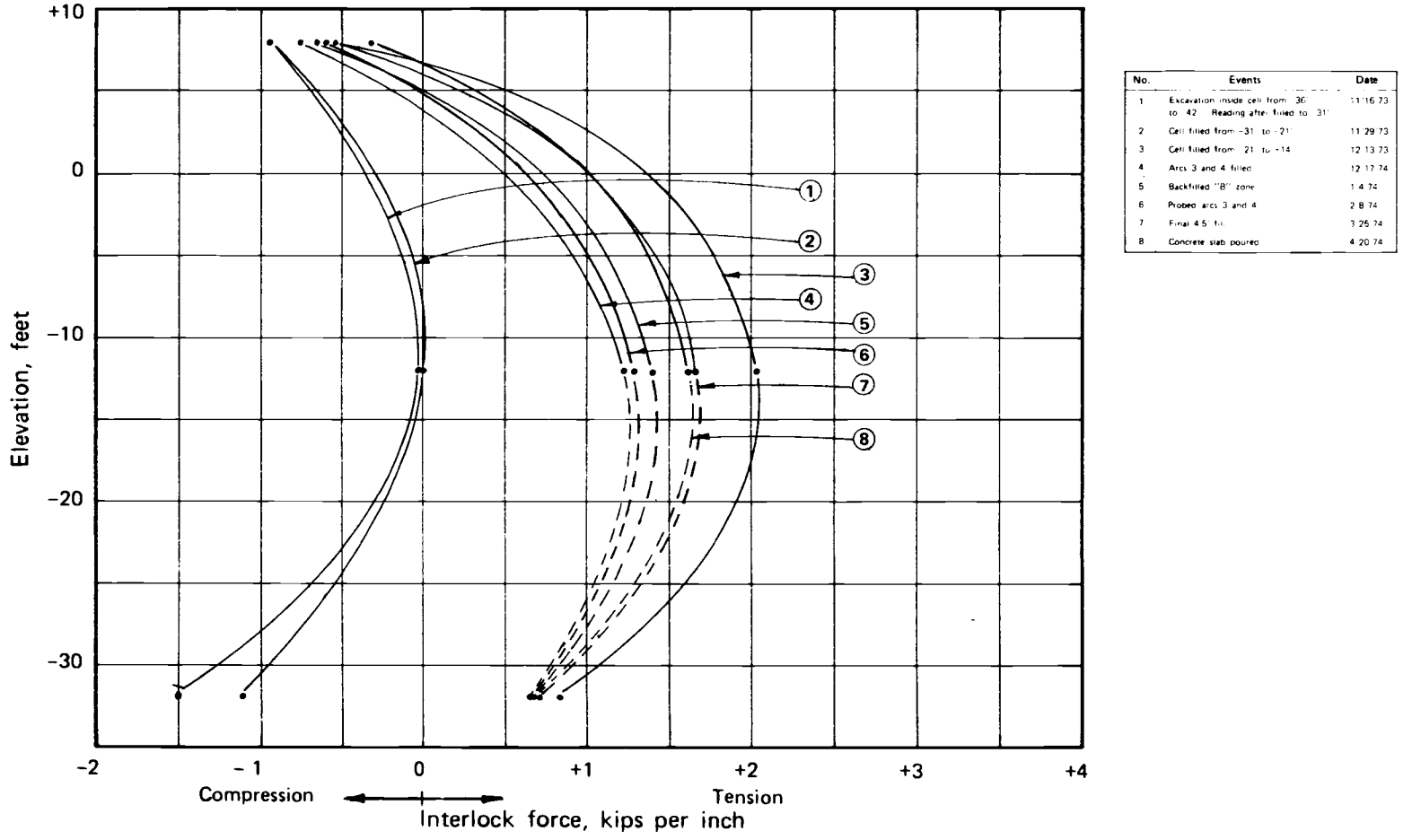

(d) Interlock forces at position 4.

Figure 94. continued

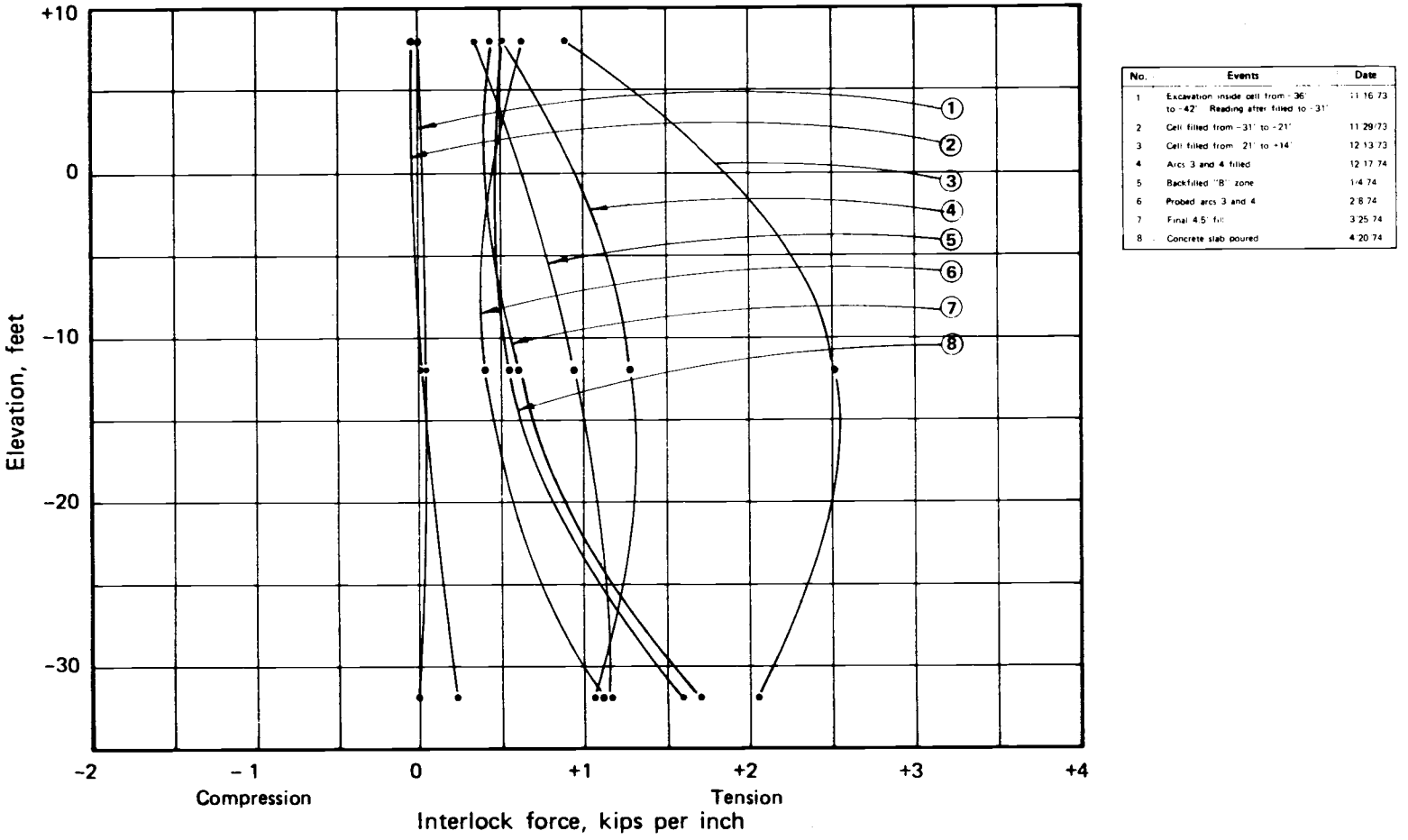

(e) Interlock forces at position 5.

Figure 94. continued

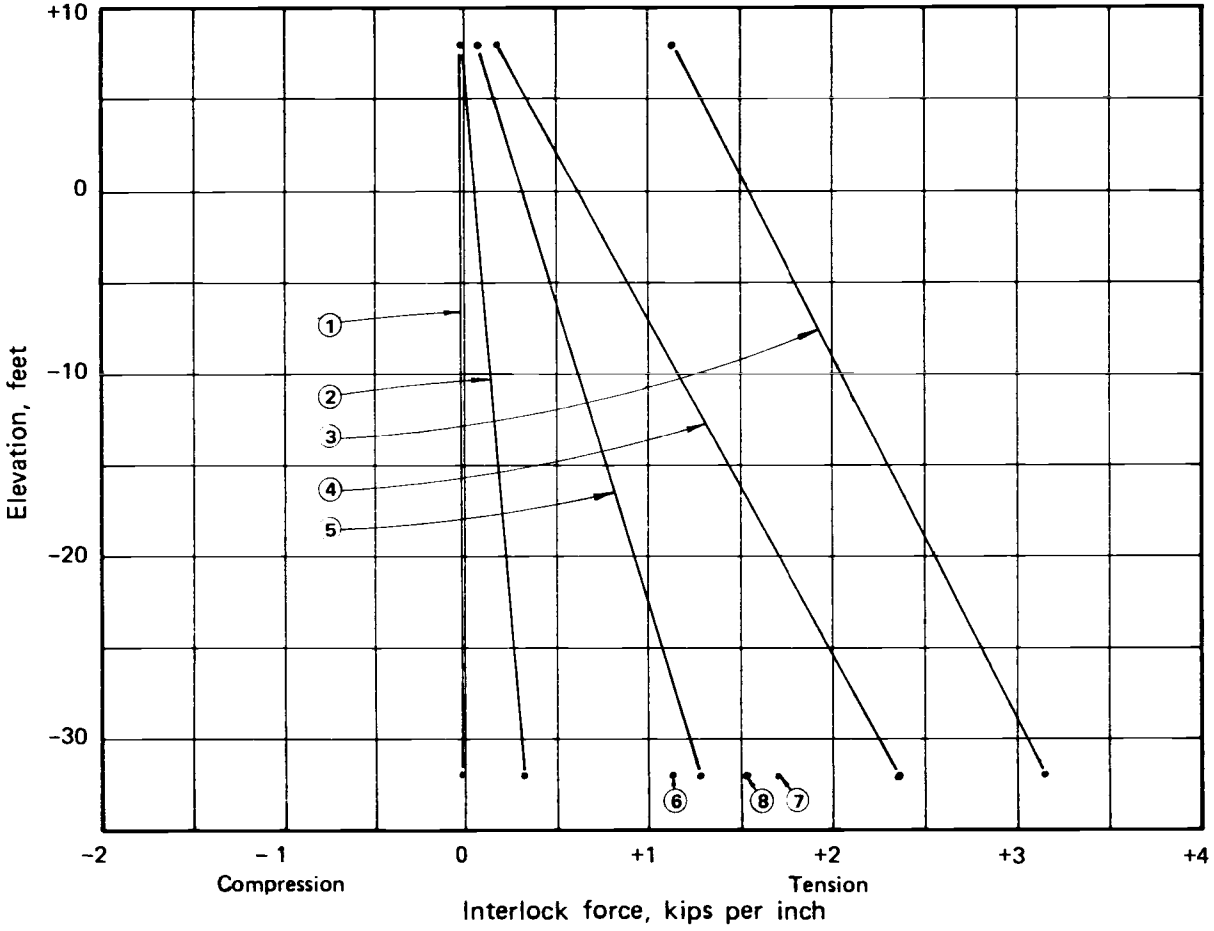

No.	Events	Date
1	Excavation inside cell from -36' to -42'. Reading after filled to -31'	11/16/73
2	Cell filled from -31' to -21'	11/29/73
3	Cell filled from -21' to +14'	12/13/73
4	Arcs 3 and 4 filled	12/17/74
5	Backfilled "B" zone	1/4/74
6	Probed arcs 3 and 4	2/8/74
7	Final 4.5' fill	3/25/74
8	Concrete slab poured	4/20/74

(f) Interlock forces at position 6.

Figure 94. continued

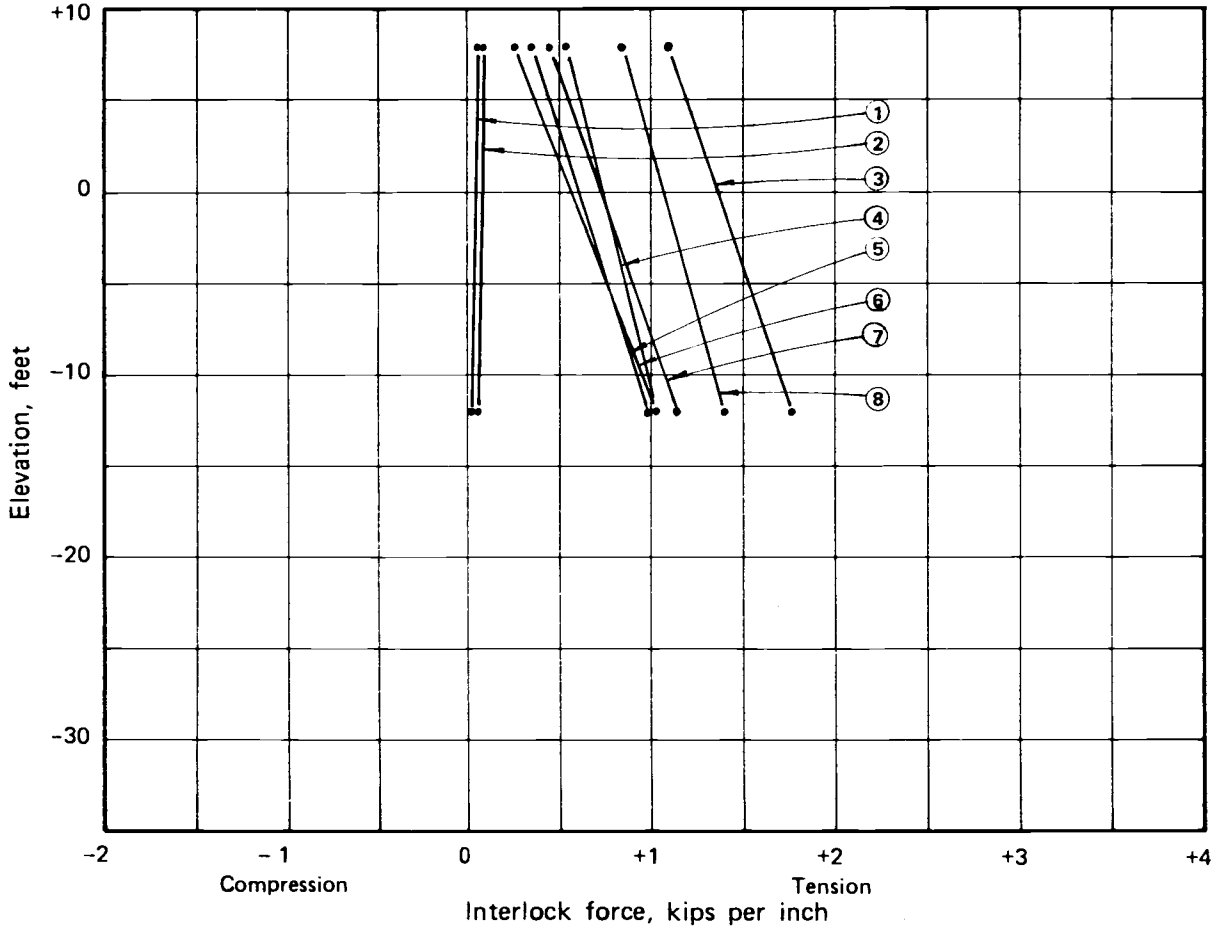

No.	Events	Date
1	Excavation inside cell from -36 to -42. Reading after filled to -31	11 16 73
2	Cell filled from -31 to -21	11 29 73
3	Cell filled from -21 to +14	12 13 73
4	Arcs 3 and 4 filled	12 17 74
5	Backfilled "B" zone	1 4 74
6	Probed arcs 3 and 4	2 8 74
7	Final 4.5' fill	3 25 74
8	Concrete slab poured	4 20 74

(g) Interlock forces at position 7.

Figure 94. continued

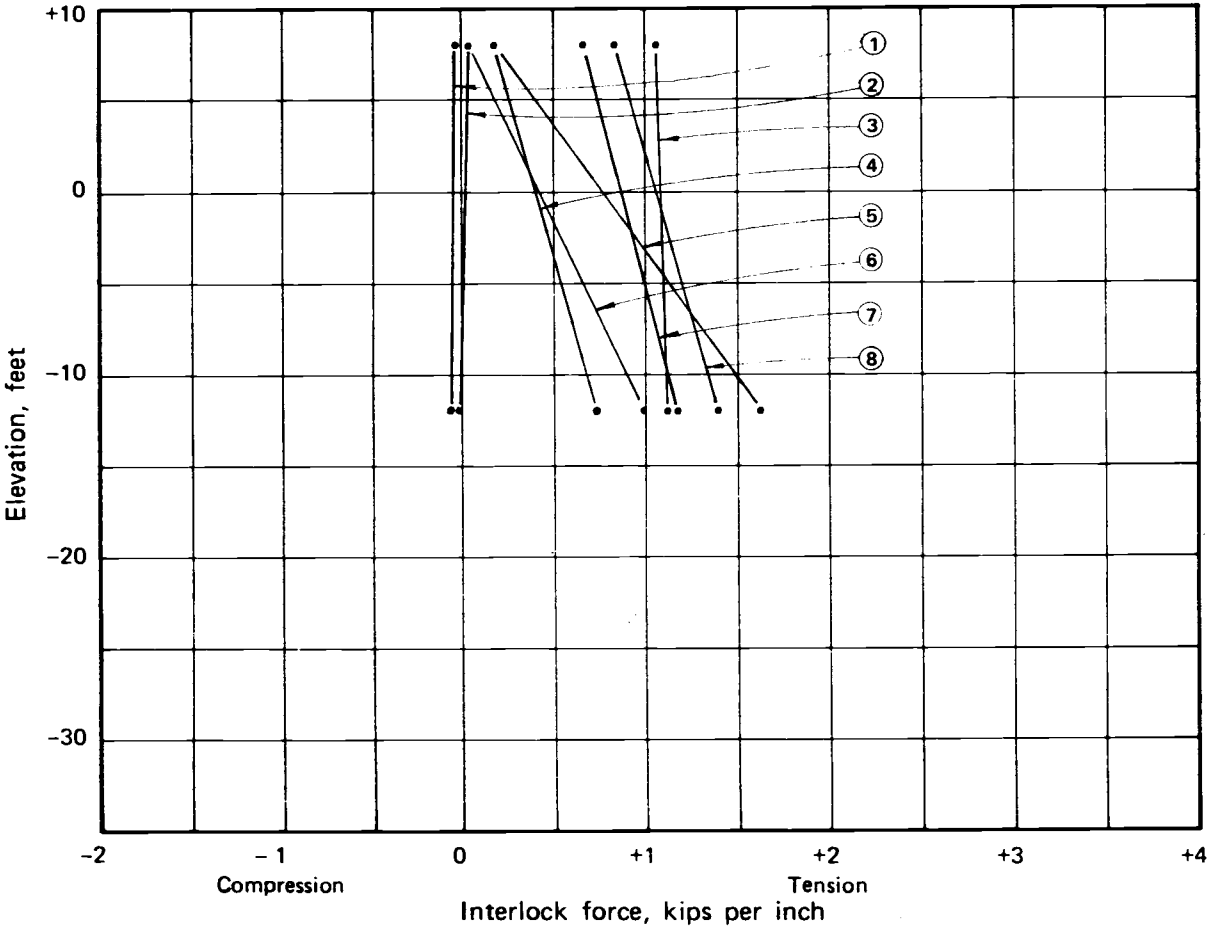

No.	Events	Date
1	Excavation inside cell from -36 to -42. Reading after filled to -31	11 16 73
2	Cell filled from -31' to -21'	11 29 73
3	Cell filled from -21' to +14	12 13 73
4	Arcs 3 and 4 filled	12 17 74
5	Backfilled "B" zone	1 4 74
6	Probed arcs 3 and 4	2/8 74
7	Final 4.5' fill	3 25 74
8	Concrete slab poured	4/20 74

(h) Interlock forces at position 8.

Figure 94. continued

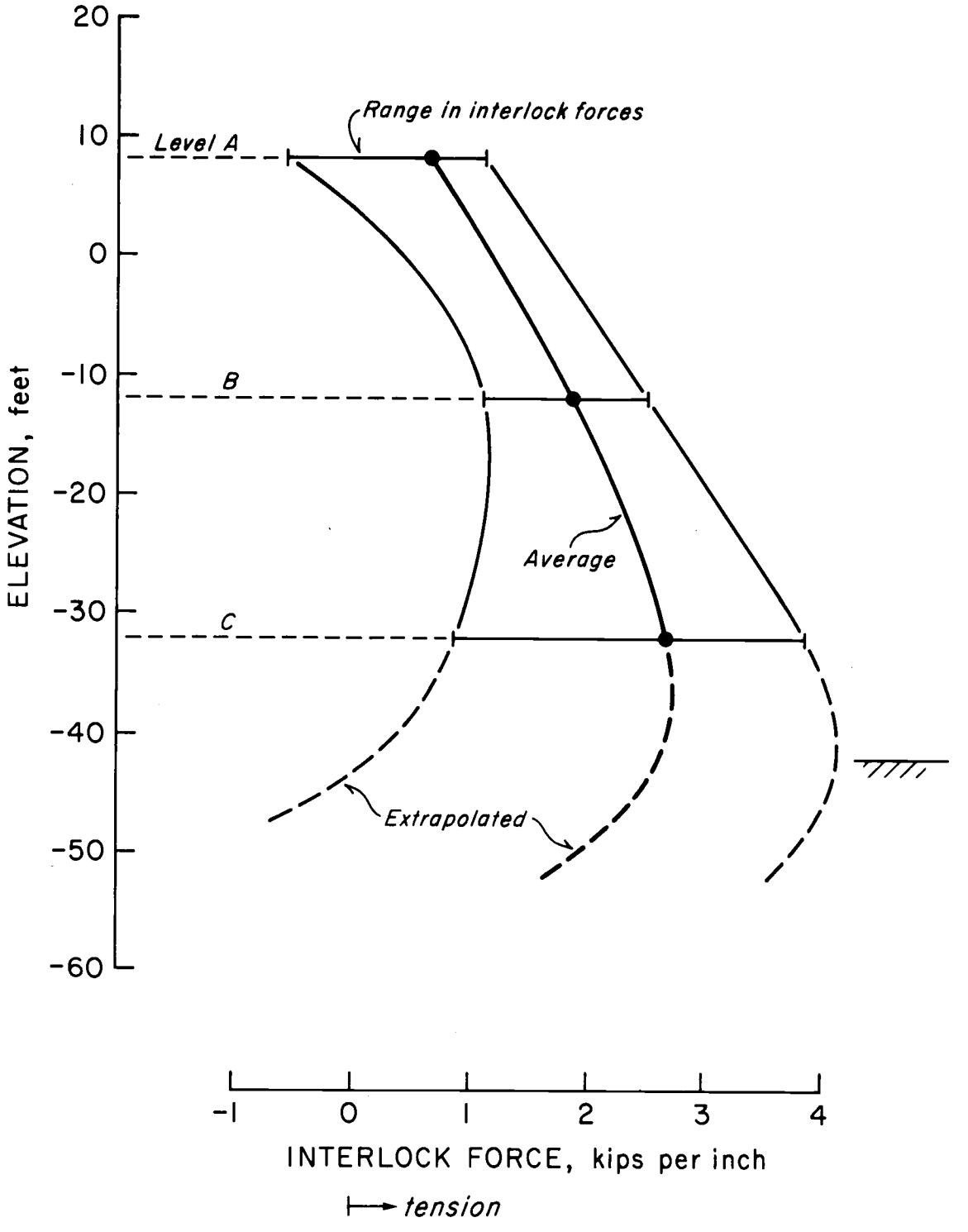

Figure 95. Average interlock forces of Terminal 4 cell.

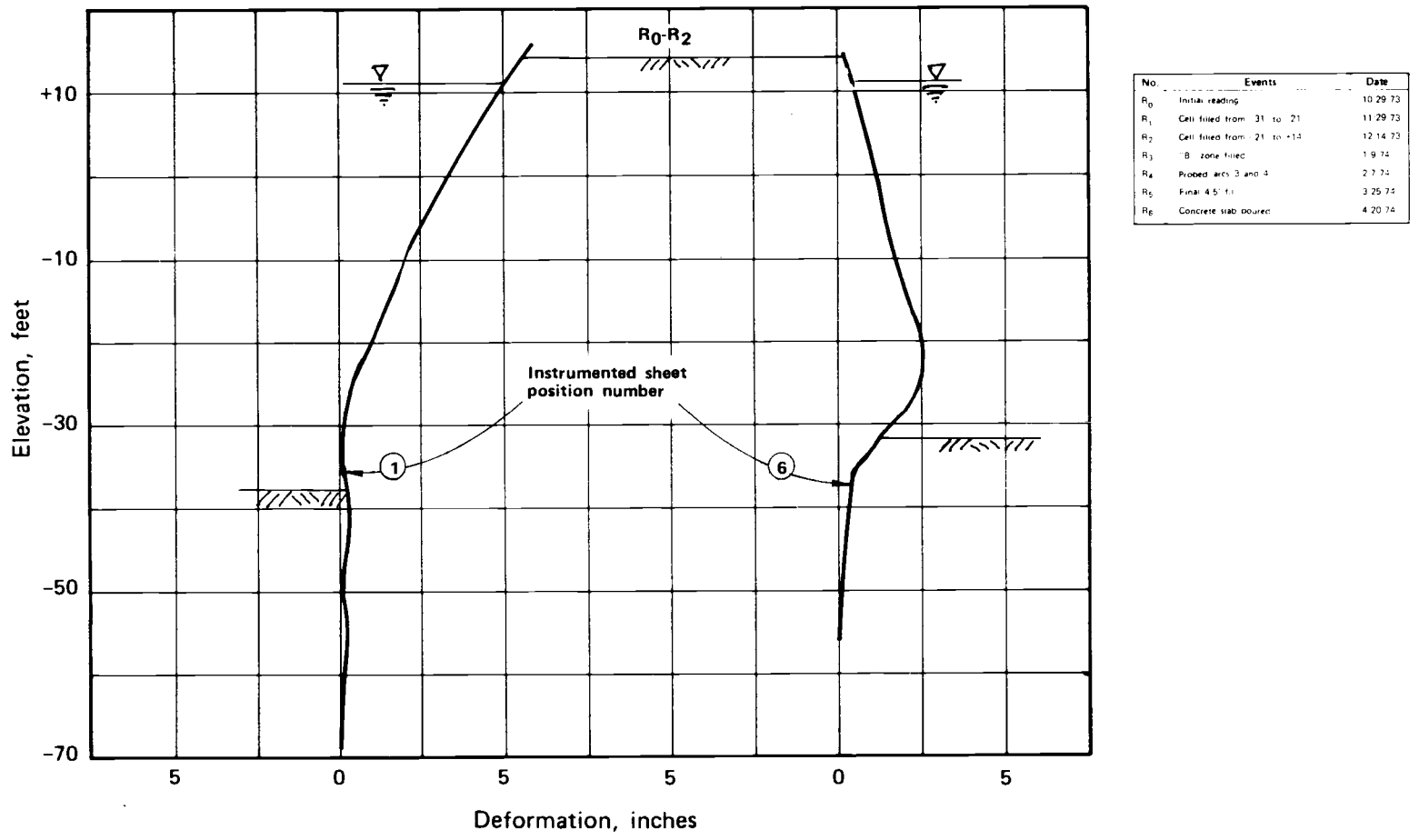

(a) Radial deformation of cell after filling from El. -31 to El. 14.

Figure 96. Radial deformation of Terminal 4 cell (after Khuayjarernpanishk).

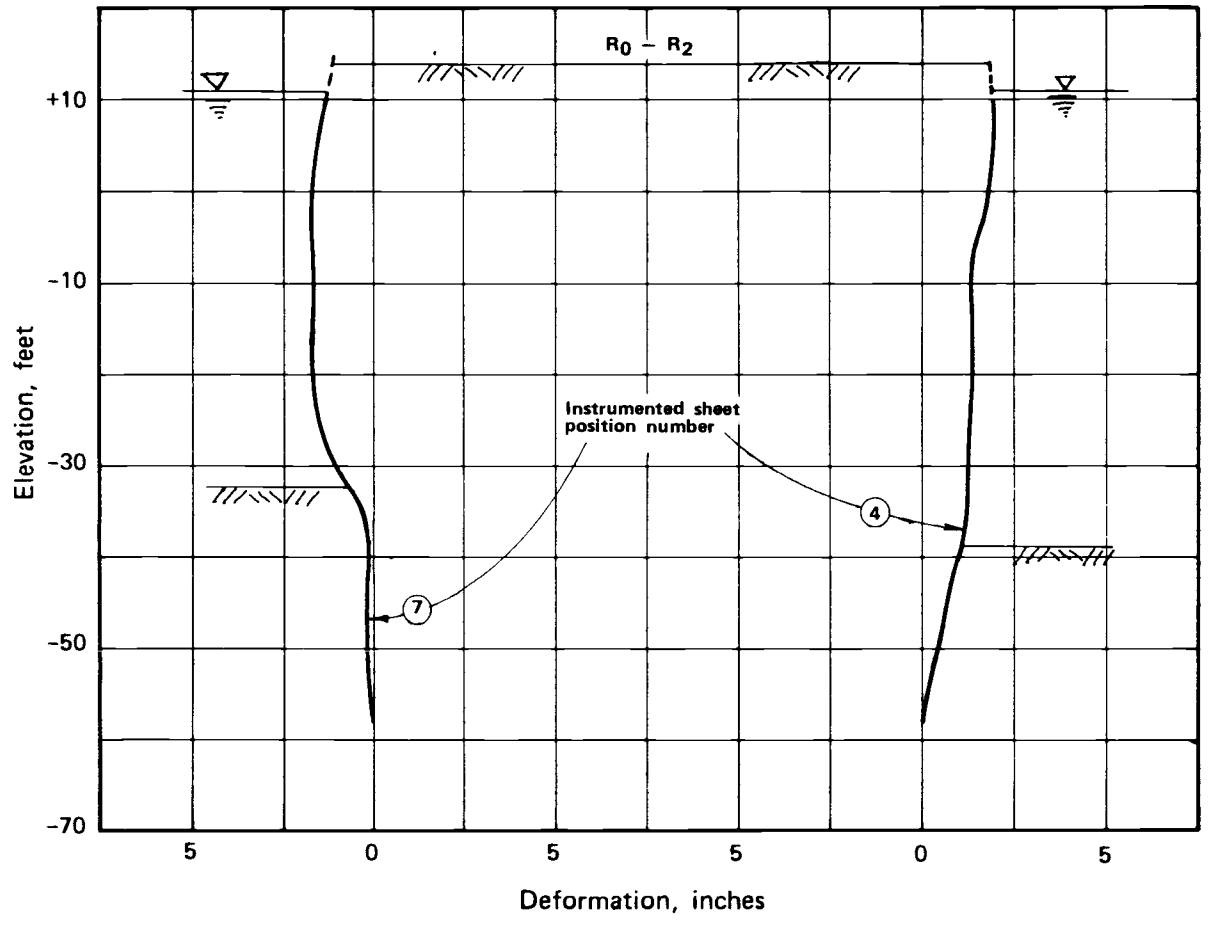

No.	Events	Date
R_0	Initial reading	10 29 73
R_1	Cell filled from -31' to -21'	11 29 73
R_2	Cell filled from -21' to +14'	12 14 73
R_3	"B" zone filled	1 9 74
R_4	Probed arcs 3 and 4	2 7 74
R_5	Final 4.5' fill	3 25 74
R_6	Concrete slab poured	4 20 74

(b) Radial deformation of cell cross section at positions 4 and 7.

Figure 96. continued

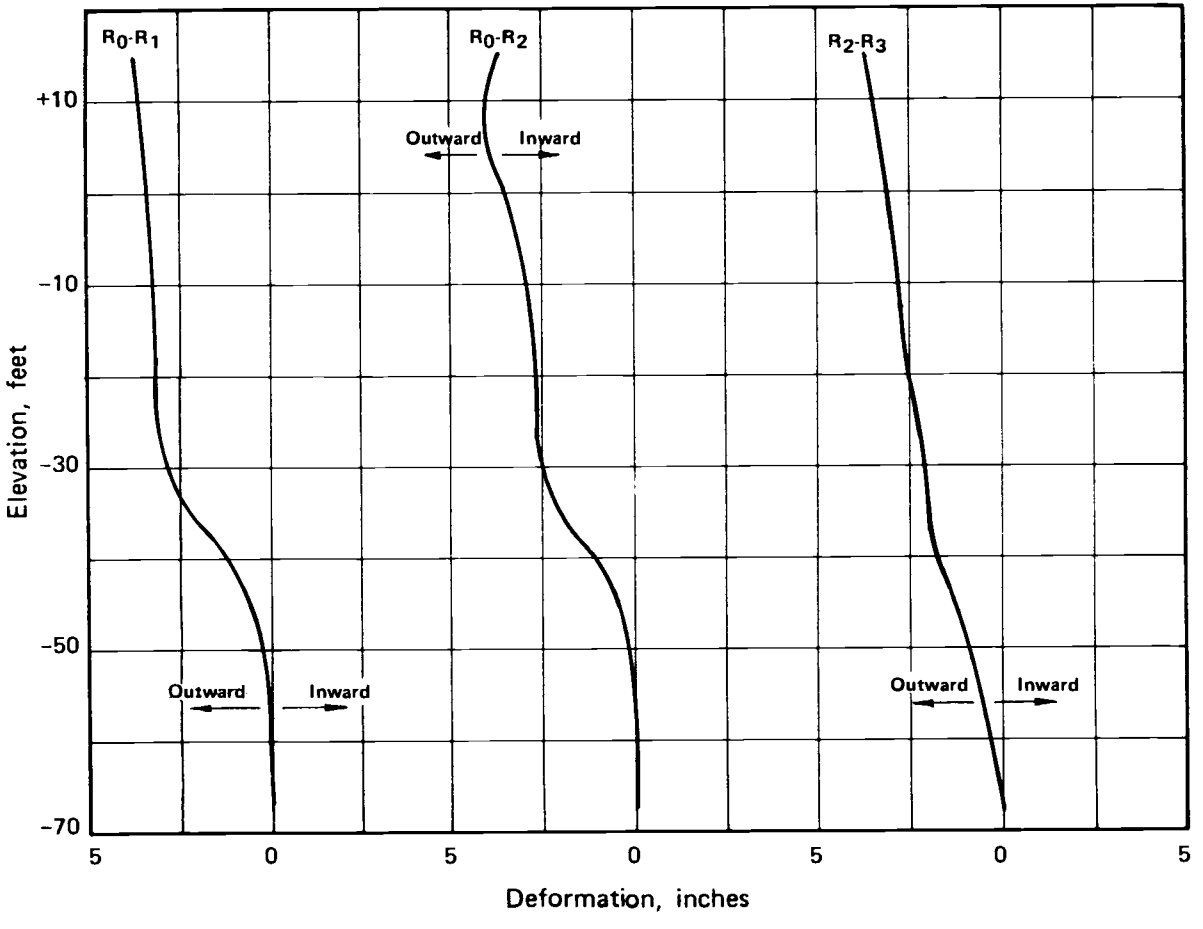

No.	Events	Date
R_0	Initial reading	10 29 73
R_1	Cell filled from -31 to -21	11 29 73
R_2	Cell filled from -21 to +14	12 14 73
R_3	"B" zone filled	1 9 74
R_4	Probed arcs 3 and 4	2 7 74
R_5	Final 4.5' fill	3 25 74
R_6	Concrete slab poured	4 20 74

(c) Radial deformation of instrumented sheet position 2.

Figure 96. continued

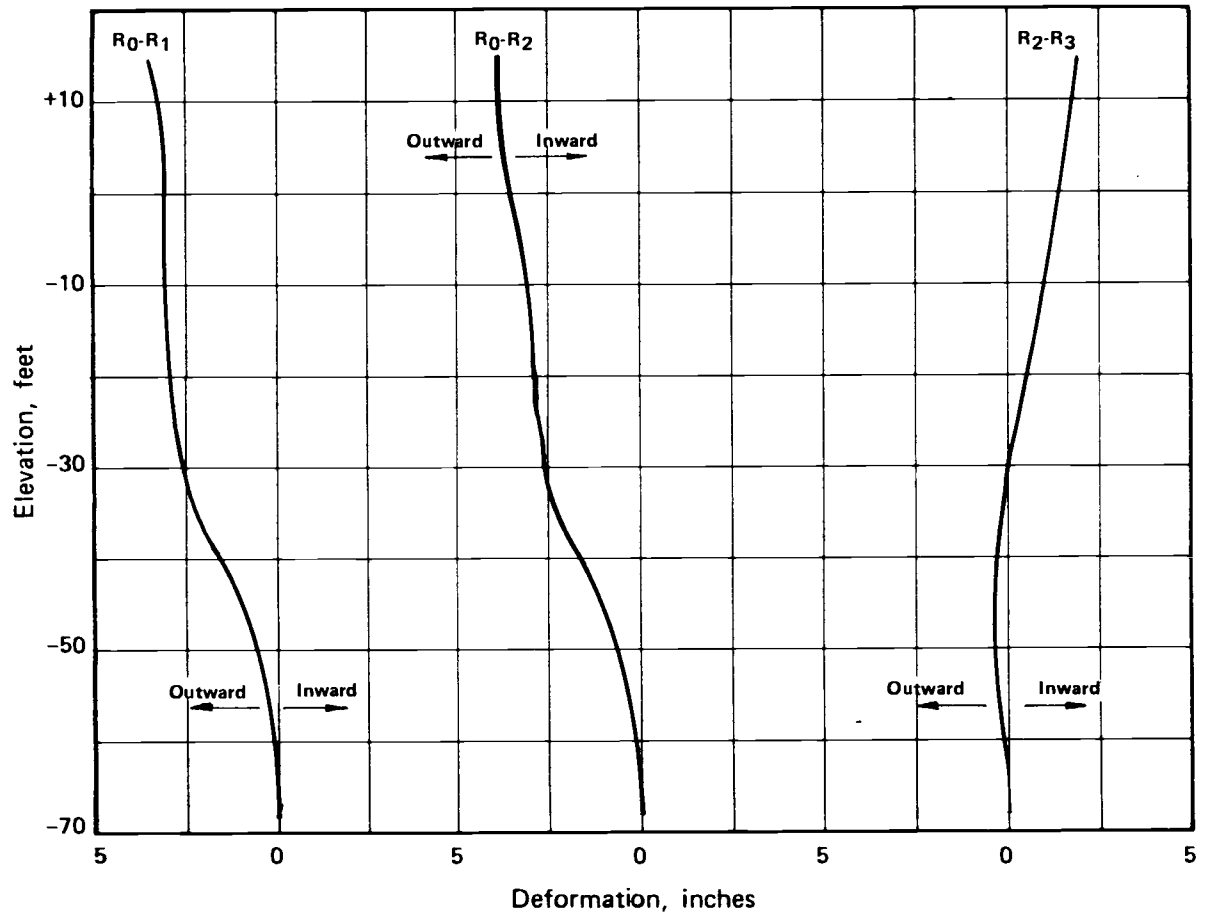

No.	Events	Date
R_0	Initial reading	10 29 73
R_1	Cell filled from -31' to -21'	11 29 73
R_2	Cell filled from -21' to +14'	12 14 73
R_3	"B" zone filled	1 9 74
R_4	Probed arcs 3 and 4	2 7 74
R_5	Final 4.5' fill	3 25 74
R_6	Concrete slab poured	4 20 74

(d) Radial deformation of instrumented sheet position 3.

Figure 96. continued

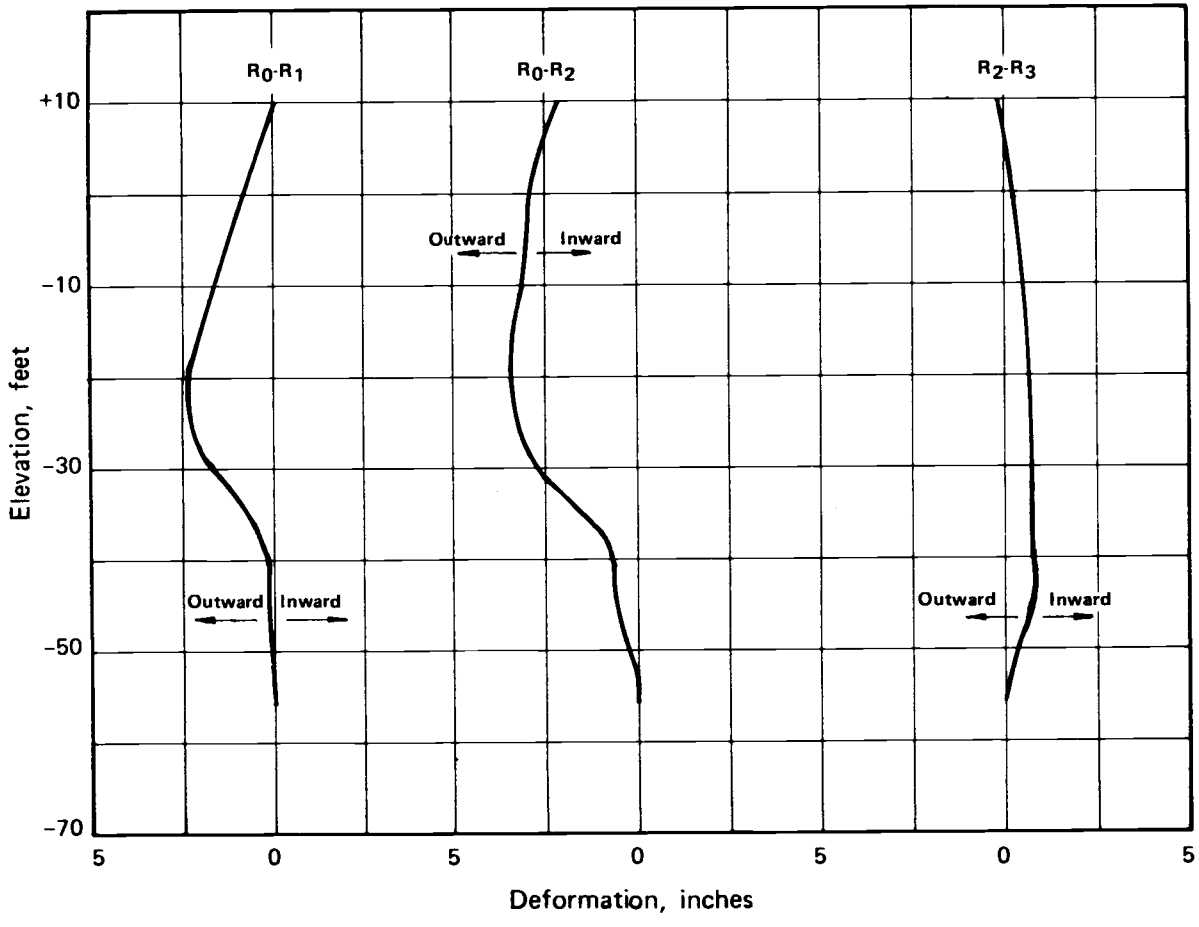

No.	Events	Date
R_0	Initial reading	10 29 73
R_1	Cell filled from -31 to -21	11 29 73
R_2	Cell filled from -21 to +14	12 14 73
R_3	"B" zone filled	1 9 74
R_4	Probed arcs 3 and 4	2 7 74
R_5	Final 4.5' fill	3 25 74
R_6	Concrete slab poured	4 20 74

(e) Radial deformation of instrumented sheet position 5.

Figure 96. continued

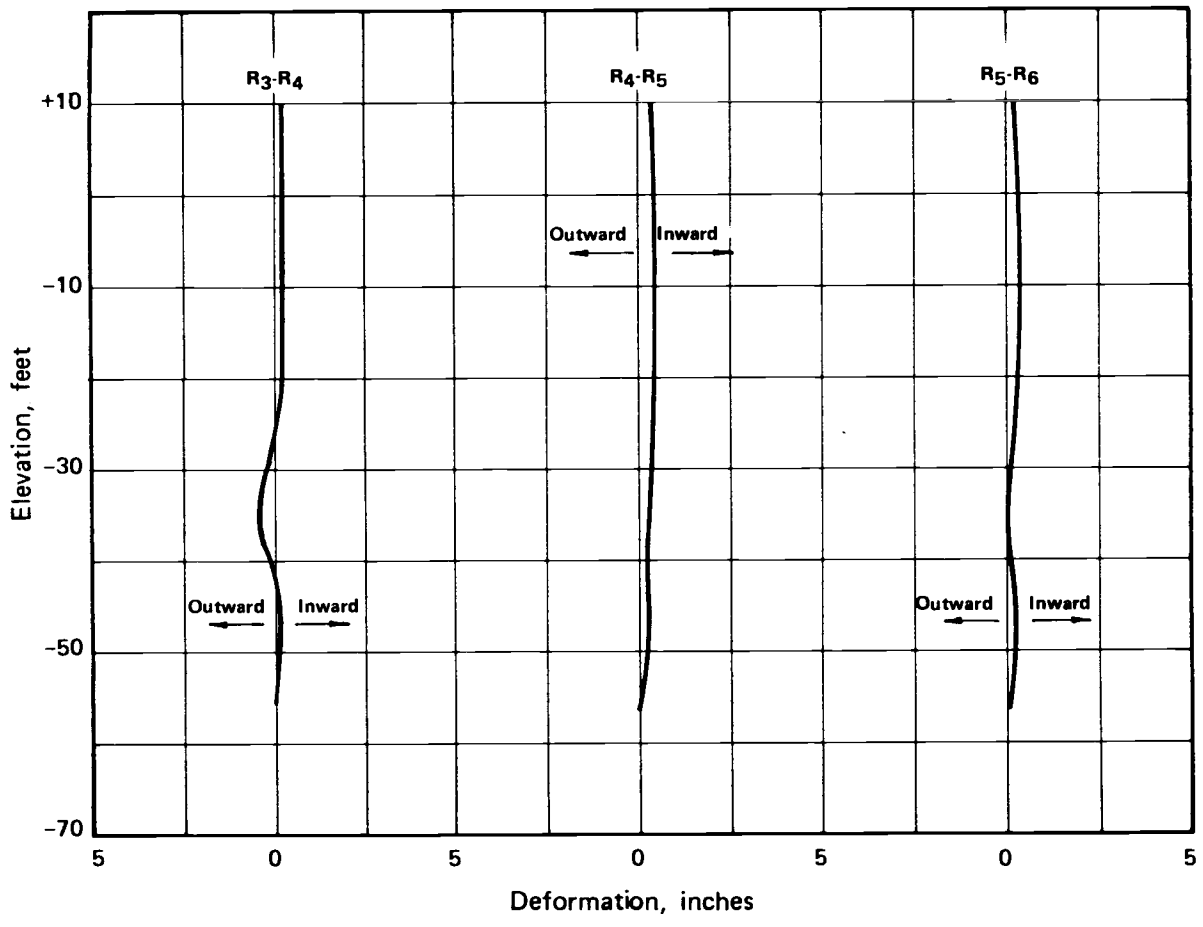

No.	Events	Date
R_0	Initial reading	10 29 73
R_1	Cell filled from -31' to -21'	11 29 73
R_2	Cell filled from -21' to +14'	12 14 73
R_3	"B" zone filled	1 9 74
R_4	Probed arcs 3 and 4	2 7 74
R_5	Final 4.5' fill	3 25 74
R_6	Concrete slab poured	4 20 74

(f) Radial deformation of instrumented sheet position 8.

Figure 96. continued

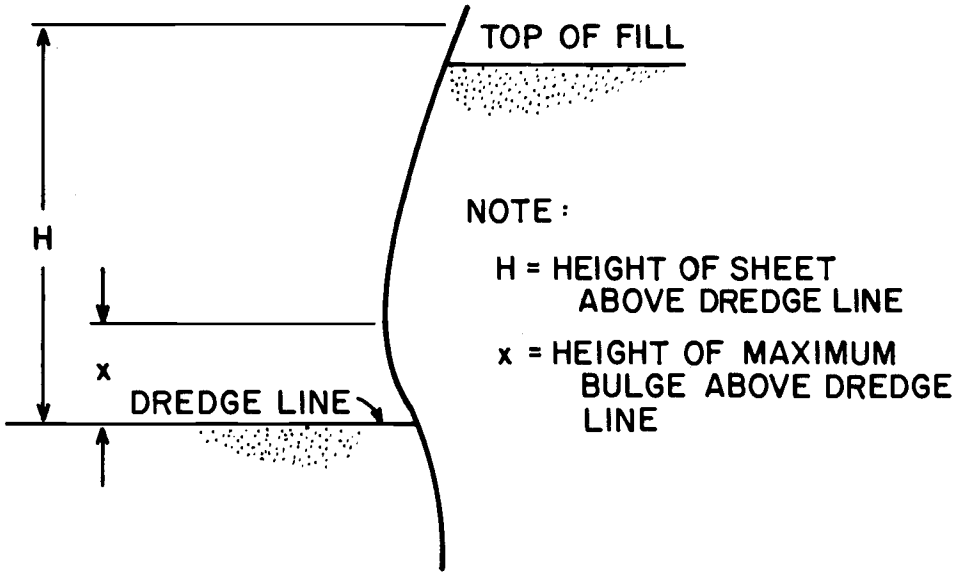

(a) Deflection of a sheetpile

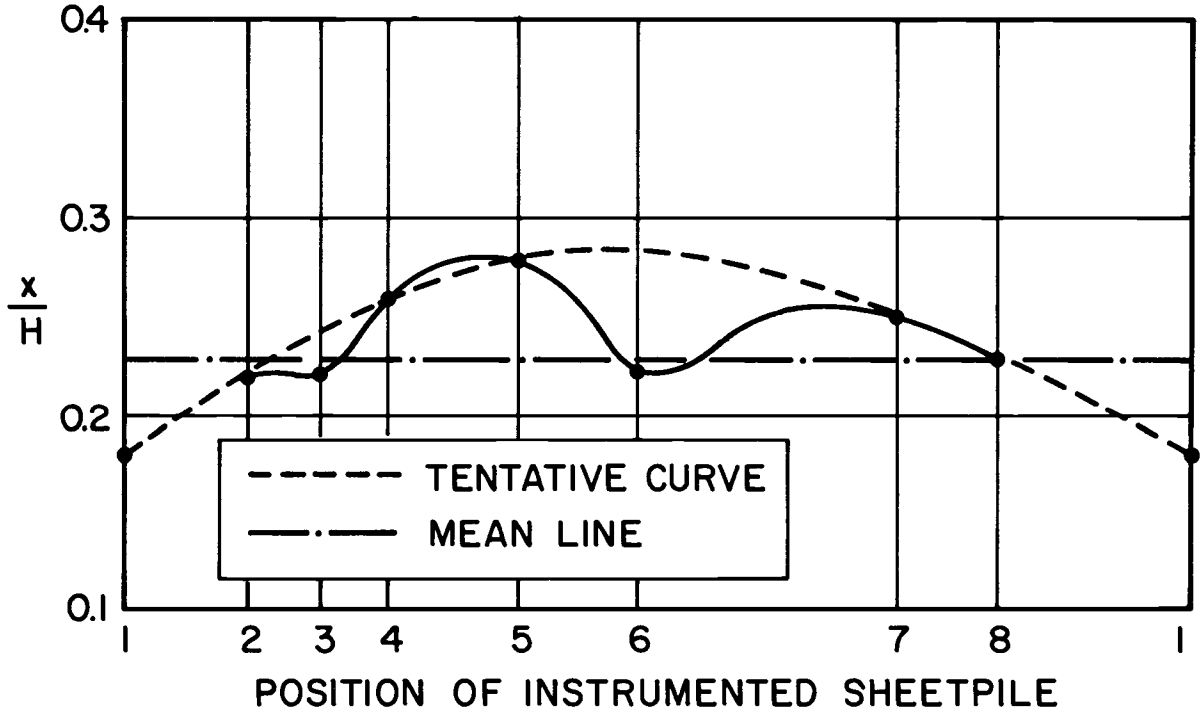

(b) Distribution of maximum bulging point

Figure 97. Positions of maximum bulging point in Terminal 4 cell (after Khuayjarernpanishk).

The point of maximum bulging at position 6 was significantly lower (and similar to the front sheetpiles).

Mechanism of Hoop Tension

Hoop stress data from the model study and available field data suggest that the magnitude and distribution of hoop tension along a sheetpile depends largely on the embedment and the flexibility of the sheetpile (i.e., the amount of radial deflections). The magnitude and distribution of the net lateral earth pressure, therefore, depends not only on the characteristics of the cell fill but also on the characteristics of the sheetpiles containing it.

The mechanism by which hoop stresses develop and deflection occurs can be, in part, understood by applying theory of elasticity to the problem of a cylindrical tank subjected to an internal hydrostatic pressure.

If the base of the tank is allowed to move and rotate, see Figure 98(a), then the maximum hoop stress and maximum radial deflection develop at the bottom. In this case no bending moments develop in the shell. Hoop stresses are calculated using thin membrane theory.

If the base of the shell is fixed against rotation and deflection, Figure 98(b), then the expression for the radial deflection, w, is

$$w = \frac{-\gamma r^2 h}{Et} \left[1 - \frac{x}{h} - \theta(\beta x) - \left(1 - \frac{1}{\beta h}\right) \xi(\beta x)\right] \qquad (48)$$

where γ = unit weight of fluid in tank

r = radius of tank

h = tank height

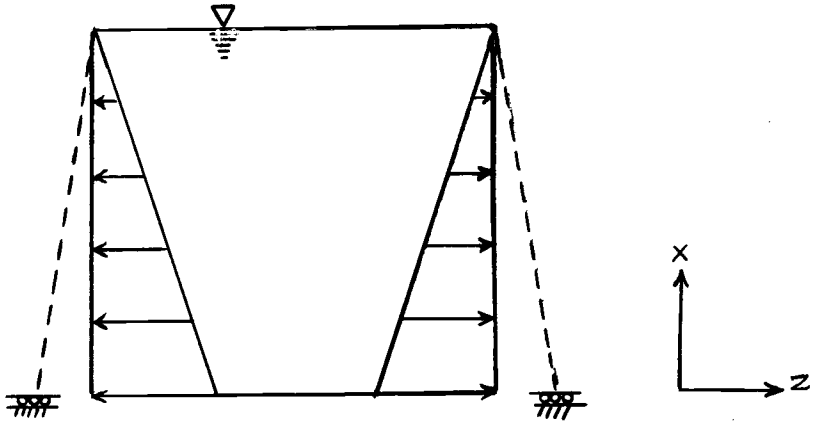

(a) Free base

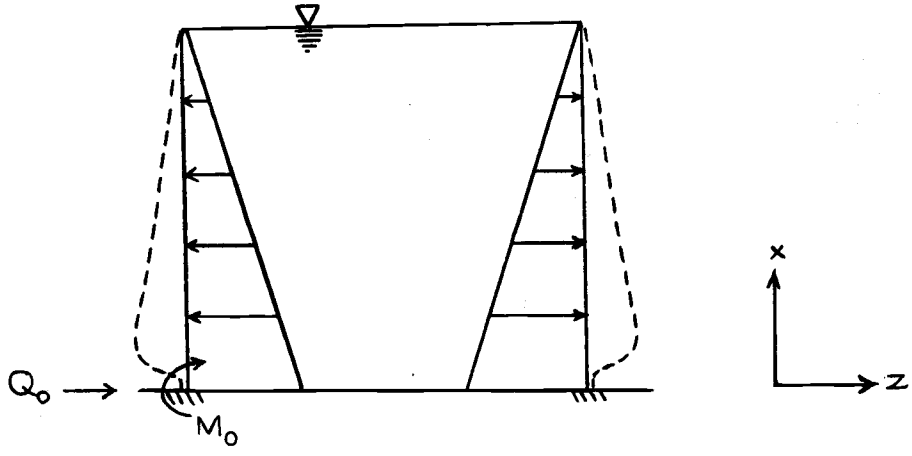

(b) Fixed base

Figure 98. Radial deflection of cylindrical tank.

t = shell thickness

x = distance from base of tank

β = flexibility term

ξ, θ = flexibility functions

The values of the functions $\theta(\beta x)$ and $\xi(\beta x)$ have been tabulated (Timoshenko and Woinowsky-Krieger, 1959). The flexibility term, β, can be tabulated from the expression

$$\beta^4 = \frac{3(1-\mu^2)}{r^2 t^2} \tag{49}$$

where μ = Poisson's ratio.

The hoop force, N_ϕ, can be obtained from the expression

$$N_\phi = - \frac{Et}{r} w \tag{50}$$

The maximum hoop force, therefore, occurs at the point of maximum bulging. The shear force, Q_o, and bending moment, M_o, that must be developed per unit length of circumference, to provide dredgeline restraint can be calculated from the expressions

$$Q_o = - \frac{\gamma r h t}{12(1-\mu^2)} \left(2\beta - \frac{1}{h}\right) \tag{51a}$$

and

$$M_o = \left(1 - \frac{1}{\beta h}\right) \frac{\gamma r h t}{12(1-\mu^2)} \tag{51b}$$

For the cell dimensions of the Terminal 4 bulkhead and equivalent shell thickness (i.e., which produce similar sheetpile rigidity), the ranges of base shear and moments computed by these methods are

$$Q_o = 3 \text{ to } 5 \text{ kip/ft}$$

$$M_o = 1.4 \text{ to } 3.8 \text{ kip-ft/ft}$$

The maximum computed radial deflection is approximately 0.25 inches and occurs between four and five feet from the dredgeline. Field measurements indicated maximum deflections on the order of two to five inches occurring between 10 and 16 feet from the dredgeline.

The difference in deflections between the theoretical calculation and field observations are due to the following factors which cause the cell to differ from the theoretical representation:

1) The slack in the sheetpile interlocks
2) A non-hydrostatic pressure diagram behind the sheetpiles
3) Rotation or deflections of the sheetpile at the dredgeline.

The slack in the interlock permits radial deflection without inducing hoop stresses. The amount of radial deflections due to interlock slack is significantly larger than that calculated from theory due to circumferential strains. Instead of the hydrostatic pressure assumed in the shell analysis, the lateral earth pressures in a sheetpile cell are a function of the local radial displacements. As displacements increase, the shear strength of the fill is mobilized

locally, reducing lateral pressures. Generally, one would expect greater mobilization of strength and, consequently, lower pressures in the lower portion of the cell. The effect of this, and interlock slack, is to cause the maximum bulging point to move up the cell. Although the passive resistance of most materials is sufficient to provide the total base shear previously calculated, the resultant of this passive constraint is not at the dredgeline as the theory discussed presumes, but at some distance below it. The deflection curves shown in Figure 96 attests to the dramatic reduction in displacements due to passive resistance (note however that there are small deflections and rotations at the dredgeline).

Although theory of elasticity does not yield accurate values of radial bulging for cellular structures, it may be used to obtain reasonable estimates of the depth to "fixity". For a structure similar to the Terminal 4 cells this depth would range (for a value of $\phi = 25°$) typically between six and nine feet below the dredgeline. Since the quality of the soil surrounding the cell affects the degree to which bulging is reduced (and therefore, hoop tension), it appears reasonable to estimate points of maximum bulging and hoop tension from the point of fixity instead of the dredgeline. TVA engineers suggested that the maximum bulging point occurred at an elevation of H/4 to H/3 above the base (for cells on rock) (TVA, 1957). It appears that the maximum bulging (i.e., the maxmimum hoop tension) occurs at about H/6 to H/4 above the dredgeline, for cells embedded in sand, based on the Terminal 4 cell. The bulging for the Long Beach cell continued to increase at the dredgeline. Whether this is due to injury

to the interlocks or the poor quality of the soil surround the cell is unknown.

The influence of sheetpile flexibility and embedment may be summarized with the aid of Figure 99 and 100. For the case of zero embedment, (Figure 99) the sheetpiles move outward as shown and no bending moments are induced. The lateral pressures diagram is nearly hydrostatic, though a small reduction near the dredge lines may occur due to arching within the fill. The hoop stresses also increase hydrostatically (with a possible small reduction near the dredgeline). The rigidity of the shell influences the magnitudes of the radial displacements. If radial displacements increase for the nearly flexible case, then the lateral pressure curve approaches the active conditions as more shear strength of the fill is mobilized.

The effect of embedding the nearly rigid sheetpile is two-fold. First, it reduces the amount of deflection at the dredgeline (Figure 100(a)). The point of maximum bulging is then at some point $\bar{y}$ above the dredgeline. Second, the net lateral earth pressure near the dredgeline is reduced because of the passive resistance below the dredgeline transmitted through the shell. The slope of the earth pressure curve (i.e., the value of K) may increase slightly because of reduced deflections.

If the embedded sheetpile approaches the nearly flexible case, the point of maximum bulging approaches the dredgeline and there is less reduction of lateral earth pressure due to passive resistance. That is, the nearly flexible shell cannot transmit passive resistance above the dredgeline. The slope of the lateral pressure diagram

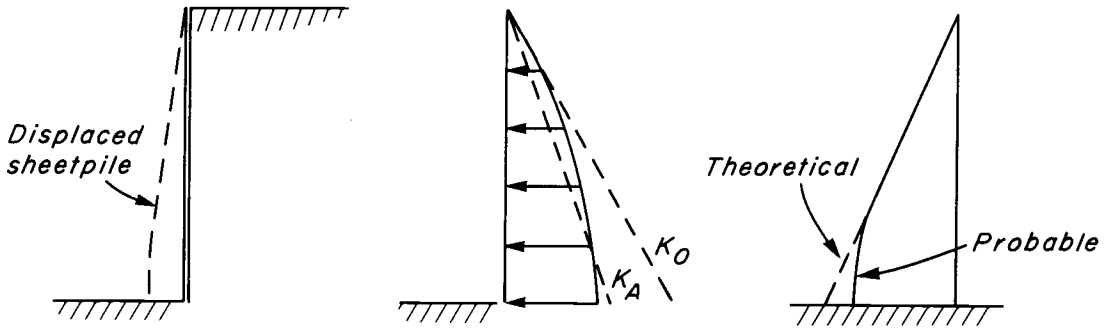

radial displacement lateral earth pressure hoop tension

(a) Nearly rigid sheetpiles.

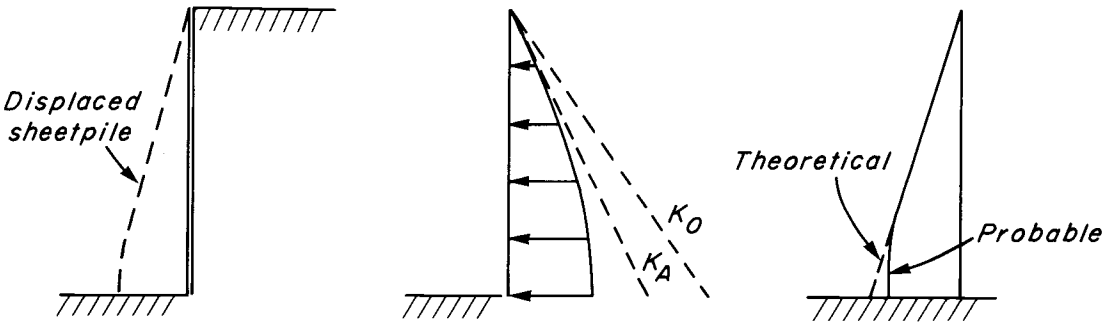

radial displacement lateral earth pressure hoop tension

(b) Nearly flexible sheetpiles.

Figure 99. Hypothetical behavior of cell walls with zero embedment.

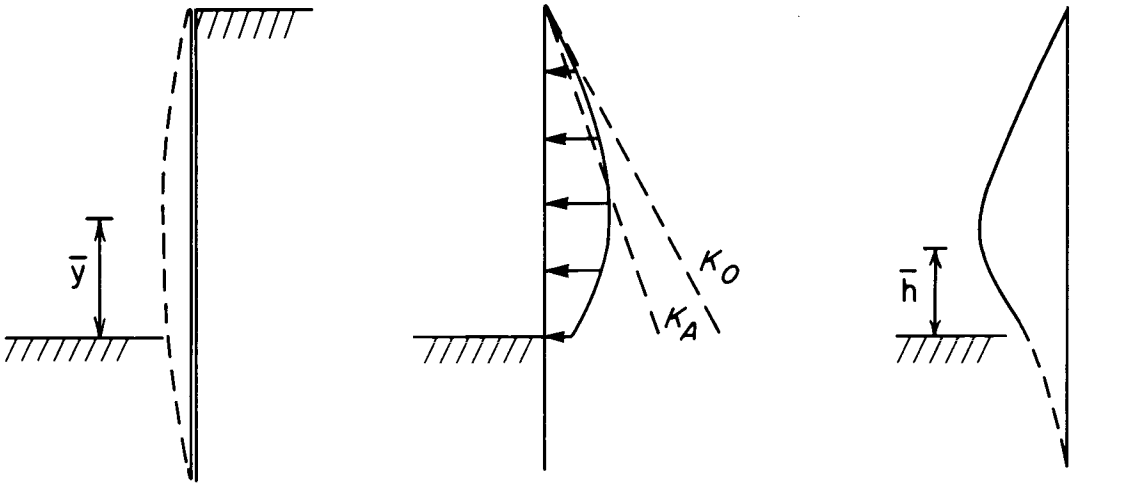

radial displacement lateral earth pressure hoop tension

(a) Nearly rigid sheetpiles.

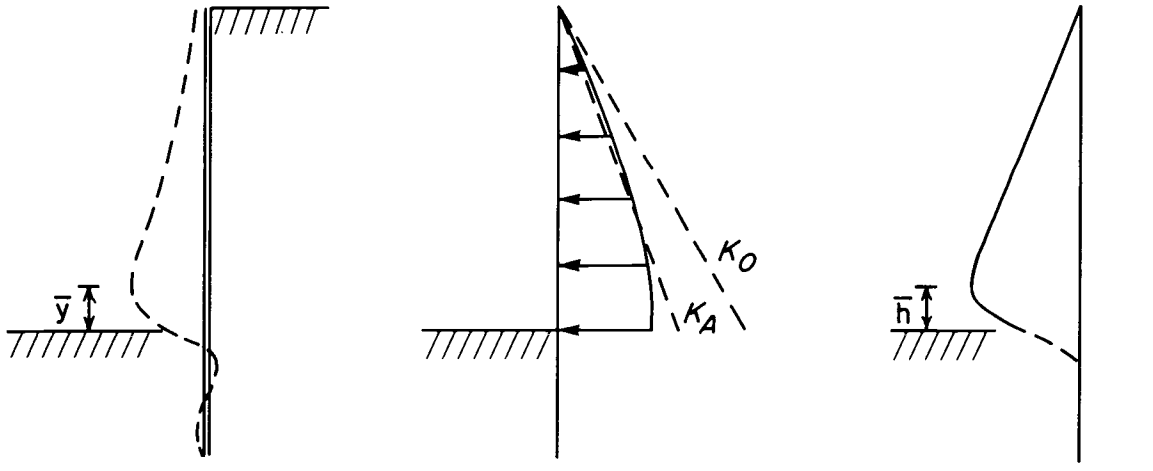

radial displacement lateral earth pressure hoop tension

(b) Nearly flexible sheetpiles.

Figure 100. Hypothetical behavior of cell walls with embedded sheetpiles.

(i.e., K) approaches that of the active case. However, since the point of hoop tension reduction is closer to the dredgeline, the magnitude of the maximum hoop tension increases above that of the rigid wall case. As the flexibility increases, one approaches the zero embedment case.

Several observations can be made about the hoop stress curves of the model summarized in Figure 94. They are:

1) The maximum hoop stress increased about 11% when the embedment depth is reduced from 22 to 10 inches (a reduction ratio of 0.45). The average maximum hoop stress over the entire cell increased only about 6%.
2) The "stepped" cell (No. 3) showed an average decrease in hoop stress of about 22% over Cell No. 1.
3) A sharp reduction in hoop stress occurred at about 0.30(H) from the dredgeline for cells No. 1, 2, and 3.
4) In all cases the hoop stress below the dredgeline were very small.
5) The slope of the hoop stress curves down to the point of maximum hoop stress was very similar for Cells No. 1, 2 and 3 (representing an average K = .183).

Observations from available field data may be summarized as:

1) Average hoop stresses continue to increase with depth (almost linearly) near to the dredgeline, for both the Long Beach and Terminal 4 cells.
2) The hoop stress at the back portion of both cells tends to be lower than for the front portions. The differences

between front and back result from decreasing sheetpile embedment and changes in soil conditions.

If the deflections of the model sheetpile are to simulate the deflections of the prototype (i.e., satisfy the similitude laws), then the slope of the elastic curves must be similar. That is

$$\left(\frac{dy}{dz}\right)_{\text{model}} = \left(\frac{dy}{dz}\right)_{\text{prototype}}$$

therefore,

$$\left(\frac{Mz}{EI}\right)_m = \left(\frac{Mz}{EI}\right)_P$$

and

$$\left(\frac{H^4}{EI}\right)_m = \left(\frac{H^4}{EI}\right)_P = \rho$$

For similitude, then, the flexibility number, ρ, for the model and the prototype should be equal (Rowe, 1952). A moment of inertia of 4.6×10^{-4} in^4 was determined for the model sheetpiles by deflection tests. Calculations of typical model and field sheetpiles indicate that the model sheetpiles were 5 to 10 times relatively stiffer. It can be expected, then, that the slope of the elastic curve in the field is considerably sharper (see radial deflection curves) than that of the model. This is evident in the available field data where hoop stresses appear to be increasing very close to the dredgeline.

Coefficient of Lateral Earth Pressure

The average apparent coefficients of lateral pressure for the first three cells and Cell No. 4 were 0.183 and 0.137, respectively. The first number represents a value of about 1.38 times the Rankine active coefficient, K_A. The second value lies closer to the active coefficient and, most probably, reflects the relatively large amount of sheetpile deflection due to lack of embedment and interlock slack.

White, et. al., reported a maximum average coefficient of 0.54 for the Long Beach cell (White, et. al., 1963). A considerable range in hoop tensions at each level was also reported. Values of the apparent coefficient as high as 0.66 and as low as 0.27 were noted. In addition, the apparent coefficient decreased over a period of time after cell filling, in some instances by as much as 50 percent.

Khuayjarernpanishk reported a maximum average apparent coefficient of 0.45 with values ranging from 0.11 to 0.71 (Khuayjarernpanishk, 1975). Typically, the lower values of Khuayjarernpanishk occurred at the lower instrumentation level (Level C). The average lateral pressure coefficient dropped to about 0.35 within five days of cell filling. The effect of time on the coefficient, K, may presumably be interpreted as the influence of consolidation of the fine to medium clean sand cell fill. The cell fill at Terminal 4 consisted of well-drained fine to medium clean sands deposited by conveyor into water-filled cells.

A drop in the apparent coefficient, K, accompanied the consolidation of the fill. Higher values of K at upper levels of instrumentation apparently indicated incomplete consolidation and the presence of an excess head of water (above the stable water level). The time decrease of K for the Long Beach cell appeared to proceed at a slower rate, possibly due to the presence of silts and fine sands in the cell fill.

The Long Beach cell indicated values of the coefficient, K, that were, on the average, higher than those calculated for the Terminal 4 cell. Both cells were dimensionally similar and borings indicate relatively similar fill materials. The Long Beach cell, however, was filled with a pipeline dredge rather than with a conveyor. The method of filling, therefore, appears to influence the magnitudes of interlock forces.

The fill material used in the Terminal 4 cells had, prior to probe compaction, an average relative density of about 40%, corresponding to a friction angle of about 33 degrees (Schroeder, et. al., 1977). Experience with a similar structure two miles away (Terminal 6) indicates that similar fill material placed under by clam shell has average relative densities of about 40% (Anderson and Ramage, 1976). A model study conducted in connection with the latter project indicated that underwater hydraulic sand fills placed by a dredge pipeline have very low relative densities (on the order of 20 percent) and that the relative density is sensitive to the orientation of the pipeline. The study also concluded that underwater hydraulic sand fills were subject to accumulations of silts at the soil/structure interface, leading to an increase in lateral pressure against the structure (Anderson and Ramage, 1976).

White, et. al., indicated values of about 37° for friction angle of the cell fill. Since the fill was placed by a pipeline dredge and was not densified, it appears, based on other evidence cited, that the indicated value for the friction angle is somewhat high. The relative density would be expected to be no higher than that of the Terminal 4 cell (i.e. about 40 percent). A value of the friction angle closer to that of the Terminal 4 fill would seem more reasonable.

The average values of K of 0.45 and 0.35 for the Terminal 4 instrumented cell represents a range of

$$K_1 = 1.53\ K_A \text{ (immediately after filling)} \tag{52a}$$

$$K_2 = 1.19\ K_A \text{ (five days after filling)} \tag{52b}$$

where K_A = Rankine active coefficient

The average values of K for the maximum levels of interlock tension (Level C) and for the entire Long Beach Cell were 0.46 and 0.54 respectively. This represents a range (using an assumed $\phi = 33°$) of

$$K_1 = 1.83\ K_A \text{ (temporary)} \tag{53a}$$

to

$$K_2 = 1.59\ K_A \text{ (long range)} \tag{53b}$$

The above ranges of values encompass the average coefficient ($K = 1.38\ K_A$) found in the model study. The average value for the model may have been higher because of differences in sheetpile stiffness and the method of cell filling. The apparent coefficient, K, is expressed in terms of the Rankine coefficient, K_A, only for convenience since it depends only on the characteristics of the fill. Friction between the fill and sheetpiles undoubtedly exists and the value of K could alternately be expressed in terms of the Coulomb coefficient.

Experience with cellular bulkheads indicates that the largest single increment in hoop tension is that due to initial cell filling. If the cell is to be backfilled and surcharged, the hoop tension may increase (depending on location). The full cell stage, then, may represent the critical level of hoop tension in the side and back portion of the cell, while hoop tension may increase towards the front part of the cell in subsequent construction stages. The interlock forces at the full cell stage should, therefore, be checked for excessive tension. Sheetpile manufacturers (U. S. Steel, 1975) recommend a minimum factor of safety of 2.0 against failure at maximum design tension. The difference in interlock tension in an isolated cell between filling and some later time, when it has decreased to a minimum, may be considered as a temporary live load which dissipates due to consolidation. The design of a circular cell bulkhead should, therefore, be checked (in particular for the back sheets) using the permanent apparent coefficient, K_2. This coefficient may have a range of $1.2\ K_A$ to $1.6\ K_A$. The range indicates the influence of the filling method and the drainage quality of the fill material. Unfortunately,

available field data is too limited to permit better resolution of the coefficient. Available evidence indicates that cells filled rapidly (i.e., by conveyor) with well-drained granular material will develop interlock tensions in the lower range of K_2. Fills that are either hydraulically placed at comparatively slow rates or that contain substantial amounts of fines will probably develop interlock tensions in the higher range. The design engineer must, therefore, evaluate the quality of the fill and the placement method before choosing an apparent coefficient to check the full cell stage.

Conclusions for Isolated Cells

Radial deflections of an isolated cell are due, for the most part, to slack in the sheetpile interlocks. This action is inelastic and is partially restrained near the dredgeline by embedment. After the interlocks tighten, the cell simulates the behavior of a steel shell and subsequent radial deflections are relatively small.

Model cells indicate that generally the hoop stress increases linearly with depth to a maximum point near the dredgeline then drops off dramatically. Field studies indicate that the hoop stress tend to increase linearly with depth almost to the dredgeline. Maximum hoop tensions at the front of the cells typically occur at an elevation of H/6 to H/4 above the dredgeline, somewhat lower than the range suggested by TVA. It would appear more reasonable, however, to include the quality of the surrounding soil in the calculation of maximum hoop tension. The point of maximum bulging (i.e., hoop tension) would then be expressed with reference to the point of sheetpile "fixity". If the cell height, to the point of "fixity" is H', then the point of

maximum hoop tension can conservatively be assumed to occur at an elevation of about (0.25)H' above the point of "fixity".

All the cells (with embedment) indicated that hoop stress at or just below the dredgeline is very small and alternates between compression and tension. Field deflection curves also show very small deflections below the dredgeline. It therefore appears reasonable to conclude that the hoop stresses drop to zero at some distance below the dredgeline. Hoop stress curves for the model indicate that this distance is, on the average, 0.04 times the exposed cell height, H.

This depth was independent of the embedment depth, for the depths considered. However, this depth must certainly depend on the quality of the soil in front of the cell. If the material is weak, the depth necessary to develop fixity will surely be larger than for a dense, strong material. If the soil is relatively soft or weak the depth may be approximately computed by the elasticity equations already presented (see Equation 51). The depth to reduced bulging is that depth required to produce a resultant passive force equal to the shear Q_o, and moment, M_o. It is the radial restraint provided by the shear force, Q_o, which tends to reduce both the deflection and hoop stress near the dredgeline. At the point of "fixity" one would expect both small radial deflection and small hoop forces.

Cell deformation profiles (for Terminal 4) indicate that radial deflections dropped to about 10 percent of the maximum bulging at depths that ranged from 12 feet below the dredgeline (position 5) to the dredgeline (positions 2 and 3). This represents a ratio of

depth to exposed cell height ranging from 0 to 0.20, or an average of 0.10. This range of depths does not appear to depend on the embedment depth, within the range of depths represented by the Terminal 4 cell. The presence of the 10-foot silt layer surrounding the cell, however, may influence the depth of fixity.

The Long Beach cell appeared to show an average increase in radius extending almost to the bottom. It is unknown whether this is due to interlock distress below the dredgeline or poor quality soil which did not restrain deflections. It does, however, explain, in part, the tendency for hoop tensions to continue to increase near the dredgeline.

The maximum hoop tension for an isolated cell can be assumed to occur at a distance 0.25 (H') from the point of "fixity" and calculated using an apparent coefficient, K_2. The hoop tension may be assumed to decrease to zero at a depth below the dredgeline of about 0.10 times the exposed height or to the point of "fixity" calculated by theory of elasticity. If the cell is embedded in weak material this depth will increase. Below this point, the interlock forces oscillate between small tensile and compression forces. The interlock forces may be assumed, therefore, to be equal to zero below the point of "fixity". Figure 101 summarizes these conclusions.

If the cell is to be backfilled and surcharged, the critical (i.e. design) interlock tension may occur at some later time, corresponding to these loadings. The apparent coefficient used for design the critical stage may, therefore, be larger than the one used to check the full cell stage.

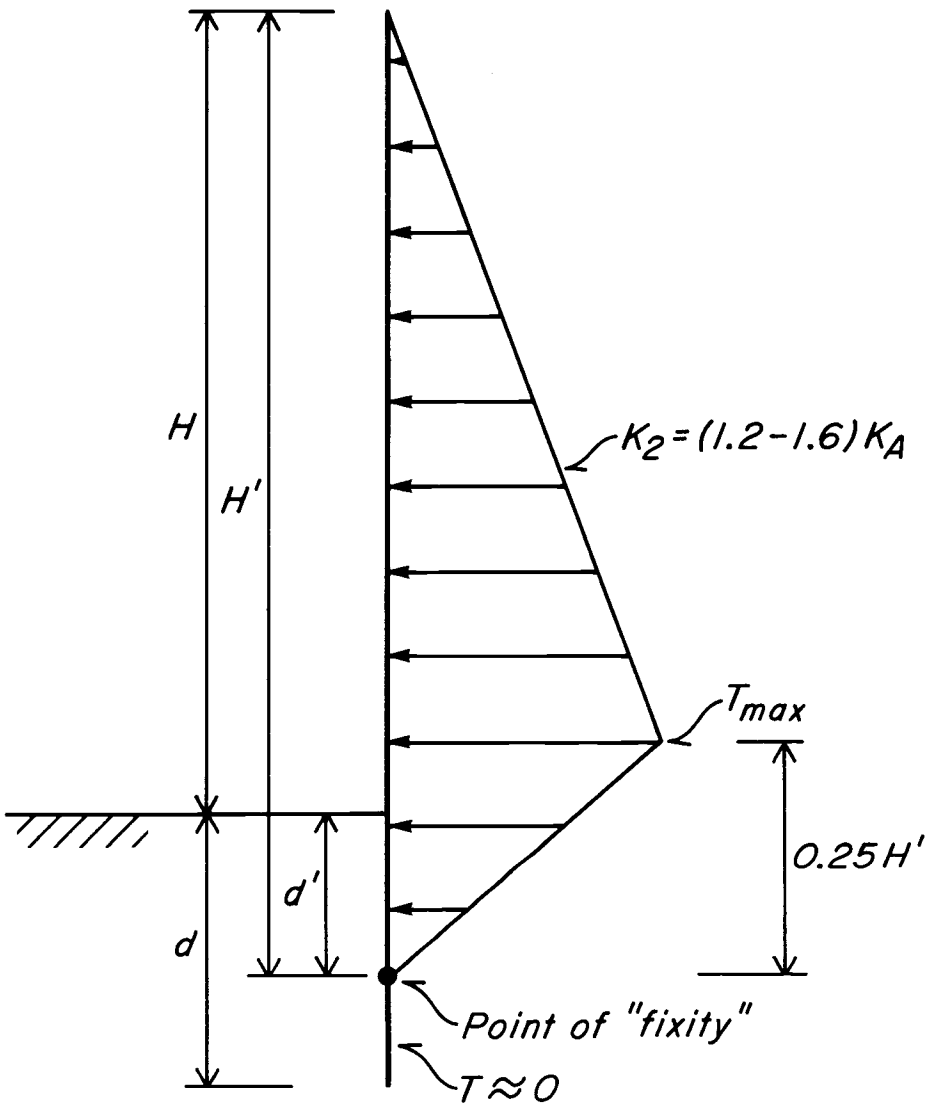

Figure 101. Net lateral pressure distribution for calculating hoop stress (isolated cell).

Discussion of Backfilled Cells

Deflections Due to Backfill

Figures 55 through 58 summarize the net radial movements of the front sheetpiles in the main model test series, due to lateral unbalanced backfill loads. The bulging due to initial cell filling has been subtracted. The magnitudes of the outward displacements due to backfill for all cells appear to be relatively equal (on the order of 0.04 to 0.08 inches). The general deflection of the cell due to backfilling appears to be that of uniform outward movement combined with a small amount of tilting. On the average the outward displacement of the top of the first three cells was about 1.5×10^{-3} times the exposed cell height. The amount of tilting was too small to draw any conclusions. Cell No. 4 showed a maximum displacement at the base since there was no restraint from sheetpile embedment.

Changes in Hoop Stress Due to Backfilling

The dashed lines in Figures 46 through 49 indicate the changes in hoop stress due to backfilling. Note in the sequence of events Table 4, 5, 6 and 7 that slight variations in backfill height occurred. The average elevation of all backfills was approximately 94% of the exposed height.

The average change in hoop stress in Cell No. 1 was relatively small. All sheets showed an increase of about 17% in hoop stress at level A. Sheetpiles P1 and P4 showed slight increases in the maximum hoop stress (about 13 and 9%, respectively). Sheetpiles P2 and P3 showed a slight decrease in hoop stress at levels B and C. Apparently the affect of backfill on sheetpile P3 (behind the Y-section) was to

decrease the hoop stress due to lateral earth pressure rather than increase it due to arc tension. No significant changes in hoop stress occurred at levels near or below the dredge line.

The changes in hoop stress at the front sheetpile (P1) due to backfilling were slightly higher for Cell No. 2 than for No. 1. The maximum hoop stress (at level C) increased by about 25%. Sheetpiles P3 and P4 showed a trend of decreasing hoop stress, with a decrease in the maximum hoop stress at the back sheet of about 27%. Again, no increase in hoop stress in sheetpile P3 due to arc tension was evident.

The front sheetpile of Cell No. 3 showed an increase in hoop stress for all three levels above the dredge line. The maxmimum hoop stress increased (between levels B and C) by about 25%. Sheetpiles P3 and P4 again show a significant (between 30 and 50%) decrease in hoop stress. It appears that the backfilling operation tends to affect hoop tension in the shorter sheetpiles (of Cell 3) more than those with larger embedment depths.

The hoop stresses in the front sheetpile of Cell No. 4 showed a relatively uniform increase in hoop stress at all levels of about 16%. The side and back sheetpiles (P3 and P1 respectively) showed a decrease in hoop stress similar to those of Cell No. 3.

Field Data

White, et. al. Sheetpile profiles presented by White indicate that the effect of backfilling (Stage V) on deflections was to cause outward displacements at the front sheetpiles and inward deflection at the back sheetpiles. The cell underwent, on the whole, some rotation and tilting. The net increase in sheetpile deflections (beyond the full cell stage)

due to backfilling was relatively small. However, when the backfill was raised approximately 13 feet (Stage VI) the cell showed significantly larger displacements. The cell as a whole tipped approximately 3° (including a southerly rotation) and racked about 2°.

The changes in average hoop stress for selected sheetpiles in the cells due to the two stages of backfill are summarized in Figures 102 through 104. The largest increase in hoop stress in the front sheetpile occurred at level 1. At lower levels the hoop stress increased by approximately 10%. The affect of backfilling on sheetpile C (behind the arc) on hoop stress was most severe at level 2 where the hoop stress almost doubled. The increase, however, took place at a level having lower than average hoop stresses at the full cell stage. Changes in hoop stress at other levels was very small. Backfilling reduced the hoop stresses along the back sheetpile (E) rather uniformly (about 18%).

Khuayjarernpanishk. Deformation profiles for the Terminal 4 cell indicate that the backfill operation caused a radial displacement at the top of the front sheetpile of about two inches. An additional outward bulging (of about two inches) also occurred at the dredgeline. The back sheetpile showed an inward bulging in the lower third of the sheetpile. Sheetpiles at the sides indicated an inward movement of the cell ranging from one half to three inches.

The hoop tension in the sheetpiles near the front portion of the cell (positions 1, 2 and 3) showed very little change due to backfilling. In particular the hoop tension behind the arcs

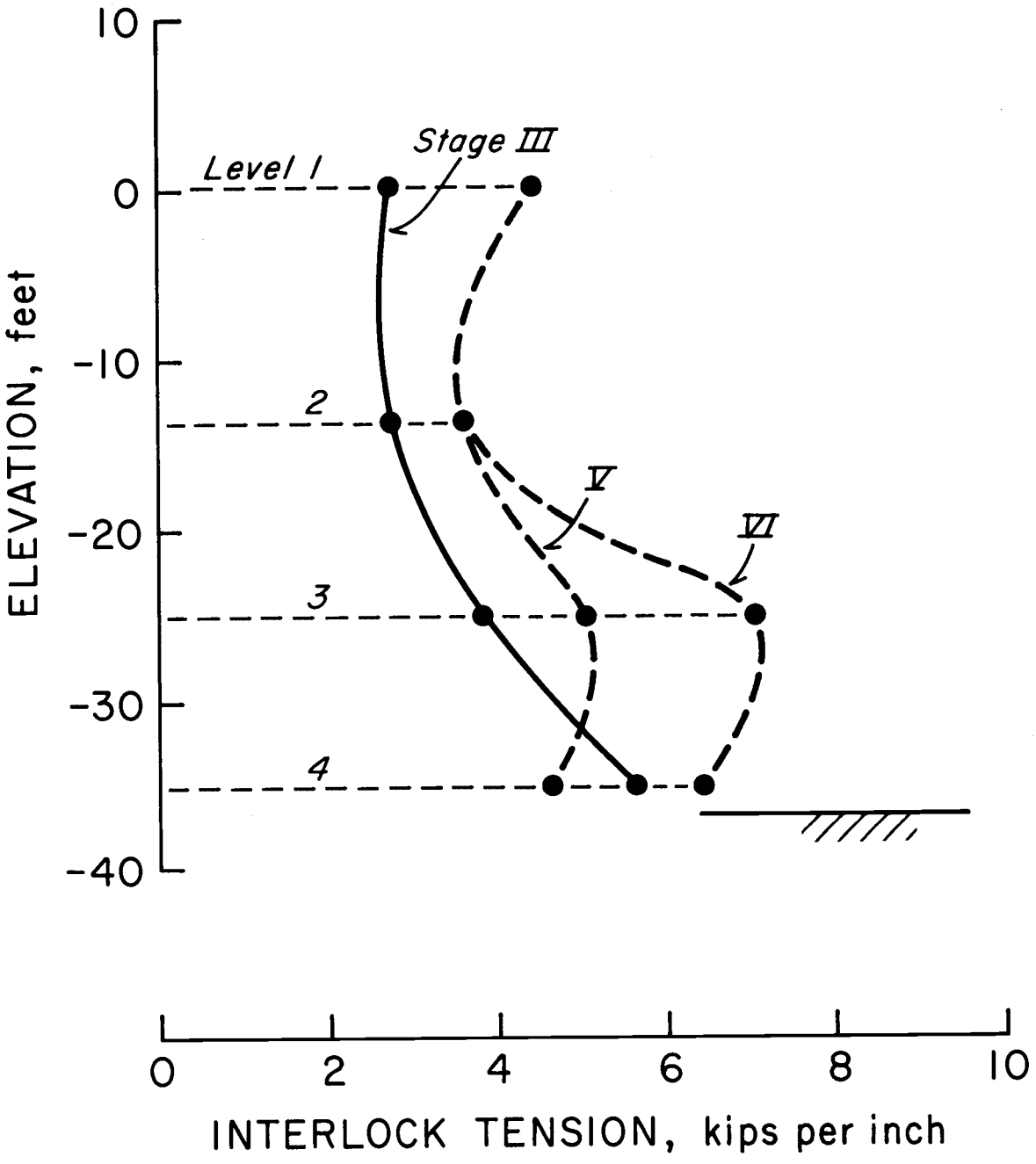

Figure 102. Interlock tension at front sheetpile (position A) of Long Beach cell.

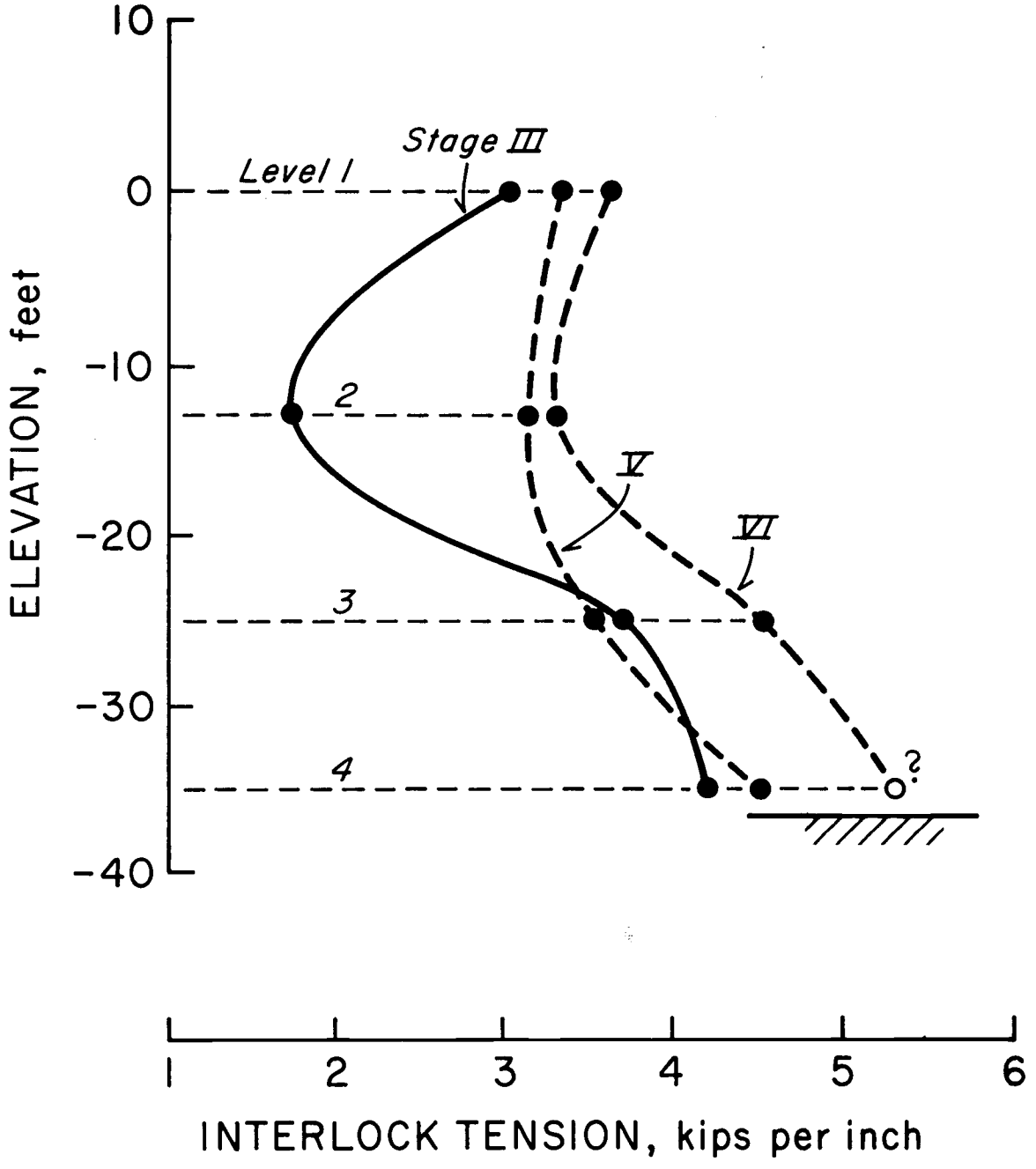

Figure 103. Interlock tension behind arc connection (position C) of Long Beach cell.

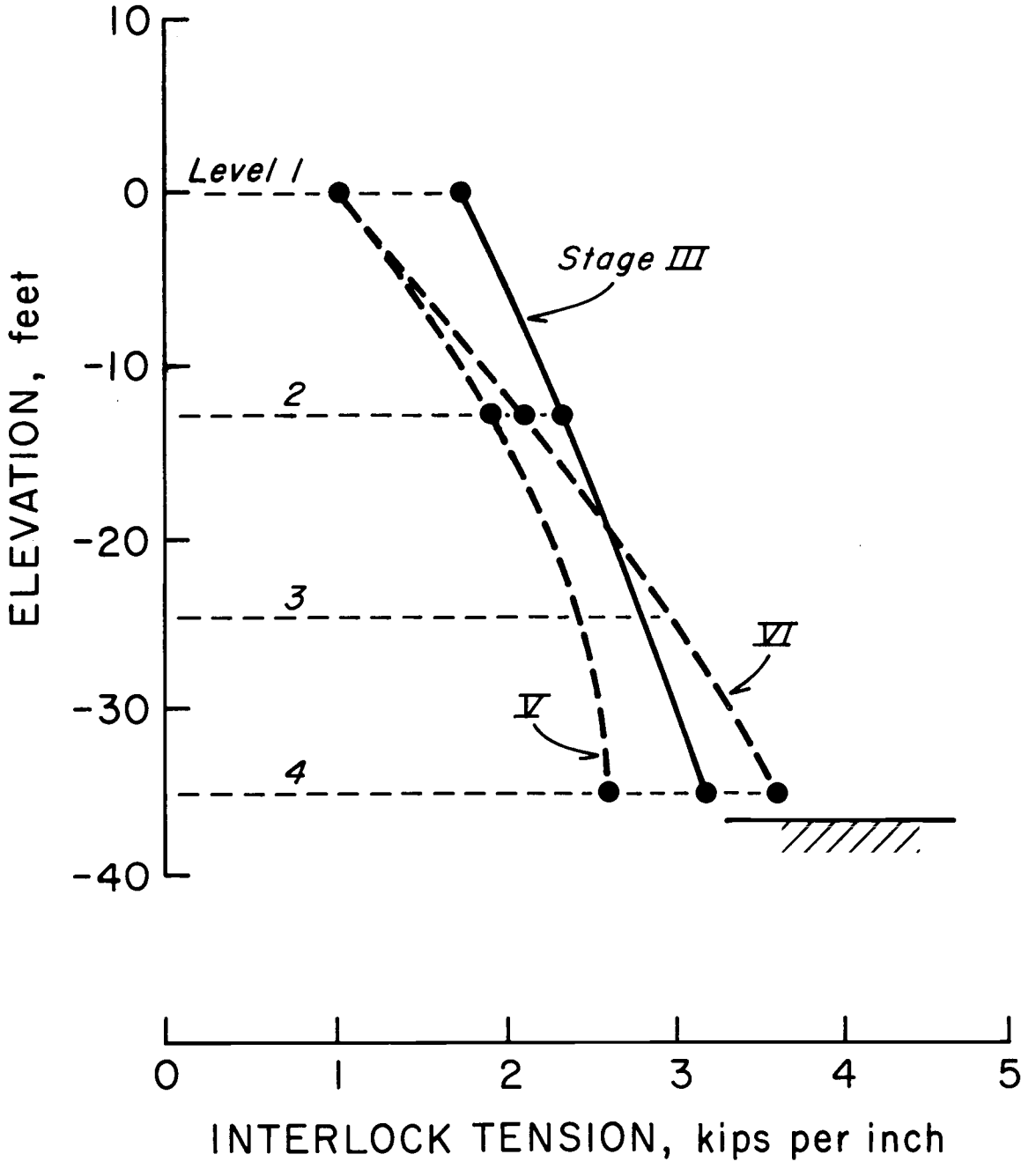

Figure 104. Interlock tension behind arc connection (position E) of Long Beach Cell.

(position 3) was insensitive to arc filling and backfilling at the upper levels of instrumentation. At lower levels the hoop tension decreased. Both side sheetpiles (positions 4 and 7) showed a consistent drop in hoop tension of about 10 to 30%. The back sheetpile (position 6) showed a substantial drop in hoop tension at all levels (over 50%).

Conclusions on the Effects of Backfilling

Deflections. The addition of a backfill appears to have a relatively small effect on cell displacements. The front sheetpile tends to tilt outward with a small additional bulging near the dredge line. The back sheetpile tends to move inward with a tendency to bulge (inward) in the lower third. The model cells indicate that additional displacements of the top of the front sheetpile (usually the critical point from a design standpoint) due to backfilling is on the order of 1.5×10^{-3} times the exposed cell height, H. Additional tilting due to backfilling at the Terminal 4 cell was on the order of about 5×10^{-3} times H. The displacement of the top of the Long Beach cell due to backfilling was about 12×10^{-3} times the exposed height. Field data also indicates inward movements at side sheetpiles. These are consistent with the tendency of cells to change from a circular shape to a roughly elliptical shape during backfilling.

The deflection of cellular bulkheads due to backfilling is one of the hardest responses to evaluate. Deflections depend on the quality of the cell fill, the interlock tension, the quality of foundation materials, sequence of filling cells and arcs, sheetpile flexibility

and probably other factors. In general, the designer should allow for a minimum of about 12 inches of outward deflection of a backfilled cellular structure. If large surcharges are to be added, then larger deflections are to be expected.

Hoop Tension. Several important conclusions can be drawn from the model study concerning the influence of backfilling on hoop tension. The trends seen in the model appear to be consistent with available field data. The main conclusions are:

1) Hoop tension at the front of the cell and near the arc connection may increase slightly.

2) Hoop tension in sheetpiles adjacent to the arc does not change appreciably at lower levels due to arc tension.

3) Hoop tension along the back of the cell decreases during backfilling.

The percent increase in interlock tension at the front sheetpiles due to backfilling is largest at the uppermost levels. However, from a design standpoint, the critical increase in hoop tension occurs near the dredgeline where interlock forces are maximum. The increase in hoop tension at the front of the cell appear to be caused by an apparent increase in lateral pressure resulting from application of an overturning moment. The proportional increase in hoop tension is larger at upper levels where

effects of embedment are minimal. The increase in hoop tension due to backfilling is slightly higher for the reduced embedment cases and the "stepped" cell. The critical increase in interlock tension due to backfilling may be estimated conservatively as 25% of the maximum tension developed after cell filling. This increase may be considered to be independent of embedment depth.

Conclusion No. 2 has several important ramifications. Although the maximum hoop tension may occur near the arc connection, the increase in interlock force due to backfilling is relatively minor. In fact, the maximum hoop tension measured in the Terminal 4 cell occurred in front of the arcs (no readings were available at the front sheetpile at level C). The largest hoop tensions developed during backfilling of the Long Beach cell occured at the front sheetpile at level 3.

The distribution of hoop tension in a single arc bulkhead is generally assumed to be that shown in Figure 4. The magnitude of hoop tension behind the arc connection is generally estimated using Equation 6 (TVA, 1957). This hoop tension concentration simply has not been observed in either the present model study or two cases in the field.

The behavior of the fill between cells and within the arcs may be partially understood by examining Figure 105. The fill inside the arcs and between the cells is partially constrained by the cell walls. As the fill is placed, substantial friction may develop between the soil and the cell walls. As the arc sheetpiles deflect, portions of

the lateral earth pressure from the backfill can then "arch" between the adjacent cell walls. This reduction in lateral earth pressure appears to be more significant at lower levels, possibly due to vertical arching or a "silo" effect in the arc space. Calculation of interlock force by the presumed free body shown in Figure 3 appears to yield hoop tensions that are very conservative.

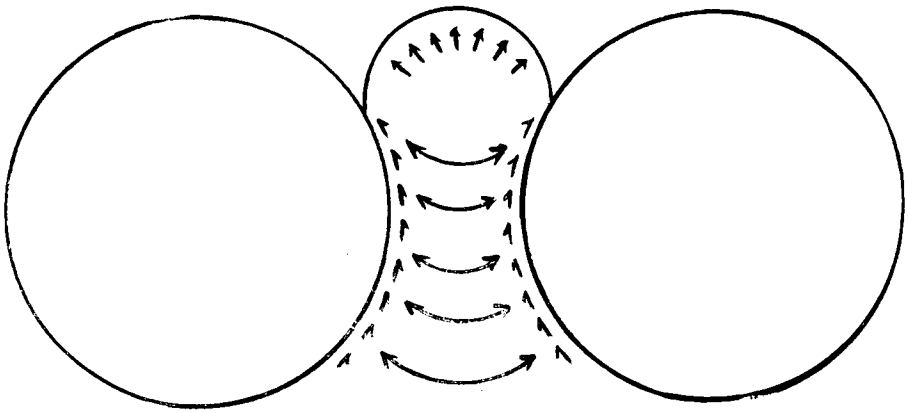

Figure 105. Arching of backfill between cells.

It also appears reasonable, then, that the majority of the load from the backfill is carried by the cells. The arcs carry only the lateral loads from the fill contained within them. A large potential for saving steel may therefore exist within the arcs themselves. Instead of counting on the arc section to resist portions of lateral loads, the arcs can be assumed to carry only a small fraction of the backfill loads between the cells. The arc sheetpiles may then be shortened with a consequent substantial savings in steel costs. In addition, the equivalent rectangular widths, b, of the bulkhead should be based on area or moment of inertia of the individual cells and not include the region between cells. The lateral loads, per foot of bulkhead, should, therefore, be calculated using nb, where n is the number of cells, instead of the entire bulkhead length. Future instrumentation of arc sheetpiles may help further define the magnitudes of hoop tension within arc sections.

Conclusion No. 3 indicates that interlock tension is not critical at the back of the cell. Reductions of at least 10 to 20% in hoop tension can be expected at all levels above the dredgeline at the back sheetpile. Field observations (Khuayjarernpanishk, 1975) indicate that hoop tension may be reduced at some levels by as much as 50 percent. The model study also indicates that the decrease in interlock tension increases for shorter sheetpiles (i.e., less embedment at the back). One might therefore propose to select sheetpile sections for the rear of cells using a maximum design condition for the isolated cell case, and neglect effects of later events in the life of the bulkhead.

Discussion of Surcharged Cells

Cell Deflections. After backfilling, the cells were subjected to a series of surcharges consisting of one to eight layers of iron bricks. This is equivalent to a range of approximately 65 to 437 psf of surcharge. Alternately, this surcharge may be expressed as the ratio of added vertical overburden to the original vertical burden due to the backfill (i.e., γH). Cell deflections and hoop stresses were monitored during the application of surcharges.

The added deflection at the front of all four cells due to surcharging consisted mainly of a uniform outward movement. In all cases the added deflection were relatively small (on the order of 0.05 inches). Figure 106 presents the deflection of the top of Cell No. 1 (as a ratio of deflection to exposed height, H) versus the added surcharge. The surcharge is expressed as the ratio of surcharge to backfill vertical overburden, γH. The deflection appears to increase almost linearly with the magnitude of surcharge. The effect of a surcharge can be assumed to act as a uniform lateral load equal to the added vertical overburden times a coefficient of lateral earth pressure (presumably active). The moment applied to the cell then increases linearly with the magnitude of surcharge. Since the tilting of a cantilever is proportional to the applied moment, the amount of cell deflection can be expected to vary linearly with the magnitude of applied surcharge.

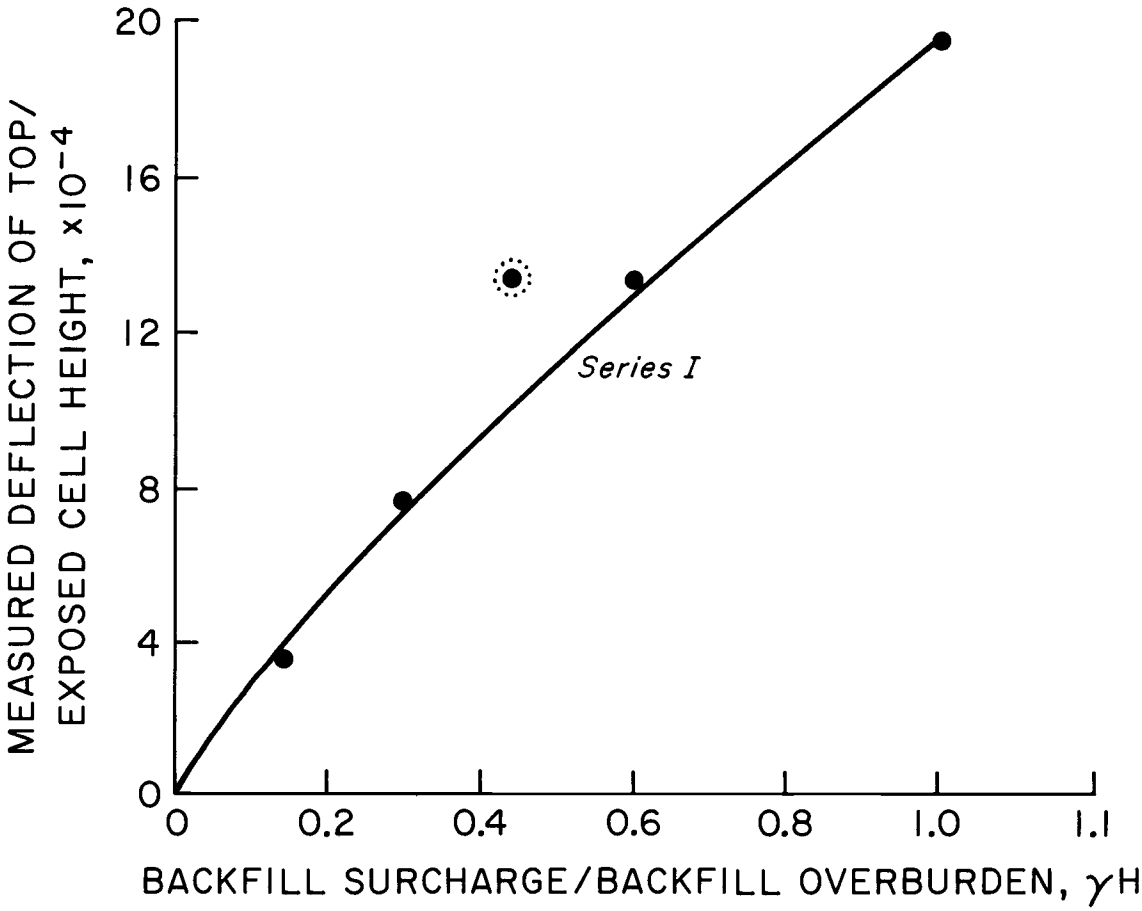

Figure 106. Deflection of model Cell No. 1 due to surcharging.

The deflection of Cells No. 2, 3 and 4 were monitored for fewer increments of surcharge. Although the magnitude of deflection did increase for Cell No. 2, the number and magnitude of subsequent readings were insufficient to relate the deflections with embedment depth. However, the application of an approximately 8400 lb. surcharge to the backfill area of Cell No. 1 appeared not to cause any significant or alarming movements of the cell or adjacent arcs. Such a surcharge was equivalent to the entire overburden due to the full backfill, well beyond anticipated field service loads.

Changes in Hoop Tension Due to Surcharging. The hoop tension in the front portion of the model cells appears to change only slightly with the addition of a 250 psf surcharge. This change consisted of a small, but relatively uniform increase in hoop tension (see Figures 46 through 49). Cell No. 1 showed an increase in hoop tension of 4 percent (at level B) while Cells No. 2 and 3 showed increases of 7 and 6 percent, respectively. Cell No. 4 indicated very little change in hoop tension. With the addition of a 437 psf surcharge, the maximum hoop stress in Cell No. 1 (P1) increase by only 7 percent.

Sheetpile P3 (behind the arc connection) showed very little change in hoop tension due to surcharging. In two cases (Cells No. 1 and 3) the hoop tension actually dropped at the upper levels.

Sheetpile P4 (of the back of the cell) showed a very dramatic drop in hoop tension due to surcharging. The drop in hoop tension at all levels ranged from 15 to 35% (Cell 2) to over 50 percent (Cell 4). The hoop tension in Cell No. 3 appeared to have dropped to about zero at all but the second levels.

The mechanism of change in hoop tension in the model due to surcharging appears to be as outlined below.

1) The added overturning moment due to the surcharge increases the lateral earth pressures in the fill at the front of the cell, thereby increasing hoop tension.

2) The added inward radial pressure due to surcharging decreases interlock tension behind the arc construction. Surcharging does not appear to increase the interlock forces in the arcs beyond the initial full cell levels.

3) Application of a surcharge to the backfill decreases the interlock forces in the back portion of the cell due to an added inward radial pressure. The drop in interlock tension is larger in sheetpiles with less embedment.

Field Data

White, et. al. A 14 foot fill surcharge was added to the backfill and cell area of the Long Beach bulkhead. This represents an overburden of about 1680 psf or a ratio of surcharge to backfill overburden of 0.44. This surcharge was applied over the cell as well as over the entire backfill area. The instrumented cell deflected 2.3 feet riverward upon application of the surcharge. This amount of deflection was considerably greater than the average of 0.55 feet for all other cells in the bulkhead. The initial cell misalignment, the loss of material through the bottom of the cell during filling and the possible injury to the interlocks below the dredgeline may have contributed to the large cell deflections (see discussions by White, et. al.).

Stage VI (surcharges stage) produced the highest interlock tensions 7 kips/in at Pile A (front) at level 3. This indicates a fairly substantial increase (nearly 40 percent) in hoop stress at the front of the cell. Sheetpile C (behind the arcs) shows an increase of about 1 kip/in in the maximum hoop tension due to surcharging (about 30 percent increase). The hoop tension at the back of the cell (sheetpile E) dropped significantly at the upper levels while increasing slightly at level 4.

Khuayjarernpanishk. After backfilling, the cell fill and backfill in the Terminal 4 cell was densified by probing and a 4.5 foot final fill was added to the cell and backfill area. This represents an addition of a 527 psf surcharge or a ratio of surcharge to backfill overburden ($q/\gamma H$) of about 0.16.

The addition of the surcharge caused an outward deflection at position 2 of about one inch. The portion of the cell behind the arcs moved outward approximately 0.3 inches. Sheetpiles at the sides and back portion of the cell tended to tilt or bulge inward in amounts ranging from one third to one inch.

The addition of the final fill tended to increase the hoop tension slightly at almost all levels and at all positions. However, with the exception of sheetpiles at position 2 and 3, even with this increase, the interlock forces were still below those developed during initial cell filling. Interlock tension increased at levels A and B in the sheetpiles at positions 2 and 3 somewhat beyond the initial cell filling stage. However, the hoop tension developed at Level C was well below the maximum developed during initial filling.

Comparison of Model and Field Data

The model study indicates that there is an approximately linear relationship between crest deflection and the magnitude of surcharge. The ratio of deflection to exposed cell height is significantly lower for the model than for field installations at comparable values of surcharge. This may be due to the added stiffness and strength of both the model sheetpile and fill. In addition, the magnitude of surcharge applied laterally to model cells was proportionally lower than in the field. No conclusion could be made concerning the influence of sheetpile embedment on deflection. One would anticipate, however, that sheetpile embedment does, to some extent, limit crest deflections.

The average ratio of crest deflections to cell height (of the entire Long Beach bulkhead) was on the order of 0.01 for a surcharge-backfill ratio of 0.44. The Terminal 4 cell deflection ratio was 0.001 for a surcharge-backfill ratio of 0.16. The Long Beach cells, therefore, showed proportionally more deflection. The difference may, in part, be attributed to the densification (and consequently strengthening) of the cell fill in the Terminal 4 bulkhead. The field data is too limited to provide a deflection/surcharge relationship. The crest deflections of each cell, however, may be considered to vary linearly with surcharge.

The effect of surcharging the backfill area on the hoop tension appears to be relatively minor. The sheetpiles in the front portion of the cell show an increase in hoop tension while it decreased in the back portion of the cell. One can also anticipate a slight increase in hoop stress in the sheetpiles adjacent to the arc.

Model data indicates that the addition of a surcharge equivalent to half the backfill overburden produces no more than a 10 percent increase in hoop tension in the front sheetpiles. Hoop tension in the back sheetpiles continue to decrease with surcharging.

Field data from the Terminal 4 cell indicates very slight all around increases in hoop tension (but still below initial maximum values). Increases in hoop tension at the upper levels (though not critical) are probably due to the addition of a cell surcharge by the final 4.5 foot fill. Cell surcharge may also play a significant role in the large increase (40%) in hoop tension at the front sheetpile of the Long Beach cell. The addition of a 29 foot fill represents a 1680 psf increase in vertical pressure. This surcharge then, more than doubled the initial 1391 psf overburden at level 3. The increase in hoop tension from surcharging is, therefore, due, most probably, to cell surcharging rather than backfill surcharges. Hoop tension also increased at the sheetpile adjacent to the arc (by about 30%). The interlock tension, however, was still well below the maximum values observed at the front sheetpile.

Backfill surcharges rarely exceed 50 percent of the backfill overburden (γH). For this limiting condition, the increase in maximum interlock tension due to surcharging can be estimated at about 10 percent. The increase in hoop tension is due mainly to an increase in lateral fill pressures at the front of the cell caused by the added lateral force and overturning moment. The quality of the backfill undoubtedly affects the magnitude of the lateral forces induced by

surcharging. If the backfill consists of poor quality material that has not been densified, the increase in hoop tension at the front of the cell should be treated conservatively.

If a cell surcharge is added, the calculation of the maximum interlock tension should include the added fill overburden. The increase in hoop tension due to cell surcharging is undoubtably critical along the exposed portion of the cell. Sheetpiles within the backfilled portion of the cell are partially confined by the fill.

Conclusions on the Effect of Surcharging

The effects of surcharging the backfill area are summarized below:

1. The cell tends to tilt towards the unloaded side. Crest deflections are highly variable, but may be expected to vary linearly with the magnitude of surcharge. Probing of the cell fill prior to surcharging causes small amounts of additional tilting but tends to reduce subsequent deflections due to surcharging.
2. A backfill surcharge of less than 50 percent of the backfill overburden will cause an increase of about 10 percent in the maximum hoop tension.
3. Interlock tension along the back portion of the cell will continue to decrease during surcharging.

If the cell area is also surcharged then:

4. Interlock tension along the front portion of the cell will increase due to the added overburden. Changes in interlock tension along the backfilled portion of the cell will be small.

Failure Mechanism of Model Cells

Failure of Large Cells

Cell No. 1 sustained a maximum lateral load of 4250 lbs applied at an elevation 31.5 inches above the dredgeline. This represents a maximum moment about the tips of the sheetpiles of 19.0 kip ft.

The cell failed by tilting (and rotating) about a plastic hinge in the front sheetpile, approximately six inches below the original dredgeline (i.e., at a depth to embedment ratio of 0.26). Deflection curves and examination of the deformed sheetpiles indicate that below the plastic hinge the sheetpile remained essentially vertical. The front sheetpile was therefore "fixed" just below the dredgeline. The 12 inch observed failure surface generated by the passive wedge is consistent with the point of tilting of the front sheetpile. The back sheetpiles did not behave the same way; they simply pulled out without developing any plastic hinge.

The interlocks showed considerable relative displacement ahead of the middle of the cell. Terraces formed in the sand at the cell fill surface near the middle and toward the rear portion of the cell (see Figure 73). No wax markers were placed in the cell fill.

Cell No. 2 sustained a maximum lateral load of 3525 lbs. applied 28.8 inches from the dredgeline or a maximum moment of 10.4 kip ft. about the tips of the sheetpiles.

Cell No. 2 failed by tilting initially about the tips of the sheetpiles then by tilting about a plastic hinge approximately six inches below the dredgeline. The longer (16 inches) passive zone observed is consistent with tilting about a point near the tips of the

sheetpiles. Figure 75 indicates the pattern of breaks in the wax markers placed in the cell fill. The pattern is consistent with a set of straight or slightly curving shear planes approximately parallel to the front sheetpile. Terraces appeared at the cell fill surface near the front and back sheetpiles. Most interlock displacement again occurred at the middle and at the front portion of the cell. Slippage at the front of the cell between the cell fill and sheetpiles was about 2.7 inches.

Cell No. 3 sustained a maximum lateral load and moment almost identical to Cell No. 1; 4450 lbs and 19.8 kip ft, respectively. A plastic hinge formed in the front sheetpiles five inches below the dredgeline (or a depth-embedment ratio of 0.21). The cell fill appeared to tilt about this point while the back sheetpiles simply pulled up with no tendency to bend. The amount of distortion of the wax markers was less at upper levels than near the base of the cell (see Figure 76). The affect of updrag by the back sheetpiles and downdrag by the front sheetpiles on the wax markers can also be seen.

Cell No. 4 sustained a significantly lower maximum lateral force and moment, 2650 lbs and 8.5 kip ft., respectively. Very little interlock displacement occurred. The cell simply tilted upon application of the lateral load. At large cell distortion, the front sheetpile was partially embedded and the cell began to rotate about its toe. As the back portion of the cell lifted above the dredgeline, cell fill ran out of the heel. Most of the distortion of the wax markers occurred at the base of the cell.

Failure loads and moments for the large cells are summarized in Table 20.

Table 20.

Moments and Lateral Loads at Model Failure

Series No.	P_{max} (lbs)	M_{max} (kip-ft)
SI	4250	19.0
SII	3525	10.4
SIII	4450	19.8
SIV	2650	6.5

Failure of Small Cells

Three smaller cells (half the scale of the large cells) were constructed in a similar manner to the larger cells and failed by application of lateral load. The cell fill was grouted after failure in each case. Thin beds of dyed sands revealed the pattern of distortion of the cell fill (see Figures 79 through 81).

Small Cell No. 1 showed a behavior similar to cells in Series I and III. The cell tilted about an inflection point in the front sheetpile while the back sheetpile pulled out of the sand. Terraces on the top surface of the cell fill were also evident. Figure 79 indicates a very definite pattern of about four distinct vertical failure planes roughly parallel to the walls of the cell. The shear in the cell fill appears to extend only to the depth of the point of inflection of the front sheetpile. Sand beds below this point and beneath the cell were not apparently disturbed.

Small Cell No. 2 showed a behavior similar to Series II. Tilting occurred about the base of the cell. Downdrag at the front of the cells by the sheetpile was also evident. Two to three distinct failure planes could be mapped between several levels. Again little disturbance at lower levels was observed.

The grouted fill in small Cell No. 3 did not remain standing long enough for measurements. Observations of the various cuts made indicated that little vertical shear displacement occurred across the horizontal marker beds. The vertical marker bed appeared to have simply tilted parallel with the cell walls.

Comparison of Proposed Mechanisms of Failure

Several methods for computing the ultimate capacity of cells to resist lateral loads and overturning moments have been proposed. These include sliding, rigid body rotation, Terzaghi's vertical shear method, Cummings' tilting method and cell slippage among others (see LITERATURE REVIEW section).

Failure by Sliding. The maximum lateral force that each cell can resist without sliding is equal to the summation of the passive and active forces outside the cell and the shear that can be developed at the base. The shear resistance, R, along the base of the cell can be calculated as the total cell fill weight times the coefficient of friction, tan ϕ' (see Figure 107). The maximum lateral force that can be applied is

$$P_{max} = \pi r^2 L \gamma \tan\phi + P_p - P_a$$

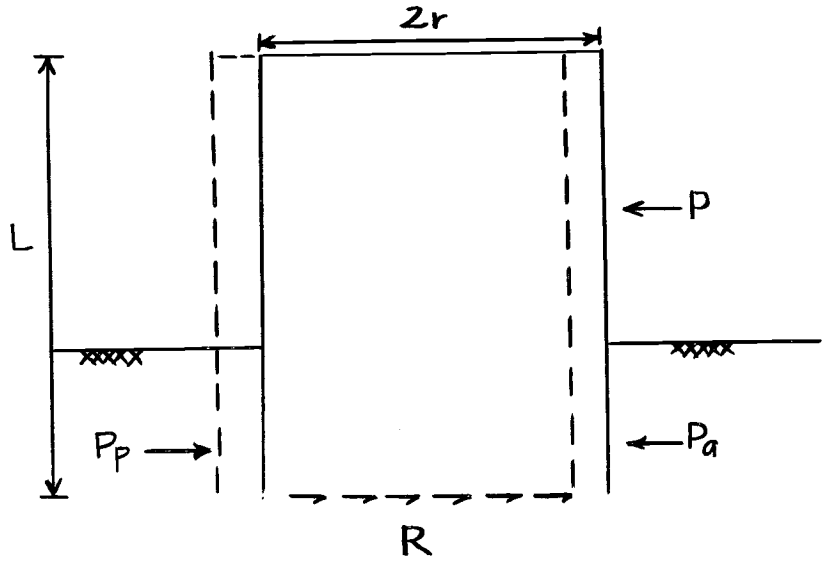

Figure 107. Sliding resistance.

Table 21 summarizes the calculated sliding resistance of each cell along with the actual maximum lateral loads applied. The passive resistance was calculated using the Rankine coefficient and assumed to act over the projected width of the cell. This represents, therefore, the most conservative estimate for the sliding resistance.

Table 21.

Sliding Resistance of Models

Series No.	Calculated Maximum Available Resisting Force P_{max} (kips)	Applied Force of Failure, P_{actual} (kips)
SI	16.1	4.3
SII	9.8	3.5
SIII	15.5	4.5
SIV	6.9	2.7

Failure by Rigid Body Overturning. The moment-resisting capacity of each test cell was computed by summing driving and resisting moments about the toe of the cell. The forces acting on the free body (the entire cell) include the cell weight, the passive and active pressures, and the friction between the outside of the cell and surrounding sand. Figure 108 summarizes the forces considered. In general, the driving moment due to the active pressure was relatively small (there was no backfill during cell failure).

Table 22 summarizes the maximum net resisting moments calculated for each cell.

Table 22.

Calculated and Measured Overturning Moments

Series No.	Maximum Applied Moment About Sheetpile Tips M_{max}, (kip-ft)	Maximum Net Resisting Moment by Cell, M_{actual} (kip-ft)
SI	21.0	19.0
SII	14.8	10.4
SIII	19.8	19.8
SIV	11.6	6.5

Failure by Rigid Body Rotation. Another method of analysis based on rigid body rotation was proposed by Hansen. The method assumes either a concave or convex circular (or logarithmic) failure surface near the base of the cell. The cell is assumed to rotate about this slip-plane as a rigid body. No evidence of such failure planes was found.

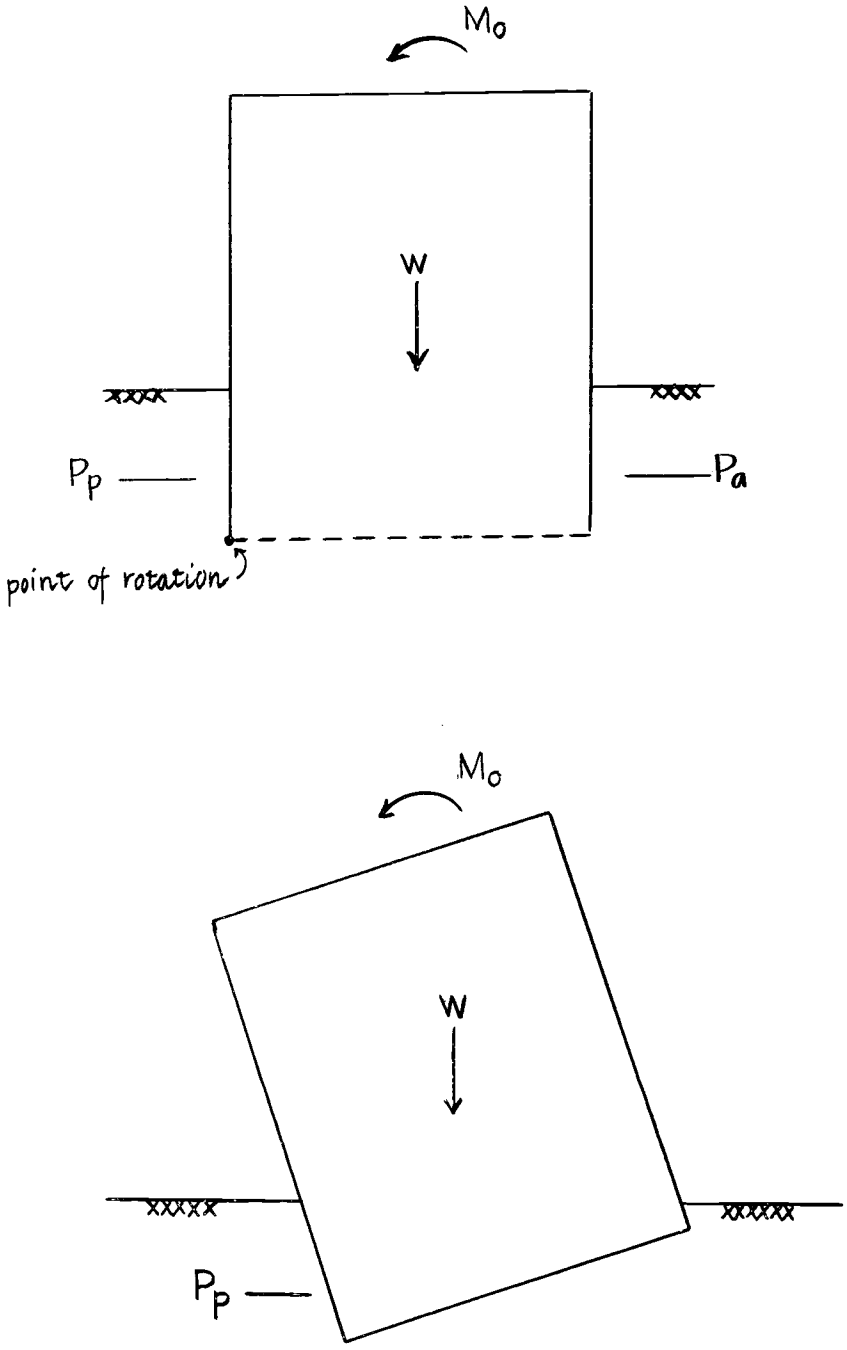

Figure 108. Rigid body overturning.

Failure by Vertical Shear (Terzaghi's Method). Analysis of failure by vertical shear was made for each cell. The total shear through the center plane due to shear resistance of the fill and interlock friction is given by Equation 17. Interlock friction was assumed to act over a length equal to the exposed cell height. An equivalent rectangular width, b, of 42 inches (based on equal moments of inertia) was used. A width of 42.5 inches was obtained from the equal area method. The moment due to passive and active pressure were included in the calculations. Krynine's coefficient of lateral earth pressure, endorsed by Terzaghi, was used (Terzaghi, 1945).

Figure 109 shows the failure mechanism schematically. The change in the pressure at the bottom of the cell can be related to the overturning moment by Equation 13.

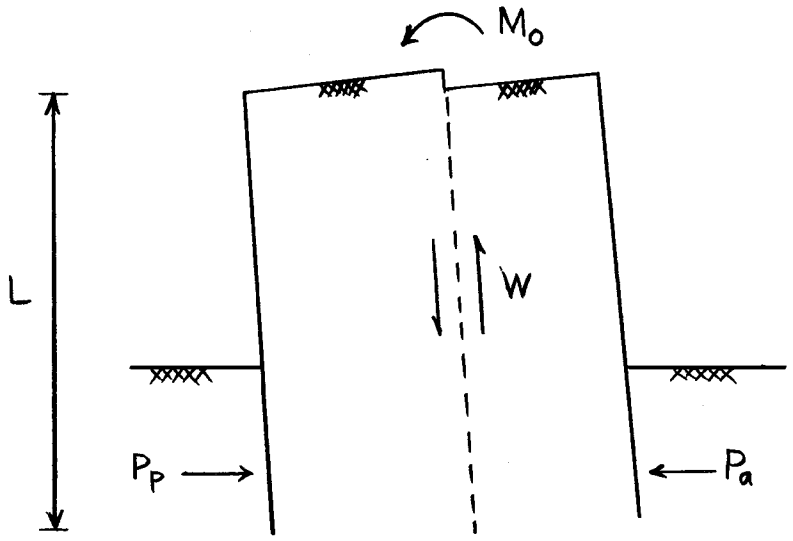

Figure 109. Vertical shear on center plane.

Table 23 summarizes the maximum moments obtained by Terzaghi's method.

Table 23.

Calculated Resisting Moment by Vertical Shear Method

Series No.	Calculated Maximum Available Resisting Moment, M_{max} (kip-ft)	Maximum Net Resisting Moment by Cell, M_{actual} (kip-ft)
SI	8.8	19.0
SII	4.4	10.4
SIII	9.0	19.8
SIV	2.8	6.5

Failure by Horizontal Shear (Cummings' method). The method of analysis by horizontal shear has been presented in the LITERATURE REVIEW section. For the value of ϕ of the sand and the cell geometry, the ϕ-line approximately intersects the top of the cell at the tip of the back sheetpile for Cells No. 1 and 2. This line extends about 1.5 inches above the top of the cell for Cells No. 3 and 4 and was assumed to be at the top of the sheetpile (i.e., c = 48 inches). Figure 110 shows the typical geometry of the method.

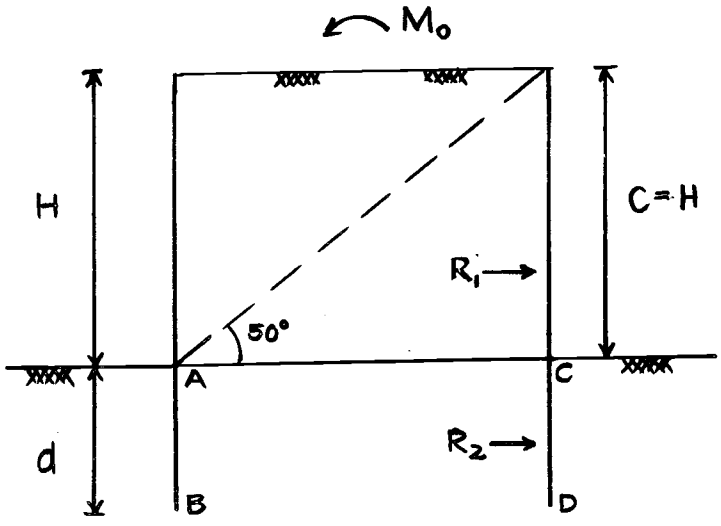

Figure 110. Failure by horizontal shear.

The shear resistance, R_2, of the material below the dredgeline (within ABCD) is taken as the weight of the fill times tan ϕ (Cummings, 1957). It is assumed to act at the midpoint of the embedded sheetpiles. The shear resistance of the material above the dredgeline, R_1, is assumed to act at a distance of (1/3)C above the dredgeline. Cummings' method also assumes that the sheetpiles above the dredgeline do not contribute to the horizontal shearing resistance.

Table 24 summarizes the results of analysis by Cummings' horizontal shear method. The actual maximum resisting moment is substantially smaller than that calculated. Cummings' method was also modified for the embedded cell case by neglecting the contribution to overturning moment from the cell fill below the dredgeline. The moments obtained by the modified method are also tabulated in Table 24.

Table 24.

Calculated Resisting Moment by Horizontal Shear Method

Series No.	Calculated Maximum Available Resisting Moment, M_{max} (kip-ft)	Modified Calculated Maximum Available Resisting Moment M^*_{max} (kip-ft)	Maximum Net Resisting Moment by Cell, M_{actual} (kip-ft)
SI	28.7	22.6	19.0
SII	16.7	15.6	10.4
SIII	28.4	21.5	19.8
SIV	8.8	8.8	6.5

Comparison of Results. Analysis of sliding stability indicates that cell failure by moment-caused distortion should occur long before the maximum lateral force resistance is reached. Values of maximum resistance to sliding ranged from three to four times the actual measured maximum lateral load. The overturning moment, then, causes failure by tilting long before sliding occurs. Sliding stability for real cells has usually been as an improbably critical mode of failure, with apparent good reason.

The value of resisting moments obtained from rigid body overturning are independent of the fill properties except density. Although rigid body rotation does not reflect the true failure mechanism it produced the best agreement with observed maximum moments. The relatively good agreement, however, may be due to the high angle of friction of the cell fill. At lower values of ϕ, the resisting moment undoubtedly decreases. The rigid body analysis produces constant values, independent of ϕ. Agreement between the two would therefore tend to break down at lower values of friction angle.

Terzaghi's method of vertical shear consistently underestimated the actual maximum overturning moment resistance available by about 130%. The calculated contribution of interlock friction to the total shear along the vertical plane was small. The resisting moment was, therefore, due mainly to shear resistance within the cell fill.

Results from the horizontal shear analysis indicate that Cummings' method predicts substantially larger moment resistance than that actually measured. The computed values ranged from 26 to 37% above the actual values. The difference, however, appears to decrease with decreasing embedment depth. If the resisting moment due to the embedded portion of the cell is neglected, the agreement with actual resisting moments is improved.

Comments on Previous Model Studies

Results from several previous model studies apparently bear out, in part, Hansen's rotation failure model (Ovesen, 1962; Scheebeli and Cavaillé-Coll, 1957; Mazurkiewicz, 1972). No evidence in either the large or small model failures indicates a convex or concave circular slip-plane. Hansen's method requires that the cell above the slip-plane act essentially as a rigid body (Hansen, 1953). In all of the previous studies the models were relatively small and stiff. Photographs of cells during failure show the cells rotating about the tip of the sheetpiles with no bending or inflection point in the sheetpiles (see photographs in Ovesen, 1962 and Mazurkiewicz, 1972). The model sheetpiles in these cases must have been fairly stiff to resist bending moments during cell failure. This added stiffness probably was the cause of rigid body rotation. The model sheetpiles in the

present study were relatively more flexible and, at failure, the cell fill showed indications of internal shear rather than rigid body behavior. Sheetpiles in cells in the field are even more flexible. The extreme stiffness of previous model sheetpiles probably dictated the mode of failure rather than allowing failure by the critical mode. Even sheetpiles that were loosely connected to prevent interlock friction probably contributed to the cell stiffness.

Proposed Mechanism of Failure

Analysis indicates that the major component of overturning resistance of the model cells is the shear resistance developed in the cell fill. Interlock friction contributed relatively little to the shear resistance of the model cell, because of the small hoop tensions developed. Interlock friction can be expected to contribute proportionally more to the total shear resistance of field cells whose interlock tension is high.

All evidence from the large and small scale model cells indicates that the overall mechanism of failure is that of tilting. Tilting occurs about a point of inflection in the front sheetpile for deeply embedded cells or about the toe for little or no cell embedment. Shear resistance in the cell fill is developed along a series of nearly vertical planes (i.e., parallel to the cell walls). Passive forces in front of the cell above the point of inflection tend to resist rotation. Passive forces are developed only to the point required to cause "fixity" (i.e., until the plastic hinge forces in the sheetpile). Skin friction in the embedded portion of the sheetpile also resists tilting to the point of interlock slippage. Figure 111 shows the proposed failure mechanism schematically.

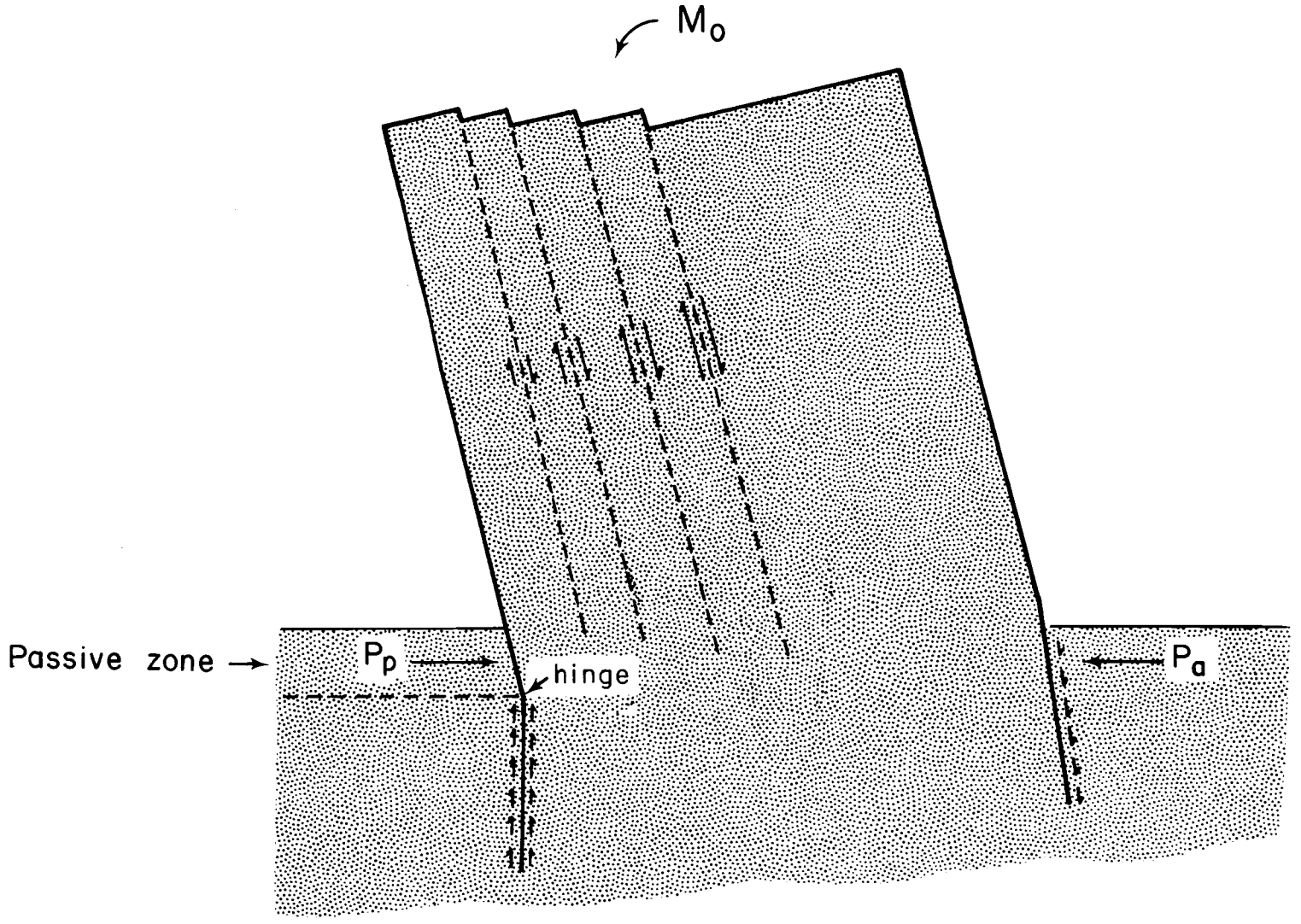

Figure 111. Proposed failure mechanism.

The depth to the point of inflection (i.e., the point of tilting) can be estimated by theory of elasticity as the depth necessary to cause fixity (i.e., to provide base shear resistance Q_o and moment M_o).

The base shear is provided by passive resistance P_p which can be calculated per foot of cell by

$$P_p = \frac{1}{2} \gamma Z^2 K_p = Q_o \tag{54}$$

The depth to cause fixity is, therefore

$$Z = \left(\frac{2Q_o}{\gamma K_p}\right)^{1/2} \tag{55}$$

The moment provided by the passive resistance about a point Z feet below the dredgeline is

$$M = P_p \cdot \frac{Z}{3} \tag{56}$$

This moment must exceed the required moment for fixity, M_o. Values of Q_o and M_o for typical structures have been calculated (see page 211).

If a layer of soft silt or clay or a layer of soil susceptible to erosion is present, the depth to the point of "fixity" must be viewed conservatively.

Analysis by Terzaghi's vertical shear method significantly underestimated the resisting moment capacity of the model cells. However, its mechanism describes the observed failure mechanism more closely than any other method. The apparent discrepancy may be understood by

examining the coefficient of lateral earth pressure used in the analysis. Krynine's coefficient, K, represents the ratio between horizontal and vertical pressure obtained from Mohr's circle but including the effect of shear on the vertical plane. The effect of lateral loads is therefore seen as a shear stress applied on the vertical plane. The application of lateral loads, however, develops passive pressures in front of the cell. This passive pressure is partially transmitted by the sheetpiles. If the sheetpiles are stiff, the passive pressures are transmitted by the sheetpiles to some distance above the dredgeline. If the sheetpiles are flexible, the extent of transmission of passive resistance above the dredgeline is limited. The net result of the lateral loads and transmitted passive resistance is a path of compression within the cell fill. Figure 112 shows this path schematically.

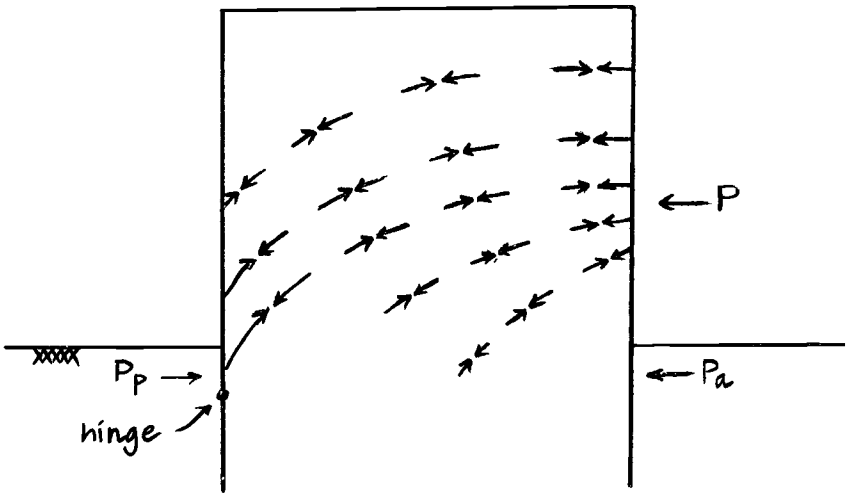

Figure 112. Zones of compression due to lateral loads.

The effect of this zone of compression is to increase the lateral earth pressure along vertical planes. Evidence for this increase is found in the pattern of interlock slippage and failure planes within the cell fill. Little interlock slippage was observed in the failed model cells in the rear portion of the cell. In addition, failure planes were much more prominent at the middle and at the front portion of the cell. Both observations may indicate a large increase in horizontal pressures especially at the rear of the cell due to lateral loads. Since vertical shear resistance increases with horizontal pressure, the tendency to shear is less at the rear portion of the cell fill. Additional evidence for the transition of the state of stress of the cell is found in Cummings' model study. Pullout tests conducted on laterally loaded cells indicated that an increase in lateral pressure occurred within the cell fill at the loaded side of the cell (Cummings, 1957).

The ultimate loads from the model tests were reexamined using the modified vertical shear failure mechanism. Interlock friction and vertical shear were assumed to extend only to the point of tilting (i.e., either the plastic hinge or the base of the cell). The apparent coefficient of lateral earth pressure, K, was calculated from the actual maximum net applied moments. Table 25 summarizes the calculated values along with the coefficient as proposed by Krynine.

Table 25.

Calculated Apparent Coefficient of Lateral Earth Pressure

Series No.	Calculated Apparent Coefficient (K)	Krynine's Coefficient
SI	1.62	0.26
SII	0.89	0.26
SIII	1.79	0.26
SIV	.71	0.26

The apparent coefficient, K, appears to depend on the cell embedment. The coefficient for full embedment (SI and SIII) is more than twice that for the unembedded cells (SIV). This appears to be consistent with the compression mechanism proposed in Figure 112.

The calculated apparent coefficients, K, lie above the value of Krynine's coefficient but well below the passive coefficient (the maximum possible value).

Figure 113 shows a plot of the active and passive (Rankine) coefficients and Krynine's coefficient as a function ϕ. The apparent coefficients, K, calculated from the model tests are also shown. All the coefficients must approach the value of 1.0 at an angle of friction, ϕ, equal to zero. Curves, approaching 1.0 asymptotically, were drawn from each apparent coefficient calculated from model failure. The curves for coefficients lying above 1.0 approach the limiting value in a manner similar to the passive coefficient curve.

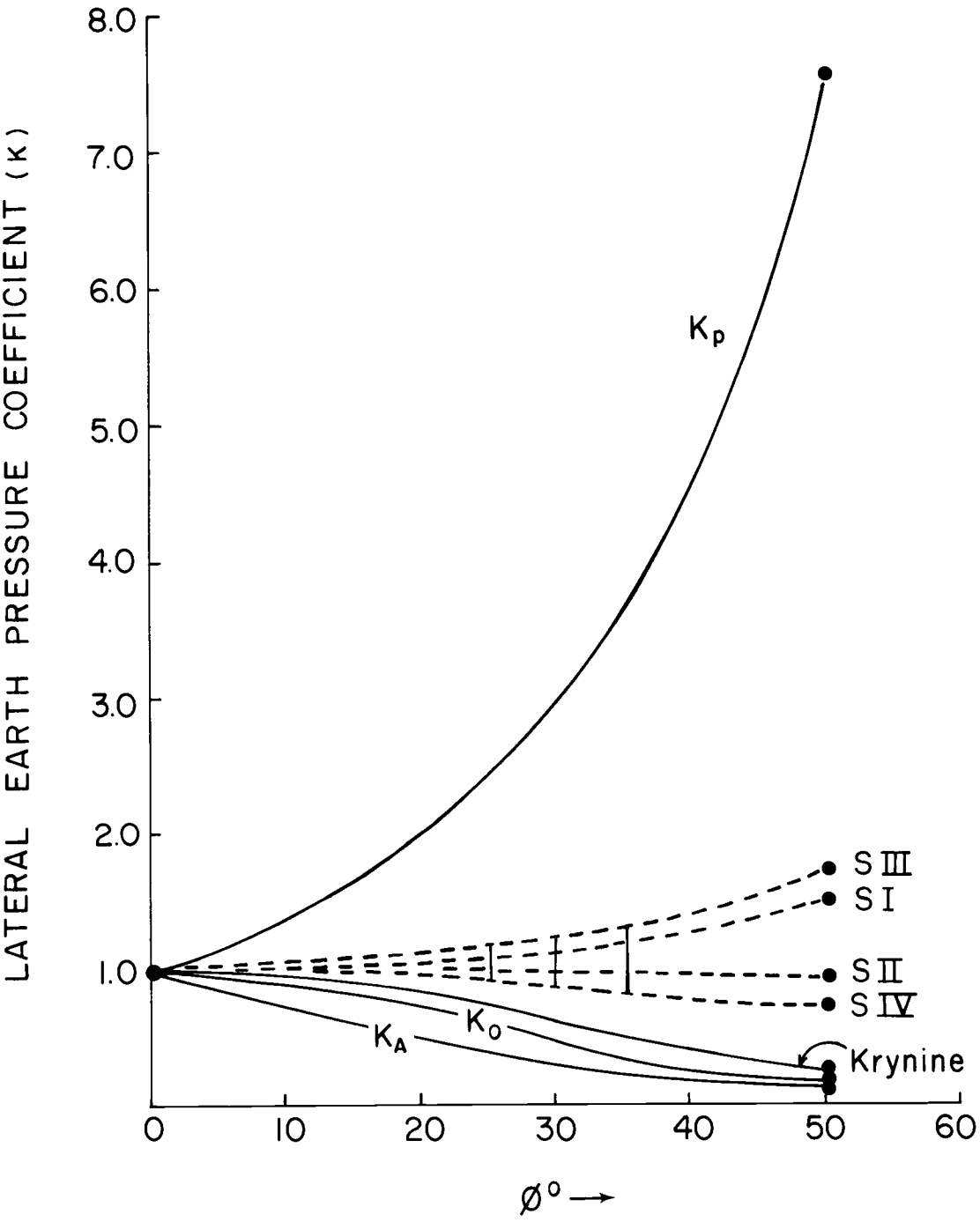

Figure 113. Coefficients of lateral earth pressure.

Curves below 1.0, approach the limiting value approximately parallel to the active, at-rest and Krynine coefficient.

Typical fill materials in the field have angles of friction ranging from 25 to 35°. Figure 114 shows a plot of the apparent coefficient, extrapolated from the model study, for the typical range of ϕ encountered in the fill. The apparent coefficient, as expected, increases with embedment depth. This increase, however, must have a limit, since, upon formation of a plastic hinge, further embedment is useless. The apparent coefficient appears to be relatively insensitive to ϕ within the range of 25 to 35°. A simple relationship, shown in Figure 115, between embedment and K may be proposed for an average angle of friction 30°.

The ultimate capacity of the model cells is based on the peak lateral load shown in Figure 83. These maximum loads, however, occur at relatively large cell displacement. Table 26 summarizes the crest deflection (expressed as the ratio of deflection to exposed cell height) for all cells.

Table 26.

Crest Deflections at Peak Lateral Loads

Series No.	Crest Deflection/H
SI	.08
SII	.04
SIII	.09
SIV	.03

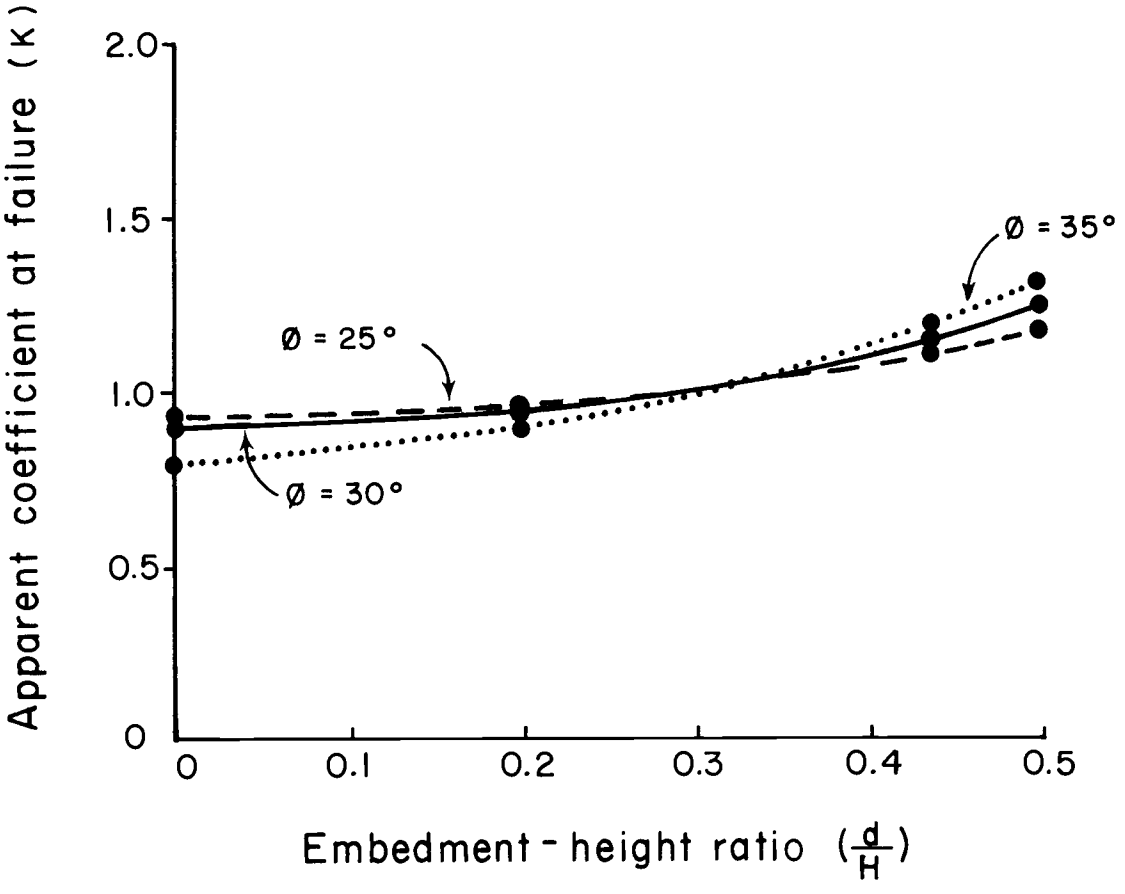

Figure 114. Apparent coefficient of lateral earth pressure.

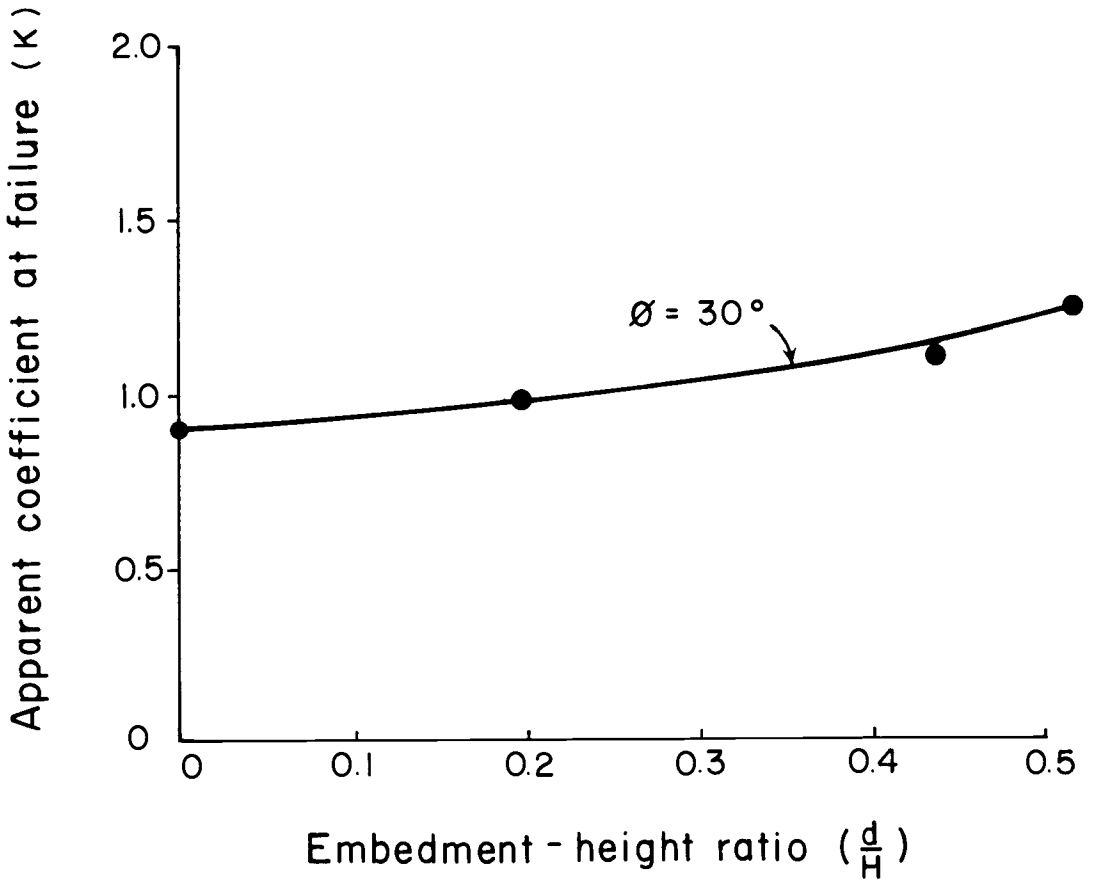

Figure 115. Apparent coefficients of lateral earth pressure for typical soils.

The maximum capacity for the cell is developed at significantly lower cell deflections for cells with shallow or no embedment (0.03 to 0.04 times the cell height, H). The embedded cells act as more flexible structures and develop their maximum resisting capacity at larger values of cell deflection. The ratio of crest deflection to exposed cell height of 0.08 represents a cell displacement of about five feet for a real cell of typical proportions. Such large displacements are intolerable in permanent bulkhead installations.

It is recommended, therefore, that the factor of safety against ultimate failure be computed using the maximum lateral loads and moments (i.e., the calculated apparent coefficient). However, the true factor of safety against excessive cell movement should also be estimated. The allowable overturning moment would then be based on a cell deflection criterion and would reflect a reduction from the ultimate moment capacity. Figure 116 shows a series of curves that could be used to estimate the allowable overturning moment, based on limiting deflections. The ultimate resisting moment is computed using the previously suggested method. A maximum crest deflection is picked and the ratio of deflection to exposed height (Δ/H) is computed. The tables are entered with this ratio value and the reduction in ultimate load is picked off of the appropriate embedment curve. Although the curves represent conditions of a relatively strong cell fill, the ultimate moment is computed with K values for typical fills. The factor of safety against excessive deflections is therefore reasonable.

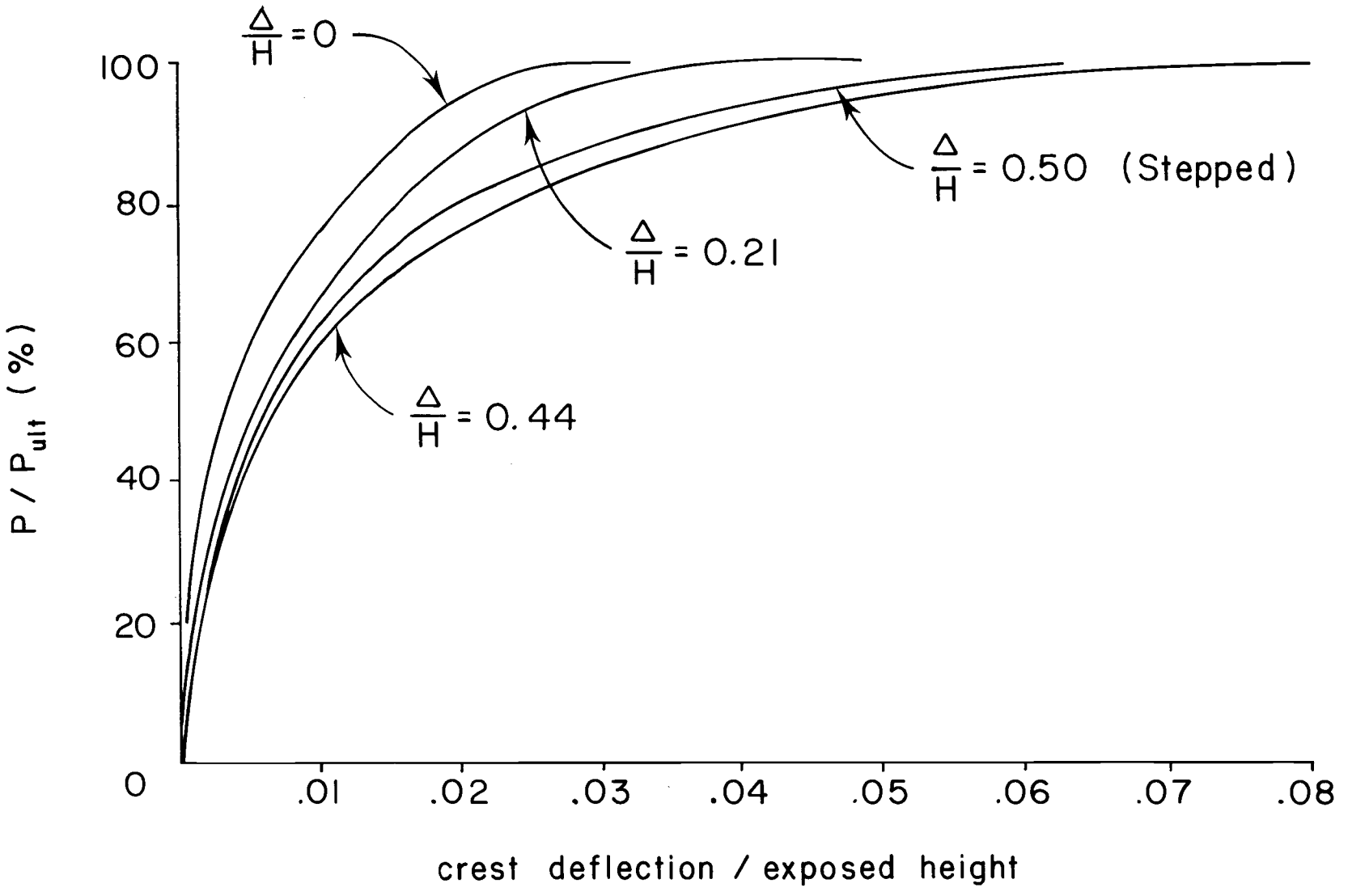

Figure 116. Reduction of ultimate overturning moment due to crest deflection.

Conclusions on Ultimate Cell Capacity

The conclusions concerning the ultimate capacity of cellular structures founded in sand can be summarized as:

1) Failure by sliding is not a critical mode of failure.

2) Analysis by rigid body overturning results in unrealistically high resisting moment and should not be used.

3) Cummings' analysis of failure by horizontal shear is applicable only to cells built on rock. Cummings' method overestimates the resisting moment for cells driven in sands.

4) Terzaghi's method of vertical shear underestimates the moment resisting capacity for embedded cells.

5) Laterally loaded cells appear to fail by tilting about either the base of the cell (for no embedment, or no fixity) or about a point of inflection in the front sheet-pile (for deeply embedded cells).

6) The maximum overturning moment a cell can sustain can be calculated by a modified model of failure by vertical shear. Shear resistance in the fill and interlock friction should be assumed to extend only to the depth of the point of tilting. An empirical value for the apparent coefficient of lateral earth given by Figure 114 should be used. This apparent coefficient, K, depends on the embedment depth and on the angle of friction of the fill material. The location of the plastic hinge (the point of fixity) may be estimated with methods of the theory of elasticity.

7) The factor of safety against overturning should be computed using a reduced moment capacity to prevent excessive cell movement.

SUMMARY OF CONCLUSIONS

Some of the most important conclusions resulting from the model study, previous analysis and model studies, and field data are summarized below:

1. Sheetpiles along the side and back portion of the cell develop their maximum interlock tension during initial cell filling.
2. The maximum interlock tension developed in isolated cells will depend on the quality of the cell fill, the method of filling, the quality of the soil in which the cells are embedded and time.
3. Maximum design interlock tension for isolated cells should be calculated at an elevation of 0.25(H') above the point of "fixity". The depth to "fixity" may be estimated from theory of elasticity (see Equation 55).
4. For sandy soils the apparent coefficient of lateral earth pressure for calculation of interlock tension will have a range of:

$$K_1 = 1.5 \text{ to } 1.8\ K_A \text{ (immediately after filling)}$$
$$K_2 = 1.2 \text{ to } 1.6\ K_A \text{ (permanent)}$$

   The apparent coefficient K_2 should be used for calculating design interlock tension for isolated cells.
5. Backfilling increases the maximum interlock tension (at the front of the cell or near the arc connection) by

25 percent or less. The design coefficient of lateral earth pressure, K, is therefore:

$$K_{backfill} = 1.25\ K_2$$

6. The increase in interlock tension behind the arc connections is not as critical as predicted by TVA engineers.
7. Equivalent rectangular widths for circular cells should be computed using only the areas or moments of inertia of the cells. The backfill should be assumed to be almost entirely carried by the individual cells.
8. Typical backfill surcharges (i.e., less than 50 percent of backfill overburden) will increase the maximum interlock tension by about 10 percent. The design coefficient, K, for interlock tension analysis is therefore

$$K_{surcharge} = 1.38\ K_2$$

9. Cell surcharges will increase the interlock tension in the front portion of the cell. This increase should be calculated using the average cell surcharge and the apparent coefficient, K_2, for isolated cells.
10. Cummings' analysis by horizontal shear overestimates the resistance to overturning of embedded cells by about one third. The method, if used, should be modified by neglecting the resisting moment of the embedded portion of the cell.

11. Cells embedded in sands will fail by tilting with approximately vertical shear of the cell fill. Ultimate resistance to overturning should be computed by a modified model of vertical shear. Interlock friction should be assumed to act only to the point of tilting and not over the entire sheetpile length. The apparent coefficient, K, for prediction of the resistance to vertical shear on the center plane depends on the angle of friction of the cell fill and on the embedment of the cell. The apparent coefficient at cell failure may be estimated from Figure 114. The use of Krynine's coefficient significantly underestimates the resistance to vertical shear.

12. The ultimate resisting moment should be reduced to prevent excessive crest deflections. Figure 116 can be used to obtain a rough estimate for the reduced resisting moment. The factor of safety against "failure" should be computed using the reduced rather than ultimate resisting moment.

13. "Stepped" cells show no reduction in capacity to resist moments due to lack of embedment of back sheetpiles. "Stepped" cells appear to be a safe design concept which provides substantial savings in steel.

RECOMMENDATIONS FOR FUTURE STUDIES

Future Model Studies

Experience with the present model study and examination of past model studies has led the author to several conclusions about such studies as analytical tools:

1. The use of relatively small models (i.e.,less than about 24" in diameter) should be discontinued.
2. Flexible interlocking model sheetpiles should be used instead of wood or stiff metal sheetpiles or continuous cylinders.

The author feels particularly strongly about these conclusions in light of attempts to use small, relatively stiff cells to predict failure of full-scale structures. By no stretch of one's imagination does the behavior of these small cells simulate the behavior of the prototype, as evidenced by the distortion of the large (4 foot) model cells.

Several recommendations for future model studies are listed below:

1. Large model cells (about four feet in diamter) should be used, despite problems in handling the fill material.
2. An attempt to increase sheetpile flexibility beyond that of the present study should be made, possibly by using thinner sheetpiles.

3. The "raining" technique of filling appears to provide good density control without disturbing the model, and may be used in future studies.
4. If grouts are to be used successfully in model studies, they should be applied under pressure rather than by gravity flow.
5. The method of applying failure loads should be improved over the cable technique (possibly with air or hydraulic pressure) to ensure a more realistic distribution of lateral forces.

Future Field Studies

The glaring need for more field studies is obvious. The ability to better understand the behavior of cellular structures will only truly be improved through the collection of substantial field data for construction under various soil and site conditions. Two recommendations for future field studies are listed below:

1. At least two cells should be instrumented per bulkhead. The variability of interlock tensions and cell deflections within a bulkhead is probably as important as the variability of these parameters within a single cell.
2. Instrumentation of arc sections should not be neglected. Arc sections may provide one of the more promising areas for savings in steel. A better understanding of the distribution of interlock forces in arcs may bear this out.

BIBLIOGRAPHY

1. Anderson, L. R. and J. Ramage. April 1976. Underwater Placement of Sand Fill at Port of Portland Terminal No. 6. Preprint, ASCE National Meeting, San Diego.

2. Belz, C. A. 1970. Cellular Structure Design Methods. Proc. Conf. on Design and Installation of Pile Foundations and Cellular Structures. Envo Pub. Co., pp. 319-338. Fang, H. Y. and T. D. Dismuke (eds).

3. Bower, J. E. October 1973. Predicted Pullout Strength of Sheet-piling Interlocks. Journ. Soil Mech. and Found. Div., ASCE, Vol. 99, SM 10, pp. 765-781.

4. Bowles, J. E. 1977. Foundation Analysis and Design. McGraw-Hill, 750 p.

5. Brown, P. P. 1963. Discussion of Field Study of a Cellular Bulkhead by A. White, J. A. Cheney, and C. M. Duke, Transactions, ASCE, Vol. 128, Part 1, Paper No. 3426, pp. 503-506.

6. Colburn, R. T. 1945. Discussion of Stability and Stiffness of Cellular Cofferdams by K. Terzaghi, Transactions, ASCE, Vol. 110, Paper No. 2253, pp. 1136-1145.

7. Cummings, E. M. September 1957. Cellular Cofferdams and Docks. Proceedings, ASCE, Vol. 83, No. WW3, pp. 13-45.

8. Hansen, B. 1958. Line Rupture Regarded as Narrow Rupture Zones. Basic Equations Based on Kinematic Considerations. Proc. Conf. on Earth Pressure Problems, Vol. 1, Brussels.

9. Hansen, J. Brinch. 1953. Earth Pressure Calculations. The Danish Technical Press, The Institution of Danish Civil Engineers, Copenhagen.

10. Hansen, J. Brinch. 1957. The Internal Forces in a Circle of Rupture. The Danish Geotechnical Institute, Bulletin No. 2, Copenhagen.

11. Kelly, P. B. June 1969. Design and Evaluation of a Foundation Model Testing Device, thesis presented to Oregon State University, at Corvallis, Oregon as partial fulfillment of the requirements for the degree of Master of Science.

12. Khuayjarernpanishk, T. June 1975. Behavior of a Circular Cell Bulkhead During Construction, thesis presented to Oregon State University, at Corvallis, Oregon in partial fulfillment of the requirements for the degree of Doctor of Philosophy.

13. Kittisatra, L. June 1976. Finite Element Analysis of Circular Cell Bulkheads, thesis presented to Oregon State University at Corvallis, Oregon, in partial fulfillment of the requirements for the degree of Doctor of Philosophy.

14. Krynine, D. P. 1945. Discussion of Stability and Stiffness of Cellular Cofferdams by K. Terzaghi, Transactions, ASCE, Vol. 110, Paper No. 2253, pp. 1175-1178.

15. Lacroix, Y., M. I. Esrig and U. Lusher. June 1970. Design, Construction, and Performance of Cellular Cofferdams. Specialty Conf. Lateral Stresses in the Ground and Design of Earth-Retaining Structures, ASCE, pp. 271-328.

16. Mazurkiewicz, B. K. 1972. The Rupture Figure for a Double-Wall Cofferdam. Proc. on the Specialty Conf. on Performance of Earth and Earth-Retaining Structures, ASCE, Vol. 1, Part 2, pp. 1271-1281.

17. Navdocks DM-7. 1962. Design Manual, Soil Mechanics, Foundations and Earth Structures. Dept. of Navy, Bureau of Yards and Docks.

18. Ovesen, N. K. July 1962. Cellular Cofferdams, Calculation Methods and Model Tests. The Danish Geotechnical Institute, Bulletin No. 14.

19. Pennoyer, R. P. June 1934. Gravity Bulkhead and Cellular Cofferdams. Civil Engineering, 4, No. 6. pp. 301-305.

20. Pietrak, P. 1974. Personal Communication.

21. Polivka, J. J. 1945. Discussion of Stability and Stiffness of Cellular Cofferdams by K. Terzaghi, Trans. ASCE. Vol. 110, pp. 1170-1187.

22. Rowe, P. January 1952. Anchored Sheet Pile Walls. Proc. Inst. of Civil Engineers, London, 1, pp. 27-70.

23. Schneebeli, G. and R. Cavaillé-Coll. 1957. Contribution to the Stability Analysis of Double-Wall Sheetpile Cofferdams. Proc. Fourth Intern. Conf. Soil. Mech., Vol. II, London, pp. 233-238.

24. Schroeder, W. L., D. K. Marker and T. Khuayjarernpanishk. March 1977. Performance of a Cellular Wharf. Journ. Geot. Eng. Div. ASCE, Vol. 103, No. GT3, pp. 153-168.

25. Swatek, E. P. August 1967. Cellular Cofferdam Design and Practice. Journ. Wtrwys. and Hrbrs. Div., ASCE, Vol. 93, pp. 109-132.

26. Taylor, D. 1948. Fundamentals of Soil Mechanics, Wiley and Sons, 700 p.

27. Tennessee Valley Authority. December 1957. Cofferdams on Rock. TVA Tech. Monograph 75. Knoxville, Tennessee, Vol. 1.

28. Terzaghi, K. 1945. Stability and Stiffness of Cellular Cofferdams. Trans., ASCE, Vol. 110. pp. 1083-1202.

29. Timoshenko, S. and S. Woinowsky-Krieger. 1959. Theory of Plates and Shells. McGraw-Hill, 580 p.

30. Tschebotarioff, G. 1973. Foundations, Retaining and Earth Structures. McGraw-Hill, 641 p.

31. United States Steel. 1975. Steel Sheet Piling Design Manual. 133 p.

32. White, A., J. A. Cheney and M. Duke. 1963. Field Study of a Cellular Bulkhead. Trans. ASCE, Vol. 128, pp. 463-508.

SUPPLEMENTARY REFERENCE LIST

1. Epstein, H. 1937. Design of a Cellular Cofferdam. Proc. 17th Annual Meeting, Highway Research Board, Nat. Research Council, Vol. 17, pp. 481-493.

2. Heyman, S. 1957. Discussion of Cellular Cofferdams and Docks by E. M. Cummings. Proc. ASCE, Vol. 83, No. WW3, pp. 34-37.

3. Kay, J. N. October 1975. Interlock Tension in Sheet Piling. Journ. Struc. Div., ASCE, ST-10, pp. 2093-2101.

4. Ovesen, N. K. 1958. On the Stability of Cellular Cofferdams on a Deep Sand Stratum. Proc. Conf. on Earth Pressure Problems, Vol. II, Brussels, pp. 155-170.

5. Schroeder, W. L. and M. L. Byington. 1972. Experiences with Compaction of Hydraulic Fills, 10th Idaho Symposium on Engineering Geology and Soils Engineering, Moscow, Idaho.

6. Teng, W. L. 1962. Foundation Design. Prentice-Hall. 466 p.

7. Verdeyen, J. 1948. The Use of Flat Sheet-Piling in Cellular Construction. Proc. Second Intl. Conf. Soil Mech., Vol. VII, Rotterdam.

APPENDICES

APPENDIX A

SAND PROPERTIES

SAND PROPERTIES

The Monterey sand used in the study was examined with a binocular microscope under low to medium (< 500x) power. The larger particles (in the coarse to very coarse range) were mostly subrounded to rounded with a high degree of sphericity. The surface of the grains were smooth and well polished, showing considerable abrasion. Particles in the medium to fine range showed considerably less roundness (angular to subangular) and a more blocky appearance, i.e., lower sphericity. Some very angular particles were also present. The surfaces in general were less polished indicating less weathering. The fine to very fine sand fraction consisted of subangular to very angular grains. More than 50% showed very sharp edges and unpolished, fresh surfaces. Over 90% of the grains consisted of quartz. Some feldspars and a few iron rich minerals were noted.

Two sieve analyses were conducted using No. 4, 10, 20, 40, 100, 200 and No. 4, 8, 16, 30, 60 and 80 series of sieves. Both resulted in essentially the same curves. Figure 117 shows the grain size distribution curves. Results have been summarized in the main text.

Relative density tests were run according to ASTM D2049 specifications. Results of these tests indicated a minimum dry density of 103.6 pcf and a maximum dry density of 120.3 pcf.

Direct shear tests were conducted on loose and medium dense sand samples using a Soil Test stress-controlled testing device. Vertical

GRAIN SIZE ANALYSIS

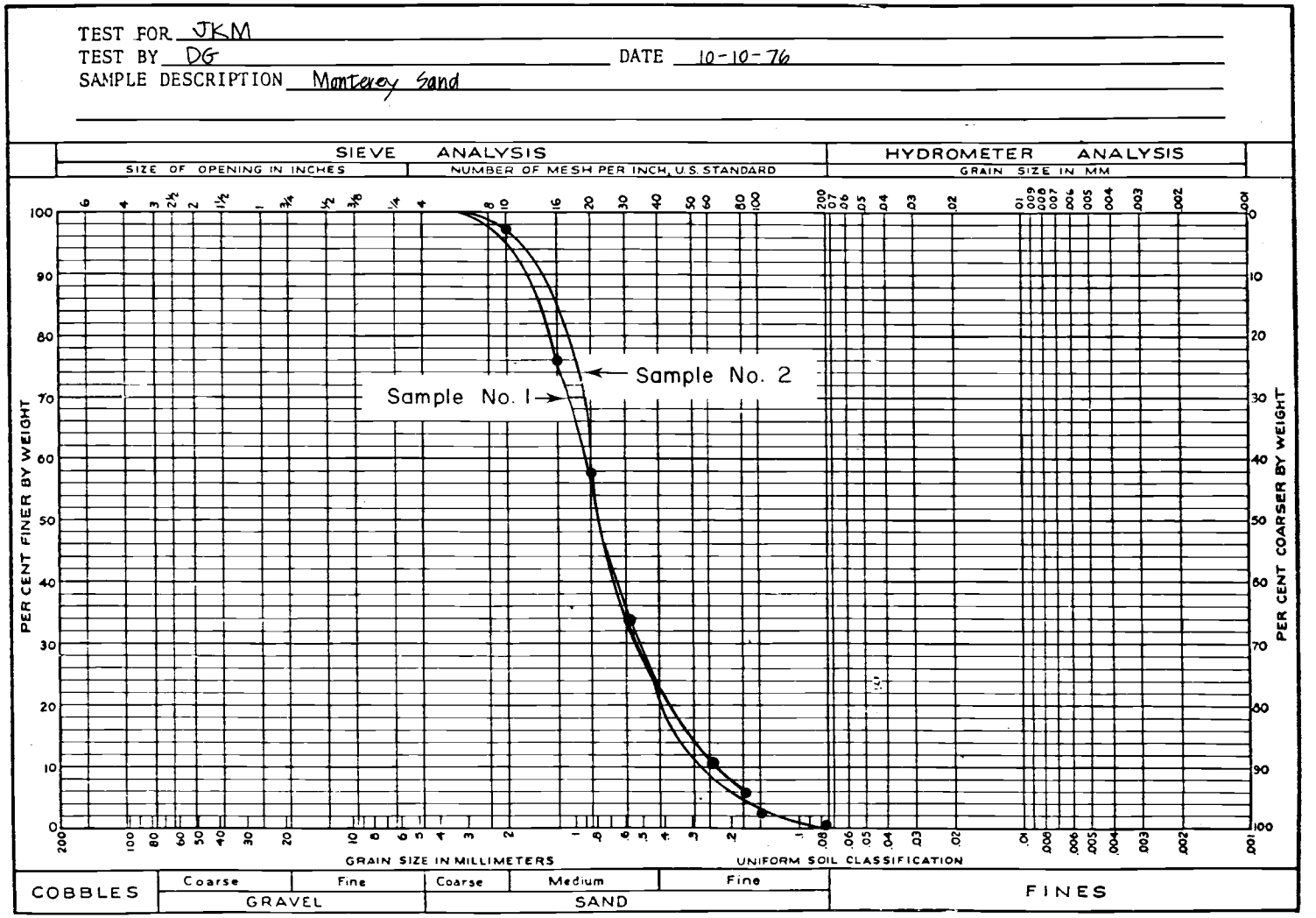

Figure 117. Grain size distribution.

overburden pressures ranged from 0.5 tsf to 2.0 tsf (6.9 to 27.8 psi, respectively). Tests could not be performed with lower vertical pressures because of excessive cap tilting. Results from direct shear tests are shown in Figure 118.

A series of triaxial tests were also run using a Wykeham-Farrence triaxial apparatus. The sand samples were 1.40 inches in diameter, 3.0 inches high and enclosed in a thin impermeable latex membrane. A special steel mold, consisting of three separate sections and held together by a thick ring, was built to form the sand samples. Testing was done on boiled saturated samples of sand. The sands were transferred from the boiling dish in a submerged state and placed in the water-filled mold using a clear plastic tube and funnel. Tests were conducted on loose, medium dense and dense samples. Densification of the samples was achieved by either vibrating the entire mold assemblage on a shaking table or by probing the sample with a vibrating wire probe. Samples of various densities were tested at confining stresses of 1.54, 2.31, 3.08 and 6.16 psi. These confining stresses were monitored by a mercury manometer tube for accuracy. A graduated burette recorded volume changes. Typical stress-strain curves for some of the triaxial tests are summarized in Figure 119.

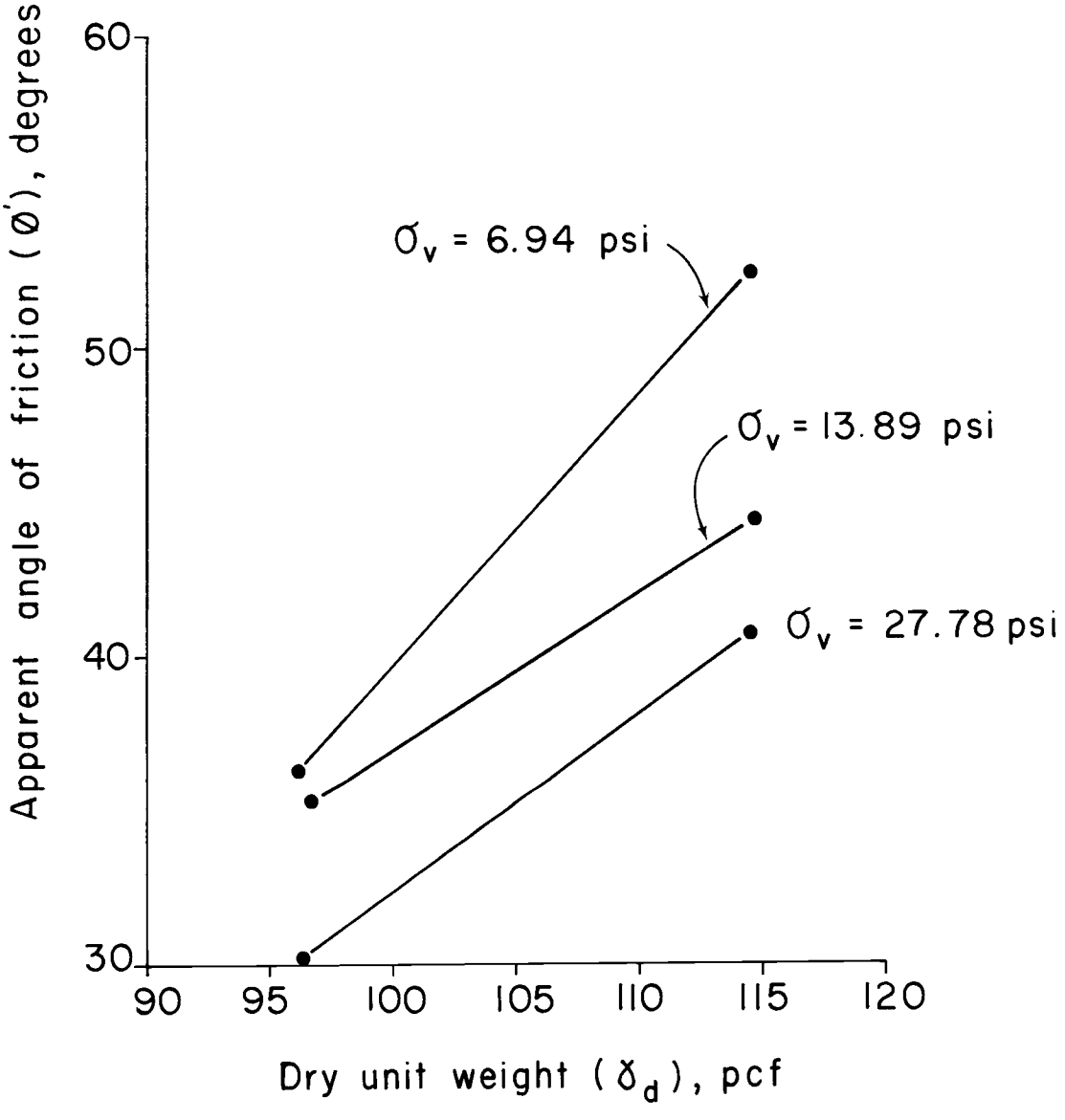

Figure 118. Direct shear test results.

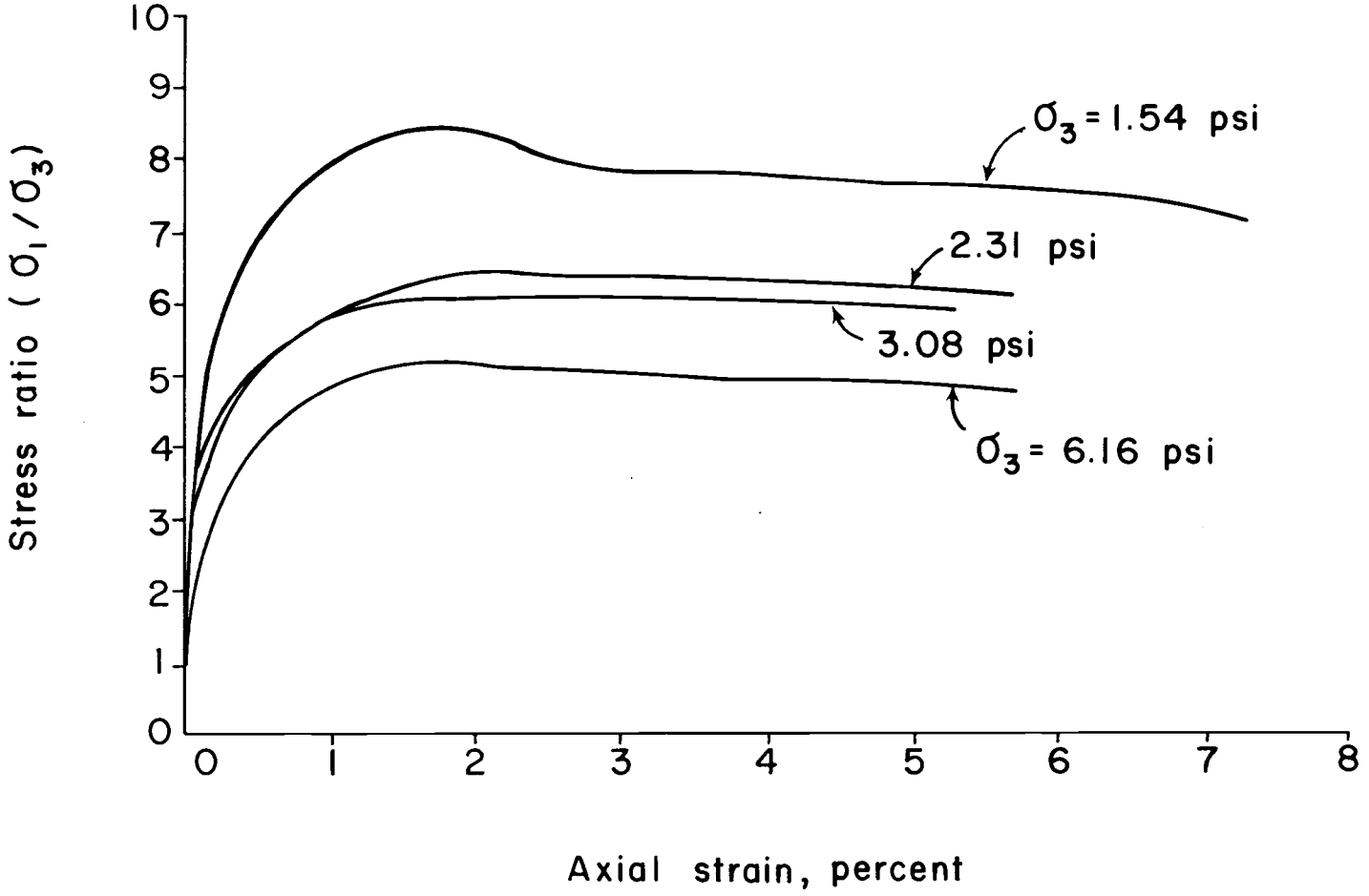

Figure 119. Typical stress-strain curves.

APPENDIX B

SUPPLEMENTARY STRAIN GAGE INFORMATION

SUPPLEMENTARY STRAIN GAGE INFORMATION

Typical Gage Installation

The strain gages used in the project were all wired in the typical quarter bridge, Wheatstone brige circuits shown schematically in Figure 120.

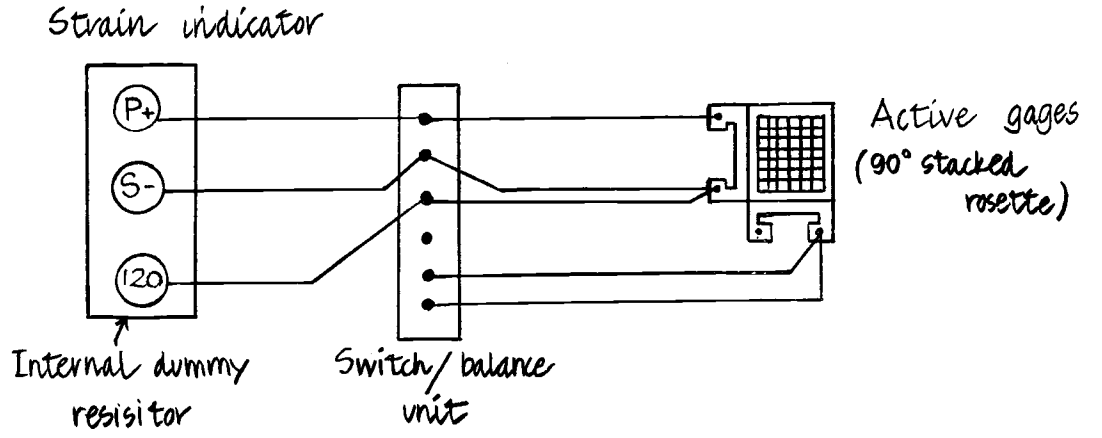

Figure 120. Typical quarter bridge circuits.

All strain gage lead wires were connected to 3 10-channel Vishay SB-1 switch and balance units wired in parallel to a Vishay P-350A digital strain indicator. A very accurate 120 ohm dummy resistor, provided internally by the strain indicator unit was used instead of an external resistor.

Lead Wire Desensitization

Long, thin lead wires may provide sufficient resistance to change the total resistance of the bridge circuit. The resistance of the leads appears as a constant resistance in the strain gage bridge and does not change with strain. As a result the overall bridge circuit is desensitized.

The gage factor may be corrected for lead wire desensitization by the equation

$$GF_i = \left(\frac{R_g}{R_L + R_g}\right) GF$$

where GF_i = corrected gage factor

R_g = nominal gage resistance

R_L = lead wire resistance

GF = original gage factor

The same correction can be made by using an internal calibration circuit provided by the strain indicator. The entire assembly (gage plus lead wires) is connected to an internal resistor of known resistance. The resistance of the lead-wire plus gage assembly is compared to the known resistance of the calibration resistor. The gage factor is then adjusted by using the Null meter. This latter procedure was used for the project.

Transverse Sensitivity

Strain gages are all affected, to some extent, by strains which are perpendicular to the primary sensing axis. The effect of transverse sensitivity should, therefore, be considered in biaxial stress analysis.

For a 90° stacked rosette the correct strains may be determined by

$$\varepsilon_x = \frac{(1 - \mu K_t)\ (\bar{\varepsilon}_x - K_t \bar{\varepsilon}_y)}{1 - K_t^2}$$

$$\varepsilon_y = \frac{(1 - \mu K_t)\ (\bar{\varepsilon}_y - K_t \bar{\varepsilon}_x)}{1 - K_t^2}$$

where μ = Poisson's ratio

K_t = transverse sensitivity of gage

$\bar{\varepsilon}_x, \bar{\varepsilon}_y$ = uncorrected strains from gages 1 and 2

$\varepsilon_x, \varepsilon_y$ = corrected strains

The corrections for transverse sensitivity were, in general, very small ($< 5\mu\varepsilon$). For most readings, this correction could be safely ignored.